AD-A175 644 RESEARCH INVESTIGATION DIRECTED TOWARD EXTENDING THE USEFUL RANGE OF THE ELECTROMAGNETIC SPECTRUM(U) COLUMBIA RADIATION LAB NEW YORK G W FLYNN ET AL. 1/3

UNCLASSIFIED 31 DEC 86 DAAG29-85-K-0049 F/G 20/14 NL

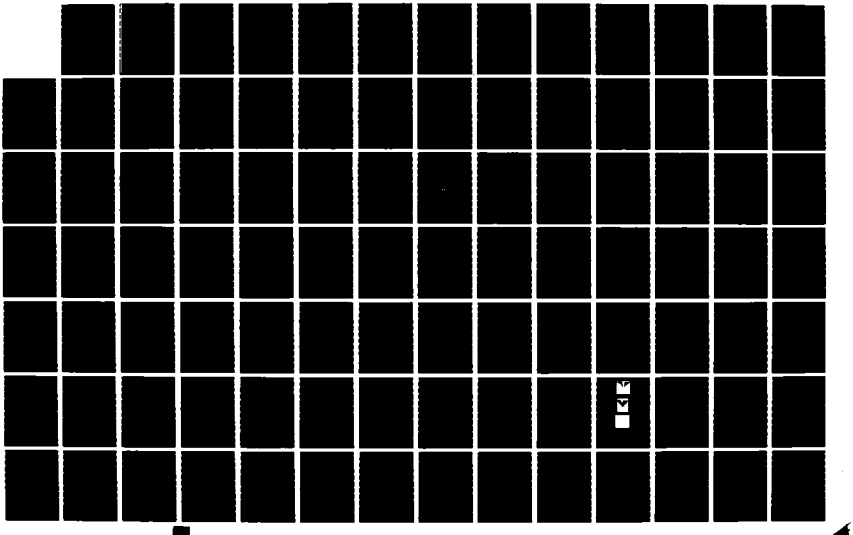

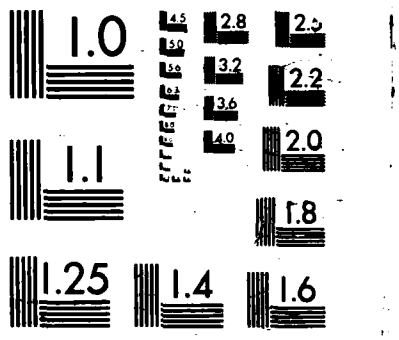
1.0
1.1
1.25
1.4
1.6
1.8
2.0
2.2
2.8
3.2
3.6
4.0

CRL

COLUMBIA UNIVERSITY

DEPARTMENTS OF PHYSICS,
CHEMISTRY, ELECTRICAL ENGINEERING

★ PROGRESS REPORT NO. 36

October 1, 1985–September 30, 1986

CONTRACT DAAG29-85-K-0049

TO:

THE JOINT SERVICES TECHNICAL ADVISORY COMMITTEE

REPRESENTING: THE U.S. ARMY RESEARCH OFFICE
THE OFFICE OF NAVAL RESEARCH
THE AIR FORCE OFFICE OF SCIENTIFIC RESEARCH

COLUMBIA RADIATION LABORATORY, NEW YORK, NEW YORK 10027

★ December 31, 1986

COLUMBIA RADIATION LABORATORY

RESEARCH INVESTIGATION DIRECTED TOWARD EXTENDING THE USEFUL RANGE OF THE ELECTROMAGNETIC SPECTRUM

Progress Report No. 36

October 1, 1985 through September 30, 1986

Contract DAAG29-85-K-0049

Object of the Research:

Basic research in the fields of quantum electronics; electromagnetic propagation, detection and sending; and solid state electronics.

The research reported in this document was made possible through support extended the Columbia Radiation Laboratory, Columbia University, by the Joint Services Electronics Program (U.S. Army Research Office, Office of Naval Research, and the Air Force Office of Scientific Research) under Contract DAAG29-85-K-0049.

Submitted By: George W. Flynn and Richard M. Osgood, Jr.
Co-Directors

Coordinated By: Karen Wingate, Departmental Administrator
Maura Schreiner, Secretary

COLUMBIA UNIVERSITY
Columbia Radiation Laboratory
Department of Physics
New York, New York 10027

December 31, 1986

The research reported in this document was made possible through support extended to the Columbia Radiation Laboratory, Columbia University by the Joint Services Electronics Program (U.S. Army Research Office, Office of Naval Research, and the Air Force Office of Scientific Research) under Contract DAAG29-85-K-0049.

Portions of this work were also supported by:

Air Force Office of Scientific Research

Contract AFOSR-84-00138
Contract AFOSR-30602-85-C-0072

AFOSR/DARPA

Grant F-49620-84-K-0022
Grant F-49620-85-C-0067

Army Research Office

Contract DAAG29-85-K-0210

National Science Foundation

Grant NSF-CHE 85-17460
Grant NSF-CHE 82-11593
Grant NSF-CHE 80-23747
Grant NSF-ECS 82-17677
Grant NSF-ECE 82-19636
Grant NSF-CDR 84-21402
Grant NSF-ECS 82-09218
Grant NSF-CHE 85-13553

Office of Naval Research

Contract N00014-78-C-0517
Contract N00014-86-0694

Department of Energy

Contract DE-AC02-78-ER-04940

Semiconductor Research Corporation

Project SRC-85-02-055

The support of these agencies is acknowledged in footnotes in the text.

SECURITY CLASSIFICATION OF THIS PAGE (When Data Entered)

REPORT DOCUMENTATION PAGE		READ INSTRUCTIONS BEFORE COMPLETING FORM
1. REPORT NUMBER Progress Report No. 36	2. GOVT ACCESSION NO.	3. RECIPIENT'S CATALOG NUMBER
4. TITLE (and Subtitle) RESEARCH INVESTIGATION DIRECTED TOWARD EXTENDING THE USEFUL RANGE OF THE ELECTROMAGNETIC SPECTRUM		5. TYPE OF REPORT & PERIOD COVERED 1 October 1985 through 30 September 1986 6. PERFORMING ORG. REPORT NUMBER
7. AUTHOR(s) George W. Flynn Richard M. Osgood, Jr.		8. CONTRACT OR GRANT NUMBER(s) DAAG29-85-K-0049
9. PERFORMING ORGANIZATION NAME AND ADDRESS Columbia Radiation Laboratory Columbia University New York, New York 10027		10. PROGRAM ELEMENT, PROJECT, TASK AREA & WORK UNIT NUMBERS
11. CONTROLLING OFFICE NAME AND ADDRESS Department of the Army U.S. Army Research Office Research Triangle Park, NC 27709		12. REPORT DATE December 31, 1986 13. NUMBER OF PAGES 184
14. MONITORING AGENCY NAME & ADDRESS(if different from Controlling Office) Department of the Army U.S. Army Research Office Research Triangle Park, NC 27709		15. SECURITY CLASS. (of this report) Unclassified 15a. DECLASSIFICATION/DOWNGRADING SCHEDULE
16. DISTRIBUTION STATEMENT (of this Report) Approved for public release; distribution unlimited.		
17. DISTRIBUTION STATEMENT (of the abstract entered in Block 20, if different from Report) Portions of this work were also supported by the Air Force Office of Scientific Research, the Army Research Office, the National Science Foundation, the Office of Naval Research, the Department of Energy, AFOSR/DARPA and NIH.		
18. SUPPLEMENTARY NOTES		
19. KEY WORDS (Continue on reverse side if necessary and identify by block number) Lightwave Communications Sub-Poisson Light Amplitude-Squeezed Light Superlattice Photodetectors		
20. ABSTRACT (Continue on reverse side if necessary and identify by block number) New developments have been achieved in the quantum generation and detection of light. The usual semiclassical theory of light detection turns out to be incomplete. The theory has been extended to include the possibility of feedback from the detector to the source which changes the theory substantially. In the revised theory the noise at the output of a detector		

DD FORM 1 JAN 73 1473 EDITION OF 1 NOV 65 IS OBSOLETE

unclassified

SECURITY CLASSIFICATION OF THIS PAGE (When Data Entered)

Block 19 continued - Key Words

Quantum-Well Heterostructures
Avalanche Photodetectors
Excess Noise Factor
Waveguide Modulator
Multiple Quantum Well Structure
Fiber Optic
Laser-Assisted Etching
Surface Spectroscopy
Infrared Spectroscopy
Metal Alkyls
Physisorbed Molecular Layers
GaAs (Gallium Arsenide)
HBr (Hydrogen Bromide)
Dry Etching
Laser Etching
XPS
Schottky Barrier
Laser Direct Writing
Chlorine
Silicon
Oxidation
AES
GaAs Oxidation
CF_4
Plasma Etching
Silicon
Plasma Polymerization
Anisotropic Etching
Interface States
Silicides
Schottky Barriers
Capacitance Spectroscopy
Low Temperature Processing
Low Energy Ion Beam
Silicon Oxidation
Leakage Current
Reverse Current
Hg
CO_2
$CH_3COCOOH$
Pt
CO
Mercury
Carbon Dioxide
Pyruvic Acid
Platinum
Carbon Monoxide
Metastable
Triplet
Photodissociation
Catalytic
Surface
Internal States
Energy Transfer
Collisions
Relaxation
Ladder Climbing
Chemical Intermediates
Dielectric Relaxation
Energy Relaxation
Excited State Structural Change
Intersystem Crossing
Liquid-Air Interface
Photodissociation
Photoisomerization
Picosecond Lasers
Solvent Effects
Surface Nonlinear Susceptibility
Surface Second Harmonic Generation
Twisted Internal Charge Transfer
Optical Coherent Transients
Photon Echoes
Sodium Vapor
Spectroscopy
Stimulated Photon Echoes
Superfluorescence
Ultrafast Modulation Spectroscopy
Four-Wave-Mixing
Broad-Band Time-Delayed
Four-Wave-Mixing
Semiconductor-Doped Glasses
$Pr^{3+}:LaF_3$
Satellite Line
Nonlinear Optics
Phase Relaxation
Quantum Wells
Phonon Relaxation
Energy Transfer

can be below shot noise even though the incident light is classical, i.e., above shot noise. However, the action of such an electron current configured in an external feedback loop can be useful for converting Poisson light into amplitude-squeezed (sub-Poisson) light. A configuration making use of transitions between the energy levels of a quantum-well heterostructure has been developed. The noise properties of superlattice avalanche photodiodes (SAPD's) have been compared with those of conventional avalanche photodiodes (CAPD's) for the detection of both amplitude-squeezed light and conventional light. SAPD's are heterostructure devices constructed in such a way that principally one kind of carrier impact-ionizes. Performance and time response have been evaluated for lightwave communication systems. These detectors exhibit promising characteristics.

A new formalism of the Kronig-Penney model, simpler than the conventional version, has been developed and applied to GaAs/AlGaAs superlattices to calculate the electron energy subbands and envelope wave functions in the superlattices, and to find the critical barrier thicknesses above which the superlattice structures can be considered uncoupled quantum well systems and below which they can be considered as coupled quantum well systems. This formalism has been applied to the design of modulators.

Low intensity, cw, uv light at 350 nm has been used to inhibit polymer formation on a silicon substrate in a plasma reactor operated with CF_4 and H_2. The dependence of the laser-enhanced etch rate, as a function of H_2 partial pressure, is due to both variation in gas-phase fluorine concentration and polymer formation on the silicon surface. The effect has been used to perform maskless patterning of a silicon wafer using an imaged laser beam.

A study has been made of excimer-laser-assisted etching of GaAs using HBr gas. The etch rate displays a temperature dependence, limited

Block 20 continued - Abstract

at lower temperatures by desorption of the reaction products and at higher temperatures possibly by formation of a contaminant layer on the surface of the GaAs. XPS surface analysis indicates that the etching proceeds through bromination of a number of monolayers of GaAs beneath the surface. Rapid etching appears to be correlated with a thicker layer. Both the XPS and the Schottky barrier measurements indicate that when the laser is incident onto the GaAs surface during the etch process,a cleaner surface results, as evidenced by a thinner surface layer and Schottky barrier measurements which are closer to ideal.

Surface electron spectroscopy has been used to investigate the laser-enhanced oxidation of gallium arsenide surfaces. The elemental composition and distribution of the oxide layer were studied by Auger electron spectroscopy (AES) depth-profiling. The thickness and chemical content of the oxide layer were studied by X-ray photoelectron spectroscopy (XPS). The oxidation was found to be much more strongly enhanced by exposure to ultraviolet light than to visible light. The presence of moisture on the surface was also found to drastically increase the rate of oxidation.

Infrared total reflection has been used to investigate the spectra of submonolayer films of dimethylcadmium on single-crystal silicon. A coverage-dependent frequency shift was observed.

Fosuced-laser etching of silicon with chlorine has been studied and a model proposed to explain the variation in etch rate versus power and pressure. The model demonstrates that the etching of silicon is a melt-enhanced reaction. Diffusion effects have also been explored. Our photodeposition work has been continued and several new metal-organic compounds have been studied. Our direct-writing work uses a unique hybrid laser system designed and built with the additional aid of a contract from the Semiconductor Research Corporation.

Block 20 continued - Abstract

A capacitance-spectroscopy technique based on accurate phase detection has been developed to measure the unoccupied states at silicide-silicon contacts. For Ni silicides, a dispersed group of states was found to exist in the Si band gap with its peak at a level 0.63-0.65 eV above the valence-band edge. Silicide formation alters their density and distribution to reflect the changes in the structural perfection and barrier height. Observations on the epitaxial $NiSi_2$-Si(111) interf[illegible]eal that the characteristics of these states are controlled [illegible] ree of structural perfection of the interface instead of the specific epitaxy. This seems to be the first correlation of the structural and electronic properties of a silicide-silicon interface.

A forward biased capacitance measurement has been made on palladium-silicon Schottky diodes. The data are interpreted in terms of the interface state density by taking into account the effect of series resistance and by using Shockley-Read-Hall statistics. Exchange of charge between the metal and the interface states is included in the model. For the as-deposited sample, an effective state is postulated to lie opposite the metal Fermi level with a concentration of 1×10^{12} cm^{-2}. Upon annealing and formation of palladium silicide, the density of states decreases by a factor of 2 and changes occur in the capture and emission time constants.

The oxidation of silicon by the use of a low energy ion beam has been studied. The electrical properties of the ultra-thin oxide layer have been investigated. The chemical properties of the oxide have been studied using Auger electron spectroscopy (AES) and angle-resolved x-ray photoelectron spectroscopy (XPS). Experiments to study the effect of process parameters, such as beam energy, composition, and substrate temperature, have been performed.

The reverse-bias leakage current in aluminum-gallium arsenide

Block 20 continued - Abstract

Schottky diodes has been reduced by over a factor of 25 by increasing the surface arsenic content.

Diode laser probing has been used to follow the time dependent changes in the populations of low lying vibrational states of CO_2 produced via quenching of $Hg(6^3P_1)$ initially excited by a pulse from a doubled dye laser. The conversion of mercury electronic energy into CO_2 vibrational energy is quite efficient and mode specific. The ratio of the number of bending mode quanta to the number of asymmetric stretch quanta produced by the quenching process is 40 ± 12. The rate of filling of both the bending and asymmetric stretch levels is identical and corresponds to 80 CO_2/CO_2 gas kinetic collisions. This data, taken in conjunction with the known quenching rate of $Hg(6^3P_1)$ by CO_2 (4 gas kinetic collisions) suggests that the quenching process produces a metastable state of CO_2 which is either a bent electronic triplet or a highly excited vibrational level of the ground electronic state.

Metal-molecule interactions have been further investigated by studying the catalytic oxidation of CO to CO_2 on a platinum surface. In a prototype experimental study, which is expected to transfer directly to the investigation of semiconductor-gas surfaces, the final vibrational states of CO_2 produced from reaction of CO with O atoms on hot platinum (700 K) have been probed with a diode laser (0.0003 cm^{-1} resolution). These experiments show that the bending and stretching modes of gaseous CO_2 ejected from the surface are produced at different temperatures.

A direct measure of the rate for the CO_2 ν_3 ladder climbing process

$$2CO_2(00^01) \rightleftarrows CO_2(00^02) + CO_2(00^00)$$

has been obtained by diode laser probing of the CO_2 00^02 ---> 00^03 transition after CO_2 laser excitation of 00^01 with a Q-switch CO_2 laser. The rate corresponds to 2-3 gas kinetic collisions.

Block 20 continued - Abstract

A tunable infrared diode laser has been employed as an absorption probe to monitor the vibrational excitation of CO_2 produced upon 193 nm excimer laser photolysis of pyruvic acid in the gas phase. Nascent relative population measurements were performed immediately after the photodissociation event for the following vibrational states of CO_2:

00^00, 01^10, 02^20, 03^30, 04^40, 00^01, 00^02, 00^03, 01^11, and 02^21.

Most of the CO_2 photoproduct is observed to be directly formed in the vibrationless ground state with a small fraction of molecules occuring with a significant degree of vibrational excitation ($N_{000} = 30 \times N_{010}$). The distribution of molecules among the excited vibrational states of CO_2 indicates the following mode temperatures:

$T_{010-040}=1800\pm150K$, $T_{001-003}=3700\pm1000K$, $T_{011-021}=2000\pm400K$.

The present experimental data suggests a dissociation mechanism which may proceed through more than a single channel.

The chemical reaction of O^1D with CO_2 to produce vibrationally excited CO_2 molecules and O^3P atoms has been studied using an excimer laser to produce O^1D and a diode laser to probe the vibrationally hot CO_2. Clear vibrational excitation of CO_2 is observed but the excitation mechanism appears to be dependent on the O^1D atom precursors. Experiments which use O_3 and 248 nm light for photodissociation are planned to increase the number of O^1D atoms.

A measurement of the absolute phase of the second harmonic light field with respect to the pump field, i.e. the phase of the surface nonlinear susceptibility, has been made. From such studies the absolute orientation of surface molecules can be determined. In the present work the liquid/vapor interface of an aqueous phenol solution was investigated.

The rates of optically induced conformational changes of excited state 1,1'-binaphthyl in alcohols and alkane solvents were measured by a picosecond laser technique. Excellent agreement with experiment was

Block 20 continued - Abstract

found using the Kramers model for the intermediate friction regime when employing the solute orientational relaxation time as a measure of solvent friction.

Solute/solvent interactions were investigated in polar solvents by using dynamical photoemission methods to follow the photoisomerization of polar probe molecules in a solvent series, in polar solvent/alkane mixtures and in a single solvent as a function of temeprature. Variation of the photoisomerization rate of p-N, N-dimethylaminobenzonitrile (DMABN) has been attributed chiefly to static solvent polarity effects rather than to dynamic frictional effects due to high solvent viscosities, as previously believed. These results were compared to data obtained for the photoisomerization of t-stilbene in alcohols, where the usual functional forms of solvent viscosity dependence also fail to account completely for the observed solvent dependence of the rate. Implications of all of these findings regarding the use of one-dimensional barrier crossing theories to describe photoisomerization in solution have been discussed.

The photophysics of a substituted oxirane as a precursor to carbenes has been investigated, using tetraphenyloxirane as the example. A short lived (70 ps) 1,3-biradical, possessing singlet state multiplicity, was found to be an intermediate to carbene formation.

We report observation of non-degenerate four wave mixing in $Pr^{3+}:LaF_3$. However we were unable to observe trilevel echoes in this sample due to low correlation in the inhomogeneous widths of the two transitions studied in this sample. Future experiments to observe trilevel echoes is planned and will be carried out in $Pr^{3+}:CaF_2$. Further observations were also made on satellite echoes and continued work on this subject is awaiting construction of single mode pulsed dye lasers currently in progress. This will allow selective excitation of satellite lines which lie very close to the central line. We have also

Block 20 continued - Abstract

begun to carry out broad band incoherent four wave mixing experiments in solids and molecular dyes in solutions. Under investigation are Nile Blue in Methanol and CdS_xSe_{1-x} semiconductor microcrystallites in glass. For the latter case we report, for the first time, observation of coherent transient effects in the femtosecond time scale using a 7 nsec broad-band incoherent source. Future plans include the application of the above technique in GaAs multiquantum wells.

Investigating the nature of the interaction of incoherent light with matter has been the focus of much theoretical and experimental work this year. Further experiments were performed to ascertain the source of the observed degradation of the Time Delayed Four Wave Mixing (TDFWM) signal with increasing pulse separation (as was reported last year in our work on TDFWM using intense incoherent light). It was predicted by Norita and Yajima that the signal intensity should not decrease with increasing pulse separation for TDFWM signals arising from incoherent light in the small pulse angle limit. As we work outside of the regime of small pulse angles, with intense incoherent light, it was necessary to do a nonperturbative analysis to include the effects of the intense pulses. An experiment was performed to determine if the cause of the observed signal degradation was indeed due to the intense nature of our pulses. Using a weak probe pulse to interrogate the TDFWM signal we still observed the signal degradation. This indicated that a more general theory was required to explain the interaction of intense incoherent light with matter. Collaboration with R. Friedberg has produced a more general theory and experiments are underway to test this theory experimentally.

A picosecond laser facility has been developed for use in optical coherent transient studies. Initial experiments have been planned which include extensions of previous work in alkali metal vapors as well as new investigations of two-photon superfluorescence.

TABLE OF CONTENTS

PUBLICATIONS AND REPORTS

Publications

C. Dupuy, D. Hrovat, J. Langan, E.V. Sitzmann, T.A. Jenny, N.J. Turro and K.B. Eisenthal, "State Selective Photochemistry of Singlet Oxygen Precursors: Kinetics and Wavelength Dependence of the Photodissociation of Anthracene Endoperoxides," J. Phys. Chem. 90, 5168 (1986).

J. Hicks, M. Vandersall, E.V. Sitzmann, and K.B. Eisenthal, "Polarity Dependent Barriers and the Photoisomerization Dynamics of Polar Molecules in Solution," Ultrafast Phenomena V, G.R. Fleming and A.E. Siegman, Eds., Springer-Verlag, Berlin, 1986.

K.B. Eisenthal, "Ultrafast Chemical Reactions in the Liquid State," Ultrafast Light Pulses, W. Kaiser, Ed., Springer-Verlag, Berlin, 1986.

J.M. Hicks, K. Kemnitz, T.F. Heinz and K.B. Eisenthal, "Studies of Liquid Surfaces by Second Harmonic Generation," J. Phys. Chem. 90, 560 (1986).

K. Kemnitz, K. Bhattacharyya, J.M. Hicks, G.R. Pinto, T.F. Heinz, and K.B. Eisenthal, "The Phase of Second Harmonic Light Generated at an Interface and its Relation to Absolute Molecular Orientation," Chem. Phys. Letts. 131, 285 (1986).

E.V. Sitzmann, J. Langan, and K.B. Eisenthal, "Effect of Solvent Polarity and Structure on Intersystem Crossing in Arylcarbenes: A Picosecond Laser Study of Dimesitylcarbene," in preparation.

J. Hicks, M. Vandersall, and K.B. Eisenthal, "Hydrogen Bonding and Polarity Effects on Barrier Crossings in Solution," in preparation.

R.M. Bowman, D.P. Millar, and K.B. Eisenthal, "Picosecond Photoisomerization in Liquids: Dynamics of 1,1'-Binaphthyl," in preparation.

E.V. Sitzmann, J. Langan, and K.B. Eisenthal, "Picosecond Laser Studies on the Photodissociation of Tetraphenyloxirane: Effect of Carbene Precursor Dissociation and Energy Decay on Pathways and Dynamics," in preparation.

B.B. Brady, G.B. Spector, and G.W. Flynn, "Vibrational Predissociation of SF_6 Clusters in a Supersonic Molecular Beam," J. Phys. Chem. 90, 83 (1986).

J.A. O'Neill, Ji Ye Cai, G.W. Flynn, and R.E. Weston, Jr., "Diode Laser Probing of Bending and Stretching Vibrational Excitation in CO_2 Caused by Collisions with Hot Deuterium Atoms," J. Chem. Phys. 84, 50 (1986).

G.W. Flynn and R.E. Weston, Jr., "Hot Atoms Revisited: Laser Photolysis and Product Detection," Ann. Review of Physical Chemistry, to be

published, Fall 1986.

B.B. Brady, G.B. Spector, L. Chia, and G.W. Flynn, "Diode Laser Probing of Product State Distributions in Metal-Molecule Collisions: $Hg(6^3P_1)$ - CO_2 $(mn^{\ell}p)$," accepted for publication.

J.A. O'Neill, C.X. Wang, J.Y. Cai, G.W. Flynn, and R.E. Weston, Jr., "Rotationally Resolved Hot Atom Collisional Excitation of CO_2 (00^01) by Time-Resolved Diode Laser Spectroscopy," J. Chem. Phys., 85, 4195 (1986).

S.S. Todorov, S. Shillinger, E.R. Fossum, "Low-Energy Ion Beam Oxidation of Silicon," IEEE Electron Device Letters, EDL-7, 468 (1986).

D. DeBeer, L.G. Van Wagenen, R. Beach and S.R. Hartmann, "Time-Delayed Four-Wave Mixing in Sodium Vapor," Proceedings of the First International Laser Conference, 18-22, (November 1985) (submitted).

S.R. Hartmann, "Spectroscopy, Relaxation and Laser Action in Pr^{3+}:LaF_3," First International Laser Science Conference, (November 1985) (submitted).

R. Beach, D. DeBeer, L.G. Van Wagenen and S.R. Hartmann, "Picosecond Modulation Spectroscopy in Sodium Vapor," Proceedings of the Fritz Haber Symposium on "Methods of Laser Spectroscopy" (Israel, December 1985) (to be published).

E.Y. Xu, F. Moshary, and S.R. Hartmann, "Noble Gas Induced Collisional Line Broadening of Atomic Li Rydberg States nS and nD (n = 4 to 30) Measured by Trilevel Echoes," AIP (1986).

E.Y. Xu, F. Moshary, and S.R. Hartmann, "Noble-Gas-Induced Collisional Line Broadening of Atomic Lithium Rydberg Superposition States 2S-nS and 2S-nD (n = 4 to 30) Measured by Trilevel Echoes," JOSA B 3, 497 (1986).

T.J. Chen, D. DeBeer, and S.R. Hartmann, "Observation and Relaxation of the Two-Photon-Excited Trilevel Echo in Sodium Vapor," JOSA B 3, 493 (1986).

T.J. Chen, D. DeBeer, and S.R. Hartmann, "Observation and Relaxation of the Two-Photon-Excited-State Trilevel Echo in Sodium Vapor," AIP (1986).

D. DeBeer, L.G. Van Wagenen, R. Beach, and S.R. Hartmann, "Ultrafast Modulation Spectroscopy," Phys. Rev. Lett. 56, 1128-1131 (1986).

P.D. Brewer, D. McClure, and R.M. Osgood, Jr., "Excimer Laser Projection Etching of GaAs," App. Phys. Lett., date of appearance unknown.

D.V. Podlesnik, H.H. Gilgen, A.E. Willner, R.M. Osgood, Jr., "Interaction of Deep Ultraviolet Laser Light with GaAs Surfaces in Aqueous Solutions," J. Opt. Soc. Am. B, 3, 775 (1986).

C.F. Yu, D.V. Podlesnik, M.T. Schmidt, H.H. Gilgen, and R.M. Osgood, Jr., "Ultraviolet-light-enhanced Oxidation of Gallium Arsenide Surfaces

Studied by X-ray Photoelectron and Auger Electron Spectroscopy," App. Phys. Lett., accepted for publication.

G.M. Reksten, W. Holber, and R.M. Osgood, "Wavelength Dependence of Laser Enhanced Plasma Etching of Semiconductors," App. Phys. Lett., 48, 8 (1986).

P.R. Prucnal, M.A. Santoro, and T.R. Fan, "Orthogonal Modulation in Fiber-optic Communications," Proc. IEEE, 74, 225-227 (1986).

P.R. Prucnal, D. Blumenthal, and P.A. Perrier, "Self-routing Optical Switch with Optical Processing," Opt. Eng., submitted for publication.

B.M. Nyman and P.R. Prucnal, "A Geometric Optics Approach to Beam Propagation Analysis," Proc. IEEE, submitted for publication.

M.C. Teich, "Laser Heterodyning," Opt. Acta, 32, 1015-1021 (1985). [Invited Paper for Special Anniversary Issue: 25 Years of the Laser'].

K. Matsuo, M. C. Teich and B. E. A. Saleh, "Noise Properties and Time Response of the Staircase Avalanche Photodiode," IEEE J. Light Tech., LT-3, 1223-1231, (1985) [joint issue with IEEE Trans. Elect. Dev., ED-32, 2615-2623 (1985)].

J. H. Shapiro, M. C. Teich, B. E. A. Saleh, P. Kumar, and G. Saplakoglu, "Semiclassical Theory of Light Detection in the Presence of Feedback, " Phys. Rev. Lett., 56, 1136-1139 (1986).

M. C. Teich, K. Matsuo, and B. E. A. Saleh, "Counting Distributions and Error Probabilities for Optical Receivers Incorporating Superlattice Avalanche Photodiodes," IEEE Trans. Elect. Dev., ED-33, 1475-1488 (1986).

M. C. Teich, K. Matsuo, and B. E. A. Saleh, "Time and Frequency Response of the Conventional Avalanche Photodiode," IEEE Trans. Elect. Dev., ED-33, 1511-1517 (1986).

F. Capasso and M. C. Teich, "Conversion of Poisson Photons into Sub-Poisson Photons by the Action of Electron Feedback," Phys. Rev. Lett., 57, 1417-1420 (1986).

E.S. Yang, D.K. Yang, Q.H. Hua, and G.S. Yang, "Tunneling in a Metal-Semiconductor-Semiconductor Thin-Film Diode," Solid-State Electronics, 29, 355-357 (1986).

P.S. Ho, E.S. Yang, H.L. Evans, and X. Wu, "Electronic States at Silicide-Silicon Interfaces," Phys. Rev. Lett. 56, 177-180 (1986).

P.S. Ho, M. Liehr, P.E. Schmid, F.K. LeGoues, E.S. Yang, H.L. Evans, and X. Wu, "Schottky Barrier, Electronic States and Microstructure at Ni: Silicide-Silicon Interfaces," Surface Science, 168, 184-192 (1986).

E.S. Yang, X. Wu, H. L. Evans, and P.S. Ho, "Silicide-Silicon Interface States," Thin Films and Interface Phenomena, Eds. R.S. Nemamich, P.S.

Ho, and S.S. Lau, 485-492 (1986).

H.L. Evans, X. Wu, E.S. Yang, and P.S. Ho, "Measurement of Interface States in Palladium Silicon Diodes," J. App. Phys., 60, 3611-3615 (1986).

Lectures and Presentations

K.B. Eisenthal, "Ultrafast Photoisomerization in Liquids," University of Miami, Miami, Florida, January 1986.

K.B. Eisenthal, "Picosecond Studies of Ultrafast Photoisomerization in Liquids," Harvard University, Cambridge, Massachusetts, February 1986.

K.B. Eisenthal, "Dynamics of Barrier Crossing in Liquids," M.I.T., Cambridge, Massachusetts, 1986.

K.B. Eisenthal, "Ultrafast Photoisomerization in Liquids," American Chemical Society Division of Physical Chemistry Conference, New York, New York, April 1986.

K.B. Eisenthal, "Photoisomerization of Polar Molecules in Solution," Fifth Topical Meeting on Ultrafast Phenomena, Snowmass, Colorado, June 1986.

K.B. Eisenthal, "Picosecond studies of Photoisomerization," M.I.T. Conference on Free-Electron Laser, Cambridge, Massachussetts, August 1986.

K.B. Eisenthal, "Picosecond Studies of Ultrafast Photoisomerization in Liquids," University of Illinois, Urbana, Illinois, September 1986.

E.R. Fossum, "Low-Energy Ion Beam Oxidation of Silicon," 1985 Semiconductor Interface Specialist's Conference, Ft. Lauderdale, FL, Dec. 1985.

E.R. Fossum, "Direct Formation of Dielectric Thin Films on Silicon by Low Energy Ion Beam Bombardment," LEIB IV, Brighton England, April 1985.

G.W. Flynn, "Diode Laser Probes of Transient Species and Dynamic Collision and Photofragmentation Events," DuPont Chemical Company, Wilmington, Delaware, April 1986.

G.W. Flynn, "Diode Laser Probes of Transient Species and Dynamic Collision and Photofragmentation Events," SUNY, Buffalo, May 1986.

G.W. Flynn, "Pulsed Infrared Lasers: Catalyst for a Revolution in Vibrational Energy Transfer Studies," Northwestern University, Evanston, Illinois, July 1986.

G.W. Flynn, "Some Like It Hot: High Energy Collisions, and the Seaarch for the Ultimate Experimental Probe in the 'Game' of Molecular Dynamics," Northwestern University, Evanston, Illinois, July 1986.

G.W. Flynn, "Probing the Bath Modes in the Quenching of Atoms, Molecules Large, and Molecules Small: Diode Lasers and the Almost Unique Properties of a Warm Bath of Carbon Dioxide," Northwestern

University, Evanston, Illinois, July 1986.

G.W. Flynn, "Diode Laser Probes of Transient Species and Dynamic Collision and Photofragmentation Events," Symposium on State to State Chemistry, American Chemical Society Meeting, Annaheim, California, September 1986.

S.R. Hartmann, "Spectroscopy, Relaxation and Laser Action in $Pr^{3+}:LaF_3$," First International Laser Science Conference, Dallas Texas, 1985.

S.R. Hartmann, "Picosecond Modulation Spectroscopy in Sodium Vapor," Fritz Haber Symposium on Methods of Laser Spectroscopy," Jerusalem, Israel, December 1985.

R.M. Osgood, "Light-Guided Microfabrication of Semiconductors in Aqueous Solution," Electrochemical Society Meeting, Las Vegas, Nevada, October 1985.

D.V. Podlesnik, "Laser-Enhanced Plasma Etching of Semiconductors," American Vacuum Society Meeting, Houston, Texas, November 1985.

R.M. Osgood, "Photon Assisted Dry Etching of GaAs," Materials Research Society Meeting, Boston, Massachusetts, December 1985.

H.H. Gilgen, "Near UV Deposition of Refractory Metals," Materials Research Society Meeting, Boston, Massachusetts, December 1985.

D.V. Podlesnik, "Ultraviolet-Induced Reactions with Water on Semiconductor Surfaces," Materials Research Society Meeting, Boston, Massachusetts, December 1985.

R.R. Krchnavek, "Near UV Deposition of Low Resistivity I.C. Interconnects," Materials Research Society Meeting, Boston, Massachusetts, December 1985.

T. Cacouris, "Laser Direct Writing of Metal Interconnects," Int. Electron Devices Meeting, Washington, D.C., December 1985.

R.M. Osgood, "Laser-Assisted Etching," SPIE, Los Angeles, California, January 1986.

D.V. Podlesnik, "Fabrication of Submicrometer Gratings on Semiconductors," Perkins-Elmer, Norwalk, Connecticut, January 1986.

D.V. Podlesnik, "The Interaction of Deep-Ultraviolet Light with GaAs Surfaces," IBM - T.J. Watson Research Center, Yorktown Heights, New York, March 1986.

R.M. Osgood, "Ultraviolet Photochemistry on Semiconductor Surfaces," American Chemical Society Meeting, New York, April 1986.

D.V. Podlesnik, "Ultraviolet Laser-Induced Reactions on GaAs Surfaces,"

American Chemical Society Meeting, New York, April 1986.

D.V. Podlesnik, "Deep Ultraviolet Induced Aqueous Etching of GaAs," Bellcore, Murray Hill, New Jersey, April 1986.

A.E. Willner, "Laser-Induced High-Aspect Etching of InP," CLEO, San Francisco, April 1986.

D.V. Podlesnik, "Direct Holographic Processing Using Laser Chemistry," IBM - T.J. Watson Research Center, Yorktown Heights, New York, April 1986.

W. Holber, "Laser-Assisted Plasma Etching," AT T - Bell Laboratories, Murray Hill, New Jersey, April 1986.

D.V. Podlesnik, "Spontaneous Ripple Formation Due to Ultraviolet Surface Oxidation of Semiconductors," IQEC, San Francisco, April 1986.

R.R. Krchnavek, Laser Direct Writing in Microelectronics," AT T - Bell Laboratories, Murray Hill, New Jersey, May 1986.

R.M. Osgood, "Laser-Induced Etching of InP," Columbia University, CTR Industrial, New York, New York, May 1986.

W. Holber, "Laser-Controlled Plasma Etching of Si and GaAs," IBM - T.J. Watson Research Center, Yorktown Heights, New York, May 1986.

R.R. Krchnavek, "Laser-Induced Direct Writing of Metallic Patterns," Bellcore, Murray Hill, New Jersey, May 1986.

D.V. Podlesnik, "Fabrication of High-Aspect Features Using Light-Guided Etching," Gordon Research Conferences, New Hampshire, July 1986.

W. Holber, "Laser-Assisted Plasma Etching," Gordon Research Conferences, New Hampshire, August 1986.

W. Holber, "Laser-Induced Anisotropic Etching," McDonnell-Douglas, Elmsford, New York, August 1986.

R.M. Osgood, "Laser Chemical Processing," Industrial Symposium on the Leading Edge of Lasers and Chemistry, MIT, Cambridge, Massachusetts, September 1986.

P.R. Prucnal, "Direct connection of optical fibers to integrated circuits," International Electronic Packaging Society, San Diego, California, November 1986.

P.R. Prucnal, "Spread and spectrum fiber-optic local area network using optical processing," FOC/LAN 86, Orlando, Florida, October, 1986.

P.R. Prucnal, "VLSI optical interconnecting networks" and "All-optical ultra-fast networks," SPIE Fiber/LASE 86, Cambridge, Massachusetts, September 1986.

P.R. Prucnal, "Fiber optic interconnects using laser assisted etching," International Optical Computing Conference, Jerusalem, Israel, July 1986.

P.R. Prucnal, "All-optical fiber networks," NSF Industry - University Workshop, Columbia University, New York, New York, May 1986.

P.R. Prucnal, "Integrated fiber optic coupler for VLSI interconnects," Society of Photooptical Instrumentation Engineering, Annual Meeting, Los Angeles, California, January 1986.

P.R. Prucnal, "Optical interconnects for VLSI local area networks," IBM/CTR Workshop on Computer Networks, Arden House, Harriman, New York, December 1985.

P.R. Prucnal, "Integrated fiber optic coupler for VHSIC/VLSI interconnections," Workshop on Optical Interconnects, MCC, Austin, Texas, November 1985.

P.R. Prucnal, "Transmission codes for optical communications," NASA Review, Greenbelt, Maryland, November 1985.

P.R. Prucnal, "Optical interconnects," Optical Processing Annual Review, DARPA, McLean, Virginia, November 1985.

P.R. Prucnal, "Local area network with spread spectrum processing" and "Integrated fiber optic coupler for VLSI interconnects,' Optical Society of America Annual Meeting, Washington, D.C., October 1985.

M.C. Teich, "Sub-Poissonian Light in Franck-Hertz Experiments," Invited Lecture, International Workshop on New Trends in Quantum Optics and Electrodynamics, Rome, Italy (October 1985).

M.C. Teich, "Neural Counting and Simple Psychophysical Paradigms," Psychophysics Seminar, M.I.T. Department of Electrical Engineering and Computer Science, Cambridge, Massachusetts (October 1985).

M.C. Teich, "Sub-Poisson Franck-Hertz Light," Invited Lecture, International Workshop on Squeezed States of Light, M.I.T. Department of Electrical Engineering and Computer Science, Dedham, Massachusetts (October 1985).

M.C. Teich, "Advances in Vision Research," Invited Lecture, Industrial Affiliates Program on New Developments in Medical Engineering, Columbia University School of Engineering and Applied Science (March 1986).

M.C. Teich, "Quiet Light Generation and Detection for Fiber-Optic Communications," Seminar, Georgia Institute of Technology Department of Electrical Engineering, Atlanta, Georgia (April 1986).

M.C. Teich, "Theory of Light Detection in the Presence of Feedback," XIVth International Quantum Electronics Conference, San Francisco,

California (June 1986), with J. H. Shapiro, P. Kumar, and G. Saplakoglu, Department of Electrical Engineering and Computer Science, Massachusetts Institute of Technology, Cambridge, Massachusetts; and B. E. A. Saleh, Department of Electrical and Computer Engineering, University of Wisconsin, Madison.

M.C. Teich, "Models of Neuronal and Human Behavior -- Shame," Invited Seminar, Rado Advanced Psychoanalytic Study Group -- Theory of Affects, Columbia University Psychoanalytic Institute (September 1986).

M.C. Teich, "Societal Benefits of Research Supported by the Department of Defense," Invited Address, Columbia University Graduate School of Journalism (September 1986).

E.S. Yang and J.S. Song, "Photovoltaic Effect in a Semiconductor Grain Boundary," MRS Meeting, Thin Film-Interfaces and Phenomena, Boston, Massachusetts, December 2-7, 1985.

E.S. Yang, P.S. Ho, M. Liehr, F.K. LeGoues, P.E. Schmid, and H.L. Evans, "Schottky barrier and Electronic States at Silide-Silicon Interfaces," MRS Meeting, Layered Structures and Epitaxy, Boston, Massachusetts, December 2-7, 1985.

E.S. Yang, H.L. Evans, X. Wu, A. Cool, and P.S. Ho, "Measurement of Interface State in pd_2S:Schottky Barriers," Semiconductor Interface Specialist Conference, Ft. Lauderdale, Florida, December 6-8, 1985.

E.S. Yang, "Interface State and Schottky Barrier Formation," EE Dept., Univ. California - Santa Barbara, California, January 17, 1986.

E.S. Yang, "Physics of Schottky Barriers," Hughes Aircraft Microwave Division, Torrance, California, January 21, 1986.

E.S. Yang, "Interface States and Schottky Barrier Formation in Silicide-Silicon Contacts," EE Dept., California Institute of Technology, Pasadena, California, January 29, 1986.

E.S. Yang, "Interface States and Schottky Barrier Formation," Hughes Research Lab., Malibu, California, February 4, 1986.

E.S. Yang, "Silicide-Silicon Interface States," Xerox Research Center, Palo Alto, California, February 7, 1986.

E.S. Yang, "Schottky Barrier Device Physics," Monolithic Memory Inc., Santa Clara, California, February 6, 1986.

E.S. Yang, "Metal-Semiconductor Interface States," IBM Europe Institute, Oberlach, Austria, August 1, 1986.

Resonance Seminars

Meetings are held periodically at Columbia University, New York, New York during the academic year and are open to all members of the New York scientific community. Guest speakers are invited to discuss work in the general area of the research in the Columbia Radiation Laboratory.

A. Flusberg, Avco Research Lab, "Stimulated Raman Scattering: Can the Stokes be Brighter than the Pump " February 7, 1986.

J. Eberly, University of Rochester, "QED in the 80's: Single Atoms in Cavities and Traps," February 21, 1986.

W. Brown, AT T Bell Labs, "Electronically Stimulated Sputtering of Condensed Gas Solids by Fast Ion Bombardment," March 4, 1986.

J. Hegarty, AT T Bell Labs, "Exciton Dynamics in 2-dimensional GaAs Quantum Wells," March 7, 1986.

G. Celler, AT T Bell Labs, "Formation of Crystalline Si Films on Insulating Substrates," March 18, 1986.

M. Feld, MIT, "Laser Treatment of Atherosclerosis: A Study in Physics, Spectroscopy and Medicine," March 28, 1986.

D. Steel, University of Michigan, "Super Position State Spectroscopy by Frequency Domain Four Wave Mixing," April 1, 1986.

A. Flusberg, Avco Research Lab, "Stimulated Raman Scattering: Can the Stokes be Brighter than the Pump " April 11, 1986.

D. Wineland, National Bureau of Standards, "Laser Cooled Trapped Ions," April 18, 1986.

B. Greene, AT T Bell Labs, "Femtosecond Molecular Spectroscopy," April 29, 1986.

P. Bernath, University of Arizona, "Laser and Fourier Transform Spectroscopy of Transient Species: Atomics to Organometallics," October 3, 1986.

M. Fayer, Stanford University, "Dynamics of Solutes in Organic Glasses at Low Temperatures: Photon Echo and Hole Burning Experiments," November 12, 1986.

I. QUANTUM GENERATION AND DETECTION OF RADIATION

A. NOISE IN THE GENERATION, PARTITION, AND DETECTION OF LIGHT

(M.C. Teich, B. Saleh, K. Matsuo)
(JSEP work unit 1, 1985 - 1988)
(Principal Investigator: M.C. Teich (212) 280-3117)

1. Conversion of Poisson Photons into Sub-Poisson Photons by the Action of Electron Feedback -- Our interest continues in generating amplitude-squeezed (sub-Poisson) light. This is light whose photon-number fluctuations are lower than those of lasers. Such quiet light, it appears, may be useful. It may have application in increasing the distance between repeaters in lightwave communication systems. In the previous period we reported the successful generation of cw amplitude-squeezed light using a Franck-Hertz apparatus excited by a space-charge-limited electron beam.[1,2] In this period we have investigated the possibilities of using external feedback from detector-to-source, instead of space charge, to create quiet electron excitations.[3]

The use of an external-feedback system for generating such light was first suggested by experiments in which feedback was used to produce sub-Poisson electrons.[4] Both the experiment of Walker and Jakeman[5] and the experiment of Machida and Yamamoto[6] involved laser (Poisson) photons illuminating a photodetector and an electronic negative feedback path from the detector to the source. In the former experiment the feedback directly controlled the photons at the output of the laser whereas in the latter experiment the feedback controlled the current at the input to the laser. Nevertheless, the principle involved in the two experiments is the same.[4] Unfortunately, these simple configurations could not generate usable sub-Poisson photons since the feedback current is generated from the annihilation of the in-loop photons. However, under special circumstances an external-feedback system can be used to produce sub-Poisson photons, such as when correlated photon pairs are available[7] or a quantum nondemolition measurement may be made.[8] The resultant light may only be weakly sub-Poisson in such cases because these multiphoton processes involve a series of detections and/or a weak

nonlinear effect.

We have developed a new approach for converting Poisson photons into sub-Poisson photons via single-photon transitions.[3] There does not appear to be any fundamental limit that would impede the technique from being used to produce an arbitrarily intense cw light source that is also arbitrarily sub-Poisson. It makes use of the action of an electron current configured in the feedback loop. Consider, for example, an optical system in which a photon emitter illuminates a detector/source combination, in the closed-loop circuit. Two alternative configurations are shown in Fig. 1. The character of the photon emitter is immaterial; we have chosen it to be a light-emitting diode (LED) for simplicity but it could be a laser. In Fig. 1(a) the photocurrent derived from the detection of light from the LED photon emitter is negatively fedback to the LED input. It has been established both theoretically[4] and experimentally[6] that, in the absence of the block labeled "source," sub-Poisson electrons will flow in a circuit such as this. This conclusion will sometimes be valid in the presence of this block, which acts as an added impedance to the electron flow. Incorporating this element into the system critically alters its character, however, since it permits the sub-Poisson electrons flowing in the circuit to be converted into amplitude-squeezed photons by means of electron transitions. The key to achieving this effect is the replacement of the detector used in other feedback configurations with a structure that acts simultaneously as a detector and a source. The electrons simply emit sub-Poisson photons and continue on their way. In the absence of the feedback path, of course, the electrons would simply emit Poisson photons. The configuration in Fig. 1(b) is similar except that the (negative) feedback current modulates (gates) the light intensity at the output of the LED rather than the current at its input.

In Fig. 2 we illustrate two possible solid-state detector/source configurations. The basic structure consists of a reverse-biased p^+in^+ diode where the p^+ and n^+ heavily-doped regions have a wider bandgap than the high-field, light-absorbing/emitting i region. Two light-generation schemes are explicitly considered here: single-photon dipole electronic transitions between the energy levels of the quantum wells [Fig. 2(a)] and impact excitation of electroluminescent centers in

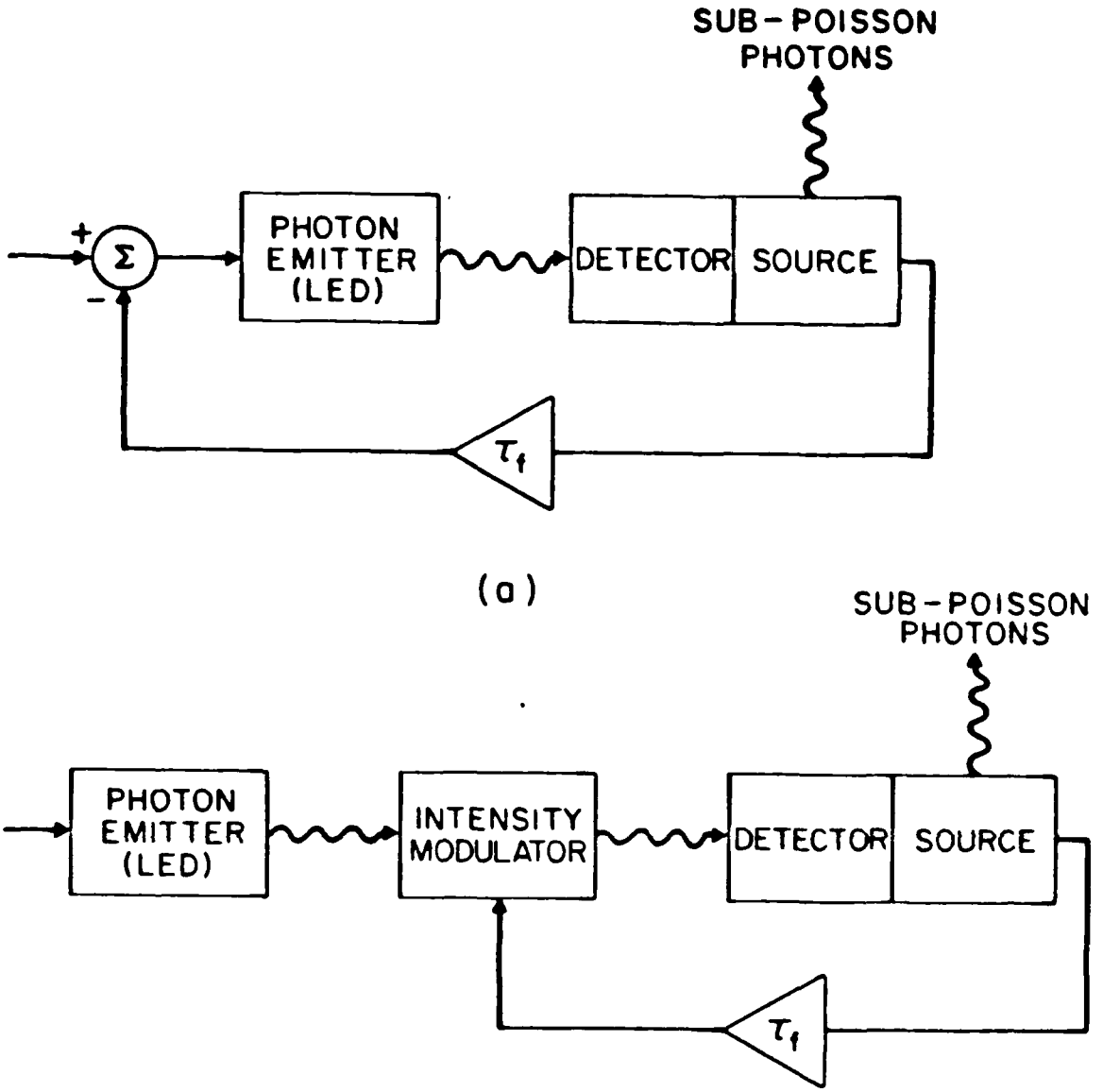

Figure 1: Generation of sub-Poisson photons by means of negative feedback. The feedback produces sub-Poisson electrons in the detector/source which, in turn, generate sub-Poisson photons. (a) Negative feedback modulating the photon-emitter input current. (b) Negative feedback modulating the photon-emitter output light. Wavy lines represent photons; solid lines represent electron current. τ_f signifies the feedback time constant.

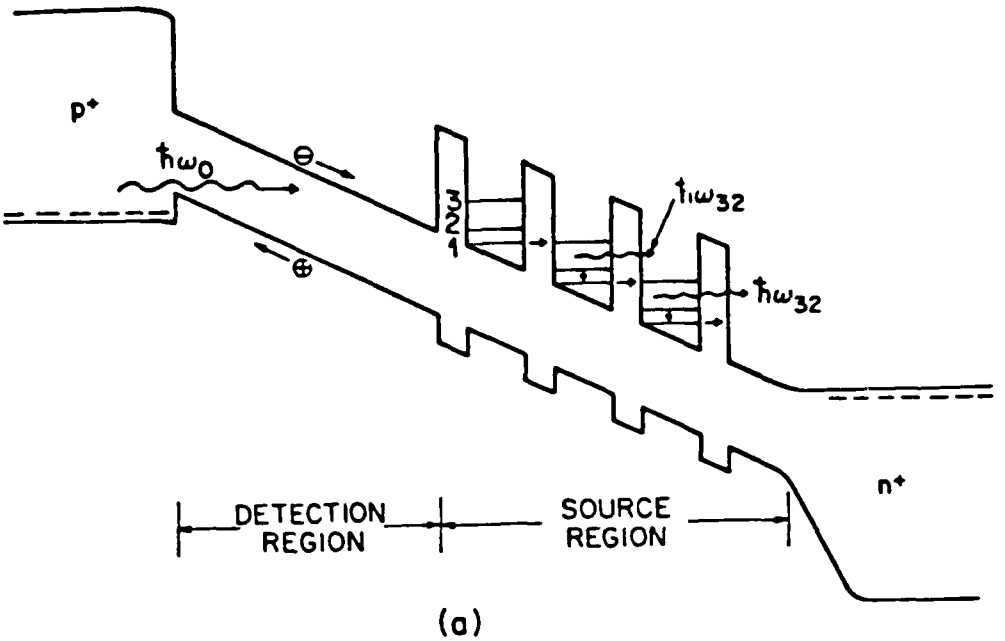

(a)

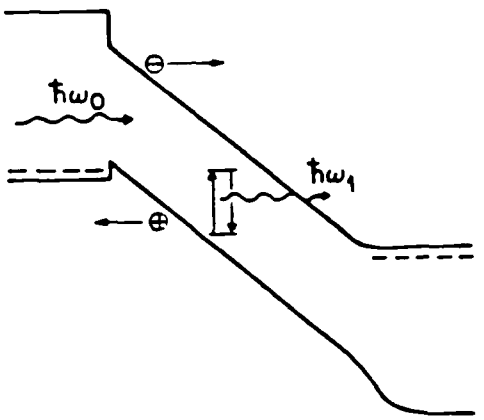

(b)

Figure 2: (a) Band diagram of the quantum-well detector/source. The energy of the incident photon emitted by the LED is denoted $\hbar\omega_o$. The absorbing region (detection region) is of $Ga_{0.47}In_{0.53}As$ or GaAs, typically 1 μm thick. In the source region, the wells are $Ga_{0.47}In_{0.53}As$ or GaAs in the thickness range 150-300 Å. The barrier layers are of $Al_{0.48}In_{0.52}As$ (in the case of $Ga_{0.47}In_{0.53}As$ wells) or AlAs (in the case of GaAs wells) and should be in the thickness range 20-50 Å to achieve tunneling times < 1 psec. Photons of energy $\hbar\omega_{32}$ are emitted via transitions from level 3 to 2. The p^+ and n^+ widegap regions are of $Al_{0.48}In_{0.52}As$ (or AlAs). The interface between the i and n^+ regions is compositionally graded. (b) Energy-band diagram of a detector/source with electroluminescent centers that are impact-excited by energetic photoelectrons, emitting photons with energy $\hbar\omega_1$.

the i region by drifting electrons [Fig. 2(b)].

The ability of configurations such as these to generate sub-Poisson light requires a number of interrelations among various characteristic times associated with the system.[3] The degree to which a light source is sub-Poisson (Fano factor) has been estimated to be $F_n \simeq 0.968$ for both the quantum-well device and the electroluminescent structure.[3] These estimates provide a significant potential improvement over the value observed in the space-charge-limited Franck-Hertz experiment.[2] Lower values of the Fano factor can be achieved in structures that exhibit higher radiative efficiency. As indicated earlier, there is no fundamental limit that impedes this scheme from being used to produce an arbitrarily sub-Poisson cw light source of arbitrarily high intensity.

2. Semiclassical Theory of Light Detection in the Presence of Feedback -- The usual formulations of the quantum[9] and semiclassical[10] theories of photodetection presume open-loop configurations, i.e., that there are no feedback paths leading from the output of the photodetector to the light beam impinging on that detector. In such configurations, the qualitative and quantitative distinctions between the quantum and semiclassical theories are well understood. In the quantum theory, photocurrent and photocount randomness arise from the quantum noise in the illumination beam whereas in the semiclassical theory the fundamental source of randomness is associated with the excitations of the atoms forming the detector. Nevertheless, the quantum theory subsumes the semiclassical theory in a natural way.[11]

The clarity of understanding associated with open-loop photodetection configurations has been extended to closed-loop systems in which there is a feedback path leading from the output of the detector back to the light beam at the detector input.[4] We have shown that the unmistakable signatures of nonclassical light associated with open-loop detection do not carry over to closed-loop systems. Nevertheless, open-loop nonclassical light can be generated with closed-loop photodetection if photon pairs are available or, alternatively, if the in-loop photons are not destroyed.[7]

3. Excess Noise Factor and Gain Distributions for Superlattice

Avalanche Photodiodes -- We have elucidated the noise properties[12-14] and time response[12] of superlattice avalanche photodiodes (SAPD's) and compared their properties with those of the conventional avalanche photodiode.[15] SAPD's promise a reduction in the feedback noise associated with conventional two-carrier avalanche devices. The expression for the excess noise factor F_e of the two carrier SAPD in the presence of residual hole ionization has been obtained.[13] F_e depends on the average overall gain of the device $\langle M \rangle$, the electron impact-ionization probability per stage P, and the ratio $k_s = Q/P$ where Q is the hole-ionization probability per stage. It turns out that even a small amount of residual hole ionization can lead to a large excess noise factor, thereby limiting the usefulness of the device.

Theoretical results have been obtained for the gain distribution and electron-counting distribution of the single carrier SAPD (in the absence of residual hole ionization).[14] The gain distribution assumes single-electron injection whereas the electron counting distribution assumes Poisson electron injection and is therefore used for calculating the bit error rate (BER) of an optical communication system. The single-carrier SAPD receiver has been found to always perform better than the single-carrier conventional avalanche photodiode receiver, for all values of the gain. It has been demonstrated that the BER advantage can attain several orders of magnitude, even though the excess noise factors for the two devices lie within a factor of two.

The (single-photon) impulse response function for the SAPD was derived in the absence of residual hole ionization, when the effects of random transit time are incorporated into the carrier multiplication process.[12] For a five-stage quaternary device, the gain-bandwidth product is calculated to be in the vicinity of 600 GHz which is quite large. These results were extended to the CAPD, which turns out to be a special case of the SAPD (in the limit of an infinite number of stages with infinitessimal gain per stage).

This research was also supported by the National Science Foundation under Grants NSF-ECE 82-19636 and NSF-CDR 84-21402.

(1) M.C. Teich, CRL Prog. Rept. No. 35, 1-6, December 31, 1985.

(2) M.C. Teich and B. Saleh, J. Opt. Soc. AM. B 2, 275 (1985).

(3) F. Capasso and M.C. Teich, Phys. Rev. Lett. 57, 1417 (1986).

(4) J.H. Shapiro, M.C. Teich, B.E.A. Saleh, P. Kumar, and G. Saplakoglu, Phys. Rev. Lett. 56, 1136 (1986).

(5) J.G. Walker and E. Jakeman, Proc. Soc. Photo-Opt. Instrum. Eng. 492, 274 (1985).

(6) S. Machida and Y. Yamamoto, Opt. Commun. 57, 290 (1986).

(7) B.E.A. Saleh and M.C. Teich, Opt. Commun. 52, 429 (1985).

(8) Y. Yamamoto, N. Imoto, and S. Machida, Phys. Rev. A 33, 3243 (1986).

(9) P.L. Kelley and W.H. Kleiner, Phys. Rev. 136, A316 (1964).

(10) Mandel, Proc. Phys. Soc. London 74, 233 (1959).

(11) H. Shapiro, IEEE J. Quant. Electron. 21, 237 (1985).

(12) K. Matsuo, M.C. Teich, and B.E.A. Saleh, IEEE Trans. Elect. Dev. ED-32, 2615 (1985); IEEE J. Light. Tech. LT-3, 1223 (1985).

(13) M.C. Teich, K. Matsuo, and B.E.A. Saleh, IEEE J. Quant. Elect. QE-22, 1184 (1986).

(14) M.C. Teich, K. Matsuo, and B.E.A. Saleh, IEEE Trans. Elect. Dev. ED-33, 1475 (1986).

(15) M.C. Teich, K. Matsuo, and B.E.A. Saleh, IEEE Trans. Elect. Dev. ED-33, 1511 (1986).

B. HOLLOW CIRCULAR MODULATOR USING LASER-ASSISTED ETCHING FOR DIRECT FIBER-OPTIC INTERCONNECT IN VLSI LOCAL AREA NETWORK

(P.R. Prucnal, H. Cho)
(JSEP work unit 1, 1985 - 1988)
(Principal Investigator: P.R. Prucnal (212) 280-3119)

1. Background -- Optical fibers as a transmission channel in telecommunications networks offer advantages such as small size, immunity to EMI/EMP, freedom from capacitive loading, and significantly increased bandwidth. However, the potential bandwidth of fiber optics has not yet been realized due to the speed limitations in the electrooptic transmitters and receivers, and electronic signal processing elements. To fully realize the channel capacity of optical fibers, it is necessary that transmission, detection and signal processing be performed using optically-based signal processing architectures.

The foundation of any all-optical network, regardless of media access protocol, is the generation of optical data and its subsequent optical processing prior to opto-electronic conversion.

The optical generation of data can be efficiently performed by using a mode locked laser to create high speed optical pulses and an electrooptic modulator driven by electronic data, which acts as a gate for the optical pulses. This technique alleviates the necessity of electronically pulsing the optical source at high speeds, and enables data to be encoded into bits less than 100 ps in duration.[1,2]

The first steps have been taken toward implementation of an all-optical network using VLSI technology. The packing density and speed of devices on VLSI chips has experienced an exponential growth in recent years, which will soon be limited by the use of electrical interconnections. Fiber optic interconnections, as a replacement for electrical pinouts, will remove this bottleneck and may re-stimulate growth in device density and speed.

Employing the available bandwidth of optical interconnects, many signals can be multiplexed onto a single optical fiber. By configuring the interconnects in a flexible topology, i.e., by using an architecture consistent with all-optical networks, the system is no longer a group of

VLSI chips communicating via point to point links, but a VLSI local area network (VLSI LAN). A VLSI LAN offers numerous advantages over current VLSI systems; most significantly the ability to be reconfigured with no physical modification, to operate in a parallel processing mode, and to incorporate soft-failure security.

For the fiber optic VLSI LAN to be viable, the devices for the opto-electronic and electrooptic conversion must be compatible with microelectronic technology. The VLSI LAN requires an optical modulator and receiver integrated onto the chip, and a technique for efficiently connectng the fibers to the chip.

A novel coupling technique consisting of the insertion of a fiber core (the fiber is chemically etched down to the core) into a high aspect ratio hole (created via a 'cold laser'-assisted etching process) on the chip's surface has been demonstrated.[3] The doping of the hole with a p-type material to create a p-n junction optical receiver has been successfully constructed and tested[4] (see Fig. 1). [This work is carried out through close collaboration with R.M. Osgood and E.R. Fossum in the Microelectronic Sciences Laboratory at Columbia University.]

A modulator employing the same coupling technique is proposed (see Fig. 2). Here the etched hole penetrates the substrate from both sides, leaving a narrow bridge. The light is intensity modulated by the electro-absorption effect, in response to an applied electric field. A good choice for the modulator design is a multiple quantum well structure because of its exceedingly high modulation depth, low power consumption, and fast response time.

Research is being conducted in the design of superlattice modulator devices, specifically GaAs/AlGaAs superlattice structures. The first step in this research was to create an analytic tool which could be used to accurately design and predict GaAs/AlGaAs superlattice behavior.

2. New Formalism of the Kronig-Penney Model -- The Kronig-Penney model[5] is an idealized representation of the energy bands in crystalline solids with periodically varying potentials. Conventionally it has been used to study the qualitative nature of band structures in bulk semiconductors,[6,7] but recently it has been used to calculate quantum confined energy subbands of electrons and holes in the smaller energy

SCHEMATIC CROSS-SECTION OF INTEGRATED FIBER-OPTIC RECEIVER

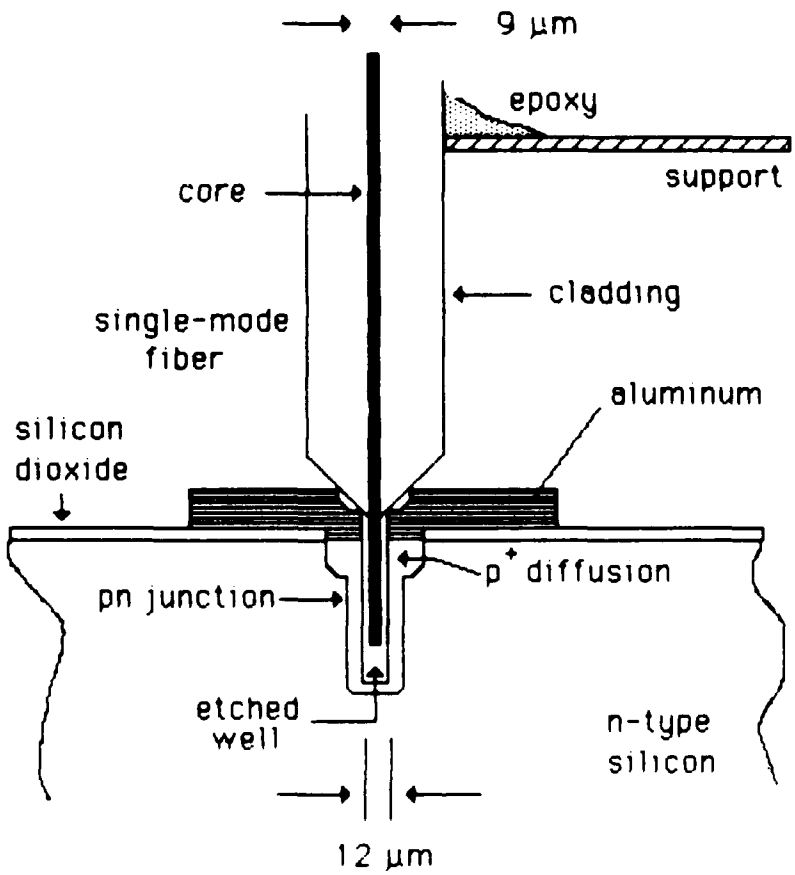

FIGURE 1

INTEGRATED ABSORPTIVE-LOSS MODULATOR

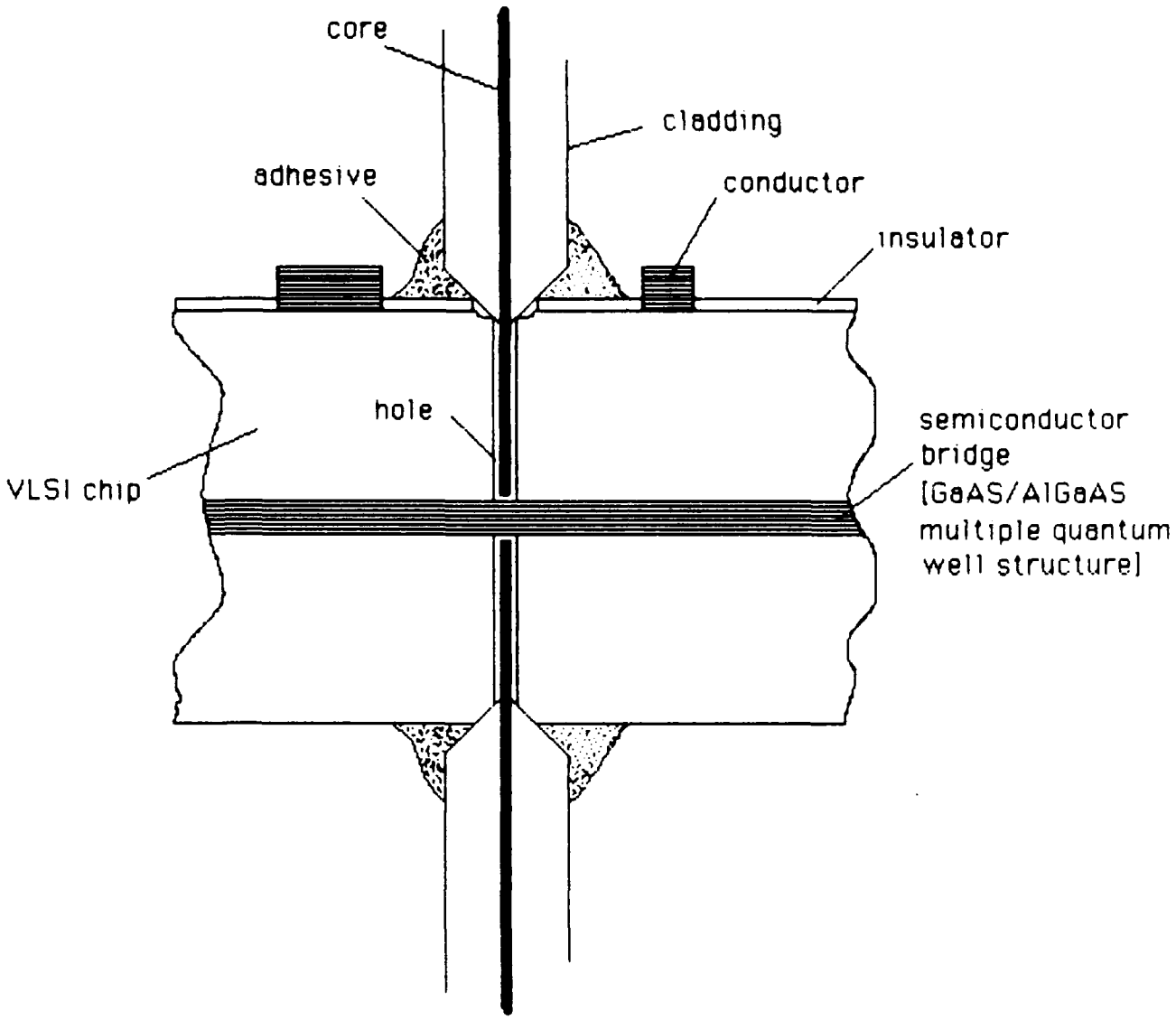

FIGURE 2

gap layers, which act as potential wells between the larger gap layers due to conduction and valence band discontinuities, in semiconductor superlattice structures.[8-11] The main difference between the two applications is that in bulk material the effective mass of an electron or hole is the same everywhere, whereas in superlattice structures the effective mass at well layers is different from that at barrier layers. The effective mass difference at the interface between the well and barrier layer necessitates a new boundary condition not needed when modelling bulk materials.

The effective mass difference has been considered by Bastard[9] in his formulation of the Kronig-Penney model to find the band structure of superlattices. By using the envelope function approximation, he has shown that the first derivative of the wave function divided by effective mass, or the probability current, is continuous at the interface under certain conditions. Although several other boundary conditions have been proposed, the one proposed by Bastard is simpler and intuitively more appealing, and the results of the particle energy calculations based upon Bastard's boundary condition are highly consistent with experimental data.

A new formalism of the Kronig-Penney model employing Bastard's boundary condition has been developed. This formalism is based upon the observation that the wave functions corresponding to the maximum and minimum energy of each band have definite parities, due to the fact that the periodic potential in a superlattice is not a real atomic potential but a result of a periodic repetition of different energy gap layers which have thicknesses typically many times larger than the period of the atomic potential. Hence, the actual wave function of a superlattice is a bulk atomic wave function modulated by the envelope wave function of the superlattice potential, and the energy bands of a superlattice are composed of a discrete series of subbands induced by the superlattice potential inside a bulk band. The new formalism is much easier to manipulate than the conventional one, and can be used to find the electron and hole energy bands and the wave functions in superlattices by simple numerical analyses.

The first five energy subbands of electrons in a GaAs/AlGaAs superlattice with fixed Al mole fractions have been calculated using

both the conventionl formalism and the new formalism, and the equivalence of the two formalisms for the calculation of energy bands, as well as wave functions, has been demonstrated.

3. Application of the New Formalism -- Since the first proposal of superlattices by Esaki and Tsu,[12] remarkable theoretical and experimental work has been performed to yield a better understanding of the electrical and optical properties of superlattices. One important parameter required to optimize modulator design which has not been rigorously discussed before is the critical thickness of barrier layers. This parameter divides superlattice structures into uncoupled quantum well systems and coupled quantum well systems dependent upon Al mole fraction and well thickness. When barrier thickness is sufficiently large, there is no wave function coupling between adjacent wells and thus the superlattice becomes an uncoupled quantum well system. As the barrier thickness decreases to sufficiently small value, interwell coupling increases and thus the superlattice becomes a coupled well system. If the coupling strength is properly described, and the criterium of the critical barrier thickness is reasonably determined, it is possible to find the critical barrier thicknesses for any Al mole fraction and well thickness.

Critical barrier thicknesses for varying superlattice parameters have been calculated employing the new formalism. To find these values it is necessary to know the strength of interwell coupling for varying superlattice parameters. Although the strength of coupling may be described in a variety of ways, we have chosen the relative bandwidth to be $\Delta E/E_\infty$, where $\Delta E = E_{max} - E_{min}$ is the energy bandwidth and E_∞ is the energy at the limit of large barrier thickness (barrier thickness = b).

For any Al mole fraction and well thickness, if b is sufficiently large, the superlattice becomes an uncoupled well system and there is no wave function coupling between adjacent wells. In this case, there is only a discrete series of allowed energy levels with vanishing bandwidth inside the wells rather than energy subbands with finite bandwidth. But as the barrier thickness decreases, energy bandwidth increases and interwell coupling also increases. Hence the coupling strength is an increasing function of bandwidth, and therefore the energy bandwidth or,

more precisely, $\Delta E/E_\infty$ is a good measure of the coupling strength.

According to the above arguments, it might be expected that it is necessary to calculate the bandwidths of all the energy bands of electron and holes (light and heavy) as functions of b, to determine the critical barrier thickness for a given Al mole fraction and well thickness. Fortunately this is not necessary because the bandwidths of holes are smaller than those of electrons for the same superlattice parameters, and only the first one or two bands are important for usual device applications.

Analysis of this case yields a definition of critical barrier thickness, b_c, as the value of b corresponding to $\Delta E/E_\infty = 1\%$ for GaAs/AlGaAs superlattices. This critical barrier thickness can be employed as a figure of merit for device applications or realization of uncoupled quantum wells for experiments of various purposes.

For the design of modulators, the absorption curve should have a large absorption coefficient and small linewidth (see Fig.3). In general, absorption coefficient increases with oscillator strength and oscillator strength decreases with interwell coupling. This means that absorption coefficient increases with b up to b_c but remains constant after b_c. Therefore, the optimum b for a modulator is b_c. This is an especially appealing result because by limiting b to only b_c, the cost of materials and time of device fabrication are also minimized.

4. Summary and Conclusions -- We have developed a new formalism of Kronig-Penney model which yields the minimum and maximum energy of superlattice energy subbands and their envelope wave functions by taking into consideration the effective mass difference between well and barrier layers, and assuming the continuity of wave function and probability current at the interface. This formalism has been compared with the conventional one and has proved to yield equivalent results in a simpler fashion. We have applied this formalism to GaAs/AlGaAs superlattices with varying parameters to calculate electron energy subbands and wave functions, and eventually to find critical barrier thicknesses for a given Al mole fraction and well thickness.

We have also discussed the applicability of the critical barrier thicknesses to modulators. It has been shown that maximum absorption

MODULATOR DESIGN CONSIDERATIONS

ABSORPTION VS FREQUENCY
(with & without an applied field)

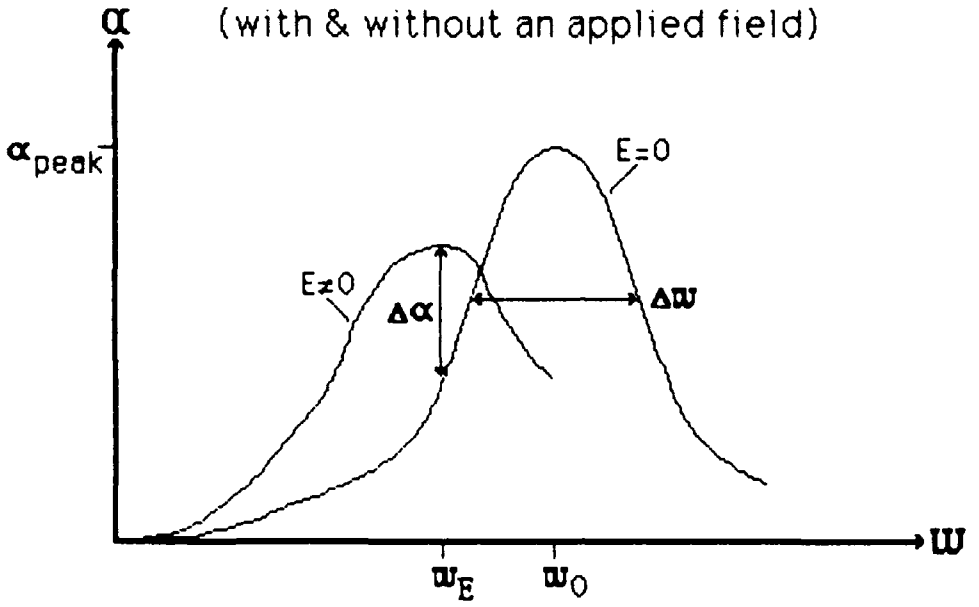

For the optimization of modulator design, the change in absorption must be maximized. This is accomplished be maximizing the peak absorption while minimizing the absorption linewidth for the case of no applied field

PEAK ABSORPTION and LINEWIDTH VS BARRIER THICKNESS
(for a fixed well thickness and Al mole fraction)

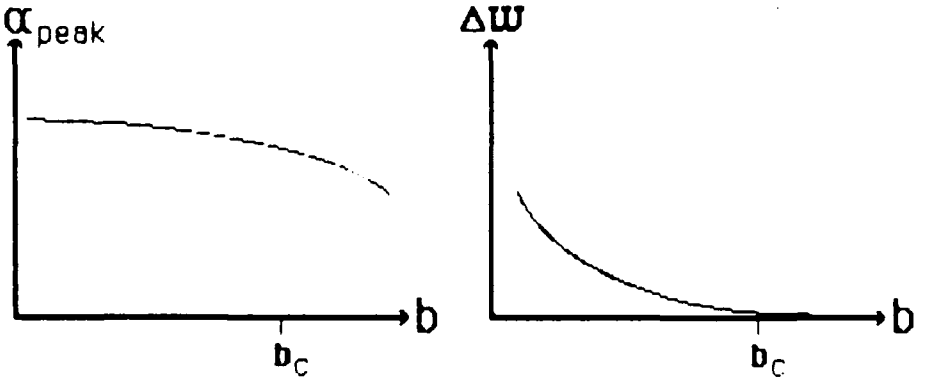

These curves illustrate that the aforementioned optimization criteria can be realized by choosing the barrier thickness to be equal to the critical barrier thickness

FIGURE 3

coefficient and minimum linewidth, which are essential for the design of modulators, can be optimized on the basis of the critical barrier thickness. Moreover, the cost and time needed to fabricate uncoupled well structures can be minimized if the barrier thickness is made the same as the critical barrier thickness.

In conclusion, the new formalism is considerably simpler and thus easier to apply to superlattices than the conventional one, and the critical barrier thicknesses obtained by applying this formalism are very reliable and useful for optimizing modulator design and other uncoupled quantum well structures.

This research was also supported by the National Science Foundation under Grant NSF-CDR 84-21402.

(1) P.R. Prucnal, M.A. Santoro, S.K. Sehgal, "Ultra-fast all-optical synchronous multiple access fiber networks," IEEE J. Select Areas Com., in press.

(2) P.R. Prucnal, D.J. Blementhal, S.K. Sehgal, M.A. Santoro, "A 10 GHz all-optical network using a mode-locked source," in preparation.

(3) P.R. Prucnal, E.R. Fossum, R.M. Osgood, Opt. Letters 11, 109-111 (1986).

(4) R.W. Ade, E.E. Harstead, A.H. Amirfazli, T. Cacouris, E.R. Fossum, P.R. Prucnal, R.M. Osgood, IEEE Trans. Electron Dev. (1986), submitted.

(5) R. de L. Kronig and W.J. Penney, Proc. Roy. Soc. London A 130, 499 (1930).

(6) J.P. McKelvey, in Solid State and Semiconductor Physics (Harper and Row), 1966.

(7) K. Seeger, in Semiconductor Physics, 3rd Ed. (Springer-Verlag), 1985.

(8) D. Mukherji and B.R. Nag, Phys. Rev. B 12, 4338 (1975).

(9) G. Bastard, Phys. Rev. B 24, 5693 (1981).

(10) J.N. Schulman and Y.C. Chang, Phys. Rev. B 24, 4445 (1981).

(11) B.A. Vojak, W.D. Laidig, N. Holonyak, Jr., M.D. Camras, J.J. Coleman, and P.D. Dapkus, J. Appl. Phys. 52, 621 (1981).

(12) L. Esaki and R. Tsu, IBM J. Res. Develop., 61 (1970).

II. PHYSICAL AND PHOTOCHEMICAL PROPERTIES OF ELECTRONIC MATERIALS

A. LASER-ADLAYER DESORPTION

(R.M. Osgood, W. Holber)
(JSEP work unit 4, 1985 - 1988)
(Principal Investigator: R.M. Osgood (212) 280-4462)

1. Introduction -- In previous work, a study was made of the effect of cw laser radiation focused onto the surface of silicon in a plasma reactor. It was found that in a CF_4/O_2 plasma, laser light focused onto the surface of silicon locally enhances the etch rate. At high laser powers, the enhancement is primarily due to thermal effects. At low laser powers, the effect is primarily nonthermal, and is dependent on the doping level of the substrate and the wavelength of the laser light.

In the work to be described in this report, hydrogen is added in varying quantities to CF_4, without O_2 present in the gas. It is found that the role of the hydrogen is to reduce the etch rate of the silicon. Under these conditions, when laser light of appropriate wavelength is incident on the silicon surface during the etching, the etch proceeds more rapidly in the illuminated region, due to the reduction of polymer deposition on the surface.

2. Experimental -- The experimental arrangement is similar to that described in the previous chapter. However, in this work a differentially pumped mass spectrometer with a high-pressure sampling head is attached to the plasma-etcher chamber. With the plasma etcher at a pressure in the 100 mTorr range, the mass spectrometer, pumped by a 50 L/sec turbomolecular pump, has a base pressure of 3×10^{-7} Torr. The plasma etcher was operated with 40 mTorr of CF_4 (flow rate = 37 sccm) and from 0 to 30 mTorr of H_2. The rf power used was 30 Watts - corresponding to an rf power density of 0.05 W/cm^2. The laser source was the krypton-ion laser, line tunable with its output between 350 nm and 800 nm. The majority of the work reported was done with the multiline near-uv output at 350-357 nm.

Typically, an unmasked sample of silicon (n(100), 1 Ω-cm, 1 cm^2 in

size) was clamped to the water-cooled base plate. The clamp also acted as a mask, to allow the etch or deposition depth to be measured with a surface profilometer after the run. For some of the runs, an aluminum masked piece of silicon was used to check the dark etch (or deposition) rate.

3. Results -- Fig. 1 shows the change in dark etch rate of the silicon, as the partial pressure of H_2 added to the 40 mTorr CF_4 was increased from 0 to 30 mTorr (corresponding to 0 to 43% of the total pressure). The dark etch rate dropped an order of magnitude over this range of H_2 concentration. If the H_2 concentration was raised much higher, deposition occurred instead of etching.

The unmasked silicon is illuminated with the 350-nm laser light, patterned and imaged onto the silicon surface. The laser power density was approximately 80 W/cm^2 in the illuminated areas. The results are shown in Fig. 2. Here, the ratio of the laser-enhanced etch rate to the dark etch rate is shown, as a function of H_2 partial pressure. From 0 to 10 mTorr of H_2, the ratio of the etch rates increased slightly. This effect could be due to a slight change in the etch/polymerization balance on the surface. However, at about 15 mTorr- H_2 pressure, there was a large, abrupt rise in the relative light-enhanced etch rate. After this point, the curve again resumed a slight rise with increasing H_2 pressure.

When some of these runs were repeated, using the 647-nm output from the krypton-ion laser, with approximately the same power density, it was found that the slow rise in the ratio of light to dark etch rates occurs again. However, the sharp increase at 15 mTorr partial pressure H_2 was missing. Since both the UV and red light heat the wafer in the same manner, the difference in the behavior with the two colors indicates that the mechanism responsible is not a simple thermal one.

When the unfocused 350-nm laser output was used to illuminate the surface of the unmasked silicon sample, formation of the polymer layer was inhibited where the laser hits. Here, the laser power density is only approximately 5 W/cm^2. Samples coated with a brownish polymer film after processing were examined with x-ray photoelectron spectroscopy (XPS) under ultrahigh vacuum conditions. Fig. 3 shows the XPS spectrum

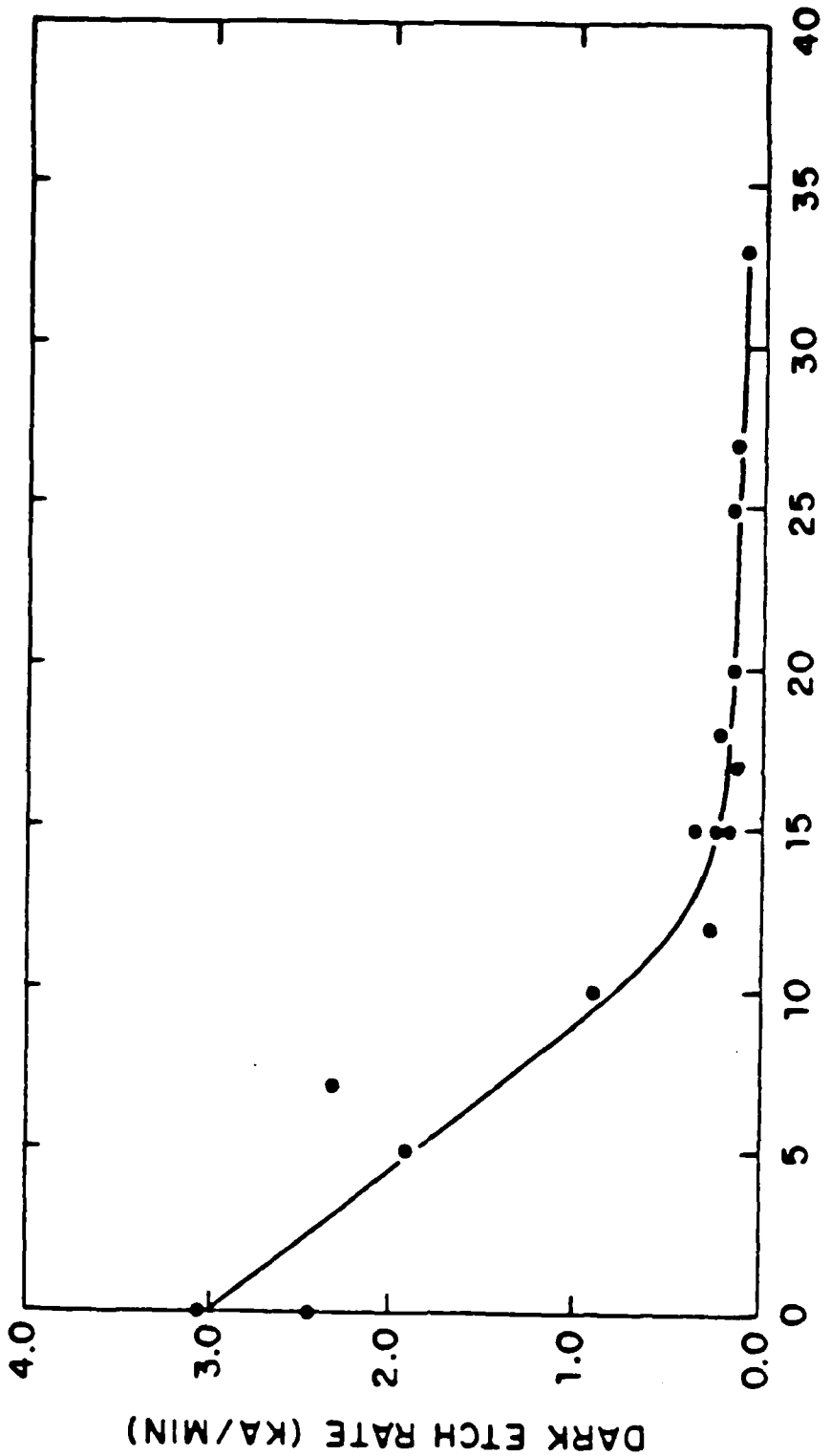

Figure 1: Plasma etch rate of silicon versus partial pressure of H_2 added to 40 mTorr of CF_4.

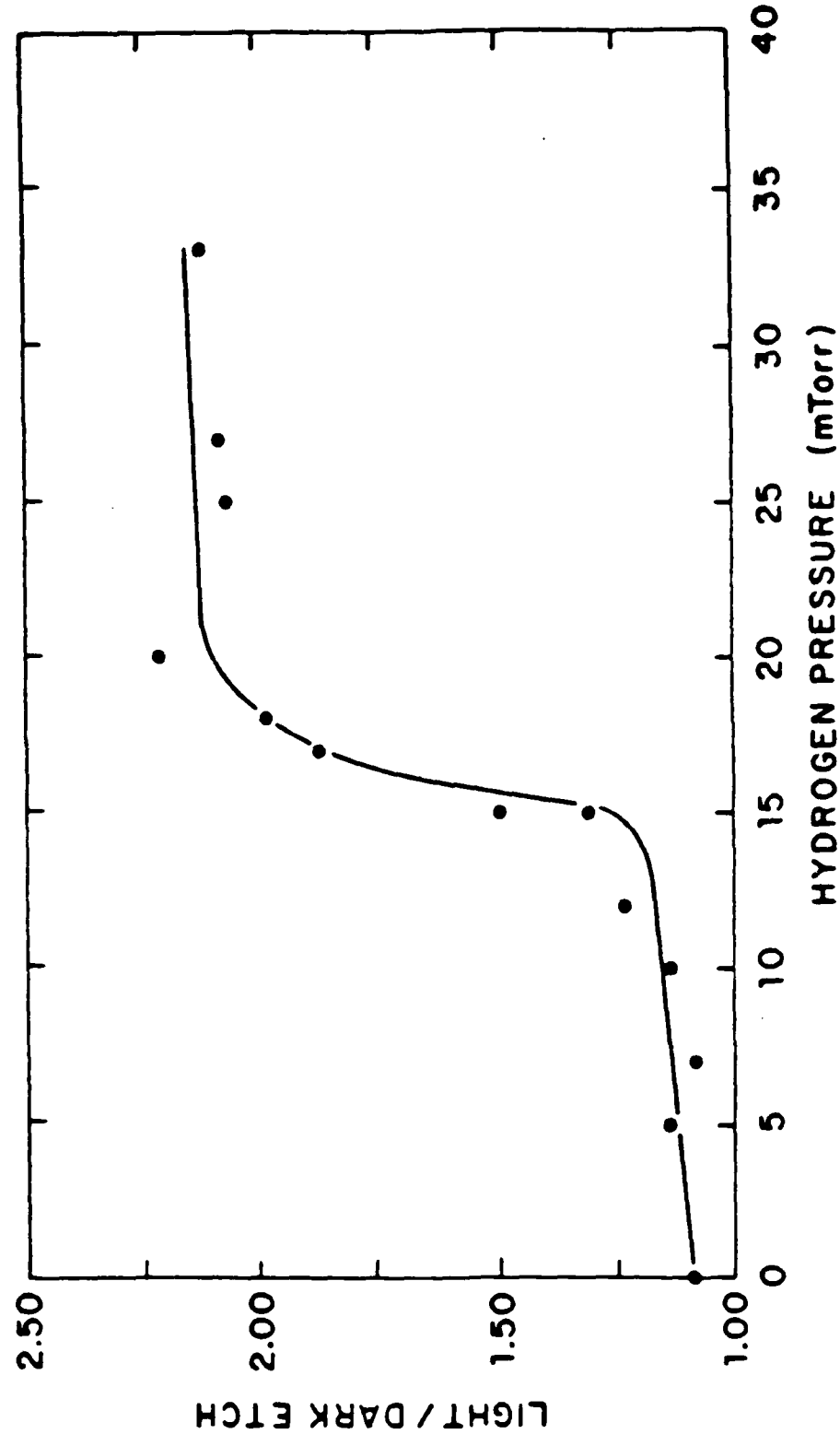

Figure 2: Laser-induced etch enhancement versus partial pressure of H_2 added to 40 mTorr of CF_4.

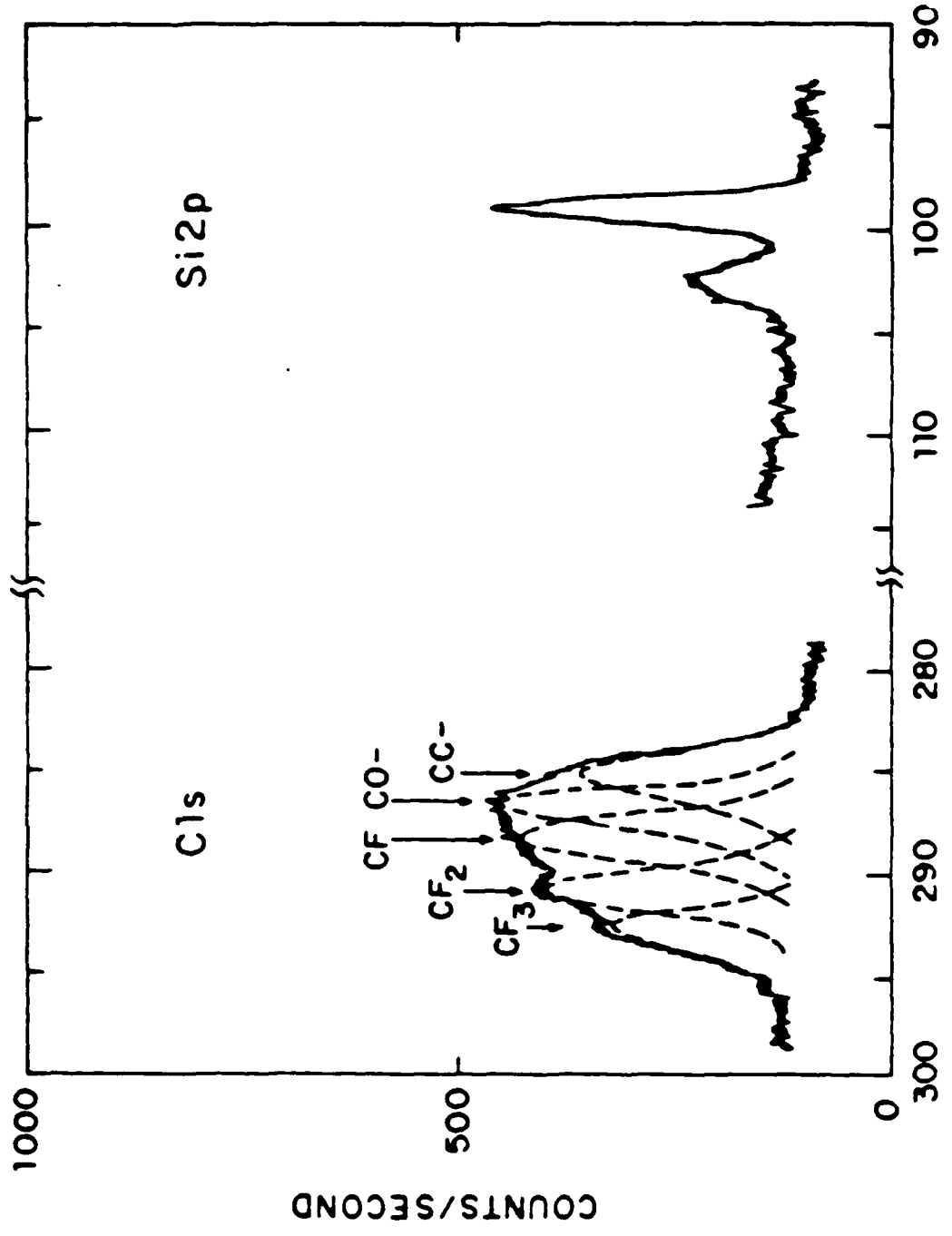

Figure 3: X-ray photoelectron spectroscopy examination of silicon surface coated with polymer.

of the coated surface. The peak corresponding to the C-1s level appears to have a multiplet structure, with five partially resolved components indicated by dashed lines. From the high binding energy side, the components represent, in succession, trifluorocarbon (292.9 ev), difluorocarbon (290.9 ev), monofluorocarbon (287.9 ev), alkyloxyl carbon (286.6 ev), and alkyl/graphitic carbon (284.6 ev).[1] The comparable intensities of all components suggest an extensively fluorinated structure for the polymer film.

In the Si-2p level, the small unresolved broader peak (binding energy at 102-103 ev) corresponds to silicon oxides and possibly some fluorides as well, although polymer deposition was the predominate process for these samples. The oxides were probably formed in air before the samples were placed in the surface analysis vacuum chamber. The larger peak at 99.3 ev corresponds to silicon from the substrate.

When the laser was directed on the sample, an area that appeared visually clear of polymer film formation resulted. Auger electron spectra were taken both inside and outside of the illuminated region. Results show a reduction of at least fifty percent in carbon, oxygen, and fluorine within the illuminated region. This indicates that the laser exposure substantially reduces the amount of polymer formation on the silicon surface; this should allow the etch process to proceed at a more rapid rate.

A differentially pumped, residual-gas analyzer (RGA) was used to look at changes in gas-phase components, as a function of H_2 partial pressure. It was not possible to monitor fluorine concentration directly, since fluorine atoms are very reactive and very few pass through the orifice into the RGA chamber without reacting via wall or gas-phase collisions. However, it was possible to monitor HF concentration. The background HF, formed in the RGA itself from CF_4 and H_2 fragments, is subtracted from the HF signal due to the plasma discharge, by looking at the signal with and without turning on the plasma.

Fig. 4 illustrates the variation in HF signal as a function of H_2 partial pressure. The curve indicates that the production of HF peaks at about 20 mTorr H_2 partial pressure, then declines. Since HF production is an important mechanism for scavenging fluorine from the

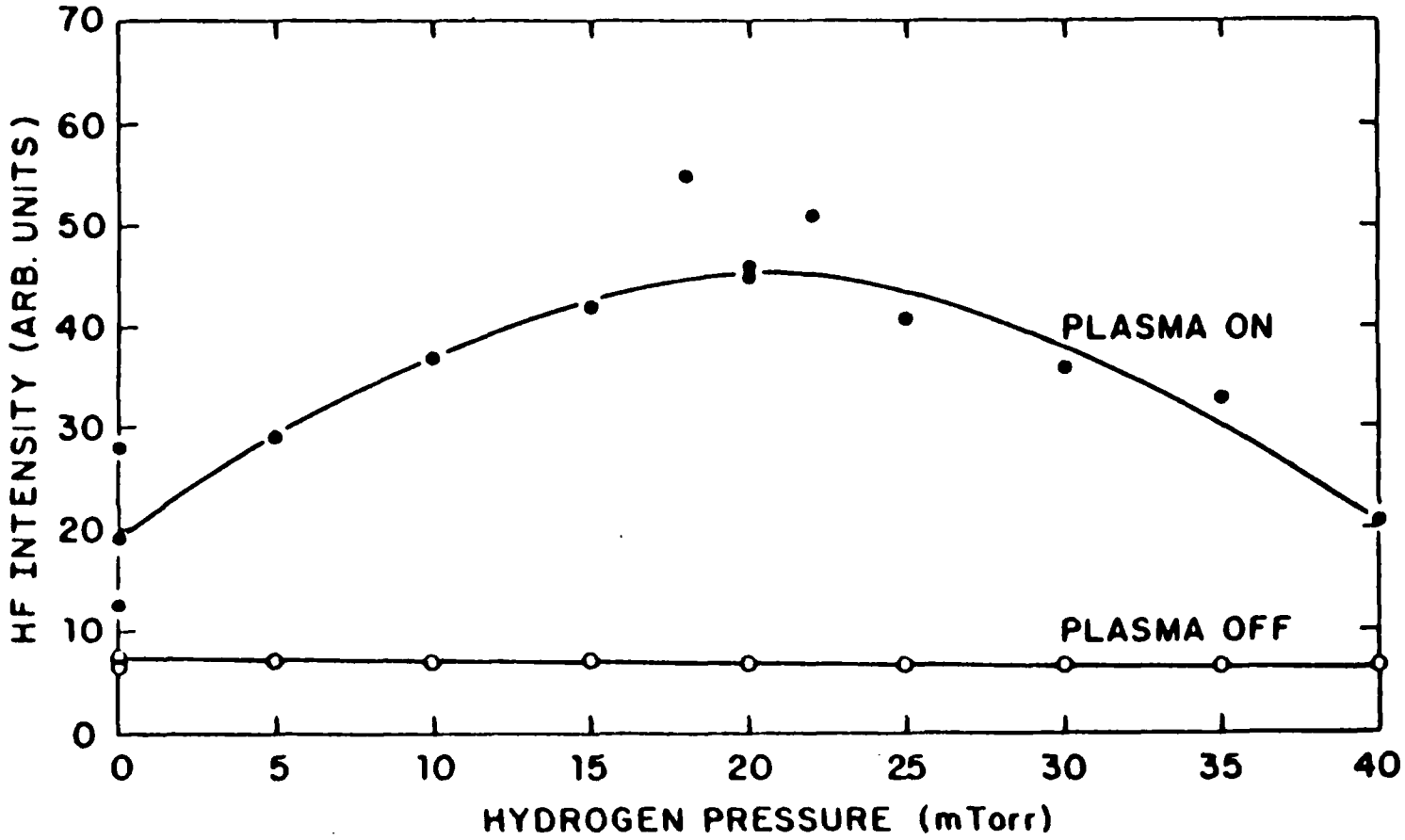

Figure 4: Mass 20 signal from differentially pumped mass spectrometer attached to etching chamber.

gas, this implies that as H_2 partial pressure is increased, the fluorine concentration falls, then rises again.

4. Discussion -- The results obtained in this set of experiments is consistent with the following model. As H_2 partial pressure is increased from 0 to 15 mTorr, the fluorine concentration in the gas drops. This causes a corresponding drop in the dark etch rate, as shown in Fig. 1. Above about 15 mTorr H_2 pressure, the fluorine concentration in the gas begins to rise. However, now polymer formation on the silicon surface prevents the plasma alone from etching at a rapid rate. At this point, the relative amount of laser-assisted etching increases abruptly, because the laser helps prevent formation of the polymer layer, and thus, since there is an adequate supply of fluorine in the gas, the laser causes a sharp increase in the etch rate. Work done by several other researchers on the role of hydrogen in CF_4/H_2 plasmas supports this explanation for the abrupt rise in the laser-enhanced etch rate. Although the role of H_2 in polymerization is very dependent on system parameters such as total pressure, flow rate, electrode spacing, and RF power, general trends observed in other systems are still supportive of this model. Ephraith[2] has found a similar reduction in the dark etch rate in a CF_4/H_2 plasma - with increasing H_2 concentration. Here, the reduction is attributed primarily to polymer formation on the silicon surface.

Using emission spectroscopy, d'Agostino et al.[3] have shown that in their plasma system, when H_2 is added to CF_4, the fluorine concentration drops to a minimum at approximately 10% H_2, and then begins to rise at higher H_2 concentrations. They suggest that the increase in fluorine after the minimum could be due to one of the following reactions:

$$HF + e^- \text{---> } H + F + e^-$$

$$H + HF \text{ ---> } H_2 + F$$

Coburn and Kay[4] have shown that addition of H_2 to a CF_4 discharge both scavenges fluorine by forming HF, and causes polymer formation -- on the silicon surface, but not on the surface of the SiO_2. Comparison in this work and also in Reference 3 of the relative decline of etch rates for SiO_2 and Si with H_2 addition may give a rough idea of the relative roles of polymerization and fluorine reduction in reducing the

etch rate of silicon.

Finally, Pang and Brueck[5] have used laser-induced fluorescence to study the effect of adding H_2 to a CF_4 discharge. They also attribute the decline in silicon etch rate to both scavenging of fluorine and polymer deposition on the silicon surface, which was observed when the H_2 percentage in the gas exceeded 35%.

In conclusion, we have demonstrated that low intensity, cw uv light at 350 nm can be used to inhibit polymer formation in a plasma reactor operated with CF_4 and H_2. The dependence of the laser-enhanced etch rate, as a function of H_2 partial pressure, is due to both variation in gas-phase fluorine concentration and polymer formation on the silicon surface.

There are several possible applications arising out of this work on laser inhibition of polymer formation on silicon. A basic issue in plasma etching is that of obtaining etching which is vertical in its wall profile, without the significant damage often associated with the high ion flux and energy often necessary for this to be accomplished. Because the silicon etch rate is greatly reduced through polymer formation, it seems reasonable that since the laser provides a directed source of photons, laser illumination might increase the anisotropy of the etch. The sidewalls will be passivated by the polymer film, but the etch will still proceed in the vertical direction, due to the action of the photons in inhibiting polymer formation.

This research was also supported by the Air Force Office of Scientific Research/DARPA under Grants F-49620-84-K-0022 and F-49620-85-C-0067, the Army Research Office under Contract DAAG29-85-K-0210, the National Science Foundation under Grants NSF-CDR 84-21402 and NSF-ECS 82-09218, the Office of Naval Research under Contract N00014-78-C-0517, and the Semiconductor Research Corporation under Project SRC-85-02-055.

(1) Lieng-Huang, ed. Characterization of Metal and Polymer Surfaces, Academic Press (1977). Vol. 2, p. 12.

(2) L.M. Ephraith, J. Electrochem. Soc: Solid State Science and Technology 126, (1979).

(3) R. d'Agostino, F. Cramarossa, V. Colaprico, and R. d'Etolle, J. Appl. Phys. 54, 1284-1288 (1983).

(4) J.W. Coburn and Eric Kay, IBM J. Res. Devlop. 23, 33-41 (1979).

(5) S. Pang and S.R. Brueck, Mat. Res. Soc. Symp. Proc. 17, (1983).

B. LASER-ASSISTED ETCHING OF GaAs

(R.M. Osgood, W. Holber, C.F. Yu)
(JSEP work unit 4, 1985 - 1988)
(Principal Investigator: R.M. Osgood (212) 280-4462)

1. Introduction -- In order to gain a better understanding of the nature of photochemically induced bromine etching of GaAs, experiments were carried out with both surface spectroscopic and electrical characterization of GaAs. This work is a continuation of work reported in the previous annual JSEP report.

2. Experimental -- In order to investigate further the nature of the laser-driven etch reaction, a study was made to correlate processing conditions, etch rate, chemical composition of the etched surface, and electrical characteristics of devices built on the etched surface. In all cases, the HBr pressure was maintained at 5 Torr, with a flow rate of 25 sccm. With a reaction cell volume of about one liter, this indicates that the gas in the entire cell is changed about every five seconds. The etch time was always five minutes. The vacuum chamber was pumped to a pressure between 10^{-4} and 10^{-5} Torr before starting the etch run. The temperature of the substrate during the etch run was varied between $40^{\circ}C$ and $90^{\circ}C$. The laser power into the cell was varied between 5 mJ/pulse and 40 mJ/pulse. The laser orientation was varied between direct (incident onto the sample) and indirect. The repetition rate of the laser was 30 Hz in all cases.

The GaAs used was of two types. For the work with etch rates and surface analysis, n-type GaAs, (100) oriented, Si doped to 3×10^{18} cm^{-3} was used. For the electronic measurements it was necessary to use material with lower doping levels, since Schottky barriers could not be readily formed on the more heavily doped material. Here, the doping was 2×10^{17} cm^{-3}.

The GaAs, used to measure etch rates and to study etch profiles, was masked by forming a chrome mask using a standard photolithographic liftoff procedure. The mask consisted of alternating bars of chrome and unmasked areas, each approximately 10 microns in width. The thickness

of the chrome mask was approximately 1800 Å.

The samples, used for the electronic measurements, required more preparation. A wafer of the lower-doped GaAs was mounted in an electron-beam evaporator. A coating of nickel-gold-germanium was applied to the backside of the wafer. After removal from the vacuum system, the wafer was annealed in a rapid thermal annealer by heating to 460°C in the presence of forming gas (N_2 + 5% H_2), for 45 seconds. This process results in a reliable ohmic contact on the back surface of the GaAs. A thin layer of gold was then evaporated onto the backside of the wafer, to ensure the integrity of the contact. The wafer was then etched briefly, to expose a fresh surface of GaAs on the front side of the wafer.

After the run, the samples were removed from the etching chamber. The samples for the electronic measurements were then always rinsed with methanol and blown dry. Some of the other unmasked samples were analyzed in the surface analysis system without having first been rinsed with methanol. Others were rinsed with methanol, then analyzed. Typically, samples remained in air for a period between hours and days, between the eth run and the surface analysis or electronic measurements.

The surface analysis was carried out in an ultrahigh vacuum system. The tools used were either Auger surface spectroscopy or X-ray photoelectron spectroscopy (XPS). For the electronic measurements, the samples to be studied were installed in a vacuum evaporator, and small (approximately 200 micron diameter) circles of gold were evaporated on the front (etched) surface. The Au-GaAs interface forms a Schottky barrier. By carrying out I-V measurements between the front and back contacts, it was possible to measure the quality of the Schottky barrier, which was created on the front surface. This provided insight into the condition of the etched surface, under the different processing conditions.

3. Results -- Fig. 1 shows the XPS results obtained with and without methanol rinsing of etched samples. Here, the substrate temperature is 60°C, and the laser orientation is indirect relative to the sample. Two transition peaks are monitored for arsenic and two for gallium. The 2p peaks are from electrons having a higher binding

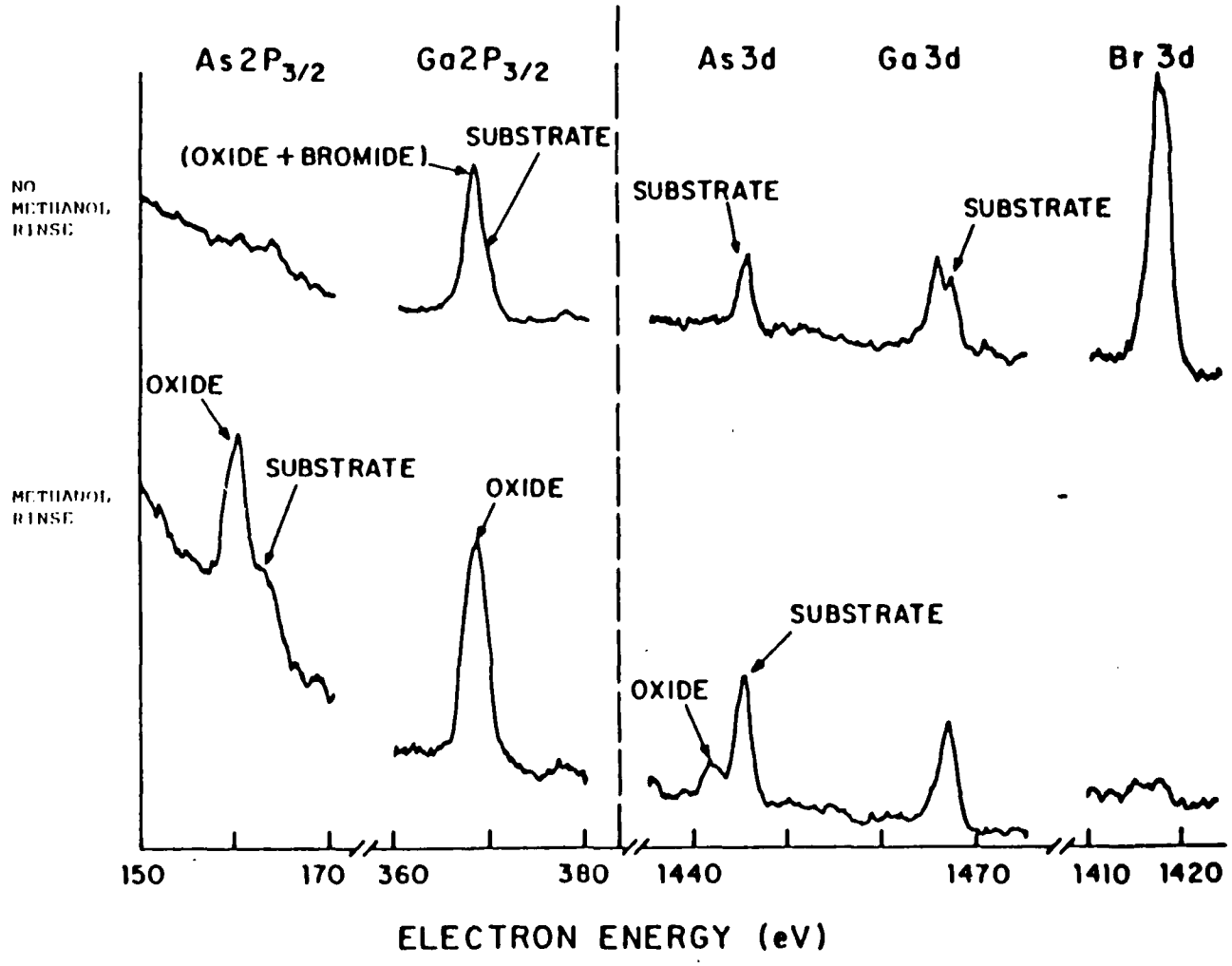

Figure 1: Effect of methanol rinse on etched GaAs surface. Laser is indirect. Substrate temperature is 60°C.

energy; consequently the escape depth of such electrons is quite shallow - approximately 8 Å. The 3d peaks are from electrons having a lower binding energy - this results in an escape depth of approximately 25 Å.

The binding energies for the gallium or arsenic atoms are shifted, according to how the atoms are bound. Thus, a peak from gallium that is from GaAs (the substrate) can be distinguished from a peak due to gallium from Ga_2O_3. The same is true for arsenic. This can be seen in Fig. 1, where the different peaks are marked. Unfortunately, the surface analysis system is unable to distinguish between $GaBr_3$ and Ga_2O_3 or between $AsBr_3$ and As_2O_3, because the binding energies in each of these cases is too close to resolve. Still, by looking at the 3d peak for bromine, an inference can be made as to whether a shifted peak represents an oxide or bromide.

Table 1 gives the binding energies of gallium, arsenic, and bromine, under various bonding conditions. The X-ray source used for this study was the Al Kα line, having an energy of 1486.6 eV.

Fig. 1 reveals several useful pieces of information. First, although the etching was carried out at a temperature high enough to allow rapid etch rates, the surface layer of the sample still displays a bromine peak before being rinsed with methanol. The gallium peaks, both 2p and 3d, display a component shifted by either an oxide or bromide - the bromine peak indicates that at least some of the shifted peak is due to $GaBr_3$. The arsenic does not show a significant oxide or bromide component, which is consistent with the greater volatility of the arsenic etch products.

When the surface is rinsed with methanol before the surface analysis is carried out, the resulting spectrum undergoes several interesting changes. First, the bromine peak disappears completely. However, there are now peaks which are associated with As_2O_3, as well as with Ga_2O_3. It is likely that the oxide peaks are a result of the substantial period of time the etched sample remains in air between etching and surface analysis.

Fig. 2 shows the thickness of this surface layer, as a function of the substrate temperature. The samples in this case were all rinsed with methanol before the surface analysis was carried out. For the

	Ga/GaAs	Ga/Ga_2O_3	$Ga/GaBr_3$	As/GaAs	As/As_2O_3	$Br/GaBr_3$
$2p_{3/2}$	1117.3	1118.4	1118.6	1322.6	1326.3	
3d	18.9	20.7	21.3	40.8	44.6	69.3

Table 1: Binding energies (eV) of species on gallium-arsenide surfaces studied with x-ray photoelectron spectroscopy.

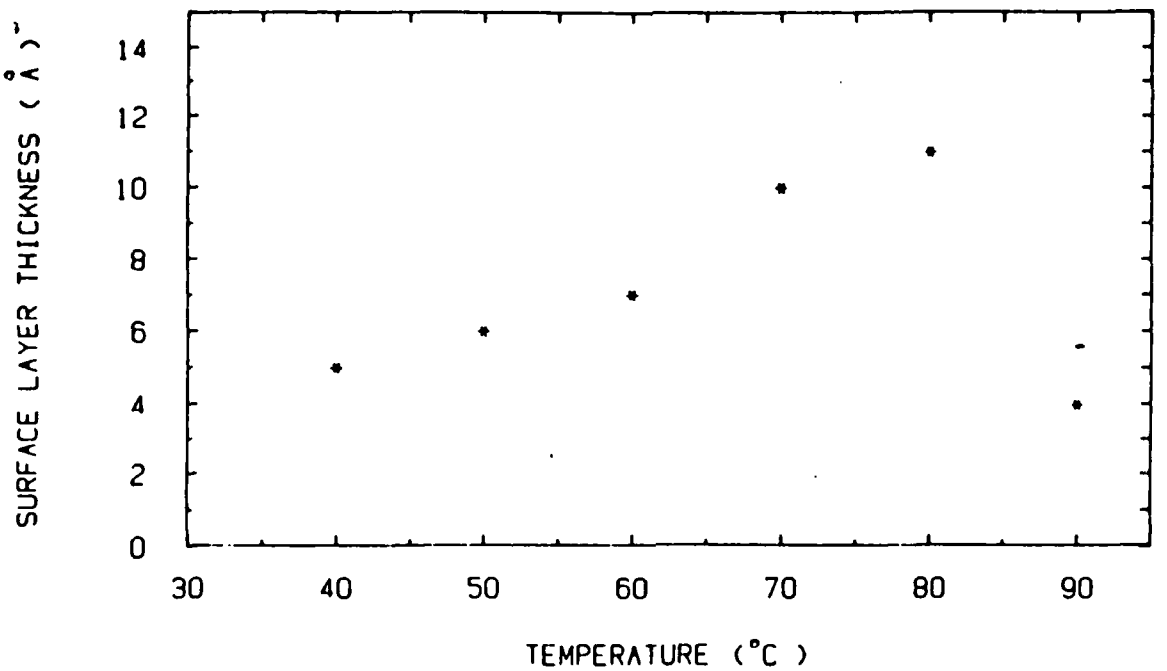

Figure 2: Thickness of surface layer on etched GaAs, as a function of substrate temperature. The laser orientation is indirect and the surface was rinsed with methanol before analysis.

indirect laser orientation, the thickness of this surface layer has a maximum value at about 70°C - 80°C, and falls off rapidly at higher or lower temperatures. For the few data points for high-power direct laser orientation (not shown), the thickness of the surface layer is much less. The peak in surface layer thickness in Fig. 2 corresponds roughly to the peak in etch rate with temperature, observed previously. These results are consistent with an etching mechanism in which, for rapid etching to occur, it is necessary for bromination of several monolayers of GaAs to occur. The temperatures which promote rapid etching also seem to be those which result in the thickest surface layers.

A similar mechanism involving subsurface fluorination of silicon has been observed by McFeeley and coworkers,[1] in their work using synchrotron radiation to probe silicon which has undergone fluorination. They found that SiF_x products could be found quite deep beneath the surface - up to 30 Å deep. They suggest that formation of this product layer is necessary for efficient etching of silicon to occur.

Fig. 3 shows the surface analysis results obtained when the substrate temperature is varied. Here, the surfaces have not been rinsed with methanol, and the laser orientation is indirect. It should be noted that for both Fig. 3 and Fig. 1, comparisons of peak heights cannot be made between samples, since differing sample sizes yield different absolute peak magnitudes. Comparisons can only be made of relative peak heights, for different peaks obtained with a single sample. The results here are consistent with those seen in Fig. 2, for the thickness of the surface layer. Here, it can be seen that the ratio of the $GaBr_3$ (or Ga_2O_3) peak to the gallium peak from the substrate is highest at about 60°C - which is the temperature yielding the fastest etching as well. Formation of the probable As_2O_3 peak at 100°C may indicate that the etch rate at that temperature is being limited by oxide layers formed from contamination in the vacuum system.

Donnelly et al.[2] have observed some similar effects in surface analysis of GaAs and InP etched in a chlorine plasma. They observed gallium-rich GaAs surfaces, with some chlorine coverage as well. For the InP etching, they saw a ~30 Å thick layer of $InCl_3$ after etching, which could be completely removed by rinsing in dionized water. In both cases, despite an attempt to minimize exposure to air by blanketing the

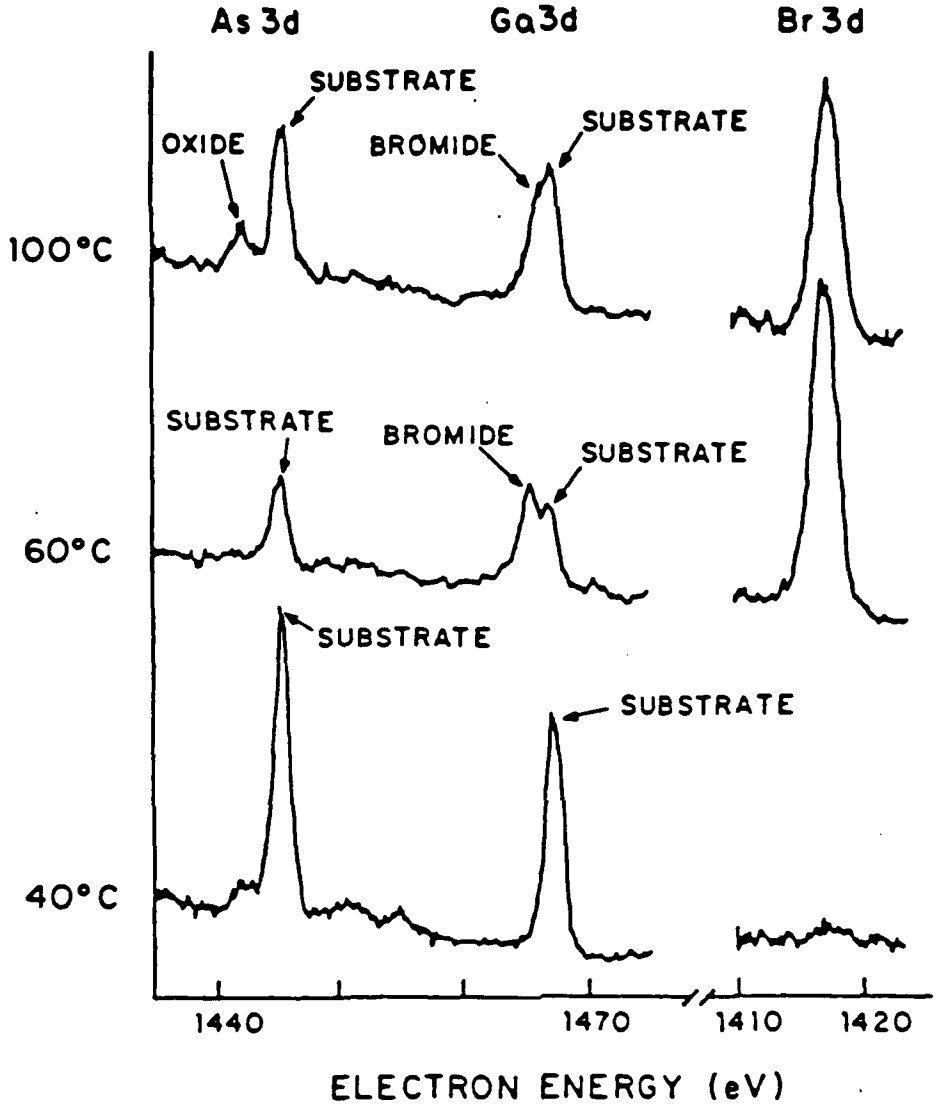

Figure 3: XPS spectra of etched GaAs surface, with varying substrate temperatures during the etch process. The laser orientation is indirect and the surface was rinsed with methanol before analysis.

etched samples in an inert gas during transport to surface analysis, some oxygen was still detected on the etched surface.

The I/V characteristics of a Schottky barrier can be given by the following relationship:

$$I = I_o(e^{V/nV_T} - 1), \text{ where}$$

V = applied forward voltage

I = measured current

$$V_T = \frac{kT}{e}$$

n = ideality factor (1 for ideal case)

I_o = saturation current

These measurements were carried out for samples processed under various conditions, to see the effects of processing on the Schottky diodes constructed on top of the etched surface.

Fig. 4 shows the Schottky barrier height obtained for the Au-on-GaAs contacts. The experimental error here is about $\pm$0.020 volts. Clearly, the barrier height obtained is less for the direct laser orientation than for the indirect. The indirect laser orientation results show a temperature dependence as well - with a peak in barrier height at about 70°C. The accepted value for the barrier height for Au-on GaAs varies somewhat in the literature, but approximately 0.85 volts seems to be typical.[3]

The peak in barrier height in Fig. 4, for the indirect illumination, corresponds well with the peak in oxide coverage shown in Fig. 4. The surface layer is most likely insulating and could be the cause of the increase in measured barrier height. With the direct laser illumination, the surface-layer thickness is much reduced - and the barrier height is nearer to the "ideal" value. This indicates that direct laser illumination can play an important role in product removal in etching of GaAs.

The leakage current and ideality factor were also measured for these diodes. The data for these factors is not as conclusive, since measurement error is greater than for the barrier height. Nevertheless, the general trend for both of these factors show a better Schottky barrier for the direct illumination than for the indirect. For the

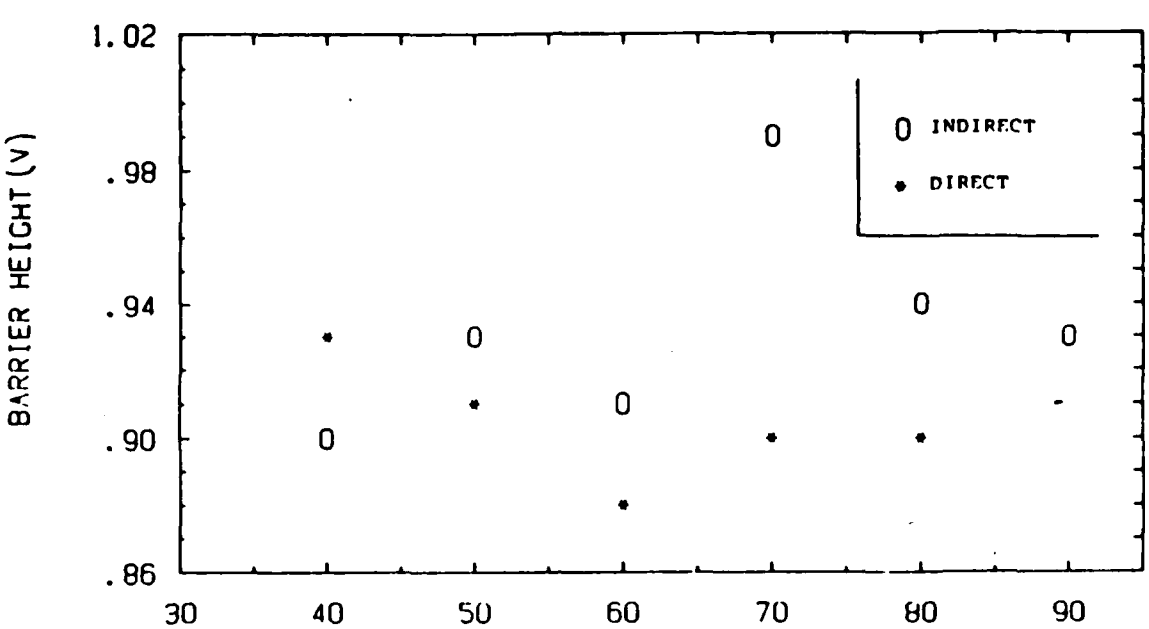

Figure 4: Measured Schottky barrier heights for etched GaAs samples, for various temperatures during etch process. The laser orientation is varied between direct and indirect.

direct laser illumination, the ideality factors measured were typically about 1.10, while the ideality factors for indirect illumination were about 20% or 30% higher.

4. Summary -- Several important new observations have been made of laser assisted etching of GaAs in an HBr ambient. The etch rate displays a temperature dependence, limited at lower temperatures by desorption of the reaction products, and at higher temperatures (possibly) by formation of a contaminant layer on the surface of the GaAs. XPS surface analysis indicates that the etching proceeds through bromination of a number of monolayers of GaAs beneath the surface - rapid etching appears to be correlated with a thicker layer. Both the XPS and the Schottky barrier measurements indicate that when the laser is incident onto the GaAs surface during the etch process, a cleaner surface results, evidenced by a thinner surface layer and Schottky barrier measurements which are closer to ideal.

This research was also supported by the Air Force Office of Scientific Research/DARPA under Grants F-49620-84-K-0022 and F-49620-85-C-0067, the Army Research Office under Contract DAAG29-85-K-0210, the National Science Foundation under Grants NSF-CDR 84-21402 and NSF-ECS 82-09218, the Office of Naval Research under Contract N00014-78-C-0517, and the Semiconductor Research Corporation under Project SRC-85-02-055.

(1) F.R. McFeely, J.F. Morar, and F.J. Himpsel, Surface Science 165, 277-287 (1986).

(2) V.M. Donnelly, D.L. Flamm, C.W. Tu, and D.E. Ibbotson, J. Electrochem. Soc.: Solid State Science and Technology 129, 2533-2537, (1982).

(3) S.M. Sze, Physics of Semiconductor Devices, 2nd edition Wiley, New York), p. 275, (1981).

C. SURFACE SPECTROSCOPIC STUDY OF THE CHEMISTRY ON SEMICONDUCTOR SURFACES

(R.M. Osgood, C.F. Yu, D.V. Podlesnik, M.T. Schmidt)
(JSEP work unit 4, 1985 - 1988)
(Principal Investigator: R.M. Osgood (212) 280-4462)

The study of the oxidation of semiconductor surfaces under photon irradiation has been of special interest because of the importance of its role in the wet-etching processes of semiconductor surfaces. It has also been recognized that the formation of native oxides on gallium arsenide surfaces after chemical etching can be utilized to provide protection and passivation prior to molecular-beam-epitaxy process. We have pursued the study of ultraviolet-light-enhanced oxidation of gallium arsenide surfaces, with a particular emphasis on understanding more about the basic processes on the surface. A newly acquired surface analysis system was used to facilitate this study. The system is equipped with an X-ray source and an electron gun to perform the X-ray photoelectron spectroscopy (XPS) and Auger electron spectroscopy (AES), and an ion gun to sputter the samples as well as to carry out the ion scattering spectroscopy (ISS).

One of the most interesting questions is regarding the composition and thickness of the oxide layer. The determination of the depth profile, that is, the elemental distribution as a function of the depth into the surface, can provide the answer to the above question. By using AES in conjunction with argon-ion sputtering, we were able to extract the depth profiles of the oxide layer on the surface after laser exposure. The various points shown in Fig. 1 are the AES peak-to-peak intensity as a function of sputtering time for two samples irradiated with 514-nm and 257-nm laser light in laboratory atmosphere. In both cases the laser power density was about 250 mW/cm^2 with exposure time of 20 minutes. The oxide layer grown with ultraviolet light is obviously much thicker than that grown using visible light. Similar results of much faster oxide growth rate with ultraviolet light exposure were also obtained for samples treated in pure water. These results clearly show that the enhancement of the oxidation process is much stronger for ultraviolet photoexcitation.

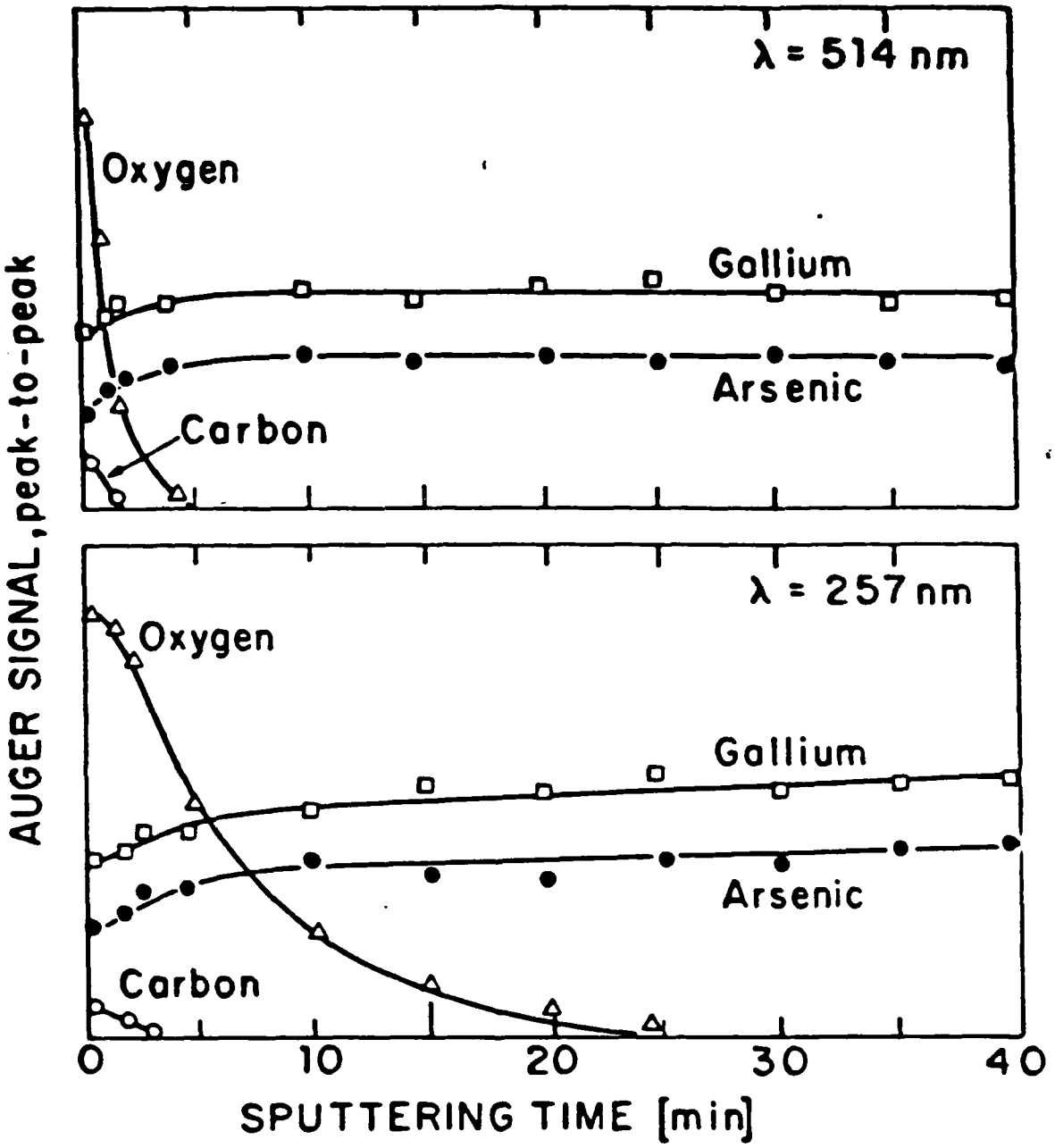

Figure 1: AES depth profiles of the oxide layer on GaAs surface exposed to 514-nm or 257-nm laser light.

XPS is particularly useful to determine the absolute thickness and the chemical composition of the oxide layer. The XPS spectra of a GaAs sample illuminated with 257-nm light, together with a sample exposed in air for 5 hours and a sample sputter-cleaned inside the vacuum chamber, are shown in Fig. 2. For the $As2p_{3/2}$ level, a second peak emerges to the left of the substrate peak in (b) and becomes the dominant peak in (c). This peak exhibits a chemical shift of 3.9 eV, referenced to the substrate peak in the sputter-cleaned surface in (a). A similar shift (3.8 eV), also due to oxide formation, is seen for the As3d peak in (c). The oxide peak is somewhat more intense than the substrate peak, which is not overwhelmed by the former because of the greater escape depth at this higher electron energy. The $Ga2p_{3/2}$ and Ga3d oxide peaks are not resolved from the substrate peaks because of the much smaller chemical shifts in gallium. The ratios of the areas of $As2p_{3/2}$ vs. $Ga2p_{3/2}$ were found to be 1.29 for the oxide peaks in (a) and 1.33 for substrate peaks in (c). This suggests that the stoichiometric relationship of arsenic and gallium is nearly preserved in the oxide layer formed during laser oxidation.

We were able to extract the oxide thickness for samples treated with varying exposure time by using the following equation:

$$d_{ox} = \lambda_{ox} * \sin\theta * \ln\left(\frac{I_{ox}}{I_{sub}} * \frac{D_{sub}}{D_{ox}} * \frac{\lambda_{sub}}{\lambda_{ox}} + 1 \right)$$

where I_{ox} and I_{sub} are the intensities of the emission from the same level, D_{ox} and D_{sub} the densities of the oxide and substrate, λ_{ox} and λ_{sub} the electron mean escape depths of oxide and substrate, d_{ox} the thickness of the oxide layer, and θ the exit angle of the photoelectron relative to the surface. Results of the oxide thickness as a function of light exposure time for two batches of samples irradiated with either 248-nm or with 257-nm photons, show the oxide growth is approximately linear in time with a growth rate of about 0.5 Å/min. This is comparable to the thermal growth rate in dry oxygen atmosphere at about 430°C.

In order to study the mechanism of oxidation on the gallium arsenide surfaces, experiments were also carried out by illuminating the samples with laser light through a quartz window in well controlled

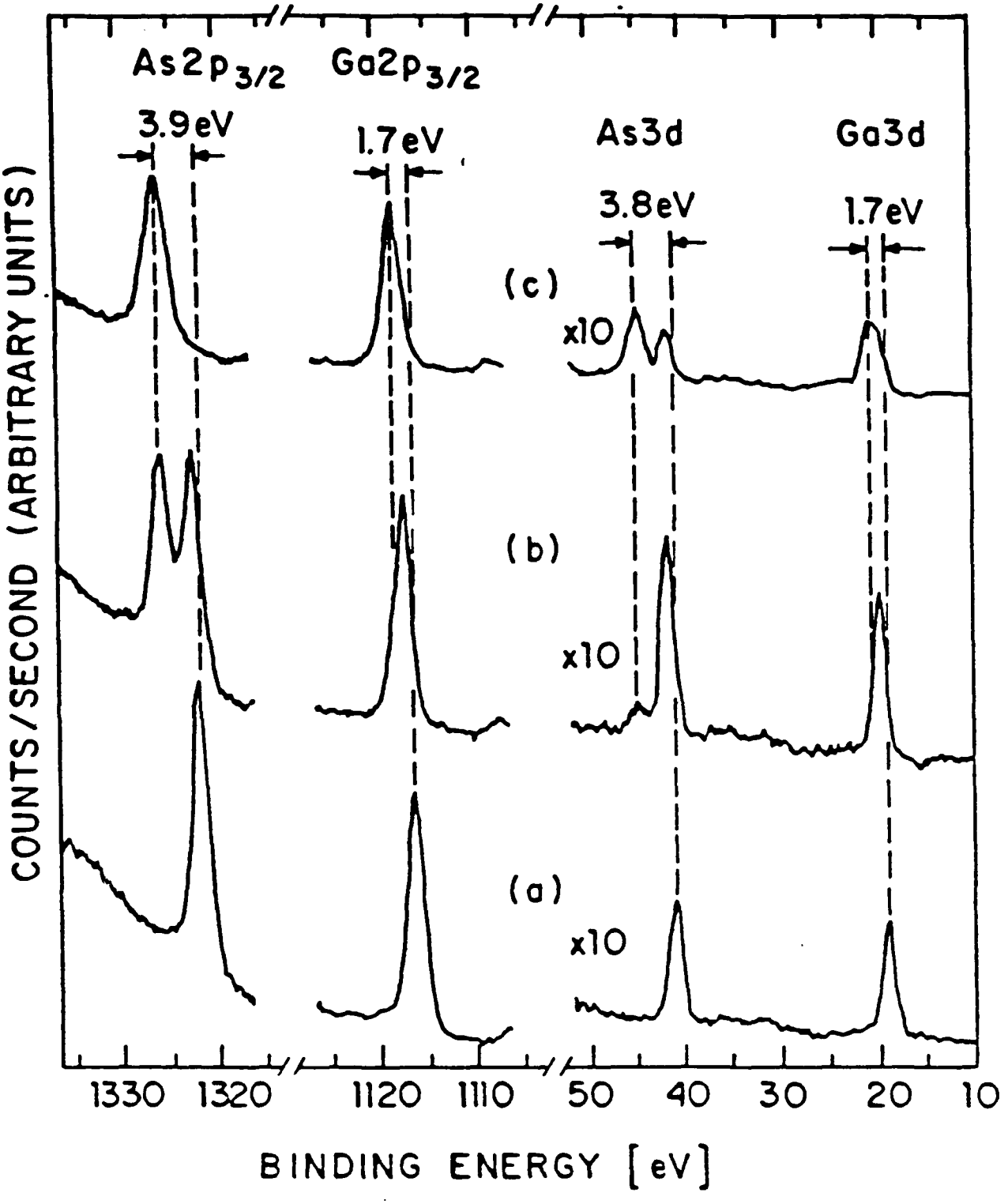

Figure 2: X-ray photoelectron spectra of GaAs surfaces: (a) sputter-cleaned in vacuo, (b) exposed in air for 5 hours after chemical cleaning, (c) irradiated with 257-nm laser light in air for 20 minutes.

ambient environment inside the preparation chamber in the system. When dry oxygen was introduced into the chamber we found that exposure of ultraviolet light made much less oxide (ca. 8 Å) than when done with wet outside air in the chamber (ca. 30 Å). The same drastic difference was also seen on p-type gallium arsenide surfaces. Further study on the wavelength dependence of the enhancement of the oxidation using an excimer laser is currently underway.

Automation of the data acquisition and control of the surface analysis system is also being carried out. The incoming gift of a IBM PC/AT microcomputer and a newly purchased Keithley DAC-500 interface system, will enable digitizing and storing of all the data acquired for much more sophisticated data manipulation and analysis.

This research was also supported by the Air Force Office of Scientific Research/DARPA under Grants F-49620-84-K-0022 and F-49620-85-C-0067, the Army Research Office under Contract DAAG29-85-K-0210, the National Science Foundation under Grants NSF-CDR 84-21402 and NSF-ECS 82-09218, the Office of Naval Research under Contract N00014-78-C-0517, and the Semiconductor Research Corporation under Project SRC-85-02-055.

D. INFRARED SURFACE STUDIES

(R.M. Osgood, E.Sanchez, P.Shaw)
(JSEP work unit 4, 1985 - 1988)
(Principal Investigator: R.M. Osgood (212) 280-4462)

1. Introduction -- The purpose of our work has been to develop a reliable infrared spectroscopic instrument capable of measuring the infrared absorption spectra of weakly adsorbed molecular layers at the interface of a gas-solid system. This apparatus which has now been completed will be used to study the physics and chemistry of metal-alkyl molecules. In particular, laser-induced changes in such systems will be studied.

2. Experimental -- The apparatus is as depicted in Fig. 1. We have employed a total internal reflection (TIR) technique because it allows us to isolate the surface adsorbant absorption signal from the gas-phase absorption signal. That this is so can be seen when one considers that the surface generated absorption signal comes from absorption of the evanescent field outside the reflection element and the evanescent field only extends into the gas sample on the order of one wavelength. Over this one wavelength path length the signal from the adsorbed species dominates because of its greater molecular density. The cell containing the TIR element is itself a novel design in that the element is mechanically butted against the entrance and exit windows so that even where the probe radiation enters and leaves the element, no gas-phase absorption signal is possible. The cell itself is backed by a turbo-molecular pump capable of pulling a vacuum of 10^{-7} to 10^{-8} torr at the cell. An important feature of the cell, which is not evident in Fig. 1, is that we have avoided the use of any viton O-rings in its construction. This is important for efficient cell pump down as some of the components we wish to study are known to be absorbed by viton. In addition, the use of all metal seals allows a significantly higher bakeout temperature than would be possible if any viton seals had been used.

The experimental control of the apparatus together with the data

IR SETUP FOR SURFACE STUDIES

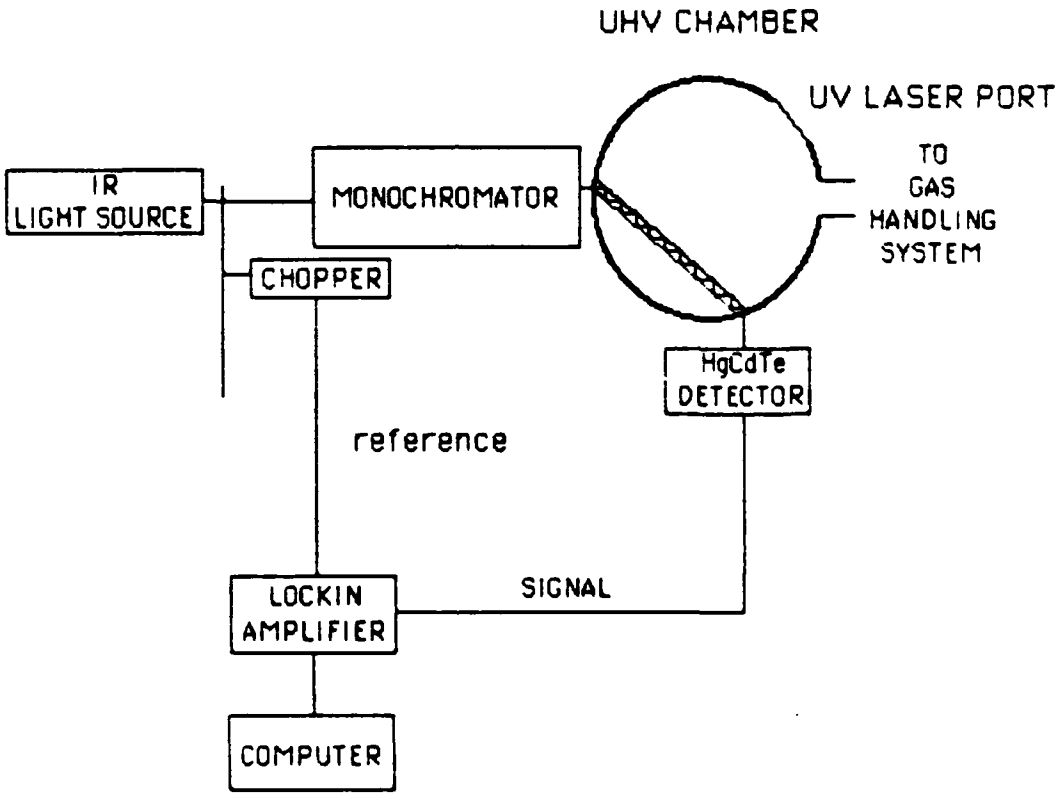

Figure 1

collection and processing was done with an IBM PC with specially designed software. Actual signal to noise is close to 0.2% but further improvement is possible by using a brighter light source and a more sensitive detector (eg. InSb) for the IR region we are working with. The signal is obtained by making a series of background runs followed by runs at a progressive sequence of pressures. After the measurements a signal-to-background substraction is performed. The results for dimethylcadmium are shown in Fig. 2.

3. Results -- The set up was initially applied to a gas-solid system of 2-propanol on silicon for trial purposes. It was then applied to dimethylcadmium (DMCd) in the spectral region from 2.5 to 4 micrometers, precisely where DMCd gas-phase shows absorption bands. Three absorption bands close to the gas ones are observed (Fig. 2) but slightly red shifted with pressure. The bands have been tentatively assigned to the vibrational numbers v = 5, 8 and 12 of CH stretching modes based on gas spectra assignments. The observed shifts as a function of coverage (or pressure) are a strong indication that the absorption is occurring on the surface. Also the isotherms for the three bands (Fig. 3) follow a BET behavior peculiar to physisorbed layers on a solid. These results contain information about the structural arrangements occurring on the surface and its thermodynamics.

4. Further Work -- We are now concentrating on interpreting these results for establishing a reasonable surface structural model that will fit the data. With it we will try to predict the photochemical behavior of the surface and then test it by shining an excimer laser on the TIR element and looking at the resulting spectra.

Within the following months we will be receiving an FTIR apparatus that will permit us to look at a broader spectral region (2-25 microns) at much faster scanning speeds.

This research was also supported by the Air Force Office of Scientific Research/DARPA under Grants F-49620-84-K-0022 and F-49620-85-C-0067, the Army Research Office under Contract DAAG29-85-K-0210, the National Science Foundation under Grants NSF-DMR

84-21402 and NSF-ECS 82-09218, the Office of Naval Research under Contract N00014-78-C-0517, and the Semiconductor Research Corporation under Project SRC-85-02-055.

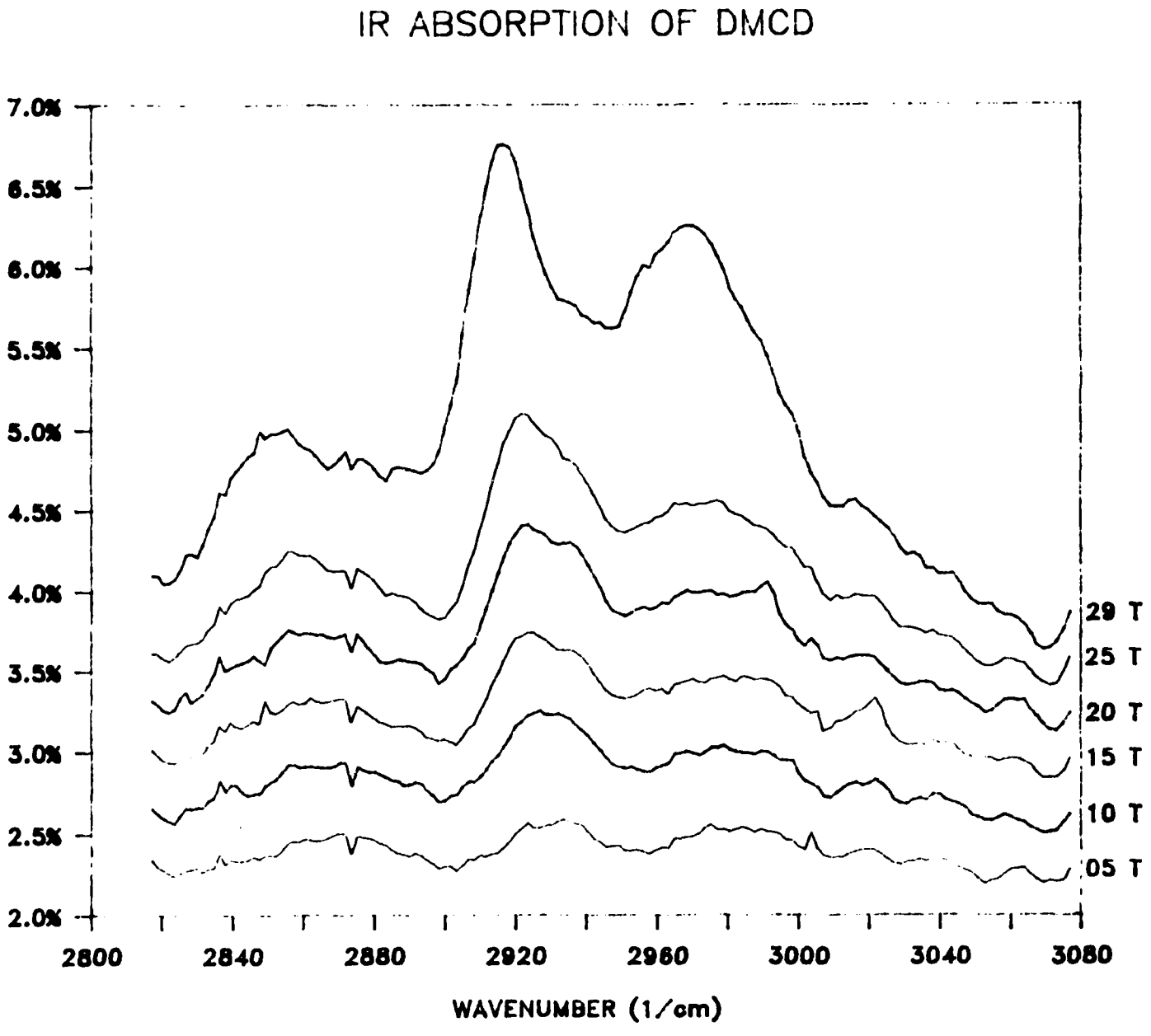
IR ABSORPTION OF DMCD
ABSORPTION
7.0%
6.5%
6.0%
5.5%
5.0%
4.5%
4.0%
3.5%
3.0%
2.5%
2.0%
29 T
25 T
20 T
15 T
10 T
05 T
2800
2840
2880
2920
2960
3000
3040
3080
WAVENUMBER (1/cm)

Figure 2

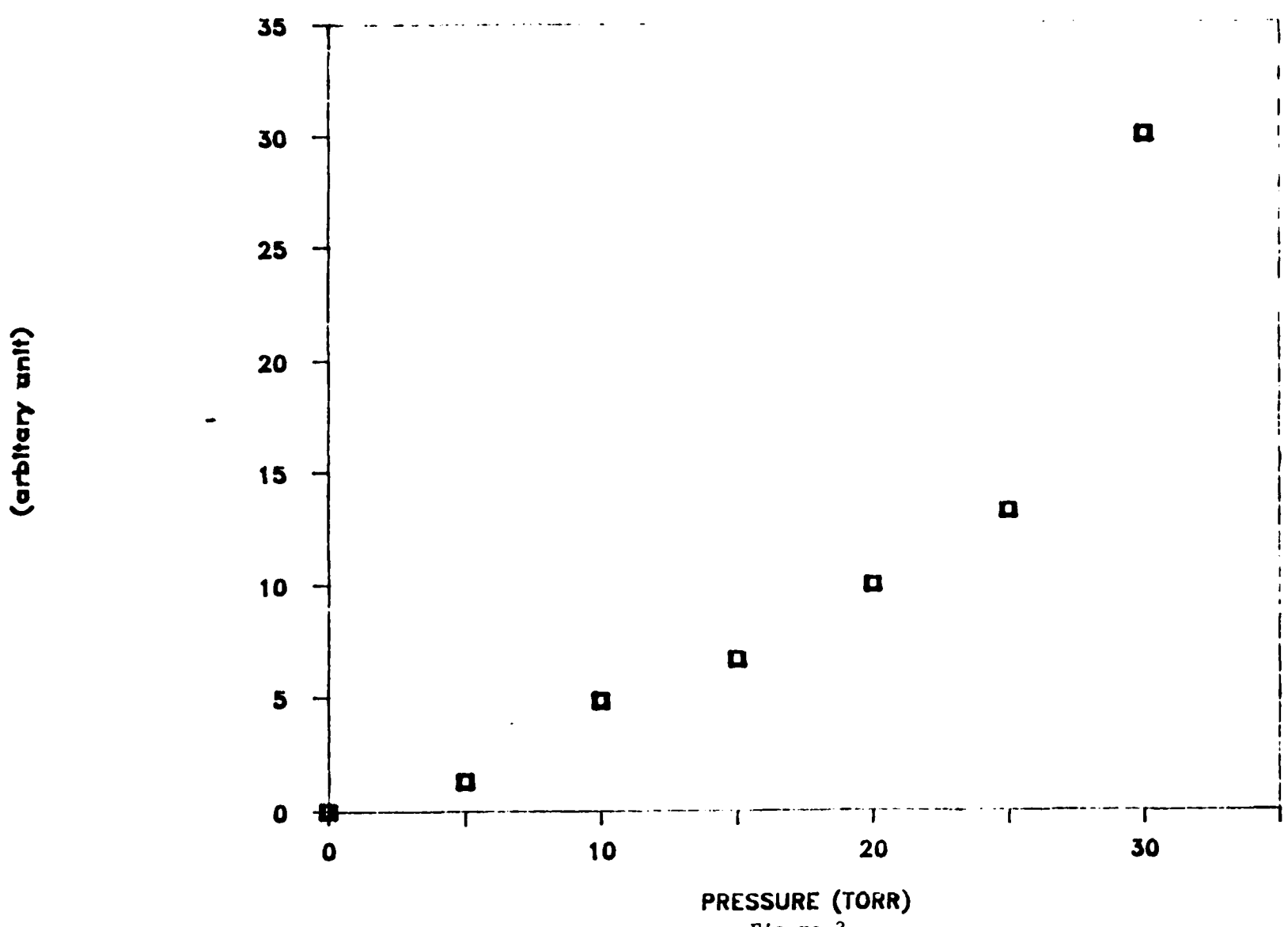
ISOTHERM OF DMCD AT 2968 /cm
35
30
25
20
15
10
5
0
0
10
20
30
(arbitary unit)
PRESSURE (TORR)

Figure 3

E. LASER-ENHANCED ETCHING OF SILICON WITH CHLORINE GAS

(R.M. Osgood, R. Beach, V. Treyz)
(JSEP work unit 4, 1985 - 1988)
(Principal Investigator: R.M. Osgood (212) 280-4462)

1. Introduction -- During this year, we have studied the process of laser enhanced etching of silicon with chlorine gas. We have also continued our study of the photodeposition of metals. A laser direct writing apparatus was designed and built in conjunction with a Semiconductor Research Corporation contract.

2. Direct Writing Apparatus

A) The Optical System

The design and construction of the laser direct writing apparatus has been completed. The entire system has been constructed on a 4' x 12' (x 2' thick) optical isolation table and placed in a new laboratory room. The system consists of two argon-ion lasers whose outputs are coupled together and then directed into a scanning optics line as depicted in Fig. 1. The optics line focuses the laser beams down to a 1.3 μm spot, which can be scanned in the x and y directions over a 4" x 4" surface. In addition to the x-y scanning capability of the system, the focused laser spot can be moved in a direction that is normal to the 4" x 4" surface that it scans over. This feature allows us to continually adjust the focus so that we can keep an optimum beam spot as we scan over surfaces of varying heights. Our system now has the capability of scanning the laser spot over the sample at speeds ranging from 5 μm/sec up to 10 cm/sec while maintaining a 0.1 μm positioning accuracy.

In addition to the laser optics, we have also coupled in a microscope and video camera at the back end of the optics line (see Fig. 1) to allow for the real-time viewing of samples while they are being processed. This has been straightforward as the optics line is essentially an infinity-corrected microscope with laser beam introduced in the microscope tube.

As already mentioned, the scanning laser spot can be moved in a

LASER PROCESSING SYSTEM

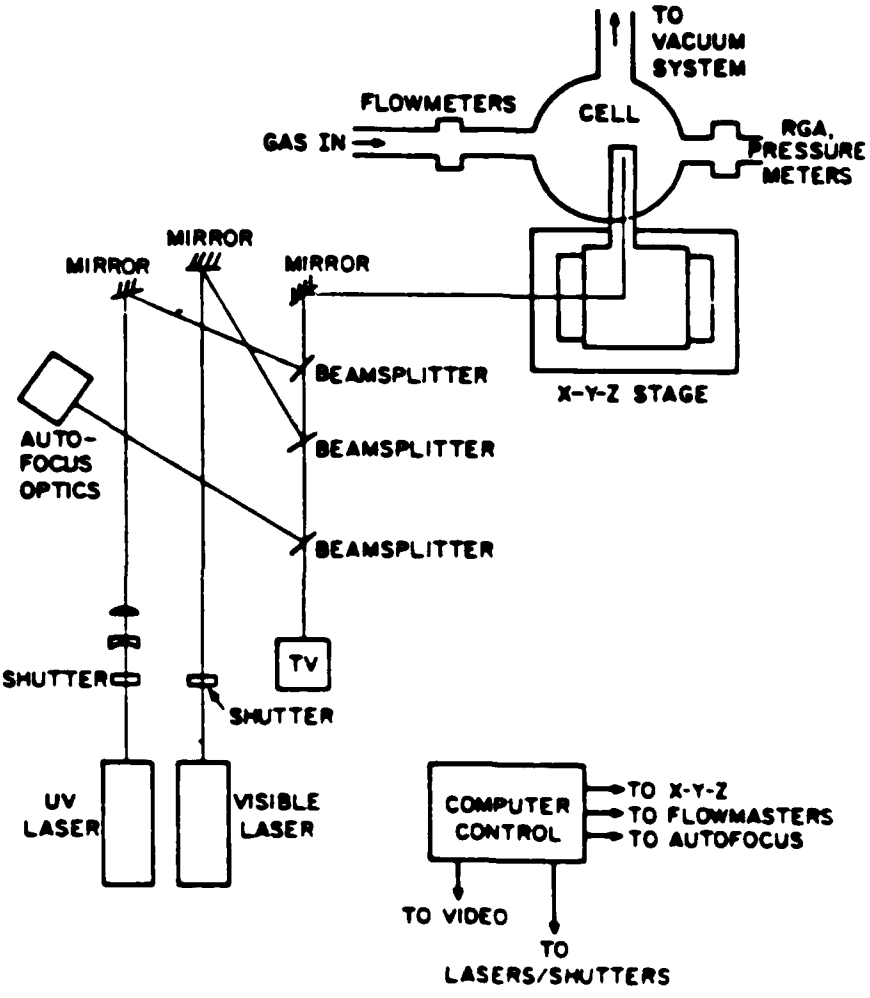

Figure 1

direction normal to the sample it scans over to facilitate optimal focusing. An autofocusing mechanism has been designed and built. This mechanism, which is very similar in design to the astigmatic autofocus mechanisms which have been popularized in commercially available laser disc optical storage devices, has been integrated into our system. Basically, the idea of this system is to analyze light reflected from the sample as it is being processed. However, because the processing we do with our lasers generally changes the reflectivity of the sample surface, we have not been able to operate the autofocus mechanism successfully in real time. This has not presented any real problems however. As it stands now, we operate in the following mode: Before we actually start a laser processing run, we use the autofocusing system to go through and register the substrate that is going to be processed. Using this registration information which is stored in the computer, we can then perform a processing run maintaining optimal focus throughout.

As already mentioned, two argon-ion laser outputs are combined together and fed into the scanning laser optics line. This gives us the capability of illuminating the substrate being studied with any two argon-ion-laser lines simultaneously. In addition, one of the lasers is equipped with an intracavity beam doubler providing 257-nm radiation at power levels in excess of 50 mW. Because the scanning optics line was designed with components that can be easily swapped in and out, we have the capability to optimize the system throughout for any particular wavelength we wish. Currently we have optics that optimize throughput for the argon-ion laser lines at 514-nm, 480-nm, 360-nm and the doubled 514-nm line at 257-nm.

One very useful diagnostic feature that has been incorporated into the optics line is the ability to make real-time reflectivity measurements of the sample while it is being processed. This has been particularly helpful in our laser-assisted etching studies of silicon using Cl_2 gas and the 514-nm, argon-ion-laser line. In particular it has allowed us to very accurately measure the laser power at which we just begin to melt the silicon surface.

An excimer laser purchased from Lambda-Physik has been delivered and is now installed. This laser has allowed us to expand the capabilities of the existing facility by providing for the imaging of

extended objects and the testing of direct writing approaches in more strongly bound molecules than can be photodissociated with the 257 μm light available from the doubled 514-nm argon-ion laser line.

B) Vacuum System and Sample Chamber

The high vacuum processing chamber has been designed, constructed, and installed in the system. Because it is not necessary to translate the processing chamber, it has no limitation on its maximum mass. This feature has given us increased freedom in its design and construction. In particular, we have been able to incorporate a residual-gas analyzer into the chamber in very close proximity to the semiconductor wafer. We have also been able to use large aperture ports in the cell construction allowing an efficient coupling of the sample chamber to the vacuum system and gas-flow system without the need for using large-surface-area, flexible, connecting bellows. The entire chamber and vacuum system is bakeable to 200°C, and, with the attached vacuum pump system consisting of an 8" cryopump from Leybold-Heraeus, we can achieve an ultimate vacuum of 10^{-7} Torr in the processing chamber. We have also incorporated heaters into the pallet of the sample chamber giving us the capability to raise the temperature of the substrate. The gas-flow system, which has been connected to the processing chamber, is halogen compatible and is capable of independently flowing four gases under computer control.

Halogen compatibility is necessary for our current experiments in which chlorine gas is used to etch silicon. In addition to the gas-flow system, two capacitance manometer pressure sensing devices are used to measure the chamber pressure in the range of 1000 Torr at the high end to approximately 0.0001 Torr at the low end.

Another feature of the sample chamber is the incorporation of in situ electrical measurements. This has been very useful in our metal deposition studies as it has given us immediate resistivity values allowing us to very quickly optimize several experimental parameters such as gas pressure, laser power, and substrate temperature.

C) Computer System

The entire apparatus is tied together by an IBM AT computer that is

used for experiment control and data acquisition. Where possible we have used the IEEE-488 parallel data bus for equipment control. A large effort has been put into developing a library of equipment control and data acquisition routines. This has paid off in that we can now very quickly develop specialized routines for performing specific experimental control sequences and measurements. In addition, we have developed menu driven software that allows first-time users to very quickly learn to use the entire system and begin their experiments.

The IBM AT computer that is presently installed in the laboratory is now heavily used for control of experiments and data acquisition. We are currently purchasing another IBM AT. When installed, this new computer will allow the simultaneous development of software and the performing of experiments in addition to giving more flexibility in experiment control and data acquisition.

3. Experimental -- We are performing an extensive series of experiments to characterize the Cl_2 etching of silicon using the 514-nm line of the argon-ion laser. Currently we are studying trench formation, concentrating our attention on using laser powers that are high enough to locally melt the substrate surface. At these powers we observe a dramatic increase in the etch rate. At this time, we have been able to etch micron deep features at scanning rates of up to 7 cm/sec. By parameterizing these various etch rates in terms of incident laser power, chlorine gas pressure, and scanning rates we have developed a simple model that connects these variables. In addition, we have also seen effects due to the polarization state of the incident 514-nm radiation that have not been previously reported. For example, Fig. 2 shows the cross section of three trenches. The straight down trench was etched with the incident laser light linearly polarized parallel to the scan velocity as shown in Fig. 3a. The trenches that bend to the left or right were etched with linearly polarized light but at a slight angle with respect to the scan velocity as shown in Figs. 3b and 3c.

We have qualitatively explained this bending and its dependence on the polarization state of the incident radiation. The bending is due to a laser-enhanced etch rate when the electric field is p polarized rather than s polarized with respect to the leading edge of the trench as it is

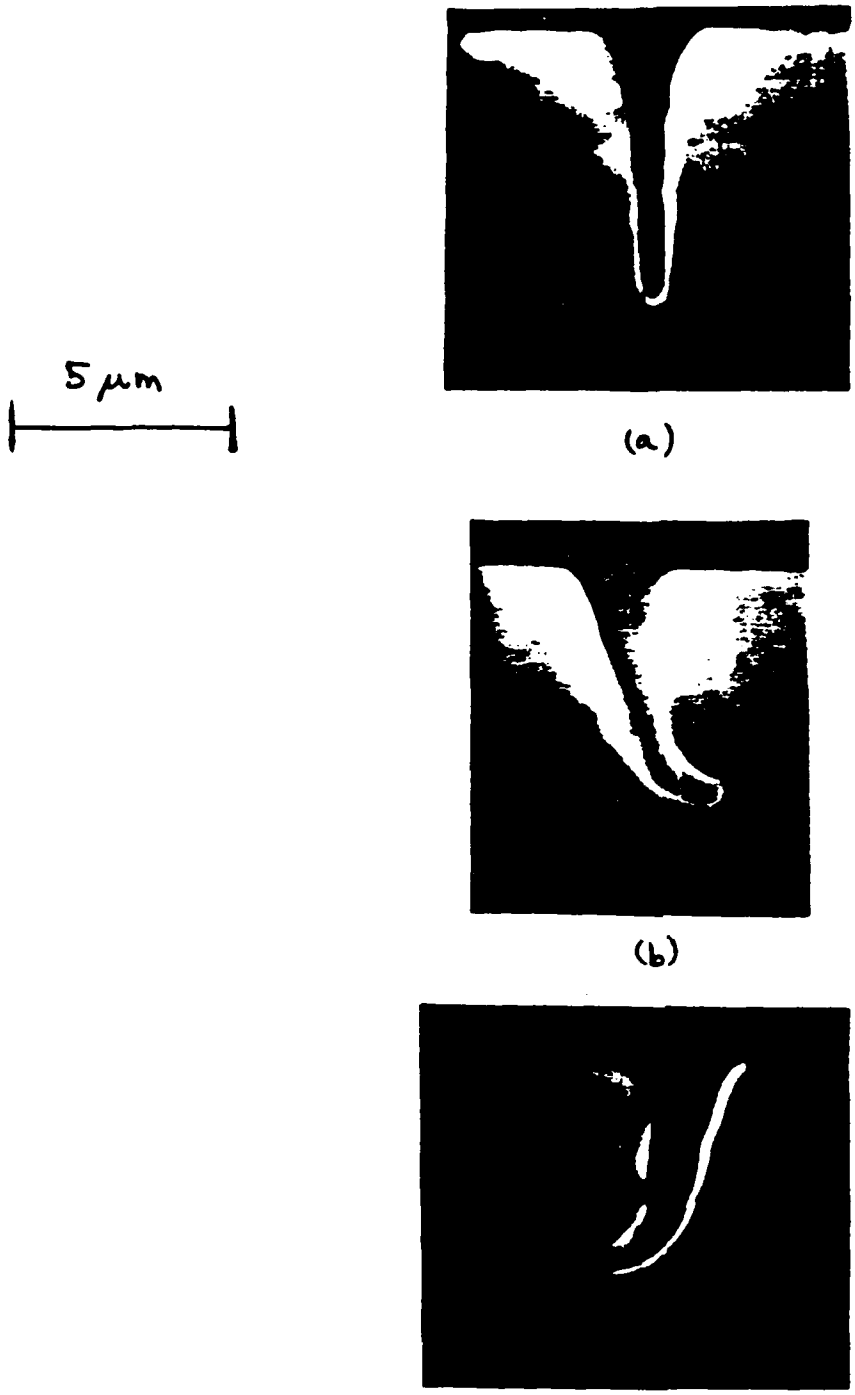

FIG. 2. SEM PHOTOS SHOWING ETCHED TRENCH PROFILES.
(A) LINEARLY POLARIZED LIGHT WAS ALIGNED PARALLEL TO SCAN DIRECTION. (B) AND (C) THERE IS A SMALL ANGLE BETWEEN POLARIZATION DIRECTION AND SCAN DIRECTION.

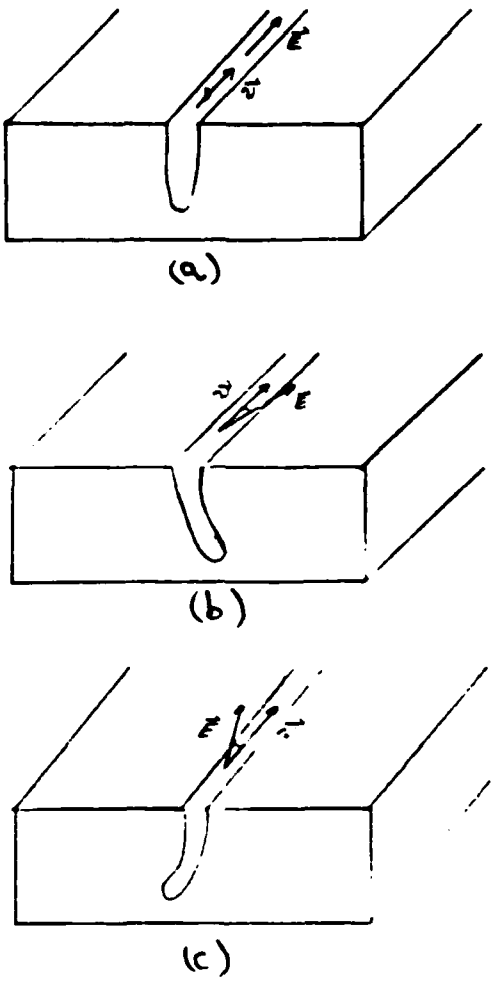

FIG. 3. SCHEMATIC DRAWING DEPICTING THE ORIENTATION OF THE INCIDENT LASER RADIATION WITH RESPECT TO SCAN VELOCITY FOR THE PICTURES SHOWN IN FIGURE 2.

being etched.

At the present, we are investigating the surface of the etched silicon by forming trench capacitors and studying the interface.

We have also explored the Cl_2 etching of silicon using the 257-nm laser radiation available in our lab. Our goal here was to parameterize these etch rates in a manner analogous to what we have done in the 514-nm etching study.

In addition to our laser-assisted etching experiments, we have also been studying metal deposition. Our current direction in laser writing of metals is to deposit metals that are of direct interest to the microelectronics industry. Theodore Cacouris, in collabortion with Dr. Krchnavek at Bellcore, has recently begun an effort to laser-deposit aluminum-metal lines. Although aluminum has been deposited previously, no quantitative information regarding film quality has been presented.

The technique of metal deposition we are using is known as the "hybrid" mode of laser deposition. In this technique, a high power uv laser source provides a combination of metal deposition by photolysis and pyrolysis and/or thermal curing. The advantage of such a technique over a purely photolytic approach is the potential for a cleaner, more complete decomposition while the advantage over a purely pyrolytic technique is a lower temperature of decomposition because of ligand stripping by the direct absorption of uv photons (photolysis). Unlike previous hybrid deposition experiments which were done at 350 nm, the intracavity frequency-doubling system provides a high power (>100 mW) 257-nm beam which should allow hybrid deposition with a stronger influence of photolysis. In addition to the improved 257-nm laser system, an apparatus has been designed and built that allows resistance measurements of deposited metal lines to be made in situ, greatly enhancing our ability to optimize the deposition reactions under study.

To date, we have met with partial success. Continuous, fine line structures have been routinely written at speeds ranging from 1-10 μm/sec. However, these lines show relatively high resistance values. In contrast, we have deposited low resistance (~ 100 Ω for lines 250 μm long) lines. In some cases, however, the lines exhibited uncontrolled pyrolytic microexplosions producing unsuitably wide (30 μm) lines. Further exploration of the parameter space should improve this

situation.

In addition to the aluminum deposition work that is now in progress, we are also studying the deposition of gold. At present we have two gold-containing compounds. From Dr. Wayne Weiner of American Cyanamid we have a sample of CYPURE DMGTF-ACAC. We have made a UV absorption spectrum of this compound and are in the process of preparing it for laser deposition studies. From Professor Carlo Floriani of Columbia University we have a sample of MESITYL gold. Currently we are attempting to make a UV absorption spectrum of this compound as a preliminary study to see if it will be useful in a laser deposition process.

This research was also supported by the Air Force Office of Scientific Research/DARPA under Grants F-49620-84-K-0022 and F-49620-85-C-0067, the Army Research Office under Contract DAAG29-85-K-0210, the National Science Foundation under Grants NSF-CDR 84-21402 and NSF-ECS 82-09218, the Office of Naval Research under Contract N00014-78-C-0517, and the Semiconductor Research Corporation under Project SRC-85-02-055.

F. ELECTRONIC STATES AT EPITAXIAL AND NON-EPITAXIAL NICKEL-SILICIDE/ SILICON INTERFACES

(E.S. Yang, H.L. Evans, X. Wu, P.S. Ho)
(JSEP work unit 3, 1985 - 1988)
(Principal Investigator: E.S. Yang (212) 280-3120)

It is known that silicide formation dominates the interfacial chemistry and the interface is structurally abrupt but contains defects such as atomic steps and misfit dislocations.[1] The Schottky barrier was found to be a true interface property and its nature can be classified as extrinsic or intrinsic, depending on the extent of the reaction.[2] In spite of the progress, the central issue regarding the nature of the interface states at the silicide-silicon interface remains unresolved. The difficulty lies in the fact that the analytical techniques used so far are primarily surface electron spectroscopies which do not have the required sensitivity and energy resolution (< 0.1 eV) to detect the presence of interface states of an amount (about 10^{13} states/cm^2) sufficient to pin the Fermi level (E_F). This is illustrated by the Auger study of the Pd_2Si-Si interface[3] where interface valence states of Si were observed and their position appears to be below E_F. However, the intensity and distribution of these states cannot be accurately measured to assess their role in determining the electrical properties of the interface.

In this regard, particularly interesting are the recent results of the $NiSi_2$-Si(111) interface, where a difference of 0.14 eV in barrier height has been reported for the twin epitaxial (A and B type) interfaces.[4] A later study found, however, that these two interfaces have similar barrier heights although both exceed the mixed type by about 0.14 eV.[5] These are the first observations on the correlation of structure to barrier height, which, if clarified, is of basic importance for understanding SB formation. So far there are no other electrical measurements available to resolve the discrepancy.

To measure the interface states, electrical techniques designed specifically for metal-semiconductor contacts are required. For this purpose, we have developed a capacitance-spectroscopy technique[6] and have used it to study a number of silicide-silicon interfaces. We

present the results of Ni silicide-silicon interfaces which were obtained from the single A and B and mixed AB types of the $NiSi_2$-Si(111) epitaxial interface. The observed interface states reveal that the characteristics for the two single type interfaces are similar but more perfect than the mixed-type interface. This establishes a direct correlation of the interface state characteristic to the structural perfection. The Ni results can clarify the discrepancy on the barrier-height measurements by suggesting that the barrier height is controlled by the structural perfection instead of the specific epitaxy of the interface.

One basic difficulty in measuring interface states at a metal-semiconductor contact arises from the localized nature of the interface states, as close as a few angstroms from the metal. This invalidates the use of standard tecnhiques, e.g., reverse-biased capacitance and deep-level transient spectroscopy. The problem is solved in our study by measurement of the induced capacitance of the contact under a foward-biased voltage with use of a phase-sensitive spectroscopy technique. A dc voltage is applied to fill the interface states below the quasi Fermi level E_F while a small ac voltage is used to probe the presence of the filled states by measuring the capacitance that they induce. The nature of the interface states can be deduced from the magnitude of the induced capacitance and its frequency dependence. One general problem in this kind of measurements arises from the conductance (in-phase) component in the Schottky contact under the forward-biased condition. Its magnitude can be several orders higher than the capacitance (out-of-phase) component; therefore, it is essential to maintain a precise zero-phase condition during the measurement.

In our experiment, n-type (111) silicon samples were chemically or UHV cleaned before metal evaporation, and an aluminum back contact was provided. The UHV cleaning was carried out by several heating steps and a flash to 1100°C for a few seconds. The barrier height was measured with I-V (in situ) and photoresponse techniques. The interface state measurement was made outside the vacuum system by carrying out capacitance-versus-voltage scans as a function of temperature and frequency (from 20 Hz to 3 kHz).

A striking correlation of the structural perfection and interface states was observed at the epitaxial Ni silicide interfaces. As shown in Fig. 1, similar densities and peak positions of the interface states were observed for the two single types, which are distinctly different from the mixed type. Again the peak positions correlate well with the difference in barrier heights. The type A and B spectra both peak at 0.34 V, signifying a band of states around 0.65 eV from the valence band. Contrasted to this, the type AB mixed interface has a much broader spectrum, peaking at 0.21 V. When we take into account the lower barrier height of this interface, the state is 0.64 eV from the valence band, the same as the single-phase interfaces. The single-type interfaces have a low density of states, about $10^{12}/cm^2$. This is about a factor of 5 to 10 times less than the mixed interface. Significantly, the type-A interface has about twice as many interface states as the type-B interface although their peak positions are identical. It is known that the type-A interface is thermally less stable and hence more difficult to form, so that the higher interface state density reflects the presence of more defects at this interface.

Our results can be represented by the schematic band diagram based on the simple charge-exchange model (Fig. 2). Even though a model including other exchange mechanisms is used, the distribution can be vastly different, possibly leading to a more dispersed band distribution. This uncertainty will not change our qualitative conclusion that the characteristics of the interface states are very similar except for the difference in the densities, which shows that the single-type interfaces are more perfect. The almost identical peak positions indicate that these states are likely associated with the same kind of imperfections, most probably bonding defects of the silicon atoms at, or very close to, the interface. This suggests that the different barrier heights of these interfaces are determined by the amount of defect states available to pin the Fermi level which, in turn, is controlled by the degree of structural perfection of the interface, rather than by the specific epitaxy.

We have studied a number of silicide-Si interfaces and found interface states with distributions and characteristics close to those reported here. In general, similar effects of annealing on the

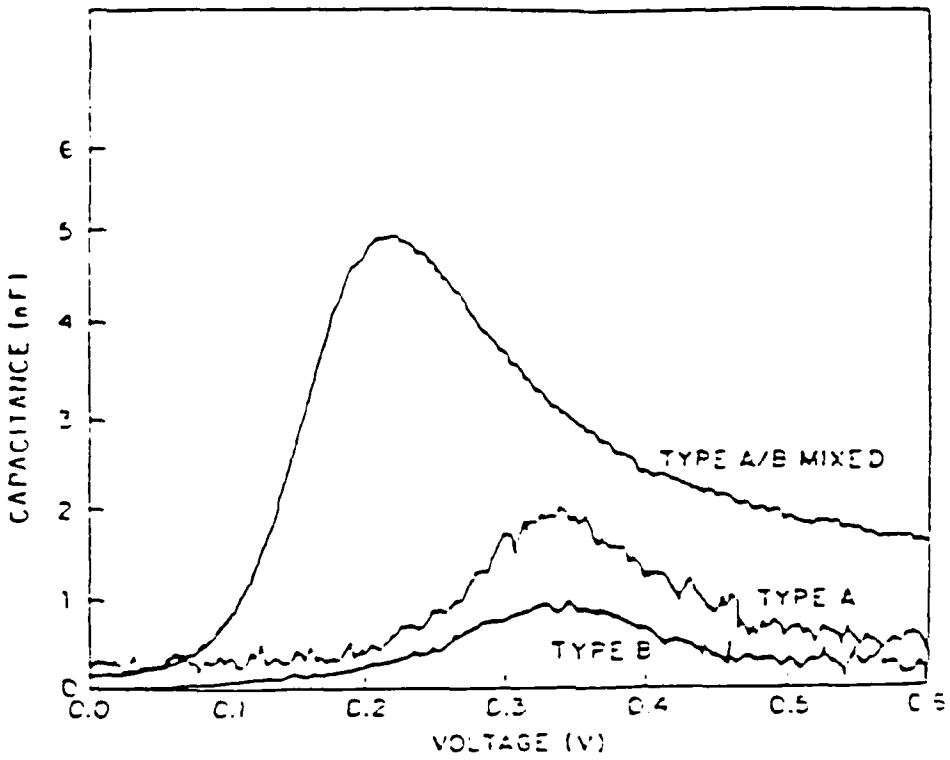

Figure 1: Capacitance spectra observed at 100 Hz for three epitaxial NiS_2-Si(111) interfaces: the A and B single-phase types and a mixed AB type.

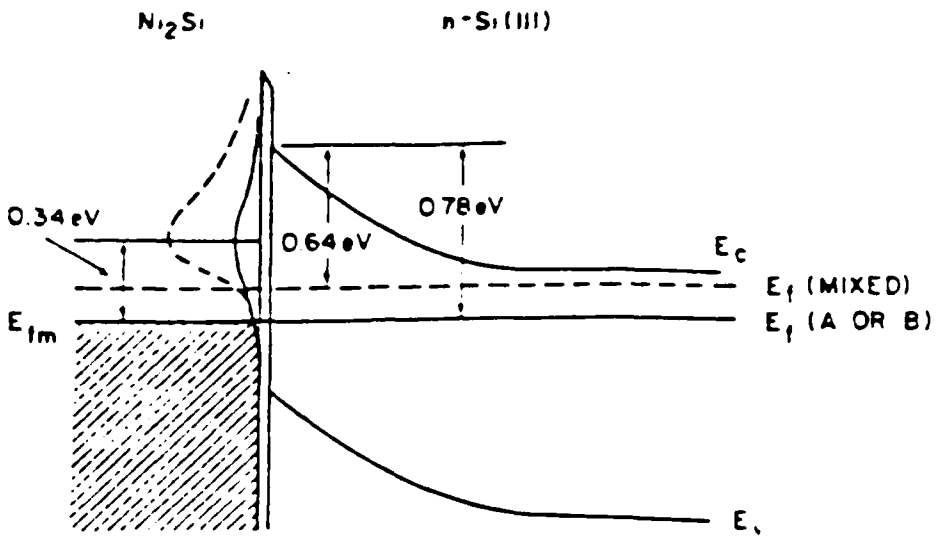

Figure 2: Schematic diagram for the distribution of the unoccupied states at $NiSi_2$-Si(111) interfaces. The solid curve represents the single-phase interface and the dashed curve represents the mixed-phase interface. Note the difference positions of the Fermi level corresponding to the difference in the barrier heights observed.

distribution and density of the states were observed and the direction and amount of the shift correlate with the change in the barrier height. This seems to be the general trend of the effect of silicide formation on the electrical characteristics of the interface.

In summary, we have observed a dispersed group of unoccupied states existing in the Si band gap at the silicide-Si interface. Upon annealing, their density and distribution change to reflect a more perfect interface as a result of silicide formation. The observation on the Ni silicides shows that their character is influenced strongly by the degree of perfection of the interface. The nature of such defects remains to be clarified. Although structural defects specific to the interface have been observed by high-resolution transmission electron microscopy for several silicide-silicon systems, including the $Pd_2Si/Si(111)$ interface,[7] it is not clear whether such defects can account for the observed states. Recently Si dangling bonds of interfacial vacancies have been proposed to account for Fermi-level pinning in silicide-silicon interfaces.[8] It would be very interesting to check whether our results which reveal the empty instead of the occupied states are consistent with this particular model.

This research was also supported by the Air Force Office of Scientific Research under Contract AFOSR-30602-85-C-0072 and by the National Science Foundation under Grants NSF-ECS 82-17677 and NSF-CDR 84-21402.

(1) P.S. Ho and G.W. Rubloff, Thin Solid Films 80, 433 (1982); G.W. Rubloff, Surf. Sci. 132, 268 (1983).

(2) P.S. Ho, J. Vac. Sci. Technol. A 1, 745 (1983).

(3) P.E. Schmid, P.S. Ho, H. Foll, and G.W. Rubloff, J. Vac. Sci. Technol. 18, 937 (1981).

(4) R.T. Tung, Phys. Rev. Lett. 52, 461 (1984).

(5) M. Kiehr, P.E. Schmid, F.F. Fetoues, and P.S. Ho, Phys. Rev. Lett. 54, 2149 (1985).

(6) H.L. Evans, P.S. Yang, and P.S. Ho, Appl. Phys. Lett. 46, 481 (1985).

(7) H. Föll, P.S. Ho, and K.N. Tu, Philos. Mag. A 45, 31 (1982); J.M. Gibson, J.C. Bean, J.M. Poate, and R.T. Tung, Thin Solid Films 93, 91 (1982).

(8) O.F. Sankey, R.E. Allen, and J.D. Dow, Solid State Commun. 49, 1 (1984).

G. INTERFACE STATES IN PALLADIUM SILICON SCHOTTKY BARRIERS

(E.S. Yang, H.L. Evans, X. Wu)
(JSEP work unit 3, 1985 - 1988)
(Principal Investigator: E.S. Yang (212) 280-3120)

Metal semiconductor contacts are perhaps the most prevalent interface in integrated circuit technology. They exist in the form of ohmic contacts needed for all device configurations and as Schottky barriers for diodes, MESFETS, and fast bipolar circuits. Yet, despite their widespread usage, the fundamental mechanism responsible for determining the barrier height is unknown. Schottky's original theory predicted a dispersion in barrier heights for different metals on silicon which was not observed experimentally.[1] On the other hand, Bardeen's intrinsic interface state description restricted the barrier for a given semiconductor to a single value.[2] The current theoretical models consider states intrinsic to the semiconductor and those due to metal deposition to be responsible for the final position of the Fermi level.

Experimental techniques to resolve the interface state distribution have not been entirely successful. Various energetic beam spectroscopies such as Auger Electron spectroscopy[3] and ultraviolet photoemission spectroscopy[4] have yielded strong evidence suggesting that [illegible] states exist at the interface, which are not found [illegible] as the chemical bonding and environment specific to [illegible] However, these techniques do not have the [illegible] the energy levels of states in the gap, nor can [illegible] when thick metal overlayers are [illegible] the final device. Electronic [illegible] capacitance and ideality factor [illegible] interfacial layer of precisely [illegible] for the case of [illegible] gained from these [illegible] present results on palladium silicon [illegible] spectroscopy and obtain a [illegible] the interface states.

The interface state capacitance is then interpreted in terms of the state distribution using a model previously proposed by Barret et. al.[7]

Palladium silicon diodes have been fabricated by thermal evaporation of palladium at 3×10^{-7} torr onto a chemically etched silicon surface. The silicon substrates were n-type, phosphorous doped, 10 Ω-cm, (111) oriented wafers. Chemical cleaning involved a degreasing procedure followed by a CP4 etch. An aluminum evaporation was performed to provide an ohmic back contact. Current-voltage and forward biased capacitance measurements were made at various temperatures on the as-deposited sample. The sample was then annealed at 275°C for 30 minutes in an Argon environment to promote the formation of palladium silicide. After annealing, the diode was subjected to the same measurements at the same temperatures as the as-deposited sample.

Forward biased capacitance measurements were made at 100 Hz using accurate phase capacitance spectroscopy (APCS) described in the last annual report. In this technique, the phase of the lockin amplifier is set precisely so that the equivalent parallel capacitance and conductance of a network can be separately recorded even when the quality factor (wC/G) is as low as .0003. This is done by placing an additional conductance in parallel with the network and adjusting the phase until the measured capacitance is the same with and without the added resistor. When measuring voltage dependent elements such as the small signal equivalent circuit of a Schottky diode added care must be taken to ensure that the voltage across the structure is the same with and without the phase adjustment resistor. Once the phase is set at a particular voltage, the equivalent parallel elements can change during the voltage sweep without any readjustment of the phase. Current-voltage (I-V) measurements were used to determine the barrier height of the diode as well as the resistance of the network in series with the depletion region of the device. This resistance, R_s, is assumed to be constant independent of bias but varies with temperature. It consists of the resistance, R_p, due to the source resistance of the supplies and the diode back contact. It is assumed that the deviation of the DC diode current characteristic from ideal exponential behavior is entirely to series resistance effects.

$$I = AA^*T^2 e^{-q\phi_{bn}/kT} \left(e^{q(V_F - IR_s)/kT} - 1\right) \quad (1)$$

where V_F is the voltage applied to the diode, I is the resulting current flow, R_s is the series resistance and A, A^*, T, θ_{bn} are respectively, the contact area, Richardson's constant, the temperature, and the diode barrier height. Taking two points on the I-V curve at a given temperature, the diode series resistance can be determined as

$$R_S = \frac{1}{I_1 - I_2} kT \ln \frac{I_2}{I_1} e^{-(V_{F2} - V_{F1})/kT} \quad (2)$$

APCS results at room temperature for both the as-deposited and annealed diode are shown in Fig. 1. I-V characteristics at the same temperature are shown in Fig. 2. ln I vs. V_F plots at low applied bias indicate that the room temperature barrier height changes 8 mV upon annealing from .744 eV to .736 eV. In both situations the ideality factor is less than 1.03 revealing good Schottky diodes. Using Eq. (2), the diode series resistance changes with temperature having values of 19 Ω, 24 Ω, and 26 Ω, for the as-deposited diode and 27 Ω, 23 Ω, and 33 Ω, for the postannealed diode at 269 K, 297 K, and 325 respectively.

Before the capacitance due to the interface states can be evaluated in terms of the interface state density, it is necessary to determine this capacitance from the measured circuit parameters. [illegible]

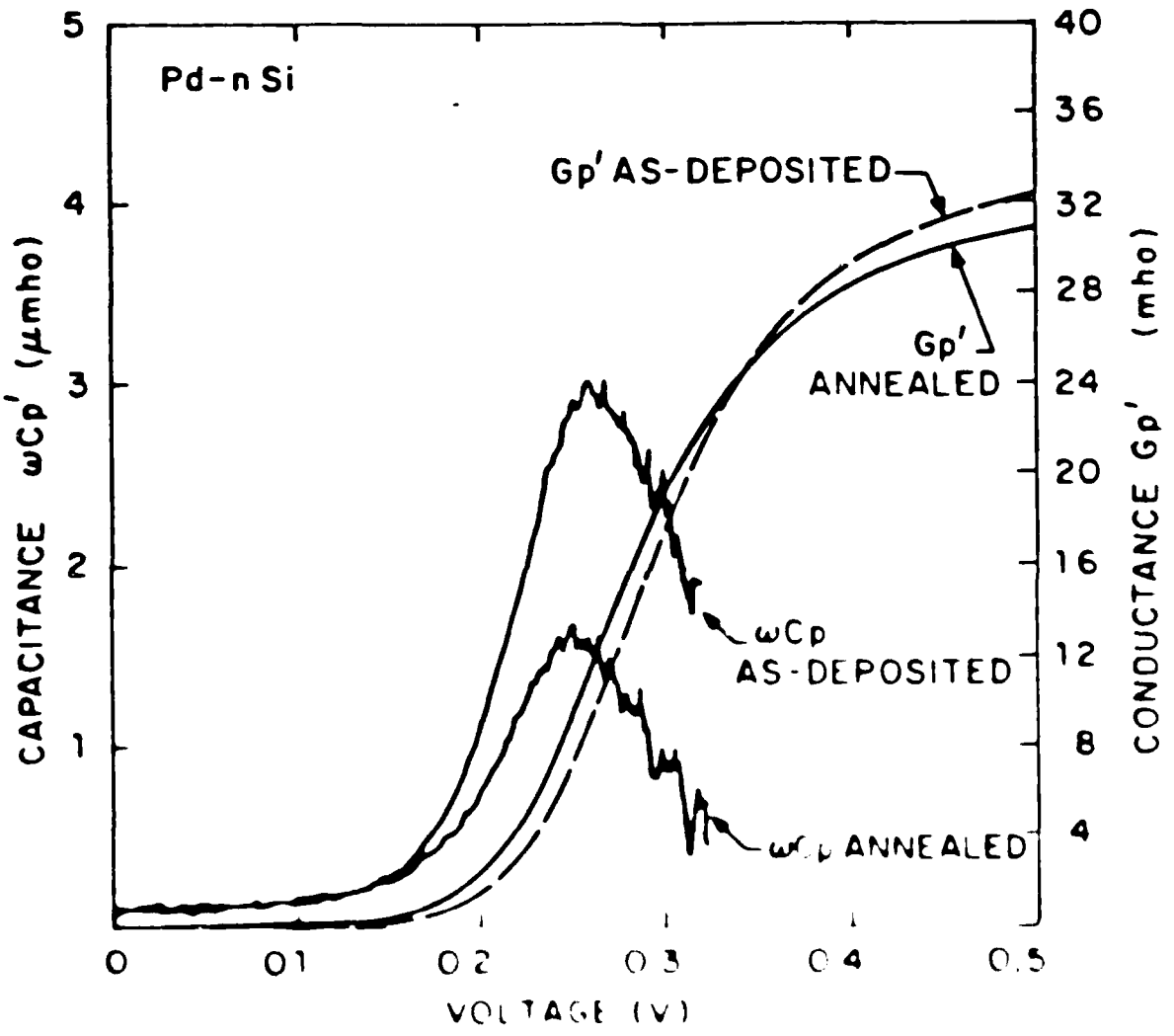
Pd-n Si
Gp' AS-DEPOSITED
Gp'
ANNEALED
ωCp
AS-DEPOSITED
ωCp ANNEALED
CAPACITANCE ωCp' (μmho)
CONDUCTANCE Gp' (mho)
VOLTAGE (V)
0
0.1
0.2
0.3
0.4
0.5
1
2
3
4
5
4
8
12
16
20
24
28
32
36
40

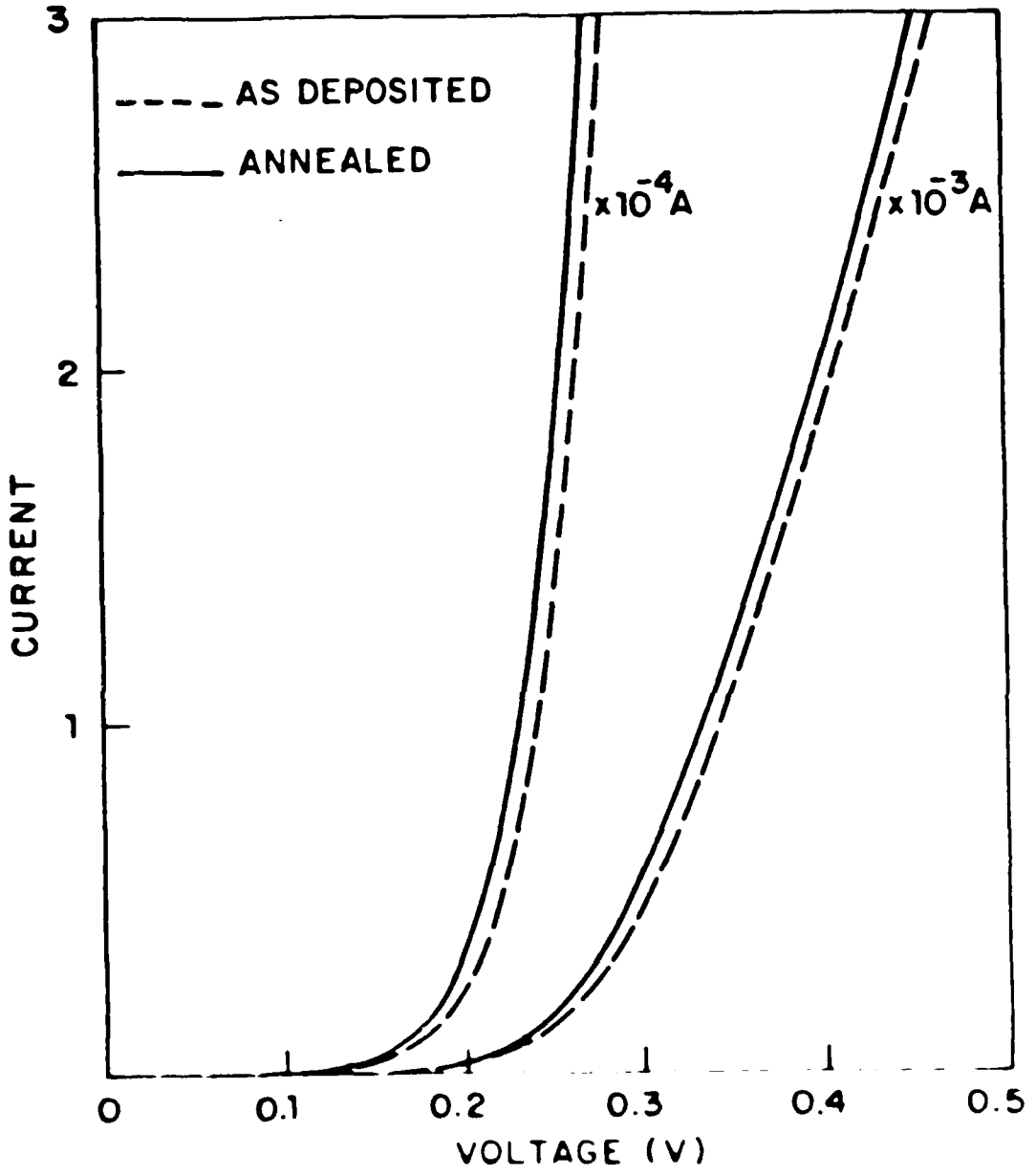
3
2
1
CURRENT
AS DEPOSITED
ANNEALED
x10⁻⁴A
x10⁻³A
0
0.1
0.2
0.3
0.4
0.5
VOLTAGE (V)

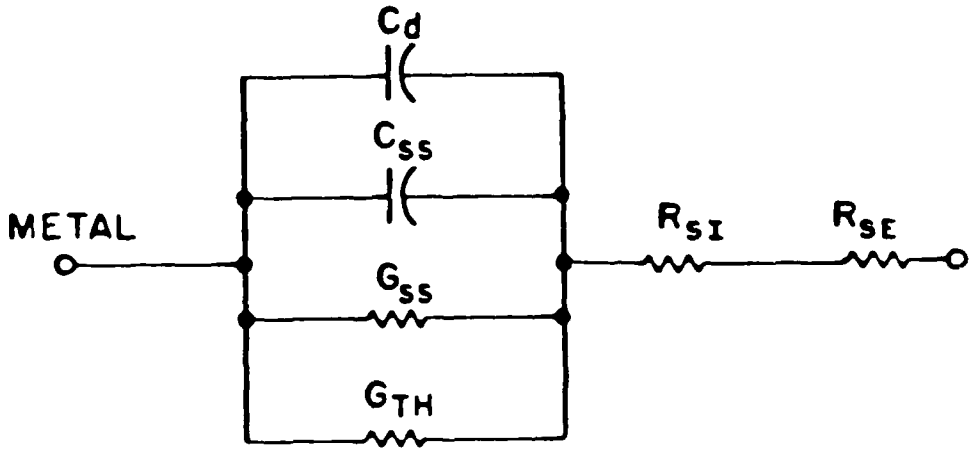

Figure 3: Small signal circuit model of the diode: C_{ss} (G_{ss})-capacitance (conductance) associated with the interface states, G_{th}-thermionic emission conductance, R_s-series resistance.

The measured conductance, G_p, approaches R_s as the thermionic emission conductance G_{th} rises with voltage. More and more of the applied ac signal is then across the series resistor and the effective current through the capacitive elements is reduced accordingly. Eq. (3) is needed to account for the changing magnitude of the ac voltage appearing across the active region of the device.

In addition to its effect on the ac signal, the series resistance also influences the position of the Fermi level at the interface. The actual DC voltage, V_D, dropped across the depletion region is reduced from V_F by

$$V_D = V_F - IR_S \tag{4}$$

Assuming the Fermi level is flat through the depletion region, the majority carrier density at the surface is given as

$$n_s = N_c e^{-(\phi_{bn}-V_F+IR_S)/kT}$$

Eq. (4) is also needed to determine C_d in Eq. (3), namely

$$C_d = \left(\frac{qe_s N_d}{2}\right)^{\frac{1}{2}} \left(\phi_{bn}-V_N-V_D-\frac{kT}{q}\right)^{-\frac{1}{2}}$$

where N_d and e_s are the doping and permittivity of the water, and V_N the Fermi potential ($kT \ln N_c/N_d$).

The measured interface state capacitance can be related to the interface state distribution using Shockley-Read-Hall statistics extended to the interface by Barret et. al.[7] With this model a state at energy E_t can exchange charge with the semiconductor conduction and valence bands and the metal giving rise to an interface state capacitance for a single level:

AD-A175 644 RESEARCH INVESTIGATION DIRECTED TOWARD EXTENDING THE USEFUL RANGE OF THE ELECTROMAGNETIC SPECTRUM(U) COLUMBIA RADIATION LAB NEW YORK G W FLYNN ET AL. 2/3

UNCLASSIFIED 31 DEC 86 DAAG29-85-K-0049 F/G 20/14 NL

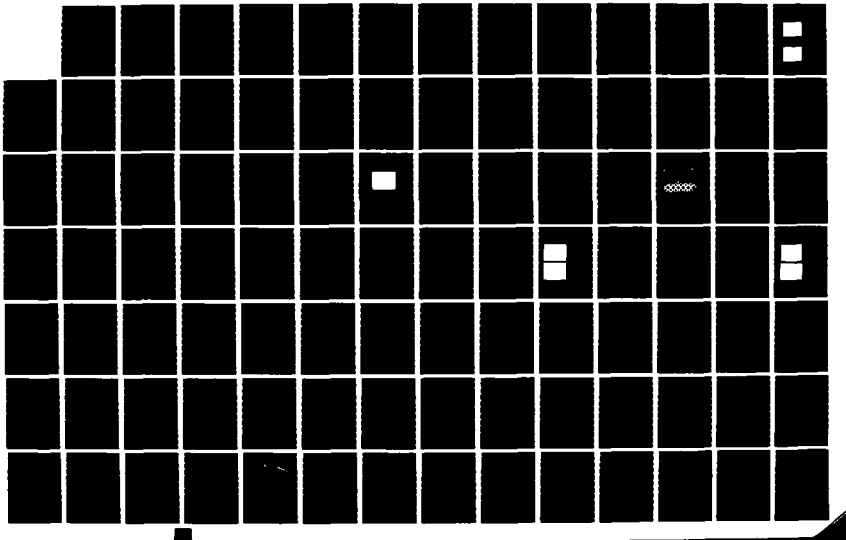

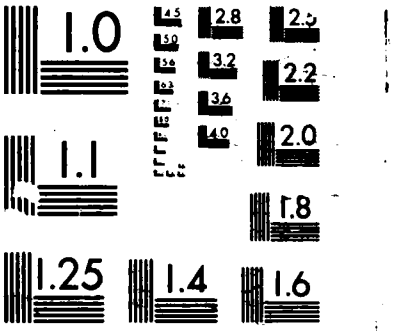
1.0
1.1
1.25
1.4
1.6
2.8
3.2
3.6
4.0
2.2
2.0
1.8

two energy limits for a band of states.

A computer analysis based on Eq. (7) was used to determine the interface state capacitance resulting from various energy level distributions and trap parameter sets. The voltage dependence of the measured capacitance requires capture from the conduction band to dominate over the other capture processes. In addition, the observed temperature shifts indicate capture and emission to be between different charge reservoirs. For all the parameter sets attempted, states closer to the conduction band than .55 eV could not fit the temperature data. The capacitance measured is thus presumably the signature of a state or group of states that lies within .19 eV of the metal Fermi level.

To reduce the number of unknown variables, an effective single level opposite the metal Fermi level which captures electrons mainly from the conduction band and emits mainly to the metal was assumed. The best match for the as-deposited data is then as shown in Fig. 4. A small shift in the concentration, N_T. and time constant product, $\sigma_n\sigma_E$, was needed to fit the experimental curves over the measured temperature range as shown. For the annealed sample, the theoretical model and experimental data match quite well with a single value of N_T and $\sigma_n\sigma_E$ as seen in Fig. 5. Upon annealing the density of the effective level decreases by a factor of 2.3, from 1.25×10^{12} cm^{-2} to $.54 \times 10^{12}$ cm^{-2}, while the time constant product increases by 2.6. This decrease in concentration is consistent with the movement of the interface into the silicon upon the formation of silicide. The original interface presumably has many extrinsic impurities which do not exist at the new interface. The increase in time constant is not yet understood and frequency measurements are being performed to determine which parameter is responsible for this change.

The necessity in using small shifts in the state parameters in order to match the data indicates the single level model is not entirely correct. After annealing, however, the distribution probably moves closer to this model as evidenced by the fit achieved using only a single parameter set. Once again, a band of states which decreases in width upon annealing is consistent with theories on silicide formation.

We conclude that the proposed effective single level, or the band of states which it represents, is responsible for the barrier height in

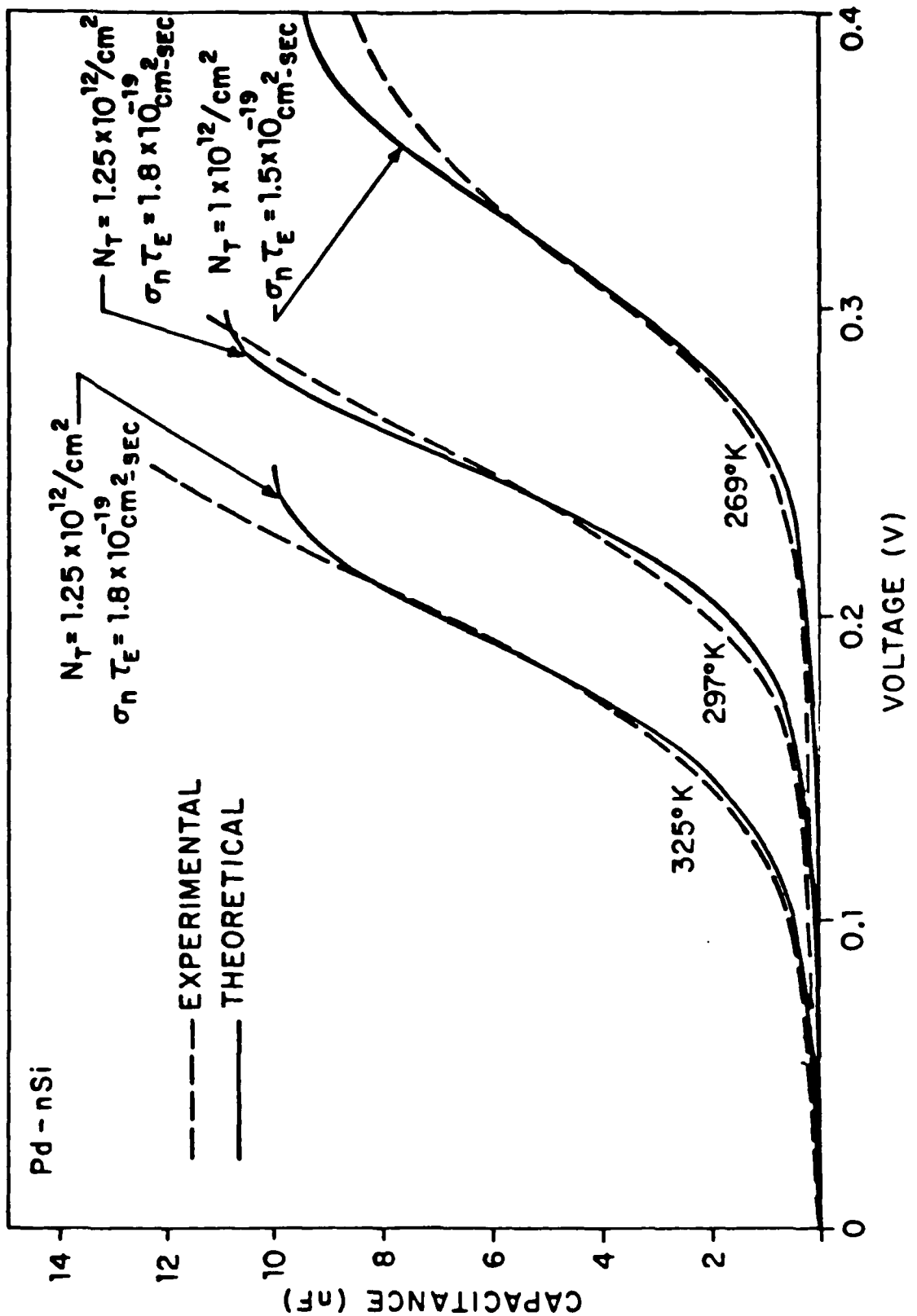

Figure 4: Match between theoretical prediction, using a single interface level opposite the metal Fermi level with the parameters shown, and the experimental results for the as-deposited diode at 269 K, 297 K, and 325 K.

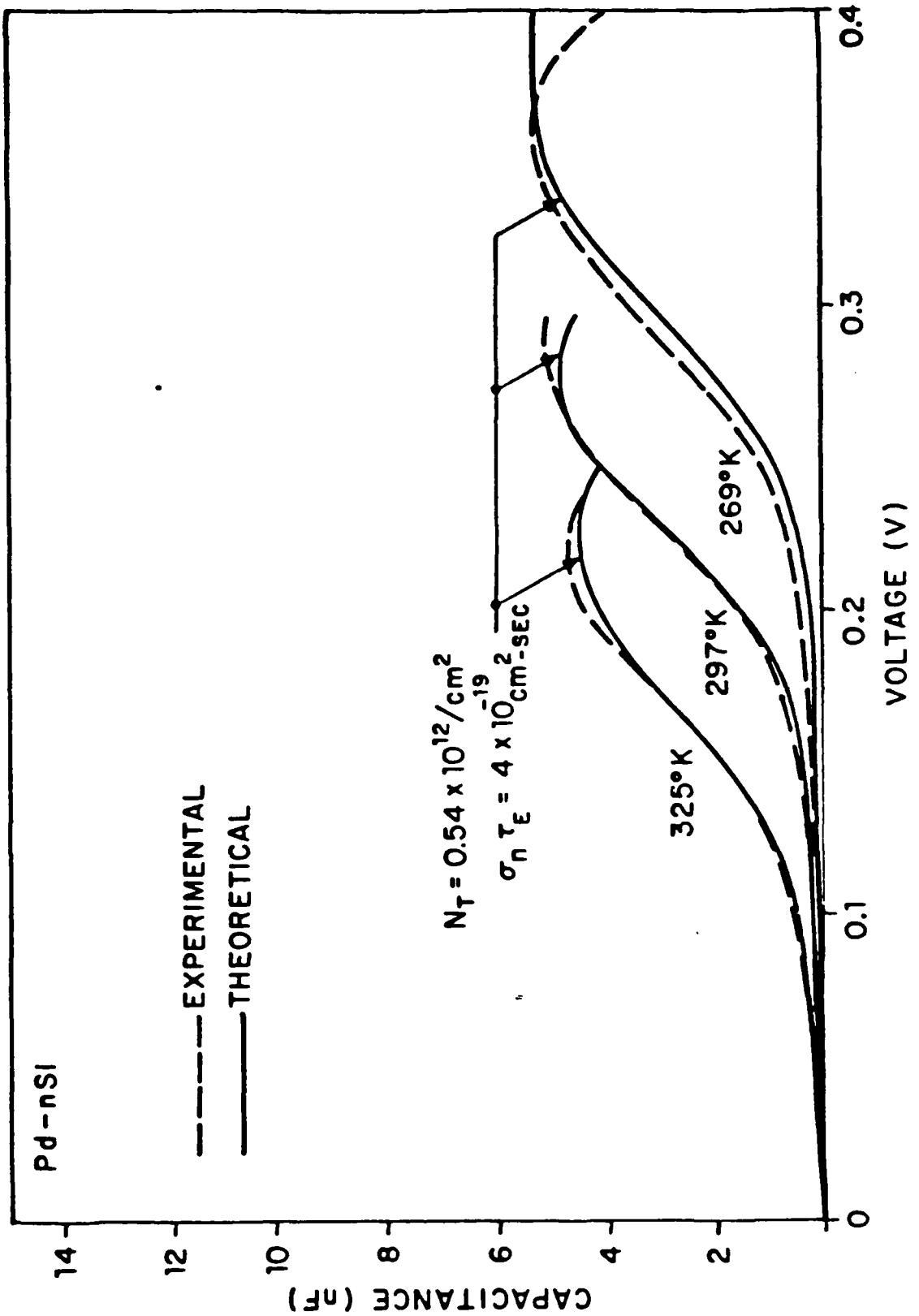

Figure 5: Match between theoretical prediction, using a single interface level opposite the metal Fermi level with the parameters shown, and the experimental results for the annealed diode at 269 K, 297 K, and 325 K.

the contact. As shown in Fig. 6, the position of the proposed state is opposite the metal Fermi level. Upon junction formation, the semiconductor bands bend until the Fermi level crosses the location of the state. Then any additional charge that needs to flow into the metal to achieve equilibrium will come from the changing occupancy of the state and the Fermi level will be pinned at this position. It is unknown whether the state is initially present on the silicon surface or induced during the nucleation and deposition processes. To determine the evolution of the state, the capacitance technique needs to be used in a layer by layer deposition scheme which is beyond our current capability.

This research was also supported by the Air Force Office of Scientific Research under Contract AFOSR-30602-85-C-0072 and by the National Science Foundation under Grants NSF-ECS 82-17677 and NSF-CDR 84-21402.

(1) W. Schottky, Naturwissenchafter 26, 843 (1938); A.M. Cowley and S.M. Sze, J. Appl. Phys. 36, 3212 (1965).

(2) J. Bardeen, Phys. Rev. 71, 717 (1947).

(3) P.S. Ho, P.E. Schmid, and H. Föll, Phys. Rev. Lett. 46, 782 (1981); P.E. Schmid, P.S. Ho, H. Föll, and G.W. Rubloff, J. Vac. Sci. Technol. 18, 937 (1981).

(4) G.W. Rubloff, Phys. Rev. B 25, 4307 (1982).

(5) H.C. Card and E.H. Rhoderick, J. Phys. D: Appl. Phys. 4, 1589 (1971).

(6) S.J. Fonash, J. Appl. Phys. 54, 1966 (1983).

(7) C. Barret, F. Chekir, and A. Vapille, J. Phys. C: Solid State Phys. 16, 2421 (1983).

(8) H.L. Evans, X. Wu, E.S. Yang, and P.S. Ho, Apply. Phys. Lett. 46, 486 (1985).

(9) W. Shockley and W.T. Read Jr., Physical Review 87, (1952); R.N. Hall, Phys. Rev. 87, 387 (1952).

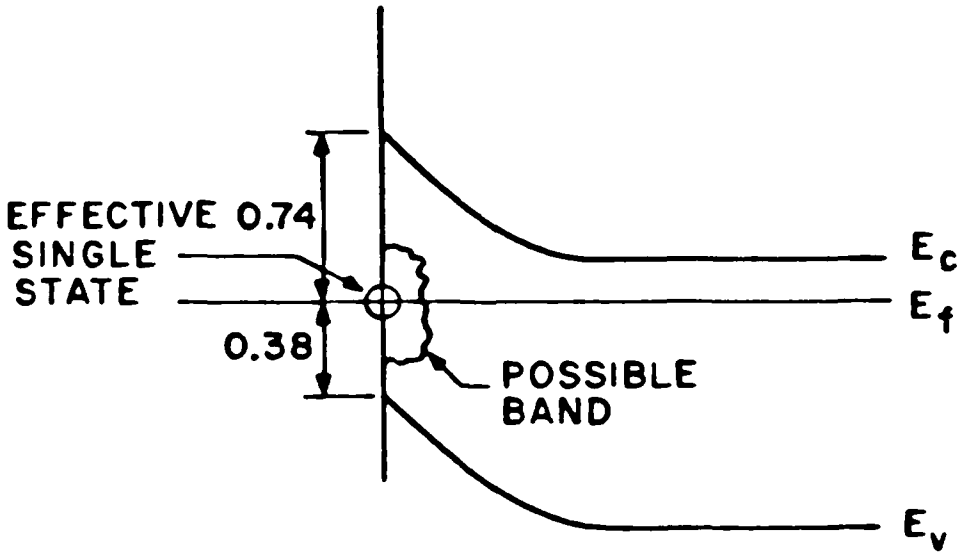

Figure 6: Position of the proposed bandgap states.

H. DEVICE FABRICATION FACILITY

(E.R. Fossum)
(JSEP work unit 4, 1985 - 1988)
(Principal Investigator: E.R. Fossum (212) 280-3107)

1. Low Energy Ion Beam Oxidation of Silicon -- The low energy ion beam oxidation of silicon, which has been demonstrated to produce very thin oxide films (40-70 Å) suitable for incorporation in MOSFET structures, has been studied. It has been found that the process is not particularly temperature sensitive and can produce high-quality oxides at room temperature. Furthermore, the growth process seems to be self-limiting so that the oxide thickness varies only by a few percent over a 200% change in dose. Thus, the ability to produce highly uniform films is enhanced. This may have technological significance.

Electrical characterization of the films has been performed using capacitance-voltage (1 MHz) and current-voltage techniques. The MOS structures typically exhibit a flat-band voltage of -0.5 volts, and a threshold voltage of -0.25 volts for a 50 Å film. The reverse leakage current of a MOSFET gate oxide is over three orders of magnitude less than the source-drain current of the transistor.

Chemical characterization of the ultra-thin layer of oxide was made possible through the use of the new ultra-high vacuum system and the collaboration of Dr. Chien-fan Yu. Auger electron spectroscopy (AES) was performed by sputtering away thf surface with an argon ion beam. The results indicate a nearly perfect match of the oxygen and silicon peak profiles between thermally grown SiO_2 and the oxide grown with the low energy ion beam. Angle resolved X-ray photoelectron spectroscopy (XPS) showed similar results, although there appears to be a higher suboxide population near the top surface of the film.

An ion implantation model has been proposed for this process. In this case, oxygen ions bombarding the surface implant themselves in the silicon crystal 10 to 20 Å deep and react with the silicon. The reaction with the silicon may be enhanced due to the damage (e.g. broken

bonds) caused by the implantation process. The thickness of the oxide is primarily determined by the range of the implanted ions, leading to an apparent self-limiting behavior of the growth process. We are currently investigating the ramifications implied by this mdoel. Preliminary results are mixed.

2. Gallium Arsenide Schottky Diode Leakage Current -- Schottky diodes fabricated on gallium arsenide often have anomalously high reverse current densities and exceed values expected from barrier height related calculations. Since the barrier height is pinned at approximately 0.8 eV, the reverse current does not have a strong dependence on gate metallization material. The consequences of such high reverse current is increased power consumption and the loss of opportunity to realize dynamic circuits which rely on conservation of gate charge.

In collaboration with J.M. Woodall at IBM Research (Yorktown), we have been investigating the reasons for such large current. One model of the GaAs-metal interface suggests that the barrier height is a microscopically varying quantity which depends on the presence or absence of arsenic microclusters at the interface. This variation can be expressed as an effective workfunction. Since arsenic microclusters dominate the interface, the effective workfunction is nearly independent of gate material.

We have been performing experiments to investigate this model. In particular, Al/GaAs Schottky diodes have been fabricated using molecular beam epitaxy (IBM) and electronically characterized (Columbia). Before the in-situ deposition of the metal gate, arsenic has been intentionally deposited on the surface of the GaAs. The leakage current of the treated diodes is reduced by nearly a factor of 25 compared to control devices. The barrier height extrapolated from the forward I-V also varies (approx. 50 mV) but this is not enough to explain the decrease in reverse current. Further experiments are underway.

This research was also supported by the National Science Foundation under Grant NSF-CDR 84-21402.

III. GENERATION AND DYNAMIC PROPERTIES OF METASTABLE SPECIES FOR QUANTUM ELECTRONICS AND LASER MICROPROCESSING

A. DIODE LASER PROBING OF VIBRATIONAL PRODUCT STATE DISTRIBUTIONS IN METAL-MOLECULE COLLISIONS: $Hg(6^3P_1)$-$CO_2(mn^{\ell}p)$

(B.B. Brady, G.B. Spector, L. Chia, G.W. Flynn)
(JSEP work unit 5, 1985 - 1988)
(Principal Investigator: G.W. Flynn (212) 280-4162)

1. Introduction — The quenching of the electronically excited states of atoms has been the subject of many studies.[1-12] A large r .r . atoms, diatomic and small polyatomic molecules have been used to quench the excited singlet, $Hg(6^1P_1)$, triplet, $Hg(6^3P_1)$, and metastable, $Hg(6^3P_0)$, states of mercury. The rate of depletion of Hg states was detected by either flashlamp absorption or laser-induced fluorescence (LIF), and the quenching cross section to the ground state or lower excited states was determined. In only a few cases, involving diatomic quenchers, have investigators looked at the states populated in the collider gas by the quenching process.[1,2,6] Polyatomic molecules, which have more than one vibrational degree of freedom, each with a different frequency, can yield more information about the quenching process and provide a better test of the theories which have been used to describe this phenomenon.[13,14] In order to take advantage of this increased information, however, a technique for probing various modes of a polyatomic quencher must be available. Such a technique has been recently developed[15,16,17] and used to study high energy collision events and photofragmentation processes.

The interaction of metals with molecules is also interesting because of its importance in catalysis. Small clusters of metal atoms have been investigated because they may be useful as models for catalysis at surfaces.[18,19] The properties of small metal clusters, however, vary greatly and in a seemingly random manner with size.[20-22] The interaction of individual metal atoms with molecules is thus important, and the investigation of such interactions is a logical first step toward understanding the catalytic activity of small metal clusters.

In this paper we have studied the internal excitation of CO_2 caused

by collisions with $Hg(6^3P_1)$. CO_2 was chosen because transitions involving a one-quantum change in its ν_3 mode have almost the largest absorption coefficient in the infrared (IR) spectral region. This fact, combined with the large number of such transitions (including hot bands) whose frequencies have been determined to a high degree of accuracy, makes CO_2 a particularly convenient quenching molecule to study using IR absorption techniques.[16]

Past experiments have shown that the rate of quenching of $Hg(6^3P_1)$ by CO_2 is extremely fast, taking place in approximately 4 gas kinetic collisions.[4,9-11]

$$Hg(6^3P_1) + CO_2 \text{ ----> } Hg(6^1S_0) + CO_2 \qquad (1)$$
$$Hg(6^3P_1) + CO_2 \text{ ----> } Hg(6^3P_0) + CO_2 \qquad (2)$$

In addition, most of the quenching is to the ground state with channel 2 above contributing less than 0.1% to the total quenching cross section.[3,10] Fig. 1 shows an energy level diagram for the Hg/CO_2 system. One other channel which has been studied and found to proceed with a quantum yield of less than 1% is the decomposition of CO_2 to CO.[5]

$$Hg(6^3P_1) + CO_2 \text{ ----> } HgO + CO \qquad (3)$$

This reaction has been found to have a CO quantum yield which increases as the square of the light intensity, and the mechanism has been postulated to involve a metastable CO_2 (perhaps a low-lying triplet state produced by process 1) undergoing collision with a second excited mercury atom.

$$Hg(6^3P_1) + CO_2 \text{ -----> } HgO + CO \qquad (4)$$

This metastable triplet has also been invoked to explain the dissociation of CO_2 in a shock tube and the recombination of $O(^3P)$ and CO to give CO_2.[23]

A significant advantage of studying CO_2 is that the asymmetric stretching vibration is metastable with respect to the bending/symmetric stretching vibrations. Approximately 30,000 collisions are required to

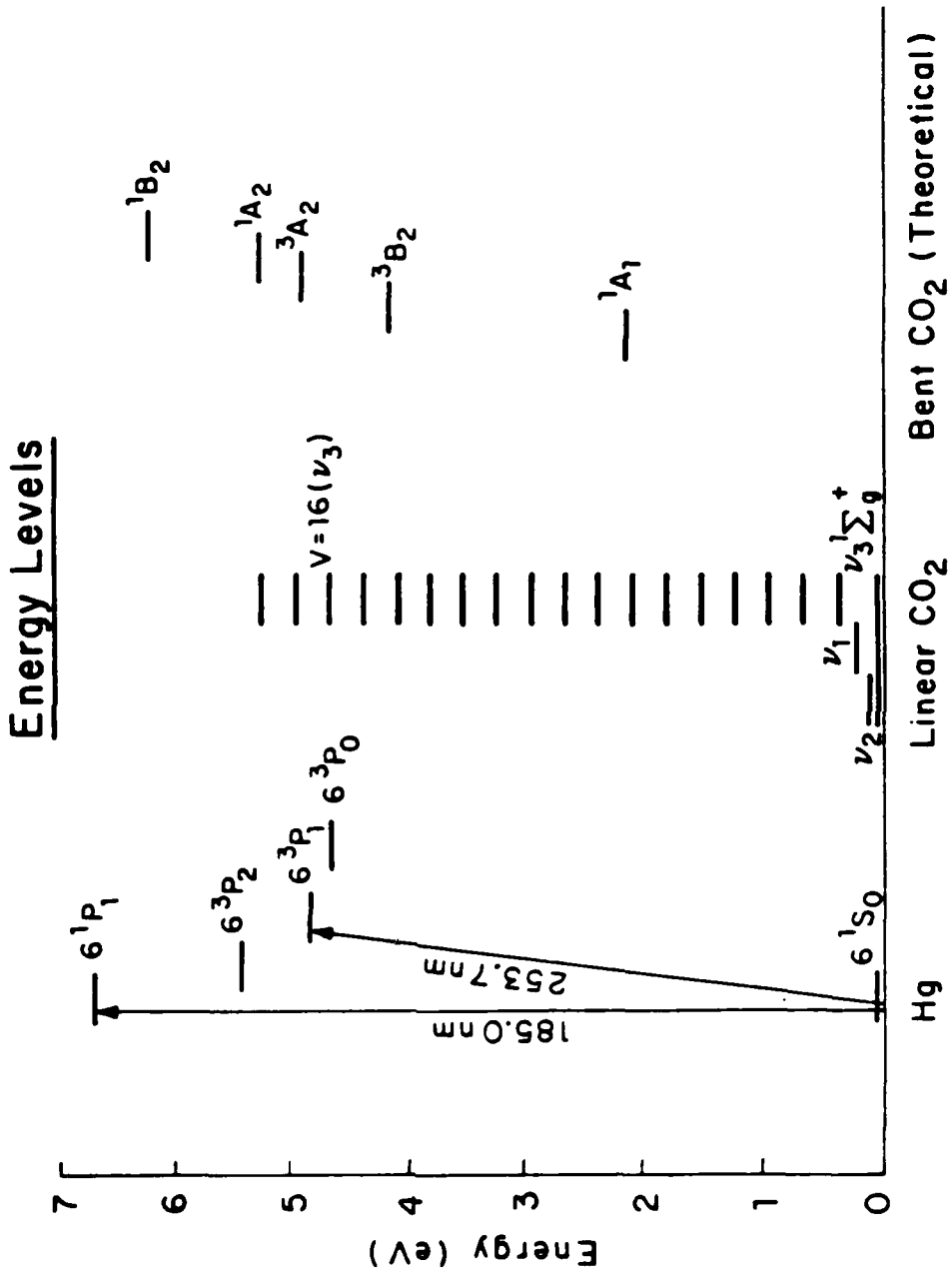
Energy Levels
Energy (eV)
0
1
2
3
4
5
6
7
Hg
Linear CO_2
Bent CO_2 (Theoretical)
6^1S_0
6^1P_1
6^3P_2
6^3P_1
6^3P_0
185.0 nm
253.7nm
ν_2
ν_1
$\nu_3{}^1\Sigma_g^+$
V=16(ν_3)
$^1B_2$
$^1A_2$
$^3A_2$
$^3B_2$
$^1A_1$

Figure 1

exchange energy between these modes.[24] Thus the asymmetric stretch and bending modes can be studied essentially independently and the importance of each in quenching can be assessed. The competition between these modes is particularly interesting since one is low frequency (667 cm^{-1}) and one is high frequency (2349 cm^{-1}). Theoretical calculations[13,14] indicate that low and high frequency modes should be affected very differently by quenching.

2. Experimental -- The diode laser probe technique used in our laboratory has been described in detail previously.[15,16,17] A Lambda Physik EMG 101 excimer laser, operating at 308 nm, 20 Hz, was used to pump an FL2002 dye laser. The output of the C-500 dye at 508 nm (10-15 mJ) was passed through a KPB crystal (Cleveland Optical Crystals) to obtain the second harmonic (254 nm, <.1 mJ). The doubled output of the dye was then tuned to coincide with the Hg absorption line at 253.7 nm. The excitation beam was passed through the sample cell collinearly with the diode laser probe beam by use of a MgF_2 optical flat coated to reflect the UV beam and pass the IR radiation.

3. Results -- A typical trace depicting the change in population of the 00^01 level due to Hg quenching is shown in Fig. 2. The rise, which corresponds to an increase in population of 00^01, can be observed in the lower panel (b). Similar traces were also taken monitoring 02^20. The rate of rise can be obtained from a non-linear least squares fit to an exponential function. A linear least-squares fit of the data points gives a slope which corresponds to a rate of $3.75 \pm .75 \times 10^{12}$ cc/molec-sec or 120 ± 24 $msec^{-1}$ $torr^{-1}$ (80 ± 17 gas kinetic collisions). Both the ν_3 and $2\nu_2$ rise time data fall on the same least squares line within experimental error.

By measuring the initial amplitude of the absorption increase (obtained by extrapolating the decay to time zero), a value for the number of vibrationally excited CO_2 molecules produced per excited Hg atom can be determined. The number of quanta in the ν_3 mode per laser shot was calculated from the intensity of the diode laser at the detector before the dye laser fires (I(4.3 μm)), the change in diode laser intensity after the dye laser fires (ΔI(4.3 μm)), the volume of

PRODUCTION OF CO_2 ν_3 ANTI-SYMMETRIC STRETCHING EXCITATION VIA QUENCHING OF $Hg^*(6^3P_1)$

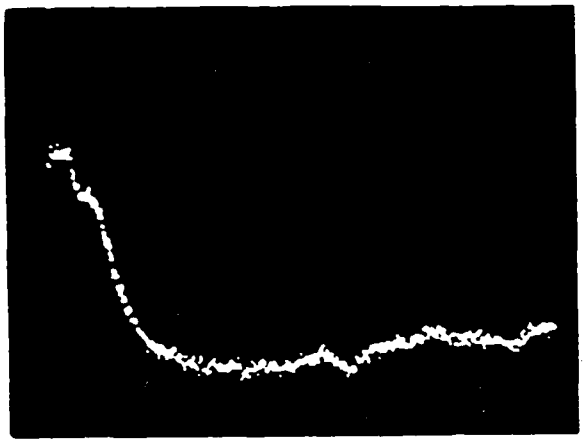

$00°1 \longrightarrow 00°2$ P(15)

P_{CO_2} = 1.0 torr

Time base = 51.2μs

1024 shots

Laser Fires

$00°1 \longrightarrow 00°2$ P(15)

P_{CO_2} = 9.86 torr

Time base = 409.6μs

1024 shots

Figure 2

the diode laser irradiation zone, and the absorption coefficient for the CO_2 line probed.[16] The number of excited Hg atoms is measured from the difference in the intensity of the dye laser after it passes through the cell with and without mercury present, ($\Delta I(254\ nm)$).

The number of quanta of ν_3 per excited Hg, $n_{00}{}^0{}_1/N_{Hg}$, was found to be $0.56 \pm .15$ (1 standard deviation) for a pressure of 1.0 torr of CO_2.

The measured rate of increase for the CO_2 vibrational energy (80 collisions) is much slower than the quenching rate k_1 (4 collisions). Thus the growth rate of CO_2 vibrational population corresponds to k_{16}, the quenching of a metastable state of CO_2, a quantity for which no previous measurements have apparently been made.

4. Discussion -- The major features of the present experimental study are as follows: (1) although the $Hg(6^3P_1)$ state is quenched by CO_2 in approximately four gas kinetic collisions, nearly 80 collisions are required for the electronic energy of mercury to show up in the low lying vibrational states of CO_2; (2) if loss of Hg electronic energy due to spontaneous emission is properly accounted for, greater than 56% of the available energy initially placed in the 6^3P_1 state by laser pumping is recovered as vibrational energy of CO_2; (3) each excited Hg atom produces 0.60 antisymmetric stretch (ν_3) quanta and 24.2 bending (ν_2) quanta; (4) the rate of filling of both the bending and antisymmetric stretch levels of CO_2 is identical within experimental error (80 collisions) even though nearly 30,000 CO_2/CO_2 collisions are required to equilibrate the bending and asymmetric stretch modes for low levels of vibrational excitation. These results clearly indicate that the mercury quenching process produces a metastable state which subsequently feeds the low lying vibrational states of CO_2.

Based on the above arguments, a tentative overall scheme for the quenching of $Hg(6^3P_1)$ by CO_2 can be proposed and is described by the following equations:

$$Hg(6^1S_0) + h\nu(254nm) \longrightarrow Hg(6^3P_1) \qquad \text{(Excitation)}$$

$$Hg(6^3P_1) + CO_2(000) \longrightarrow Hg(6^1S_0) + CO_2(^3B_2) \qquad \text{(Quenching)}$$

$$CO_2(^3B_2) + CO_2(000) \longrightarrow CO_2(mn^{\ell}p) + CO_2 \qquad \text{(Intersystem Crossing)}$$

$$CO_2(mn^{\ell}p) + CO_2(000) \longrightarrow CO_2(mn\text{-}1^{\ell}p) + CO_2(01^10) \qquad \text{(Harvesting)}$$

$$CO_2(mn^{\ell}p) + CO_2(000) \longrightarrow CO_2(mn^{\ell}p-1) + CO_2(001) \quad \text{(Harvesting)}$$
$$CO_2(mn^{\ell}p) + CO_2(000) \longrightarrow CO_2(m-1n^{\ell}p) + CO_2(100) \quad \text{(Harvesting)}$$

The identification of the metastable CO_2 state as $^3B_2$ is of course only a hypothesis at this point. As noted above, other CO_2 triplet states have been calculated to be too high in energy to be populated during collisions with mercury.[24] Furthermore, the identification of the metastable as an excited electronic state is also tentative until spectroscopic proof of its existence is forthcoming.

Assuming that the present tentative explanation for quenching of Hg through the CO_2 triplets is correct, the collisional lifetime of the CO_2 triplet corresponds to 80 CO_2/CO_2 collisions. This is comparable to the collision controlled lifetime of the SO_2 triplet states.[7] Because of the highly bent nature of the triplet state in CO_2, the radiative lifetime is expected to be quite long due to poor Franck-Condon factors.

5. Conclusions

1) Although the quenching of $Hg(6^3P_1)$ by CO_2 takes place in 4 gas kinetic collisions, 80 collisions are required for the mercury electronic energy to show up in the low lying vibrational levels of CO_2. This suggests the existence of a metastable state of CO_2 which is produced by the quenching process.

2) Both the ν_2 bending mode and the ν_3 antisymmetric stretching mode of CO_2 are filled at the same 80 gas kinetic collision rate during the quenching process, suggesting that both modes are filled from a common origin.

3) For each electronically excited mercury atom quenched by a CO_2 molecule, 24.2 ± 7.2 quanta of bending excitation and 0.60 ± 0.16 quanta of antisymmetric stretch excitation are produced in CO_2, suggesting that statistical considerations based on the density of vibrational states play at least some role in the partitioning of energy among the vibrational modes.

4) The conversion of mercury electronic energy into CO_2 vibrational energy appears to be quite efficient. If radiative loss due to spontaneous emission from Hg is properly accounted for, in excess of 56% of the mercury electronic energy is converted to CO_2 vibrational

energy.

5) Based on the above observations, the metastable state of CO_2 produced in the Hg quenching process is tentatively identified as CO_2 ($^3B_2$) which has been calculated to have an energy of 33,653 cm^{-1}. Production of triplet CO_2 allows spin to be conserved during the quenching of Hg. This postulate also agrees well with earlier photochemical data in which triplet CO_2 has been suggested as an intermediate in the two photon production of CO from Hg, CO_2, and light. Definitive confirmation of the nature of the metastable CO_2 level awaits spectroscopic detection of this interesting species.

This research was also supported by the National Science Foundation under Grants NSF-CHE 85-17460 and NSF-CHE 80-23747 and by the Department of Energy under Contract DE-AC02-78-ER-04940.

(1) G. Karl, P. Kruus and J. Polanyi, J. Chem. Phys. 46, 224 (1967); G. Karl, P. Kruus, J. Polanyi and W. Smith, J. Chem. Phys. 46, 244 (1967).

(2) Y. Fushiki and S. Tsuchiya, Chem. Phys. Lett. 22, 47 (1973).

(3) H. Horiguchi and S. Tsuchiya, Bull. Chem. Soc. Japan 44, 3221 (1971).

(4) A. Vikis, G. Torrie and D. LeRoy, Can. J. Chem. 50, 176 (1972).

(5) O. Strausz and H. Gunning, Can. J. Chem. 39, 2244 (1961).

(6) G. Karl and J. Polanyi, J. Chem Phys. 38, 271 (1963).

(7) H. Okabe, Photochemistry of Small Molecules (J. Wiley and Sons, New York), 1978.

(8) J. Calvert and J. Pitts, Jr., Photochemistry (J. Wiley and Sons, New York), 1966.

(9) R. Cvetanovic, Prog. React. Kinet. 2, 39 (1964).

(10) A. Callear and J. McGurk, J. Chem Soc. Faraday Trans 2 69, 97 (1973).

(11) J. Deech, J. Pitre and L. Krause, Can. J. Phys. 49, 1976 (1971).

(12) H. Horiguchi and S. Tsuchiya, Bull. Chem. Soc. Jap. 47, 2768 (1974).

(13) R. Levine and R. Bernstein, Chem. Phys. Lett. 15, 1 (1972).

(14) M. Gonzalez, G. Karl and P. Watson, J. Chem. Phys. 57, 4054 (1972).

(15) C.F. Wood, J.A. O'Neill, and G.W. Flynn, Chem. Phys. Lett. 109, 317 (1984).

(16) J. Chu, C. Wood, G. Flynn, and R. Weston, Jr. J. Chem. Phys. 81, 5533 (1984).

(17) J. Chu, C. Wood, G. Flynn and R. Weston, Jr., J. Chem. Phys. 80, 1703 (1984).

(18) L.S. Brown and S.L. Bernasek, J. Chem. Phys. 82, 2110 (1985).

(19) S.L. Bernasek and S.R. Leone, Chem. Phys. Lett. 84, 401 (1981).

(20) R.E. Smalley, Laser Chemistry 2, 167 (1983).

(21) A. Kaldor, E. Rohlfing, and D.M. Cox, Laser Chemistry 2, 185, (1983).

(22) E. Parks, K. Liu, S. Richtsmeier, L. Pobo and S. Riley, J. Chem. Phys. 82, 5470 (1985).

(23) M.C. Lin and S.H. Bauer, J. Chem. Phys. 50, 3377 (1969).

(24) W. England, B. Rosenberg, P. Fortune and A. Wahl, J. Chem. Phys., 65, 684 (1976).

B. IR DIODE LASER STUDIES OF CO_2 VIBRATIONAL DISTRIBUTIONS PRODUCED BY UV EXCIMER LASER PHOTOFRAGMENTATION OF PYRUVIC ACID

(J.A. O'Neill, T.G. Kreutz, G.W. Flynn)
(JSEP work unit 5, 1985 - 1988)
(Principal Investigator: G.W. Flynn (212) 280-4162)

1. Introduction -- In recent years, the photodissociation dynamics of many small molecules has become a subject of great interest.[1-5] Measurements of fragment energy distributions and angular orientations have yielded a wealth of state-specific experimental information about these dissociation processes. Such information can provide insight into the geometry of the dissociating species and the nature of the potential energy surfaces involved.[3-5] Also, theoretical models involving "half-collision" arguments and molecular dynamics on potential energy surfaces have been developed to a high degree of refinement. The vast majority of this experimental and theoretical work has sought to provide a detailed interpretation of the dissociation dynamics of predominantly diatomic and triatomic species, while the photolysis of most larger polyatomic molecules is less well understood.

Of particular interest in photofragmentation processes are experimental studies of vibrational energy disposal that yield information about mode-specific excitation of photolysis products, which can in some cases be extrapolated back to provide an understanding of the dissociation mechanism.[6-8] A variety of techniques, including infrared fluorescence, laser-induced fluorescence and infrared laser absorption, have been employed to probe these product state energies.[1] A new technique which is presently being developed in our laboratory investigates various dynamic molecular processes using a tunable diode laser absorption probe.[9-11] This technique has been employed previously to monitor the time resolved IR absorption of CO_2 molecules undergoing collisions with fast hydrogen and deuterium atoms as well as with electronically excited mercury, NO_2 and azulene.[9-14] The high resolution (0.0003 cm^{-1}) and wide tunability of the laser makes rotationally state-specific studies possible in a wide variety of molecules. Also, through the proper choice of absorption transition, any vibrational state of a molecule can be studied. In the case of CO_2,

all the ro-vibrational levels in the molecule can be probed by taking advantage of the strong ν_3 absorption coefficient and the anharmonicities inherent in the molecule and by tuning the diode laser to a transition of the type:

$$CO_2(mn^{\ell}p,J) + h\nu(4.3\ \mu m) \longrightarrow CO_2(mn^{\ell}p+1,J+1) \qquad (1)$$

The letters m,n,p and J are the quantum numbers for the symmetric stretching, bending, and antisymmetric stretching vibrations, and the rotational motion of the molecule.

In the present experiments, the UV photolysis of pyruvic acid is studied by monitoring the IR absorption of its CO_2 dissociation product. Pyruvic acid has been studied in both the gas and liquid phases, and it is found to undergo both thermal and photochemical decomposition to yield predominantly acetaldehyde and CO_2.[15-20] A previous experiment, which examined the vapor phase photolysis of pyruvic acid at 366 nm measured a small amount (1-2%) of methane and carbon monoxide among the photolysis products.[18] Several mechanisms for the dissociation of this molecule have been proposed. One of these involves a four-center mechanism which leads to the direct production of acetaldehyde and CO_2, while another involves a five-center process which yields an hydroxycarbene intermediate species. A recent experiment which measured the 4.3 μm CO_2 IR fluorescence as a function of dissociation wavelength supports the five-center mechanism involving the hydroxycarbene intermediate.[19] In another experiment, the infrared multiphoton decomposition of pyruvic acid was observed, and the results of this work suggest that the dissociation process occurs by unimolecular decomposition in high vibrational levels of the ground electronic state.[21] It is also thought that the UV photolysis of pyruvic acid procedes through an internal conversion step where highly vibrationally excited ground state molecules decompose to form acetaldehyde and CO_2.[19]

In the present experiments, the diode laser absorption probe is employed to monitor the vibrational states of CO_2 which are produced in the 193 nm photolysis of pyruvic acid. Previous work on this system in our laboratory investigated the relative production of CO_2 ν_2 bending and ν_3 antisymmetric stretching quanta after the photofragmentation process by probing the $01^10 \rightarrow 01^11$ and $00^01 \rightarrow 00^02$ transitions in the

molecule. The present work investigates the distribution of energy in the CO_2 bending, stretching and combination state manifolds by examining such overtone levels as 02^20, 03^30, 04^40, 00^02, 00^03, 01^11 and 02^21 as well as the 00^00 ground state. Also, the rotational resolution of the diode laser is used to obtain preliminary information concerning the degree of rotational excitation in the CO_2 photofragment.

2. Experimental -- These experiments are similar to several previous IR diode-UV excimer laser double resonance experiments carried out in our laboratory.[9-11,14] The details of these types of experiments have been discussed previously, and only the new features will be described here. The photolysis mixture, consisting of either neat pyruvic acid or pyruvic acid and argon, flows through a cylindrical gas sample cell 207 cm long (see Fig. 1). The cw output of a tunable IR diode laser (Laser Analytics) operating at about 4.3 μm and the pulsed output of a UV excimer laser (Lambda Physik) operating at 193 nm are collinearly propagated through the cell by the use of an IR transparent MgF_2 beamsplitter coated for high reflectivity at 193 nm. The excimer laser is operated in an unstable resonator configuration which minimizes the divergence of the UV beam in the far field and allows for the propagation of the photolysis beam over the long distances (5-7 m) necessary for the present experiments. Changes in the absorption of the diode laser beam caused by CO_2 which is produced in the photolysis process are monitored with an InSb liquid nitrogen cooled infrared detector and matched amplifier (300 nsec response time). The signals are temporally resolved with a Biomation 8100 transient recorder and signal averaged with a Nicolet 1174 averager. Analysis of time-resolved signals is performed on a Vax 11/780 computer.

Using a 207 cm cell at a CO_2 pressure of 10 torr, where pressure broadening begins to make the direct spectral observation of weak absorption features difficult, the present apparatus can be used to detect the presence of molecules in states whose ambient population at room temperature is about 5×10^{-6} that in the ground state. This makes the direct spectral observation of such states as 00^02 and 01^11 very difficult using our conventional phase-sensitive detection techniques. In order to locate and identify transitions corresponding to states with

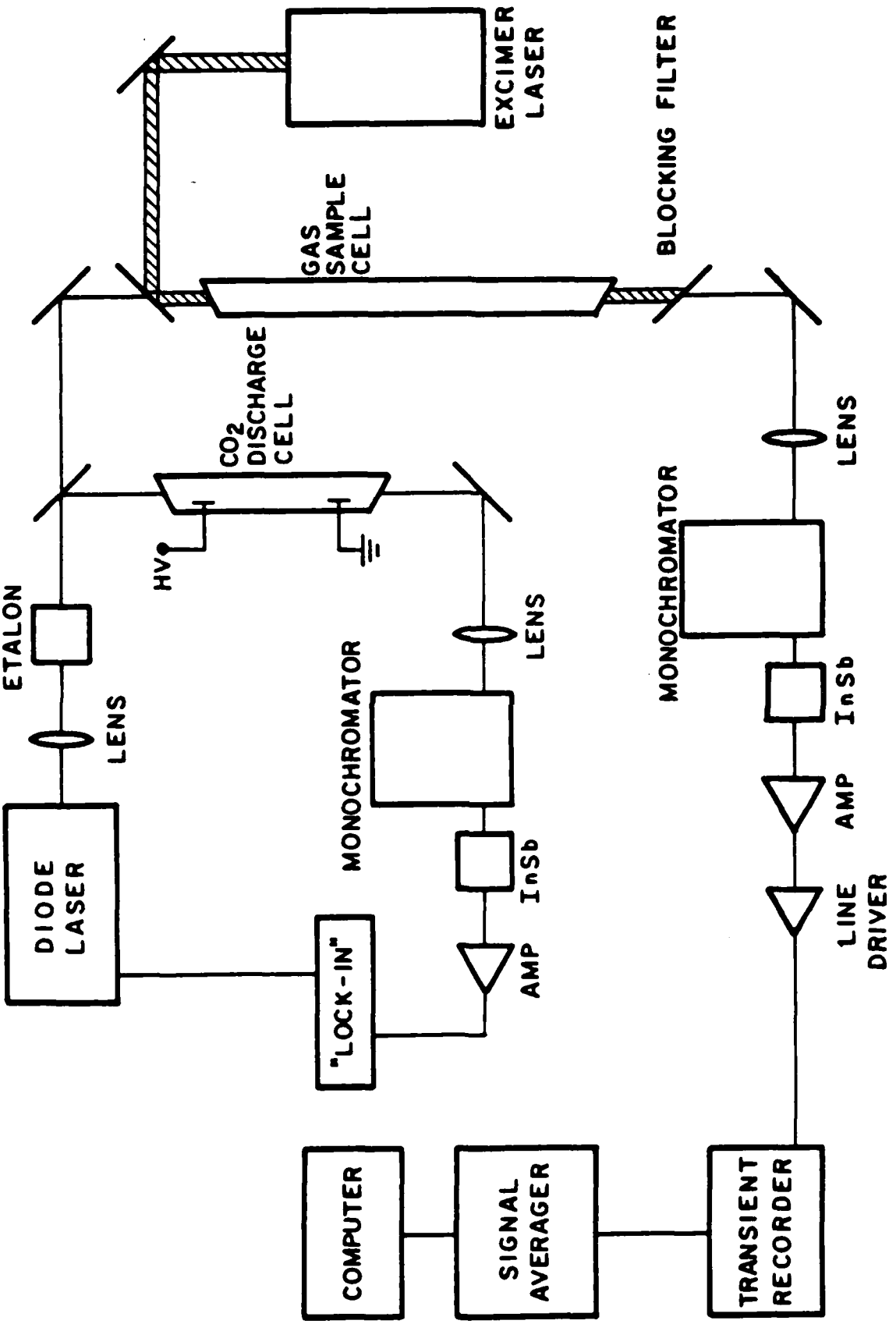
EXCIMER LASER
GAS SAMPLE CELL
BLOCKING FILTER
CO_2 DISCHARGE CELL
HV
ETALON
LENS
DIODE LASER
"LOCK-IN"
MONOCHROMATOR
LENS
InSb
AMP
MONOCHROMATOR
LENS
InSb
AMP
LINE DRIVER
COMPUTER
SIGNAL AVERAGER
TRANSIENT RECORDER

Figure 1

such a small ambient population, a technique was employed which selectively populates these high levels. This method involves the use of a high voltage dc CO_2 discharge cell similar to that described by Dang et al, through which 8% of the diode laser beam is diverted (see Fig. 1).[22,23] The discharge excites via "anharmonic pumping" those states in the molecule which contain ν_3 quanta. Fig. 2 presents typical absorption spectra observed through the auxiliary cell with the discharge both on and off. Under conditions where the high voltage is applied, the ν_3 mode temperature is selectively increased to approximately 2000 K making such transitions as $00^03 \rightarrow 00^04$ readily observable. (At 300 K there is less than 1 molec./cm^3 in a given rotational level of the 00^03 vibrational state!) Using this technique we have been able to populate and identify highly vibrationally excited levels such as 05^50 and 00^04. This auxiliary cell also allows for the frequency stabilization of the diode laser on a specific spectral line over long periods of time through the use of a lock-in amplifier and a feedback loop which corrects for any drift in the controlling current (frequency) of the diode laser.

In order to account for the shot to shot instabilities of our excimer laser photolysis source, part of the UV beam is diverted to a Gentec power meter, and the total number of photons entering the cell during a given experimental run is counted using a signal averager. The data is subsequently normalized by this factor. In the present experiments, relative vibrational population changes are obtained for various vibrational states in CO_2 through a comparison of the observed transient absorption intensities caused by the photolysis process.

The pyruvic acid used in these experiments (Aldrich 98%) was purified by repeated fractional distillation under partial vacuum conditions, and NMR techniques were used to detect the presence of major contaminant species such as acetaldehyde. In order to flow different mixtures of pyruvic acid and argon through the sample cell, a mixing chamber was designed which allows various amounts of Ar to flow across a reservoir of the liquid acid while maintaining a constant pressure of 5 torr in the cell. In each mixture, the partial pressure of pyruvic acid was determined by calibration of the transient signal observed under photolysis conditions with those obtained with a known pressure of

CO_2 DISCHARGE CELL ABSORPTION SPECTRUM

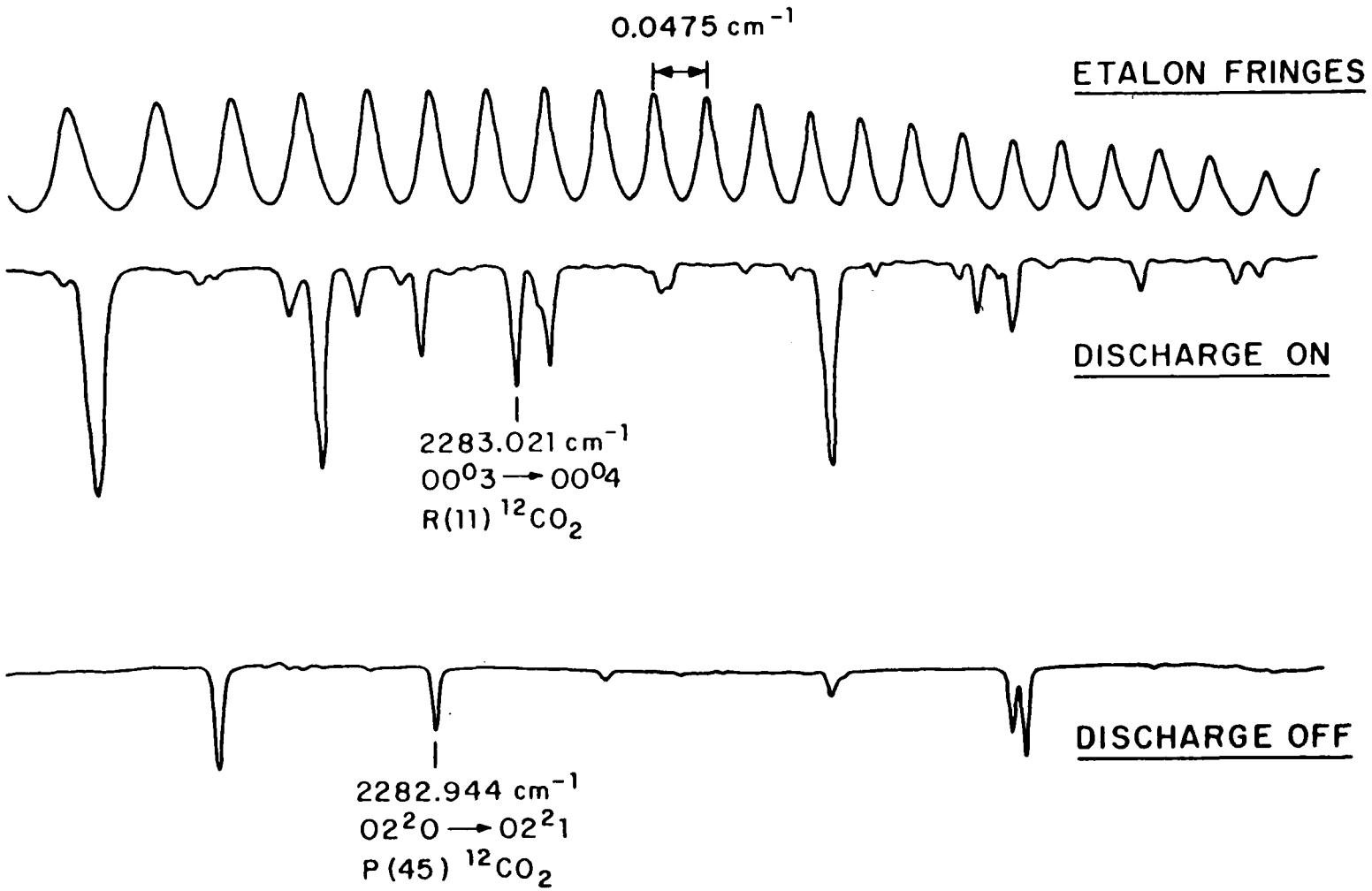

Figure 2

pure pyruvic acid in the cell.

3. Results -- Upon 193 nm irradiation of pyruvic acid, we observed transient IR absorption signals for the following transitions in CO_2:

$00^00 \rightarrow 00^01$ P(60)	$00^01 \rightarrow 00^02$ P(37)
$01^10 \rightarrow 01^11$ P(49),P(35),P(30)	$00^02 \rightarrow 00^03$ P(10)
$02^20 \rightarrow 02^21$ P(37),P(22),P(17)	$00^03 \rightarrow 00^04$ R(23)
$03^30 \rightarrow 03^31$ P(24),P(8)	$01^11 \rightarrow 01^12$ P(8)
$04^40 \rightarrow 04^41$ P(10)	$02^21 \rightarrow 02^22$ P(10)
$00^00 \rightarrow 00^01$ R(40), $^{13}CO_2$	

The absorption signals obtained in these experiments are actually a measure of the difference in population between the upper and lower levels of any given transition ($N_\ell - N_u$). In order to determine the absolute population change in a particular level, the following relation can be used:[23]

$$N_{mn^\ell p} = \Sigma(N_{mn^\ell p'} - N_{mn^\ell p'+1}) \qquad (2)$$

It is usually the case that only the first few terms contribute to this sum, and these levels are easily probed with the diode laser. In the present experiments, the contributions of the upper states to the transitions which originate on the bending mode states (01^10, 02^20, 03^30) are determined by examining transitions such as $01^11 \rightarrow 01^12$ and $02^21 \rightarrow 02^22$. For the bending states, the population of the upper energy state of each pair was always found to be much smaller than the population of the lower energy state; however, corrections were made for the upper state contributions in all calculations of nascent vibrational populations determined in these experiments.

A) Bending Excitation in the CO_2 Photoproduct

Typical signals obtained while monitoring the bending mode vibrations (01^10, 02^20, 03^30, 04^40) in CO_2 immediately after the UV photolysis of neat pyruvic acid at pressures of 0.04-0.5 torr demonstrate an initial prompt rise which is limited by the response time of the detector.

In order to carry out an accurate determination of the relative population distribution among the vibrational levels in CO_2 after the photolysis process, it is necessary to insure that the rotational

distribution within each vibrational state is completely relaxed. Studies were performed on mixtures of pyruvic acid (40 mtorr) in a large excess of Ar (1-10 torr), and it was determined that at Ar pressures of 5 torr rotational equilibration in all CO_2 vibrational states was essentially complete within the risetime of the detector. Fig. 3 presents the results of these relative nascent vibrational population measurements for the 01^10, 02^20, 03^30 and 04^40 bending states of CO_2. This figure illustrates that while the number of molecules produced in each of the higher bending states decreases with increasing energy, it falls off much more slowly than does the room temperature Boltzmann distribution for the bending mode of CO_2.

B) Antisymmetric Stretching Excitation in the CO_2 Photoproduct

Transient absorption signals obtained while monitoring the 00^01, 00^02 and 00^03 antisymmetric stretching states in CO_2 immediately following the photodissociation process demonstrate an initial change in absorption which is detector limited followed by a much slower process of large amplitude. The fast rise observed in these signals is attributed to CO_2 molecules which are directly produced in this antisymmetric stretching vibration as a result of the photolysis process. The nascent population distributions for these levels are presented in Fig. 3. These results indicate that while the absolute number of molecules produced in each of the antisymmetric stretching states is much less than that found in the vibrational states of the bending manifold, the relative number of molecules within the stretching mode suggests a distribution which is substantially hotter than that indicated by the ν_2 bending states.

C) Bend/Stretch Excitation in the CO_2 Photoproduct

In order to examine the excitation of bend/stretch combination states in the CO_2 photoproduct, the 01^11-->01^12 and 02^21-->02^22 transitions were monitored directly. Population distributions for the 01^11 and 02^21 levels are also presented in Fig 3.

D) Formation of Ground State CO_2 (00^00) Photoproduct

In order to determine whether any of the CO_2 produced in the UV

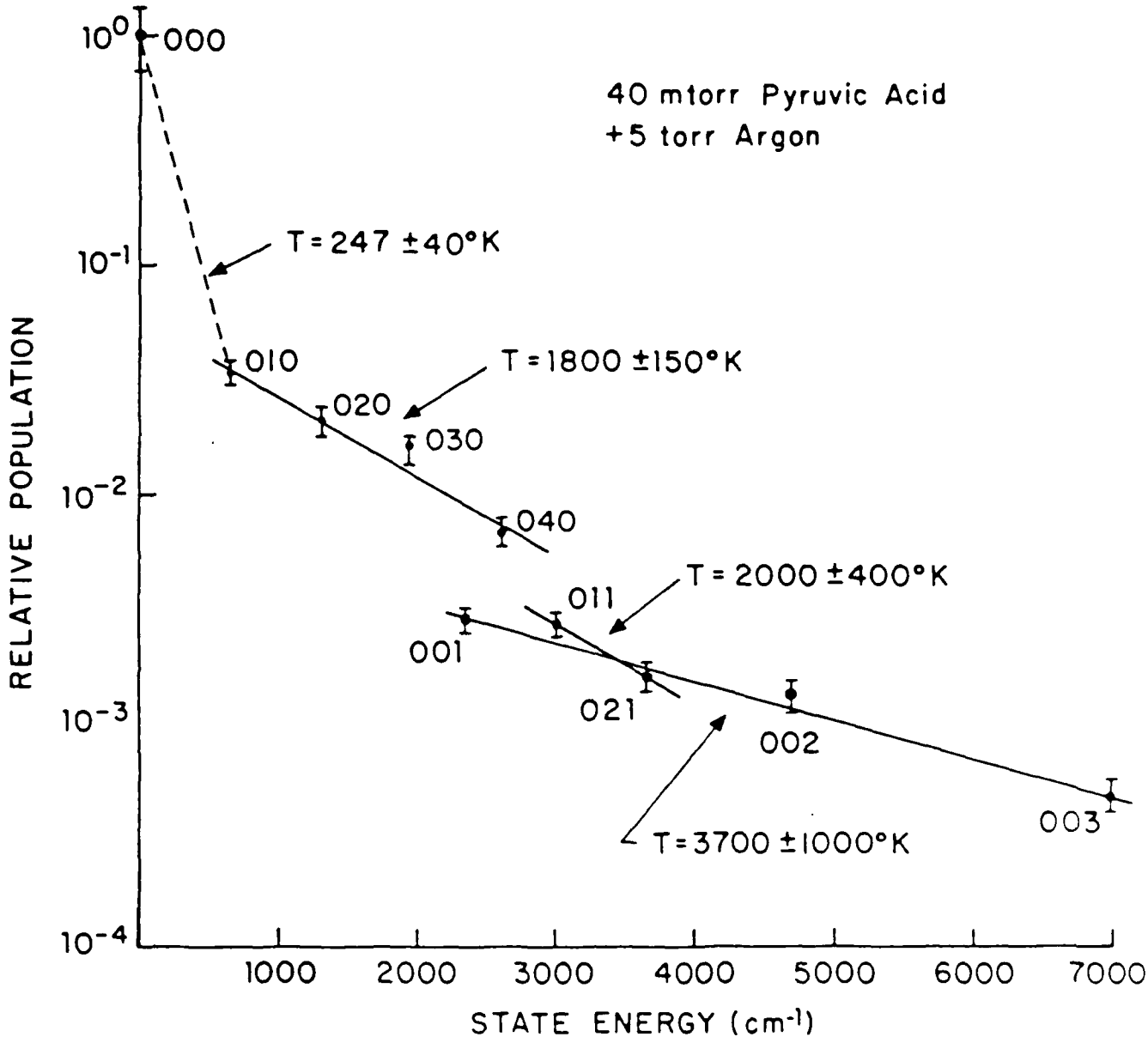
PYRUVIC ACID PHOTOLYSIS
NASCENT CO_2 VIBRATIONAL DISTRIBUTION
40 mtorr Pyruvic Acid
+5 torr Argon
T = 247 ±40°K
T = 1800 ±150°K
T = 2000 ±400°K
T = 3700 ±1000°K
000
010
020
030
040
001
011
021
002
003
RELATIVE POPULATION
STATE ENERGY (cm^{-1})
10^0
10^{-1}
10^{-2}
10^{-3}
10^{-4}
1000
2000
3000
4000
5000
6000
7000

Figure 3

photolysis of pyruvic acid is formed with no vibrational motion, the 00^00 ground state of the molecule was examined directly by monitoring the $00^00 \rightarrow 00^01$ transitions which originate on very high rotational levels (J = 60) or which correspond to the less abundant isotopic $^{13}CO_2$ species (1% natural isotopic abundance).

Present experimental results which examine the $00^00 \rightarrow 00^01$ transition in $^{13}CO_2$ reveal an initial prompt change in absorption of very large amplitude after the excimer laser photolysis pulse. Relative population measurements show that the number of molecules directly formed in this state during the photolysis process is approximately 30-40 times that produced in the 01^10 bending state (see Fig. 3).

4. Conclusions

1) A tunable IR diode laser absorption probe technique was employed to examine nascent vibrational population distributions in the CO_2 photoproduct resulting from the 193 nm laser photolysis of pyruvic acid.

2) The majority of the CO_2 product is formed directly in the vibrationless ground state, and only a small fraction of molecules are produced with a significant degree of vibrational excitation (N_{000}/N_{010} = 30 - 40).

3) Without considering the molecules formed in the ground state of CO_2, the vibrational distribution among the excited states of the molecule indicates the following mode temperatures:

$$T(\nu_2) = 1800 \pm 150 \text{ K}$$
$$T(\nu_3) = 3700 \pm 1000 \text{ K}$$
$$T(\nu_2+\nu_3) = 2000 \pm 400 \text{ K}$$

4) The present data suggests that the ground state and bending states of CO_2 are formed with a significant degree of rotational excitation.

5) The observed nascent distribution of population among the vibrational states of the CO_2 photoproduct is not consistent with a statistical model which is expected to apply to a unimolecular decomposition process. The present data suggests a dissociation process with striking dynamical constraints which may procede through more than a single photolysis channel.

6) The vibrational excitation of the CO_2 fragment accounts for only a small fraction of the energy available in the dissociation process. The remaining available energy is sufficient to produce an electronically excited acetaldehyde species as well as fragmentation of the acetaldehyde molecule (see Fig. 4).

7) Further experiments are planned to examine the nascent rotational distributions in various vibrational states of CO_2 after the UV photolysis of pyruvic acid. Future work will also study changes in the Doppler linewidth of the nascent CO_2 product in order to gain information about the translational recoil velocity of the receding fragments.

This research was also supported by the National Science Foundation under Grants NSF-CHE 85-17460 and NSF-CHE 80-23747 and by the Department of Energy under Contract DE-AC02-78-ER-04940.

(1) S.R. Leone, Adv. Chem. Phys. 50, 255 (1982).

(2) R. Bersohn, J. Phys. Chem. 88, 5145 (1984).

(3) W.M. Gelbart, Ann. Rev. Phys. Chem. 28, 323 (1982).

(4) K.F. Freed and Y.B. Band, in: Excited States, Vol. 3, ed. E.L. Lim (Academic Press, New York, 1977) p.110.

(5) M. Shapiro and R. Bersohn, Ann. Rev. Phys. Chem. 33, 409 (1982).

(6) W.H. Hermann and S.R. Leone, J. Chem. Phys. 76, 4759 (1982).

(7) W.H. Hermann and S.R. Leone, J. Chem. Phys. 76, 4766 (1982).

(8) S.L. Baughcum and S.R. Leone, Chem. Phys. Lett. 89, 183 (1982).

(9) J.O. Chu, C.F. Wood, G.W. Flynn and R.E. Weston, Jr., J. Chem. Phys. 80, 1703 (1984).

(10) J.O. Chu, C.F. Wood, G.W. Flynn and R.E. Weston, Jr., J. Chem. Phys. 81, 5533 (1986).

(11) J.A. O'Neill, J.Y. Cai, G.W. Flynn and R.E. Weston Jr., J. Chem. Phys. 84, 50 (1986).

(12) B.B. Brady, G.B. Spector, L. Chia and G.W. Flynn, manuscript in preparation.

(13) B.B. Brady, L. Chia and G.W. Flynn, work in progress.

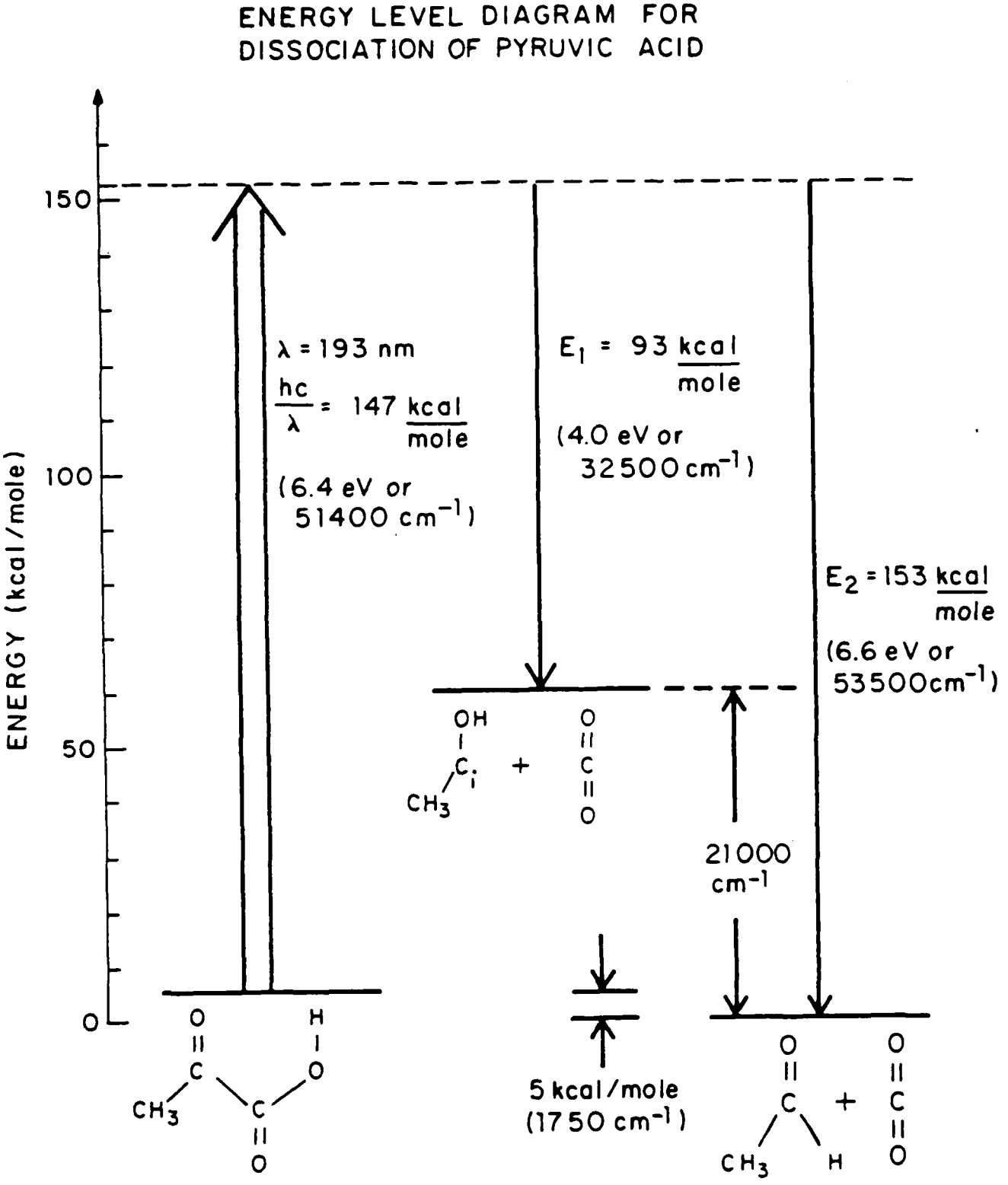
ENERGY LEVEL DIAGRAM FOR
DISSOCIATION OF PYRUVIC ACID
ENERGY (kcal/mole)
150
100
50
0
λ = 193 nm
hc/λ = 147 kcal/mole
(6.4 eV or
51400 cm⁻¹)
E1 = 93 kcal/mole
(4.0 eV or
32500 cm⁻¹)
E2 = 153 kcal/mole
(6.6 eV or
53500 cm⁻¹)
21000
cm⁻¹
5 kcal/mole
(1750 cm⁻¹)

Figure 4

(14) W. Jalenak, R.E. Weston, Jr., T.J. Sears and G.W. Flynn J. Chem. Phys. 83, 6049 (1985).

(15) M. Urion, Ann. Chem. 1, 5 (1934).

(16) J.F. Arnett, D.B. Larson and S.P. McGlynn, J. Am. Chem. Soc. 95, 7599 (1973).

(17) P.A. Leermakers and G.F. Versley, J. Am. Chem. Soc. 85, 3776 (1963).

(18) G.F. Versley and P.A. Leermakers, J. Phys. Chem. 68, 2364 (1964).

(19) R.N. Rosenfeld and B. Weiner, J. Am. Chem. Soc. 105, 3485 (1983).

(20) C.F. Wood, J.A. O'Neill and G.W. Flynn, Chem. Phys. Lett. 109, 317 (1984).

(21) J.L. Beuchele, E. Weitz and F.D. Lewis, Chem. Phys. Lett. 77, 280 (1981).

(22) T.G. Kreutz, J.A. O'Neill and G.W. Flynn, manuscript in preparation.

(23) C. Dang, J. Reid and B.K. Garside, Appl. Phys. B 27, 145 (1982).

C. DIODE LASER ABSORPTION PROBE OF V-V ENERGY TRANSFER IN CO_2

(T.G. Kreutz, J.A. O'Neill, G.W. Flynn)
(JSEP work unit 5, 1985 - 1988)
(Principal Investigator: G.W. Flynn (212) 280-4162)

1. Introduction -- The CO_2 laser is one of the most powerful and efficient laser systems ever developed.[1] Consequently, the dynamics of both pulsed and cw CO_2 lasers have been the subject of extensive research for many years.[2-3] The behavior of these systems is now rather well understood, and kinetic models agree well with experimental results. These models are based upon numerous rate contants for vibration-to-vibration (V-V) and vibration-to-translation (V-T) energy transfer between CO_2, N_2, and rare gases, values for which have been measured in infrared fluorescence and CO_2 laser double resonance studies. Perhaps the most fundamental V-V energy transfer process in CO_2 is the near resonant "collisional uppumping" process:

$$CO_2(00^01) + CO_2(00^01) \rightleftarrows CO_2(00^02) + CO_2(00^00) \quad \Delta\varepsilon = -25 \text{ cm}^{-1} \qquad (1)$$

which serves as a model for how vibrational energy is rapidly distributed within the asymmetric stretch (ν_3) mode of CO_2. The rate k for this process has been calculated by Pack[4] to be 9.2×10^6 $\text{sec}^{-1}\text{torr}^{-1}$ at 300 K (i.e. approximately one gas kinetic collision), but an experimental value has not been published to date.[5] We have recently measured this rate using the powerful combination of a tunable diode laser (TDL) spectrometer and a CO_2 discharge reference cell. The diode laser provides a high resolution probe ($< 10^{-4}$ cm^{-1}) for time domain absorption spectroscopy,[6] and has been recently used to probe CO_2 laser dynamics.[3] The CO_2 discharge reference cell creates steady state populations of vibrationally hot CO_2 and provides frequency references for thousands of high lying rovibrational lines which are normally inaccessable at room temperature. The TDL/discharge cell combination allows virtually every important rovibrational level in the CO_2 laser to be probed with extremely high temporal and spectral resolution.

2. Experimental -- In this double resonance experiment, the 9.6 μm output of a Q-switched CO_2 laser is propagated through a 2 m long sample cell containing a 1:10 mixture of CO_2 and argon, populating (00^01) J = 21. The argon promotes rotational relaxation within each CO_2 vibrational level without significantly affecting vibrational relaxation, so that the rotational levels are described by a Boltzman distribution throughout the experiment. In addition, it also limits radial diffusion of excited CO_2 molecules out of the probe beam. The diode laser is used to monitor the time dependent populations in the (00^01) and (00^02) levels. Its 4.3 μm cw output is copropagated along the cell axis, passed through a monochromator (to discriminate against competing spatial and longitudinal modes), and detected with a cooled (77 K) InSb detector. Time resolved changes in the transmitted intensity of the diode radiation are acquired with a Biomation 8100 transient digitizer and averaged with a Nicolet 1170 signal averager. A trigger is provided by detecting a portion of the CO_2 laser beam with a cooled (77 K) HgCdTe detector having a response time of ~0.1 μs. A typical time domain absorption signal for the (00^02) level is shown in Fig. 1; the diode laser is tuned to the (00^02) --> (00^03) R(20) transition at 2310.959 cm^{-1}. In order to locate this absorption line and lock the diode laser to this frequency, a portion of the beam is split off before the sample cell, directed through a CO_2 discharge reference cell, and into a monochromator/IR detector. The reference cell absorption signal is sent to a lock-in detector whose output is fed back into the diode laser current controller for frequency stabilization. This configuration fixes the frequency of the diode laser at the peak of a single absorption line throughout the duration of the experiment.

The discharge reference cell consists of a high voltage DC discharge (16 kV; 25 mA) applied to a low pressure mixture of CO_2, N_2, and He. It provides a steady state, non-Boltzman population of highly vibrationally excited CO_2, with 'effective' (Treanor-type[7]) vibrational mode temperatures as high as 2920 K.[8] In this experiment, the discharge enhances the (00^02) population by more than eight orders of magnitude (from 10^{-10} to 0.05 of the ground state population), providing a precise frequency reference for each (00^02) --> (00^03) absorption line.

Accurate assignments of the additional lines present in the discharge are made possible by high resolution FTIR spectroscopy of discharge excited CO_2.[9]

3. Results -- The kinetics of the collisional uppumping process given in Eq. (1) may be modelled simply by:

$$N_2(t) = k[N_1(t)]^2 - k_{-1}N_0N_2(t) \quad (2)$$

where $N_n(t)$ is the population in (00^0n), and k and k_{-1} are the forward and backward rates. Since N_0 and $N_1(t)$ are not significantly perturbed by this process, the solution to Eq. (2) may be written:

$$N_2(t) = k\int_0^t [N_1(\tau)]^2 \exp[-N_0k_{-1}(t-\tau)]\, d\tau \quad (3)$$

In theory, time domain absorption signals for $(00^02) \rightarrow (00^03)$ (e.g. Fig. 1) may be fit directly to the right hand side of Eq. (3). Note that k is the only free parameter in Eq. (3); k_{-1} is related to k by microscopic reversibility, and $N_1(t)$ is proportional to the measured $(00^01) \rightarrow (00^02)$ absorption signal. This procedure accounts for the time dependence in $N_1(t)$ due to: 1) the risetime of the CO_2 laser (pulsewidth ~400 ns FWHM), and 2) depletion (~8%) by the fast process:

$$CO_2(00^01) + CO_2(01^10) \rightarrow CO_2(01^11) + CO_2(00^00) \quad \Delta\varepsilon = -13 \text{ cm}^{-1} \quad (4)$$

which has a rate of $(5.3 \pm 1) \times 10^6 s^{-1}torr^{-1}$ [ref. 10]. However, this is unnecessary when the $N_1(t)$ transients are fast compared with 1/k, and $N_2(t)$ may be expressed as:

$$N_2(t) = N_1k[1-\exp(-k_{-1}N_0t)] \quad (5)$$

where N_1 is the (constant) amplitude of the (00^01) population. The right hand side of Eq. (5) is used as a fitting form for the time domain (00^02) signals. In addition, we add an exponential decay to account for diffusion of excited CO_2 out of the probe beam.

Time domain absorption signals were taken on the (00^02) P(14) line at total pressures ranging from 0.3 to 10 torr (i.e CO_2 partial pressures of 27.3 - 909 mtorr). Fitted values for the rise time ($k_{-1}N_0$) are graphed as a function of pressure in Fig. 2, and linear behavior is observed up to CO_2 partial pressures of 200 mtorr. The slope of these data points is given by $k_{-1} = (3.15 \pm 0.8) \times 10^6\ s^{-1}torr^{-1}$, i.e. a rate $k = (3.55 \pm 1.0) \times 10^6\ s^{-1}torr^{-1}$. The observed rates roll off at a maximum of 1400 ms^{-1}, corresponding to the detector/amplifier response time of ~0.7 μs.

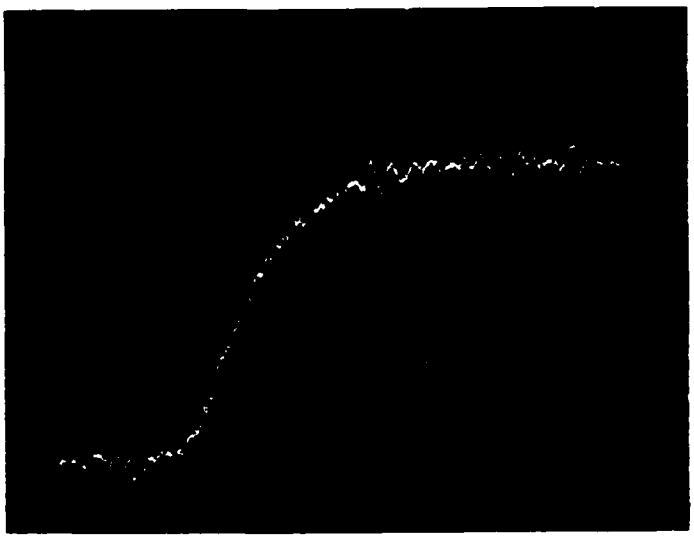

Fig. 1. Time domain absorption signal for the $(00^02) \rightarrow (00^03)$ R(20) transition of CO_2 following excitation of the (00^01) level by 9.6 μm radiation from a Q-switched CO_2 laser. The sample is a 1:10 mixture of CO_2:Ar at a total pressure of 1.0 torr (CO_2 partial pressure of 90.9 mtorr) and a temperature of 298 K. The trace represents the average of 32,000 signals and has a time base of 20 μs full scale.

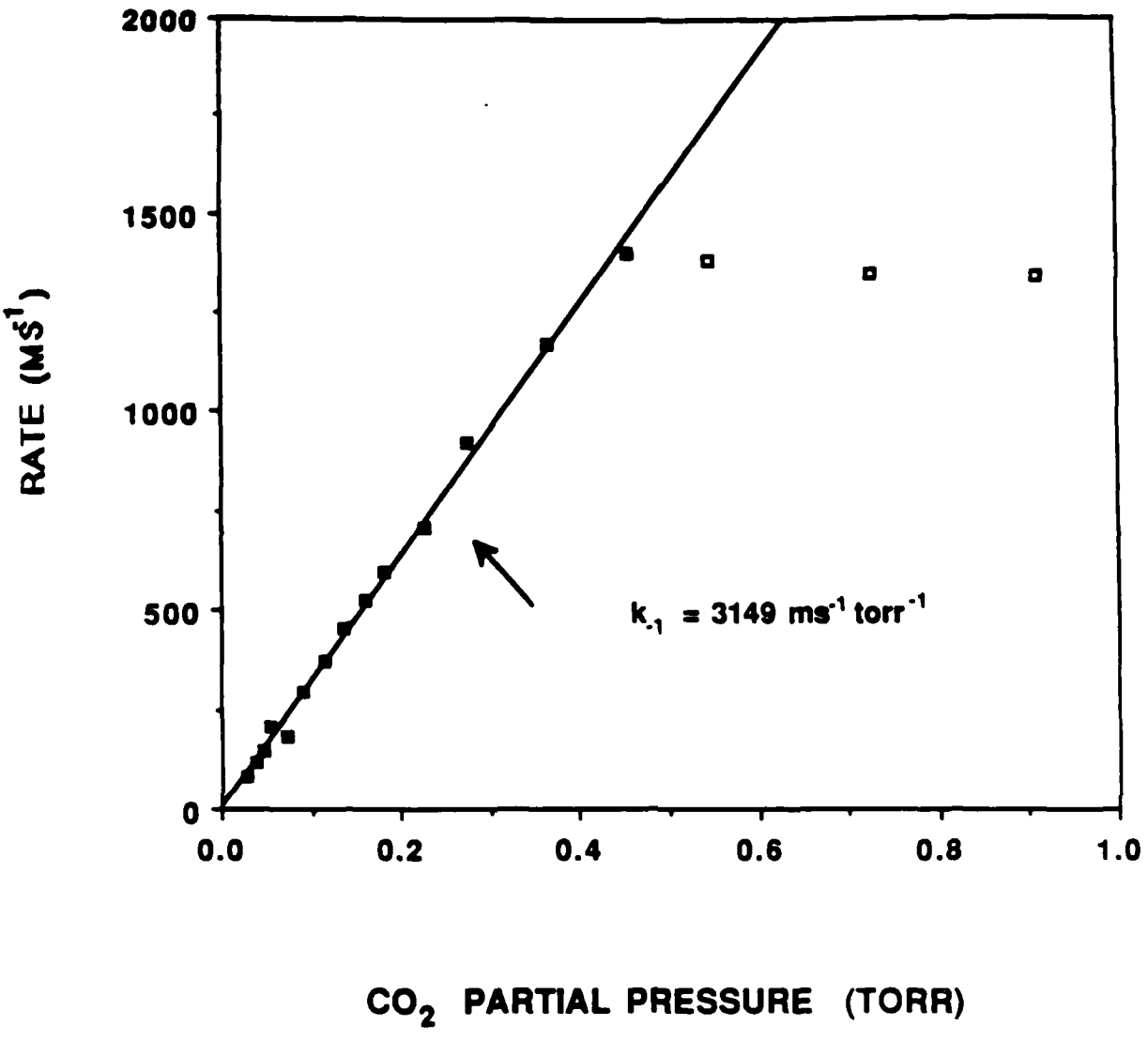

Fig. 2. Plot of signal rise rate, $k_{-1}N_0$ versus CO_2 partial pressure, N_0. The slope of this curve is k_{-1}=3.15 ms^{-1}torr^{-1}, or a value for the forward rate (see Eq. 1) of $k = 3.55 \times 10^6$ s^{-1}torr^{-1}. The rolloff at 450 mtorr corresponds to the 1.4 MHz cutoff of the detection system.

4. Conclusion -- We have measured the rate for collisional uppumping in CO_2 using the powerful combination of a tunable diode laser spectrometer and CO_2 discharge reference cell. The rate for this important V-V energy transfer process is found to be $(3.55 \pm 1.0) \times 10^6$ $s^{-1}torr^{-1}$ or $(1.00 \pm 0.3) \times 10^{-10}$ cm^3s^{-1} at 298 K, a value which is close to previous estimates[4,5] and rates for similar near resonant processes.[10] This apparatus provides a high resolution absorption probe capable of measuring CO_2 populations in rovibrational levels as high as 3 electron volts in energy. We are presently using the TDL/discharge cell combination to measure the nascent rotational and vibrational distributions of excited CO_2 molecules created by a variety of chemically interesting processes such as photodissociation,[11] electronic quenching,[12] and bimolecular and surface chemical reactions.

This research was also supported by the National Science Foundation under Grants NSF-CHE 85-17460 and NSF-CHE 80-23747 and by the Department of Energy under Contract DE-AC02-78-ER-04940.

(1) C.K.N. Patel, Phys. Rev. Lett. 12, 588 (1964); 13, 617 (1964); Appl. Phys. Lett. 7, 290 (1965).

(2) B.F. Gordictz, N.N. Sobolev, V.V. Sokovikov, L.A. Shelepin, IEEE J. Quantum Electron. 4, 796 (1968); C.B. Moore, R.E. Wood, B.E. Hu, J.T. Yardley, J. Chem. Phys. 46, 4222 (1967).

(3) C. Dang, J. Reid, and B.K. Garside, Appl. Phys. B27, 145 (1982); B31, 163 (1983); IEEE J. Quantum Electron. 19, 755 (1983).

(4) R.T. Pack, J. Chem. Phys. 72, 6140 (1980). Pack notes that the actual rate is expected to be ~75% of his reported value, i.e. 6.9 $\times 10^6$ $s^{-1}torr^{-1}$.

(5) M.D. Thomason, Ph.D thesis, University of Virginia, 1982. Thomason gives a value of $(7.61 \pm .24) \times 10^6$ $s^{-1}torr^{-1}$ at 700 K, measured by CO_2 laser double resonance.

(6) J.A. O'Neill, C.X. Wang, J.Y. Cai, G.W. Flynn, and R.E. Weston, Jr., J. Chem. Phys. 85, 4195 (1986); J.A. O'Neill, J.Y. Cai, G.W. Flynn, and R.E. Weston, Jr., J. Chem. Phys. 84, 50 (1986); J.O. Chu, C.F. Wood, G.W. Flynn, and R.E. Weston, J. Chem. Phys. 80, 1703 (1984); 81, 5533 (1984).

(7) C.E. Treanor, J.W. Rich, and R.G. Rehm, J. Chem. Phys. 48, 1966 (1970).

(8) D. Bailly, C. Rossetti, and G. Guelachvili, Chem. Phys. 100, 101 (1985).

(9) D. Bailly, R. Farrenz, and C. Rossetti, J. Mol. Spectry. 70, 124 (1978); D. Bailly, R. Farrenq, G. Guelachvili, and C. Rossetti, J. Mol. Spectry. 90, 74 (1981); D. Bailly, 3 eme Cycle Thesis, University of Paris-Sud, (1970).

(10) I. Burak, Y. Noter, and A. Szoke, IEEE J. Quantum Electron. 9, 541 (1973).

(11) J.A. O'Neill, T.G. Kreutz, and G.W. Flynn, "IR Diode Laser Studies of Vibrational Distributions Produced by UV Excimer Laser Photofragmentation of Pyruvic Acid," submitted: J. Chem. Phys.; C.F. Wood, J.A. O'Neill, and G.W. Flynn, J. Chem. Phys. 109, 317 (1984).

(12) B.B. Brady, L. Chia, and G.W. Flynn, "Diode Laser Probing Vibrational Product State Distributions in Metal-Molecule Collisions: $Hg(6^3P_1)$-CO_2, accepted, J. Chem. Phys.

D. TUNABLE DIODE LASER PROBE OF VIBRATIONLLY EXCITED CO_2 FORMED BY CATALYTIC OXIDATION OF CO ON A PT SURFACE

(T.G. Kreutz, J.A. O'Neill, L.S. Brown, S.L. Bernasek, G.W. Flynn)
(JSEP work unit 5, 1985 - 1988)
(Principal Investigator: G.W. Flynn (212) 280-4162)

1. Introduction -- The catalytic oxidation of carbon monoxide on a platinum surface has been investigated in numerous studies dating back to the work of Langmuir.[1] Aside from its enormous practical importance, the reaction is particularly interesting to the molecular dynamicist because the CO_2 product does not fully accommodate with the surface before desorbing, as is typical of chemical reactions on catalytic surfaces. Instead, CO_2 molecules leave the surface with translational, vibrational, and rotational temperatures far in excess of the surface temperature, and like gas phase reactions, can be probed for mode specific energy disposal in the internal degrees of freedom. Such data provides a wealth of information about the reaction dynamics and the activated complex. Although little is known about the potential hypersurface which governs the reaction dynamics, significant vibrational excitation is expected to be present in the CO_2 product on the basis of reactant --> product geometry. Studies of chemisorbed CO on clean Pt surfaces[2] show that the CO molecule is oriented with the carbon end toward the surface with a C-O bond distance of 1.15 Å. The distance between the carbon atom and the nearest adsorbed oxygen atom is on the order of 2.62 Å, the diameter of the surface Pt atoms. In this configuration (see Fig. 1), the incipient CO_2 molecule has a bond angle of 90° and two dissimilar C-O bond lengths. As it evolves to the usual linear, symmetric CO_2 species, substantial excitation is expected in the bending and asymmetric stretch modes. This mode specific deposition of reaction energy is likely to appear as a non-statistical population distribution in the vibrational energy levels of the unaccommodated gas phase CO_2 reaction product.

Several time-of-flight[3] and angular desorption[4] studies have demonstrated that the CO_2 reaction product desorbs from platinum with kinetic energy far in excess of that expected from the surface temperature. Similarly, measurements of the reaction IR

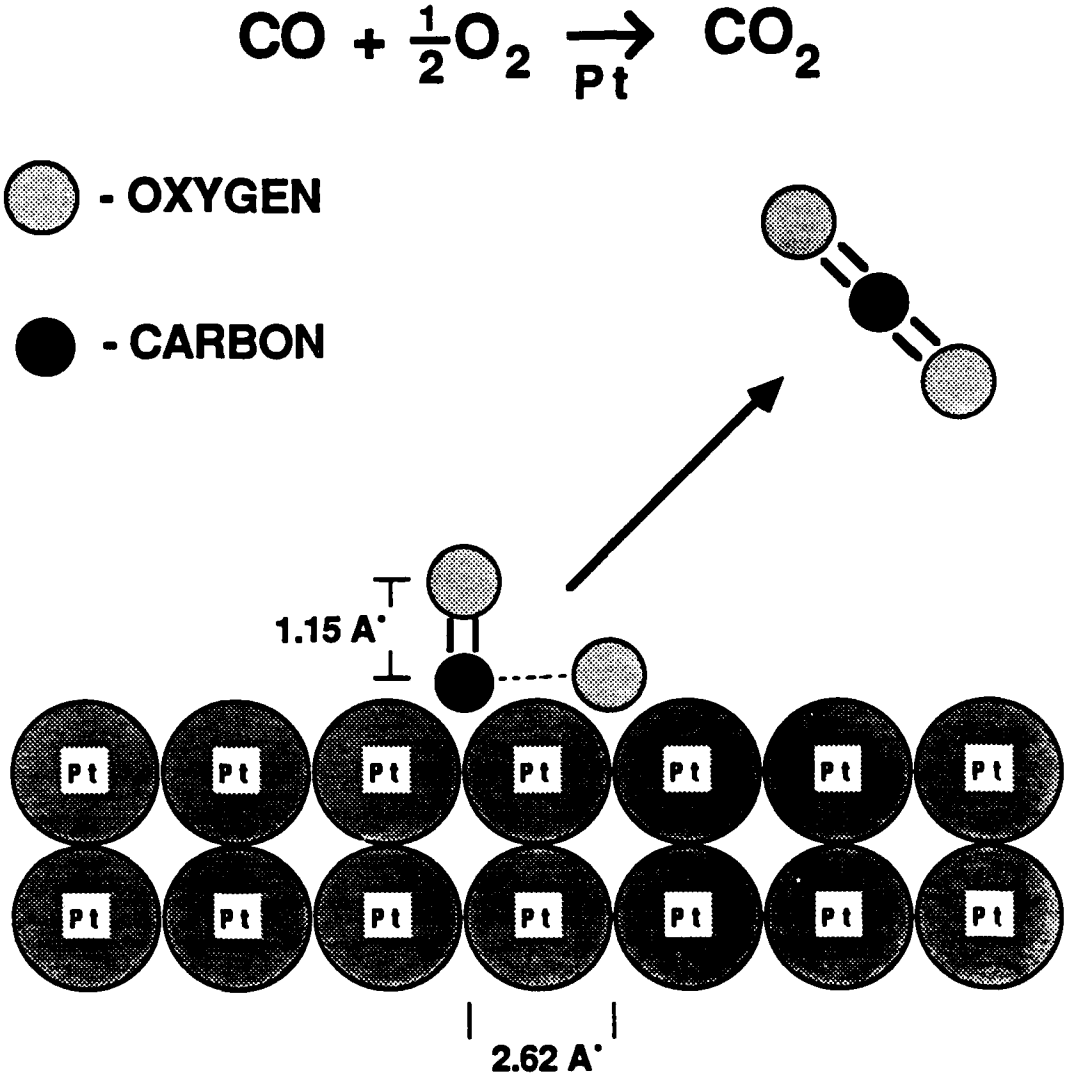

Fig. 1. Conceptual picture of adsorbed CO + O reacting on a platinum surface and evolving to the linear, symmetric CO_2 molecule. Vibrational excitation is expected in the bending (ν_2) and asymmetric stretch (ν_3) modes.

chemiluminescence have shown a high degree of vibrational excitation in the CO_2 product.[5,6] Vibrational mode temperatures as high as 1500 and 2000 K were seen in the bending (ν_2) and asymmetric stretch (ν_3) modes of CO_2 formed on an 800 K platinum surface. However these studies were hampered by the moderately high density of states of CO_2 and the typically poor resolution of IR chemiluminescence detection. Brown and Bernasek[5] measured the infrared emission spectrum using a circular variable filter (~30 cm^{-1} resolution) while Mantell, et al.[6] employed low resolution (~0.1 cm^{-1}) FTIR detection. While these experiments were capable of estimating the degree vibrational excitation, they lacked sufficient spectral resolution to clearly measure the nascent population distribution within each vibrational mode, data which can potentially provide a wealth of information about the nature of activated complex and reaction pathways.

We report the use of high resolution diode laser absorption spectroscopy to probe vibrational excitation in CO_2 formed on a platinum surface under steady state conditions. Tunable Pb-salt diode lasers have recently become an important tool in high resolution infrared spectroscopy, having a number of important features such as a linewidth of ~10^{-4} cm^{-1}, broad and continuous tunability, and operation from 3-30 μm. With this device, we are able to measure the amplitude of CO_2 absorption lines and map out the state specific deposition of reaction energy in the nascent CO_2 product. The population of virtually any rovibrational level (n, m, p) may be measured by diode excitation to the state (m, n, p+1). These transitions lie in the 4.3 μm region and benefit from the large oscillator strength of the asymmetric stretch fundamental. We report here vibrational mode temperatures measured for the vibrationally equilibrated bending and asymmetric stretch modes. We are presently extending this technique to measure the nascent (unequilibrated) vibrational energy distibution within each mode.

2. Experimental -- Diode laser absorption spectroscopy is used to monitor the degree of vibrational excitation in CO_2 formed in a reaction flow tube under steady state conditions. A schematic view of the experimental apparatus is shown in Fig. 2. The highly divergent 4.3 μm radiation from a Laser Analytics diode laser is collimated with an f/1

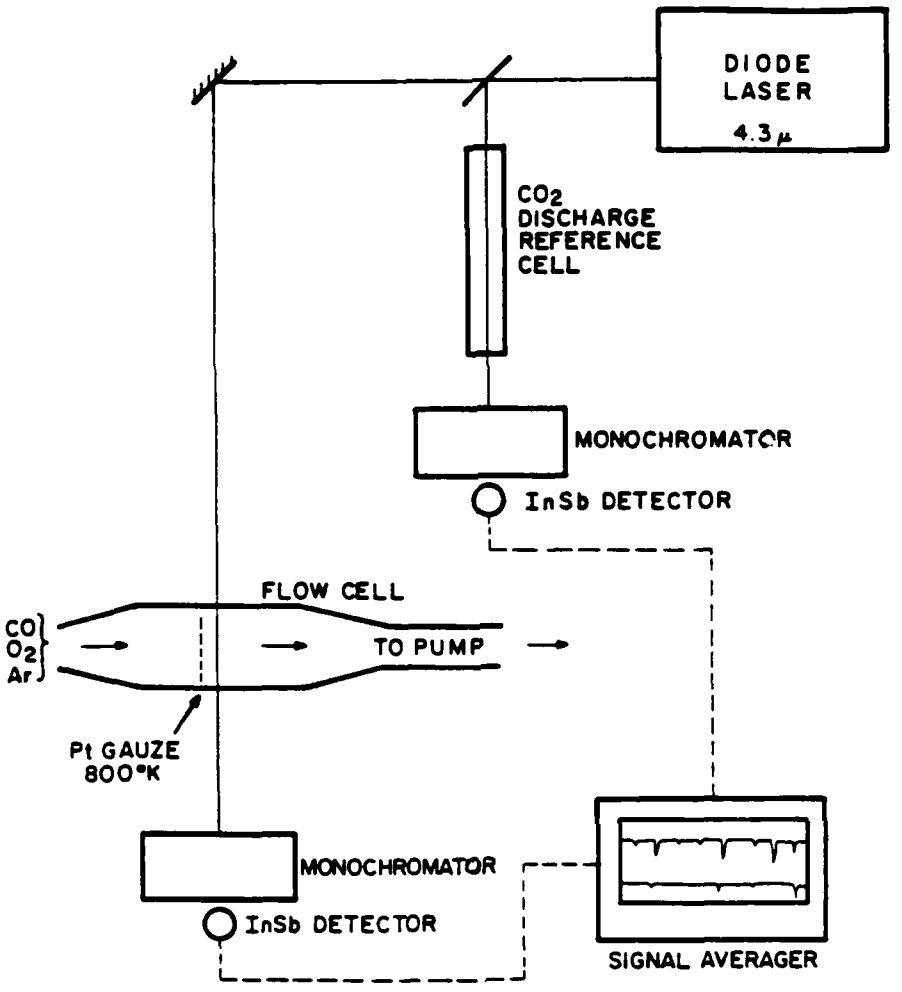

Fig. 2. Schematic view of the experimental apparatus. Vibrationally excited CO_2 is produced in a reaction flowtube by catalytic oxidation of CO on an 800 K platinum gauze. The CO_2 IR absorption spectrum is measured with diode laser light (4.3 μm) which is directed through the flow tube and detected with a cooled IR detector. A portion of the diode beam is split of and sent through a CO_2 discharge reference cell in order to provide frequency references for high lying vibrational lines of CO_2. The laser frequency is repetitively scanned over ~1 cm^{-1} (at 200 Hz); yielding an absorption spectrum which is acquired and averaged on a signal averager.

lens and directed through a reaction flow tube in which CO is oxidized on a heated platinum surface. The transmitted light is dispersed with a monochromator (to discriminate against competing longitudinal and spatial frequency modes) and is detected with a cooled (77 K) InSb detector. A portion of the laser beam is split off with a MgF_2 flat before the flow tube and sent through a CO_2 discharge reference cell consisting of a high voltage DC discharge (16 kV; 25 mA) applied to a low pressure mixture of CO_2, N_2, and He. The cell creates steady state populations of vibrationally hot CO_2 having mode temperatures as high as 2920 K [ref. 7], and provides frequency references for thousands of high lying rovibrational lines which are normally inaccessable at room temperature.

The reaction flow tube (shown in Fig. 2) consists of a 2 inch diameter pyrex tube with a gas inlet and a 6 L/s mechanical pump at each end. A 1 in^2 platinum gauze is supported in the center of the tube by stainless steel feedthroughs which provide a 40 A current through the gauze. Typical gauze tempertures are 600-1200 K, measured with a thermocouple spot welded to the center of the gauze. Calcium fluoride windows, which are mounted flush on each side of the flow tube, allow the 4.3 μm diode laser light to intersect the flow at 90^o immediately downstream of the gauze. High purity CO, O_2, and Ar gas (typical ratio = 2:1:6) are mixed in a gas manifold and admitted into the flow tube. At total pressures ranging from 0.75 to 8.0 torr, measured with a capacitance manometer, the gas flows at an axial speed of ~250 cm/s. As it passes through the heated gauze, CO is oxidized to CO_2 and is swept downstream into the path of the laser. The vibrationally excited CO_2 molecules undergo ~1500 CO_2-CO_2 collisions as they travel from the gauze through the sampling region. This allows vibration-to-vibration (V-V) relaxation to occur (rate ~2-25 CO_2-CO_2 collisions) but does not permit vibration-to-translation (V-T) relaxation (rate ~100,000 collisions) or intermode energy transfer between the bending and asymmetric stretch modes (rate ~30,000 CO_2-CO_2 collisions). As a result, the CO_2 reaction product sampled by the diode laser has two vibrational modes which are individually at equilibrium and have separate mode temperatures.

The laser frequency is scanned repeatedly (at 200 Hz) over a frequency range of ~1 cm^{-1} by a stabilized current controller which

provides a 200 mA current sawtooth to the diode laser element. The detector output is amplified, acquired on a Biomation 8100 transient digitizer, and averaged on a Nicolet 1170 signal averager. The resulting time domain signal represents a nonlinear frequency domain absorption spectrum as shown in Fig. 3. Frequency calibration is provided with a 1 in thick solid germanium Fabry-Perot etalon (F.S.R. = 0.0475 cm^{-1}). The final spectrum (typically 2048 averaged signals), baseline, and etalon trace are analyzed on a VAX 11/780 computer.

3. Results -- The CO_2 rotational/translational temperature T_R can be found from the intensity ratio of two absorption lines which have the same initial vibrational state but different rotational quantum numbers. T_R may be expressed as:

$$T_R = \frac{B}{k}[J'(J'+1)-J(J+1)] \; / \ln[R\frac{L(J')}{L(J)}] \qquad (1)$$

where R is the ratio of I_{vJ} and $I_{vJ'}$, the rovibrational line intensities, B is the rotational constant, and L(J) equals J for the P branch and J+1 for the R branch. The sensitivity of T_R to experimental error, given by

$$d\ln T_R/d\ln R = -1/\left\{\frac{B}{kT}[J'(J'+1)-J(J+1)]\right\} \qquad (2)$$

is minimized when J and J' have disparate values, i.e. when the absorption lines are measured in two, widely separated spectral regions. Within a given vibrational mode, the relative population in each vibrational state, N_v is given by

$$N_v \sim I_{vJ}/[(v+1)f(J;T_R)] \qquad (3)$$

where $f(J;T_R)$ is the rotational Boltzman distribution and $1/(v+1)$ accounts for the v dependence in the dipole matrix element.

Vibrationally excited CO_2 was created on an 800 K platinum gauze by flowing 100 mtorr CO and 50 mtorr O_2 in 5 torr Ar buffer gas. Values of T_R were obtained with pairs of absorption lines (in the 2281 and 2310 cm^{-1} regions) for a number of different vibrational levels, then averaged to give a final value of 890 K. The vibrational population distributions for both the bending and asymmetric stretch modes are shown in Fig. 4. The symmetric stretch (ν_1) and bending (ν_2) modes, which are in thermal equilibrium, were found to be quite cold, having a temperature of 680 K. In contrast, the ν_3 mode was found to have a temperature of 1600 K. These temperatures are lower than expected from

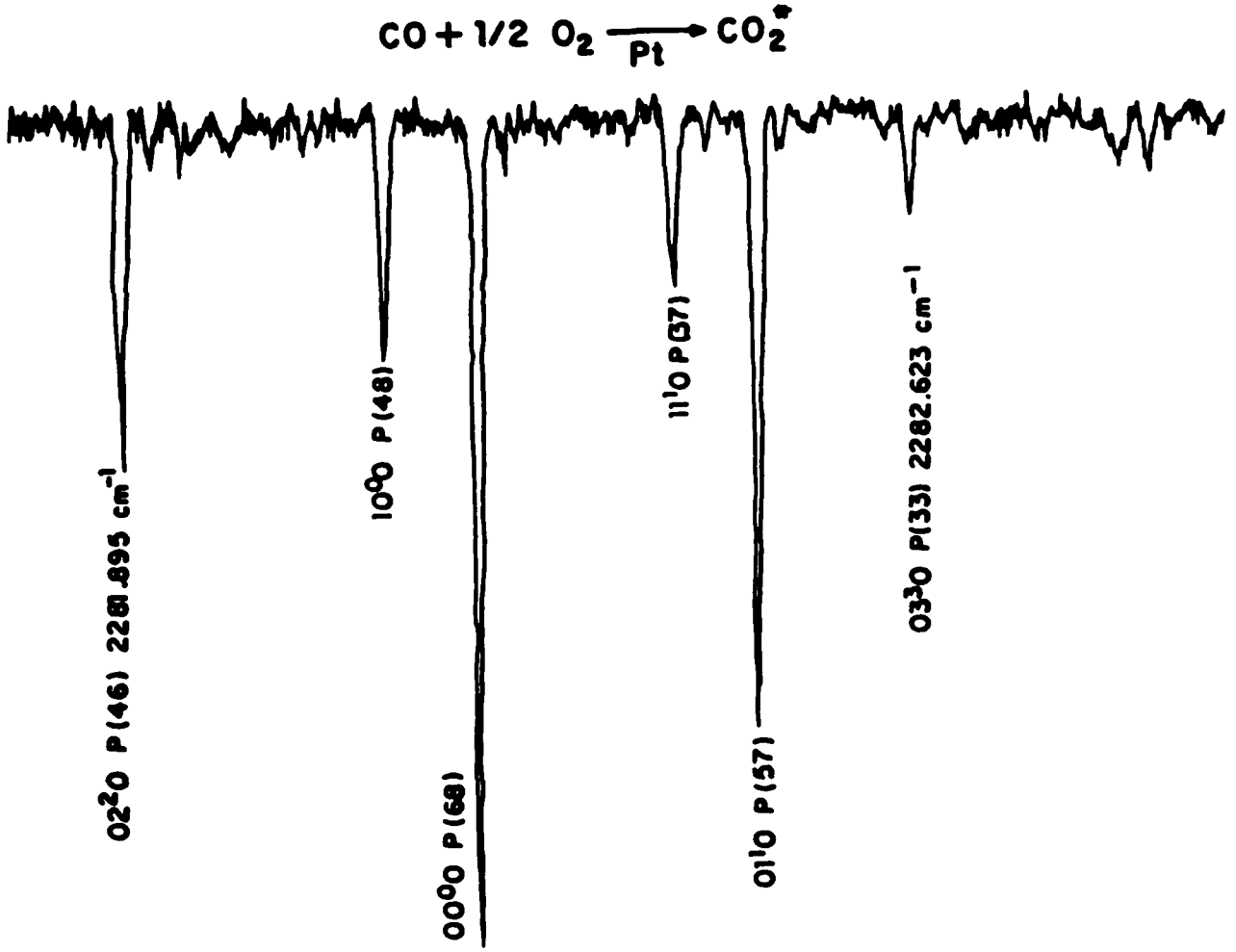

Fig. 3. Typical diode laser absorption spectrum of the CO_2 reaction product in the 2281 cm^{-1} region. The spectrum has been normalized to the incident laser intensity and linearized along the frequency axis.

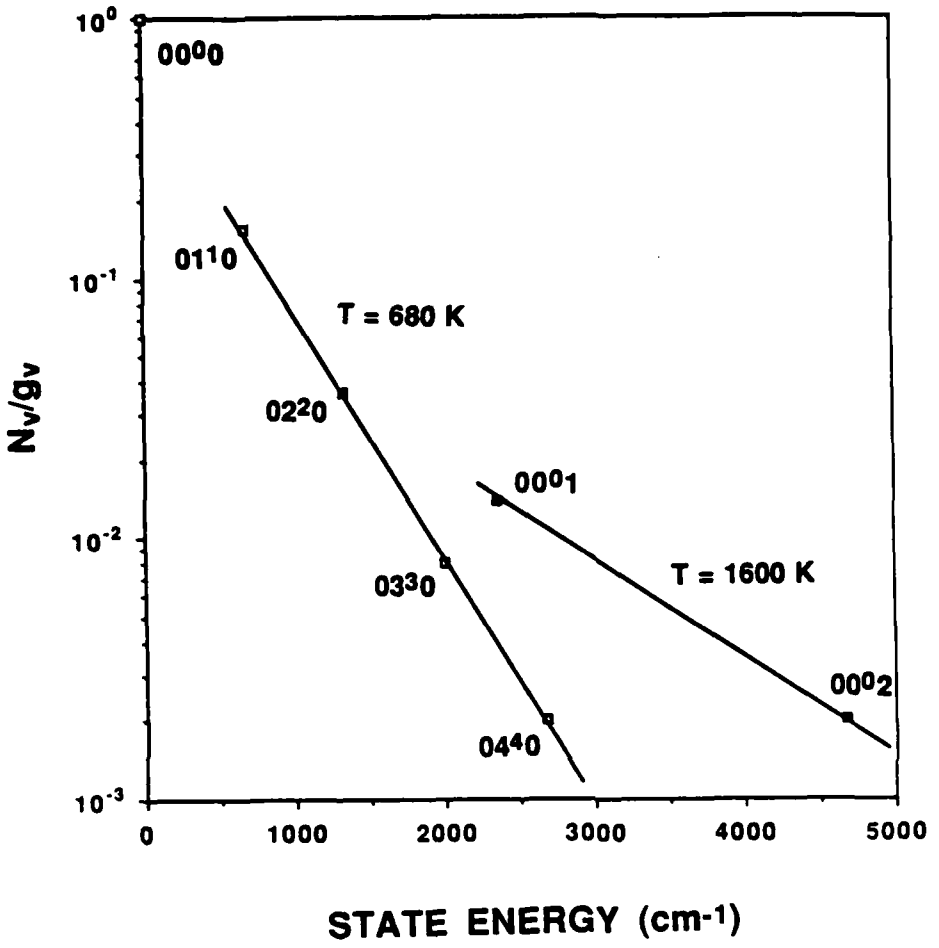

Fig. 4. Measured vibrational populations for the bending (v_2) and asymmetric stretch (v_3) modes, graphed as a function of vibrational state energy. Vibrationally equilibrated mode temperatures are given by the slopes of the lines which are fitted to these points.

previous studies,[5,6] and may be attributed to the presence of cold CO_2 in the path of the laser. Despite experimental conditions which insure vibrational equilibrium within a given mode of the CO_2 product, the vibrational populations in each mode (see Fig. 4) do not fall on a straight line corresponding to a single mode temperature. Instead, there is a preponderance of ground state molecules relative to excited molecules, implying inhomogeneity in the temperature of the CO_2 molecules along the transverse laser beam path. This non-equilibrium situation can occur only when different fractions of CO_2 molecules having different mode temperatures are separated spatially to such an extent that they are unable to equilibrate before being sampled by the laser. Inside the flow cell (see Fig. 2), there are two distinctly different regions in the beam path which may create CO_2 molecules with two different temperatures: 1) the area directly downstream of the gauze, and 2) the regions between the gauze and the cell walls. At total pressures less than 8 torr, CO_2 formed on the gauze can diffuse a significant distance upstream, relax on the cell walls and flow back either through or around the gauze. CO_2 molecules emanating from these two regions have markedly different temperatures and are unable to reach equilibrium in the ~10 ms transit time through the beam. As a result, the measured vibrational distributions correspond to the sum of the distributions for at least two separate fractions of CO_2 molecules, each having a different vibrational mode temperature. Future studies using a modified apparatus should eliminate these difficulties. Gas velocities are vastly increased (to $\sim 10^4$ cm/s)d in the flowtube at lower gas pressures (~10 mtorr) when the mechanical pump is replaced with a 1/2 in diffusion pump. Furthermore, cooling the flowtube walls to 77 K effectively eliminates sampling of CO_2 which has diffused throughout the cell and cooled on the walls. These modifications will allow us to measure the population distribution within each vibrational mode before vibrational relaxation can occur.

4. Conclusion -- A tunable diode laser has been used as a high resolution probe to investigate the degree of vibrational excitation in CO_2 formed on an 800 K polycrystalline platinum surface. With a translational/rotational temperature of 890 K, the bending (ν_2) and

asymmetric stretch (ν_3) mode temperatures were found to be 680 and 1600 K respectively. We believe that the level of vibrational excitation in the CO_2 reaction product is significantly higher than suggested by these temperatures. However, the present flowtube configuration permits cooling of a portion of the CO_2 before sampling by the diode laser. Nonetheless, high resolution diode laser absorption spectroscopy has been shown to provide an excellent means of probing vibrational excitation in the reaction product, and will be employed in upcoming studies of this important catalytic reaction.

This research was also supported by the National Science Foundation under Grants NSF-CHE 85-17460 and NSF-CHE 80-23747 and by the Department of Energy under Contract DE-AC02-78-ER-04940.

(1) I. Langmuir, Trans. Faraday Soc. 17, 621, 672 (1922).

(2) T. Engel and G. Ertl. Advan. Catal. 28, 1 (1979).

(3) C.A. Becker, J.P. Cowin, L. Wharton, and D.A. Auerback, J. Chem. Phys. 67, 3994 (1977).

(4) R.L. Palmer and J.N. Smith Jr., J. Chem. Phys. 60, 1453 (1974).

(5) S.L. Bernasek and S.R. Leone, Chem. Phys. Lett. 84, 401 (1981); L.S. Brown and S.L. Bernasek, J. Chem. Phys. 82, 2110 (1985).

(6) D.A. Mantell, S.B. Ryali, B.L. Halpern, G.L. Haller, and J.B. Fenn, Chem. Phys. Lett. 81, 185 (1981); D.A. Mantell, S.B. Ryali, and G.L. Haller, Chem. Phys. Lett. 102, 37 (1983).

(7) D. Bailly, C. Rossetti, and G. Guelachvili, Chem. Phys. 100, 101 (1985); C. Dang, J. Reid, and B.K. Garside, Appl. Phys. B27, 145 (1982).

E. DIODE LASER PROBE OF CO_2 VIBRATIONAL EXCITATION PRODUCED BY QUENCHING OF $O(^1D)$ ATOMS

(A.S.M. Hewitt, T.G. Kreutz, G.W. Flynn)
(JSEP work unit 5, 1985 - 1988)
(Principal Investigator: G.W. Flynn (212) 280-4162)

1. Introduction -- The first electronically excited state of oxygen, $O(^1D)$, plays an important role as an intermediate in radiation and photochemical systems and in the chemistry of the stratosphere and planetary atmospheres. This is due to the moderately short wavelengths required to produce $O(^1D)$ by ultraviolet photolysis of many gases and to the 100-sec radiative lifetime of $O(^1D)$ which essentially allows all the excited oxygen atoms to react or be quenched even at low pressures. Because $O(^1D)$ is a highly reactive species, it is also used to etch surfaces. Furthermore, studies of the physical and chemical quenching of singlet oxygen atoms are of interest to physical chemists for comparison with the established behavior of ground state, triplet oxygen atoms.

Carbon dioxide quenching of $O(^1D)$ is a matter of much controversy as to whether $O(^1D)$ is collisionally deactivated to $O(^3P)$ (physical quenching), reacts to form products (chemical quenching), or is quenched by both of the above mechanisms. Katakis and Taube[1] were the first to propose the formation of CO_3 from the reaction between $O(^1D)$ and CO_2. Since then, CO_3 has often been invoked in infrared studies of solid matrices,[6,12,13] isotopic exchange of $O(^1D)$ with CO_2[2,3,5] ultraviolet flash photolysis,[4,11] CO_2 laser plasmas,[14] CO_2 photolysis,[7,8,9] and a liquid O_3-N_2 actinometer study[10]. The lifetime of the CO_3 complex has been reported to be as short as 10^{-11} to 10^{-12} sec[11] and as long as 0.04 sec.[6] Theoretical studies of the geometry and electronic structure of CO_3 seem to favor a planar, isosceles triangular (C_{2v}) geometry.[15-18] On the other hand, there have been many studies employing resonant LIF,[19] monitoring the 6300-Å emission from $O(^1D)$,[20] ultraviolet flash photolysis,[21] and CO_2/N_2O photolysis[22] to name a few which do not invoke a CO_3 intermediate species. Furthermore, the experimentally determined rates of deactivation of $O(^1D)$ by CO_2 vary from 2×10^{-13} to 2.3×10^{-10} $cm^3 molecule^{-1} s^{-1}$. Consequently, more

experimental work is necessary to resolve these discrepancies.

In the present study, we employ a high resolution cw diode laser probe technique to monitor time-resolved absorption in $C^{16}O_2(C^{16}O^{18}O)$ molecules undergoing collisions with $^{16}O(^1D)$ $\{^{18}O(^1D)\}$. From these measurements the vibrational distribution of collisionally excited CO_2 molecules will be determined. In addition, we can easily distinguish between the ro-vibration transitions of $C^{16}O_2$, $C^{16}O^{18}O$, and $C^{18}O_2$ because of the narrow bandwidth (0.0003 cm^{-1}) of the diode laser. Consequently, by using an isotopically substituted $O(^1D)$ precursor and monitoring a specific ro-vibration transition of $C^{16}O^{18}O$, we can determine whether chemical quenching occurs through the $C^{16}O_2{}^{18}O$ intermediate. The nature of the CO_3 transition state and the O/CO_2 potential surface may be inferred from these measurements.

O_3, NO_2, and N_2O are used as $O(^1D)$ precursors. The $O(^1D)$ atoms are produced by excimer laser photolysis of the precursor molecules at 193 and 248 nm. The diode is a continuous wave (cw) laser device having excellent amplitude stability, high resolution, and a tuning range of 3 to 30 cm^{-1}. Due to the anharmonicities in CO_2, this allows separate individual ro-vibration transitions of the type

$$CO_2(mn^{\ell}p,J) + h\nu(\sim 4.3\mu m) \longrightarrow CO_2(mn^{\ell}p+1,J\pm 1).$$

to be monitored. m, n, and p are the numbers of vibrational quanta in the symmetric stretching mode ν_1, the bending mode ν_2, and the asymmetric stretching mode ν_3, respectively. Since these transitions "ride" the strong ν_3 absorption coefficient (i.e., they have essentially the same effective oscillator strength as the $00^00 \longrightarrow 00^01$ transition), even the IR inactive ν_1 symmetric stretch mode (10^00) and the bending ν_2 mode (01^10), whose emission at 15 μm is difficult to detect, can be observed. Consequently, all three normal vibrational modes of CO_2 can be specifically studied. Moreover, absolute population changes can be determined by direct calibration of the absorptions using cold unexcited CO_2 gas. Finally, the time response of the system is limited only by the bandwidth of the IR detection system since the diode laser contiuously monitors the transition of interest.

2. Experimental -- The diode laser probe technique employed in this study has been described previously.[23-25] Briefly, a Lambda Physik

EMG 101 excimer laser, operating at 193 nm, 0.5 Hz, was used to photodissociate O_3, NO_2, or N_2O, producing electronically excited $O(^1D)$ atoms. The excitation beam and diode laser probe beam pass collinearly through the cell. Various mole fractions of O_3/CO_2, NO_2/CO_2, or N_2O/CO_2 (sometimes He or Xe was added to the gas mixtures) were flowed through the sample cell. The diode laser was tuned to various ro-vibrational transitions of $C^{16}O_2(C^{16}O^{18}O)$ and time-resolved changes in the transmitted intensity of the IR probe beam after the photolysis pulse are detected by a SBRC InSb IR detector and matched amplifier after passing through the cell. The IR detector output was digitized with a Biomation 8100 transient recorder, summed with a Nicolet 1170 signal averager, and transferred to a PDP 11/34 or a VAX 11/780 for storage and further analysis. The overall response time of the detection system was 300 ns. An auxiliary CO_2 discharge cell is used to lock the diode laser at the desired frequency by use of a Keithley 840 lock-in detector and feedback loop.[26]

3. Results -- To date, the vibrational distributions of $C^{16}O_2$ molecules following 193 nm excimer laser photolysis of O_3, NO_2, and N_2O have been measured. Transient absorption signals were obtained while monitoring pure asymmetric stretch levels, pure bend levels, the fundamental symmetric stretch level, and combination states of CO_2 after UV photolysis of the $O(^1D)$ precursor at pressures varying from 10 torr to 50 mtorr.

Two conflicting sets of data have been obtained. In one set, the O_3, NO_2, and N_2O signals are all similar in amplitude and correspond to most, but not all, of the vibrationally excited CO_2 molecules being in the 00^01 state. Some population was also observed in the 01^10 and 02^20 bending states, and very small amounts were detected for the 03^30, 10^00, 01^11, and 10^01 states of CO_2. However, the risetimes using NO_2 or N_2O as a precursor correspond to about 25 gas kinetic collisions compared to a risetime using O_3 of about 1 gas kinetic collision (the consensus in the literature is that $O(^1D)$ is quenched by CO_2 in approximately 1 gas kinetic collision) (Fig. 1A). In the other set of data, the NO_2 and O_3 signals are similar in both amplitude and risetime. All of the vibrationally excited CO_2 molecules appear to be in the 00^01 state.

E-V EXCITATION OF CO_2 BY O(1D)

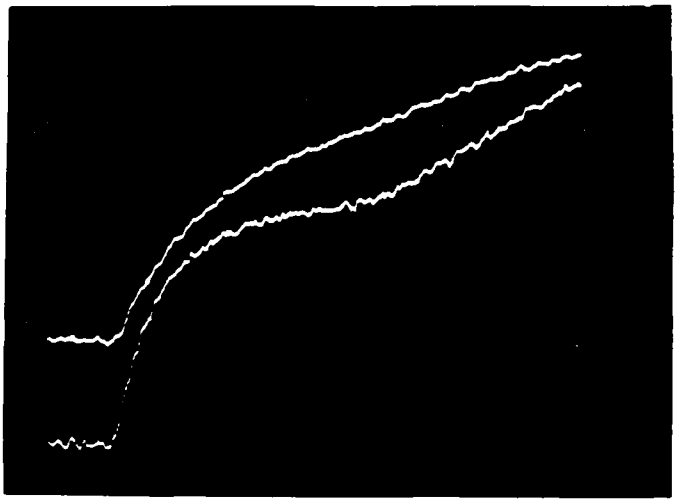

Figure 1A
$00^01 \rightarrow 00^02$ P(37)
20μs full scale
TOP: NO_2/CO_2 1/4 mixture
20 shots
250 mtorr
BOTTOM: O_3/CO_2 1/5 mixture
128 shots
1 torr

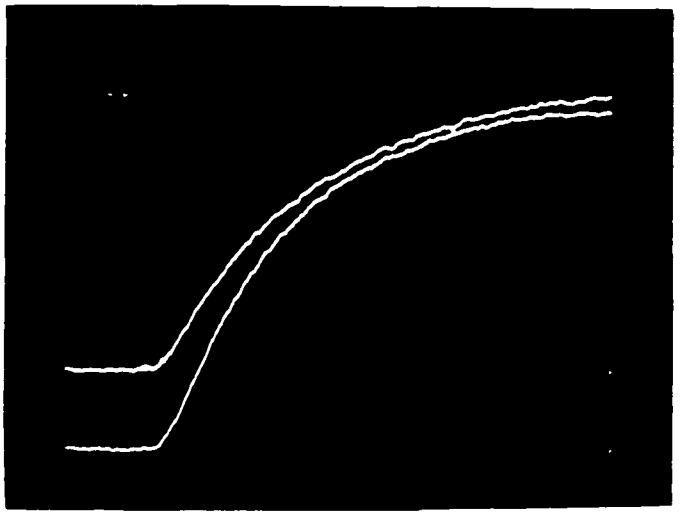

Figure 1B
$00^01 \rightarrow 00^02$ P(17)
20μs full scale
250 mtorr
64 shots
TOP: NO_2/CO_2 1/20 mixture
BOTTOM: O_3/CO_2 1/4 mixture

Figure 1. Diode laser absorption changes for the $00^01 \rightarrow 00^02$ transition following 193 nm excimer laser photolysis of the $O(^1D)$ precursor. Absorption increases downward

Furthermore, none of the signals have a fast rise as in the first set of data reported (Fig. 1B). Each of these sets of data have been observed numerous times, with the same and different gas mixtures, and with different optical alignments. Differences in the translational energy of $O(^1D)$, due to excimer laser photolysis of different $O(^1D)$ precursors, should not be the cause of the discrepancies in our results.[27] It is possible that a nascent rotational distribution of the 00^01 vibrational level of CO_2 which is peaked at a much higher rotational level than that predicted by thermalized room temperature Boltzmann statistics may reconcile the two disparate sets of data.[28]

Rare gases were added to the N_2O/CO_2 gas mixtures in order to confirm that the previous signals were due to CO_2 quenching of $O(^1D)$. It was expected that the 00^01 signal would decrease in amplitude with the addition of Xe due to the heavy atom effect but would not be affected by the addition of He. However, the data showed that the 00^01 signal was decreased in amplitude to the same extent by both He and Xe (Fig. 2A,B).

4. Discussion -- The abrupt change in signals from day to day and the unexpected effect of rare gas addition must be cleared up before beginning the isotope studies. Moreover, there have been problems with diode ripple and low signal-to-noise which have exacerbated the situation. We plan to switch from ArF to KrF gas in the excimer laser which will increase the S/N since the absorption coefficient of O_3 at 248 nm is 13 times greater than that at 193 nm.

Once we are positive that the signal being observed is due to the CO_2 quenching of $O(^1D)$ and that the correct vibrational distribution has been determined, we will begin the isotope experiments.

This research was also supported by the National Science Foundation under Grants NSF-CHE 85-17460 and NSF-CHE 80-23747 and by the Department of Energy under Contract DE-AC02-78-ER-04940.

(1) D. Katakis and H. Taube, J. Chem. Phys. 36, 416 (1962).

(2) D.L. Baulch and W.H. Breckenridge, Trans. Faraday Soc. 62, 2768 (1966).

(3) K.F. Preston and R.J. Cvetanovic, J. Chem. Phys. 45, 2888 (1966).

(4) M. Clerc and A. Reiffsteck, J. Chem. Phys. 48, 2799 (1968).

(5) H. Yamazaki and R.J. Cvetanovic, J. Chem. Phys. 40, 582 (1964).

(6) M. Arvis, J. Chem. Phys. 66, 517 (1969).

(7) P. Warneck, J. Chem. Phys. 41, 3435 (1964).

(8) A.Y. Ung and H.I. Schiff, Can. J. Chem. 44, 1981 (1966).

(9) J.G. Slanger, J. Chem. Phys. 45, 4127 (1966).

(10) W.B. DeMore and C.W. Jacobsen, J. Phys. Chem. 73, 2935 (1969).

(11) W.B. DeMore and C. Dede, J. Phys. Chem 74, 2621 (1970).

(12) E. Weissberger, W.H. Breckenridge, and H. Taube, J. Chem. Phys. 47, 1764 (1967).

(13) N.G. Moll, D.R. Clutter, and W.E. Thompson, J. Chem. Phys. 45, 4469 (1966).

(14) J. Freudenthal, J. Appl. Phys. 41, 2447 (1970).

(15) B.M. Gimarc and T.S. Chou, J. Chem. Phys. 49, 4043 (1968).

(16) M. Cornille and J. Horsley, Chem. Phys. Lett. 6, 373 (1970).

(17) J.F. Olsen and L. Burnelle, J. Am. Chem. Soc. 91, 7286 (1969).

(18) J.A. Pople, U. Seeger, R. Seeger, and P.v.R. Schleyer, J. Comp. Chem. 1, 199 (1980).

(19) T.G. Slanger and G. Black, J. Chem Phys. 54, 1889 (1971).

(20) J.F. Noxon, J. Chem. Phys. 52, 1852 (1970).

(21) R.J Donovan, D. Husain, L.J. Kirsch, Trans. Faraday Soc. 67, 375 (1966).

(22) L.F. Loucks and R.J. Cvetanovic, J. Chem. Phys. 57, 1682 (1972).

(23) J.O. Chu, C.F. Wood, G.W. Flynn, and R.E. Weston, Jr., J. Chem. Phys. 81, 5533 (1984).

(24) C.F. Wood, J.A. O'Neill, and G.W. Flynn, Chem. Phys. Lett. 109, 317 (1984).

(25) J.O. Chu, C.F. Wood, G.W. Flynn, and R.E. Weston, Jr., J. Chem. Phys. 80, 1703 (1984).

(26) C. Dang, J. Reid, and B.K. Garside, Appl. Phys. B27, 145 (1982).

(27) R.J. Cvetanovic, Can. J. Chem. 52, 1452 (1974).

(28) J.A. O'Neill, C.X. Wang, J.Y. Cai, G.W. Flynn, and R.E. Weston, Jr., J. Chem. Phys. 85, 4195 (1986).

E-V EXCITATION OF CO_2 BY $O(^1D)$

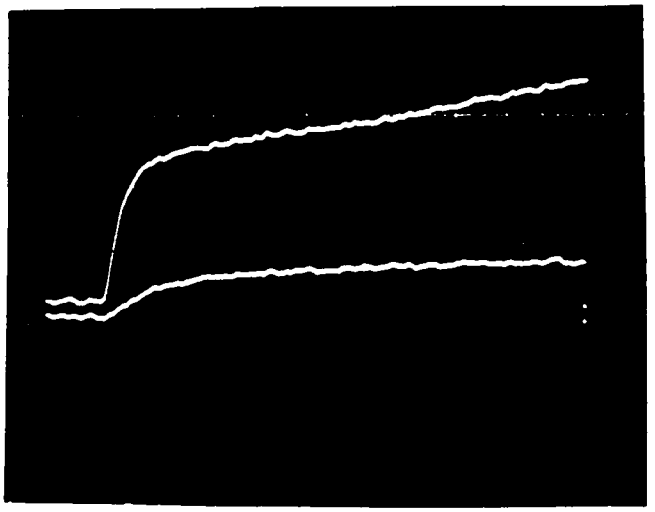

Figure 2A
$00^01 \rightarrow 00^02$ P(37)
20 μs full scale
50 shots
TOP: CO_2/N_2O 4/1 mixture
2.5 torr
BOTTOM: $He/CO_2/N_2O$ 16/4/1
mixture
10.5 torr

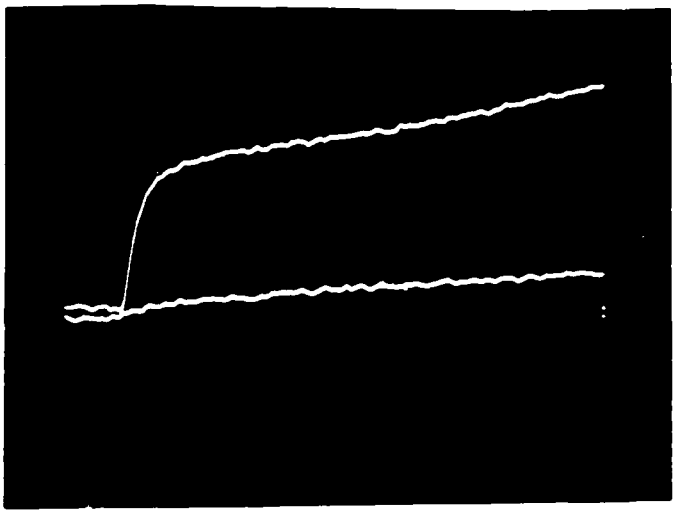

Figure 2B
$00^01 \rightarrow 00^02$ P(37)
20 μs full scale
50 shots
TOP: CO_2/N_2O 4/1 mixture
2.5 torr
BOTTOM: $Xe/CO_2/N_2O$ 16/4/1
mixture
10.5 torr

Figure 2. Diode laser absorption changes for the $00^01 \rightarrow 00^02$ transition following 193 nm excimer laser photolysis of the $O(^1D)$ precursor. Note the decrease in signal amplitude due to rare gas addition. Absorption increases downward

IV. PICOSECOND ENERGY TRANSFER AND PHOTOFRAGMENTATION SPECTROSCOPY

A. SECOND HARMONIC GENERATION FROM LIQUID SURFACES

(K. Kemnitz, J. Hicks, G.R. Pinto, K. Bhattacharyya, T.F. Heinz, and K.B. Eisenthal)
(JSEP work unit 6, 1985 - 1988)
(Principal Investigator: K.B. Eisenthal (212) 280-3175)

1. The Phase of Second Harmonic Light Generated at an Interface and its Relation to Absolute Molecular Orientation -- In recent years the nonlinear optical process of second harmonic generation (SHG) at an interface has been shown to provide a substantial amount of new information on a number of interfacial properties.[1] In our continuing effort to understand the behavior of small molecules at the air-water interface we have earlier studied a monolayer of phenol on the surface of an aqueous solution and from the polarization dependence of the SHG, determined the average orientation of the principal molecular axis (passing through the phenyl-oxygen bond) with respect to the surface normal.[2] We have now extended these studies to measure the absolute phase of the SH electric field and develop a scheme for inferring the absolute sense of the molecular orientation, namely, whether the phenyl-oxygen bond is pointing towards or away from the water.

The principle of the method can be outlined as follows. If the surface nonlinearity arises from an electric-dipole response, one can write the surface nonlinear susceptibility, $\overleftrightarrow{\chi}_s^{(2)}$, as a sum of the nonlinear polarizibilities $\overleftrightarrow{\alpha}^{(2)}$ of the molecules:

$$\overleftrightarrow{\chi}_s^{(2)} = N_s \langle \overleftrightarrow{\alpha}^{(2)} \rangle \tag{1}$$

where N_s is the number of molecules per unit area and the angular bracket indicates an average over molecular orientations. If the nonlinear polarizability is dominated by a single component $\alpha^{(2)}_{\zeta\zeta\zeta}$ and if we assume that the molecules are arranged isotropically with respect to azimuthal directions, the individual elements can be expressed in terms of the polar angle θ between the molecular ζ-axis and the positive surface normal,

$$(\chi_s^{(2)})_{zzz} = N_s \langle \cos^3\theta \rangle \alpha^{(2)}_{\zeta\zeta\zeta} \tag{2a}$$

$$(\chi_s^{(2)})_{xzx} = (\chi_s^{(2)})_{zxx} = (N_s/2) \langle \cos\theta \sin^2\theta \rangle \alpha^{(2)}_{\zeta\zeta\zeta} \qquad (2b)$$

Thus, from a comparison of the signs (or more precisely, the phases) of the elements of $\overleftrightarrow{\chi}_s^{(2)}$ and $\overleftrightarrow{\alpha}^{(2)}$ one can determine the absolute molecular orientation.

In order to determine the phase of nonlinear susceptibility, the SH light from the surface was allowed to interfere with the SH light generated in a reference crystal.[3] For the measurement of the absolute phase, comparison is made with a calibrated standard, a right-handed quartz crystal. The interference patterns are shown in Fig. 1. The experimental data indicate that the trace for the phenol solution is delayed by 90° with respect to the quartz standard. From the known phase of the $\chi^{(2)}_{xxx}$ for the bulk quartz[4] the absolute phase of $(\chi_s^{(2)})_{xzx}$ for the liquid is then found to be 180°. Theoretical calculations[5] indicate that for phenol $\overleftrightarrow{\alpha}^{(2)}$ is dominated by $\alpha^{(2)}_{\zeta\zeta\zeta}$, with ζ lying along the principal molecular axis. With this definition of the molecular ζ-axis the experimental data imply that the sense of phenol molecules is such that the hydroxy group points into the bulk water.

In conclusion, we have performed the first measurement of the absolute phase of surface nonlinear susceptibility.[6] We have shown that if the nonlinear response is due to electric dipole contributions the phase data can be related to the absolute molecular orientation. This information cannot be obtained directly from ordinary linear optical methods. Our work on the phenol-water system confirms the intuitive notion that the hydroxy end is directed towards water. A point of further interest is when surface structural information is available, one can use measurements of the type outlined here, to obtain the phases of the elements of the molecular nonlinear polarizibility.

This research was also supported by the Air Force Office of Scientific Research under Contract 84-0013B and by the National Science Foundation under Grants NSF-CHE 85-13553 and NSF-CHE 82-11593.

(1) Y.R. Shen, "The Principles of Nonlinear Optics," (Wiley, New York, 1984), Ch 25; J. Vac. Sc. Tech. B 3 (1985) 1464.

(2) J.M. Hicks, K. Kemnitz, K.B. Eisenthal and T.F. Heinz, J. Phys.

Chem. 90 (1986) 560.

(3) J.J. Wynne and N. Bloembergen, Phys. Rev. 188 (1969) 1211.

(4) R.C. Miller and W.A. Norland, Phys. Rev. B 2 (1970) 4896.

(5) J. Zyss, J. Chem. Phys. 70 (1979) 3341.

(6) K. Kemnitz, K. Bhattacharyya, J.M. Hicks, G.R. Pinto, K.B. Eisenthal and T.F. Heinz, Chem. Phys. Lett. (to be published).

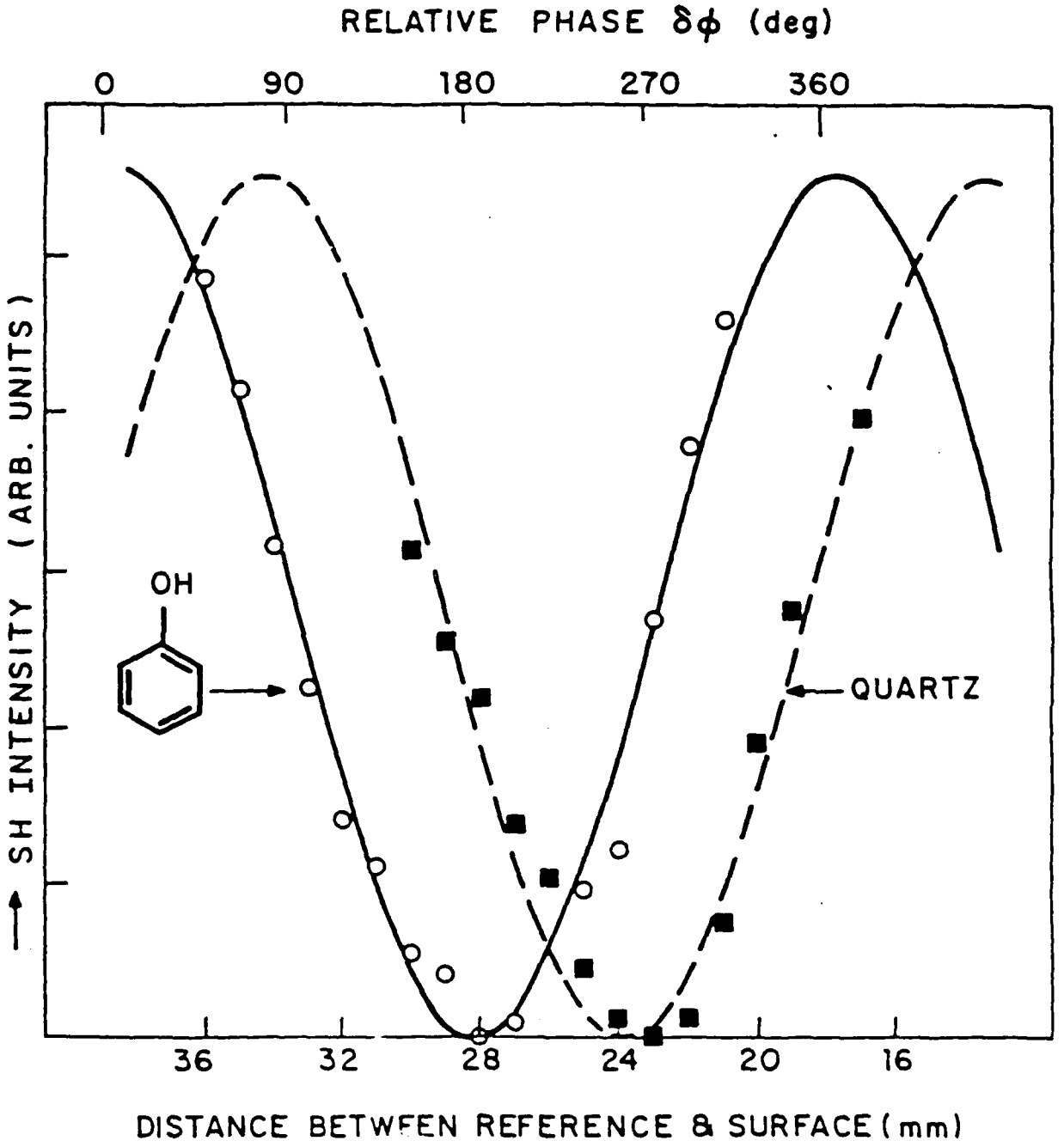

Figure 1: Interference pattern of the SH fields for the surface of a 0.4 M aqueous phenol solution (open circles) and for the quartz standard (filled boxes). The points are experimental data and the curves through them represent the best fits to $\cos^2$ functions.

B. PICOSECOND PHOTOISOMERIZATION IN LIQUIDS: DYNAMICS OF 1,1'-BINAPHTHYL

(R.M. Bowman, D.P. Millar and K.B. Eisenthal)
(JSEP work unit 6, 1985 - 1988)
(Principal Investigator: K.B. Eisenthal (212) 280-3175)

One of our major interests is the influence of the solvent on reactions which involve structural changes. An important reaction we have examined in this regard is the photoisomerization of 1,1'-binaphthyl, which involves only the twisting of the naphthalene moieties about a single bond.[1-4] Since this process is one-dimensional, comparisons can be made to one-dimensional barrier crossing theories,[5-7] in particular to Kramers' theory.[8]

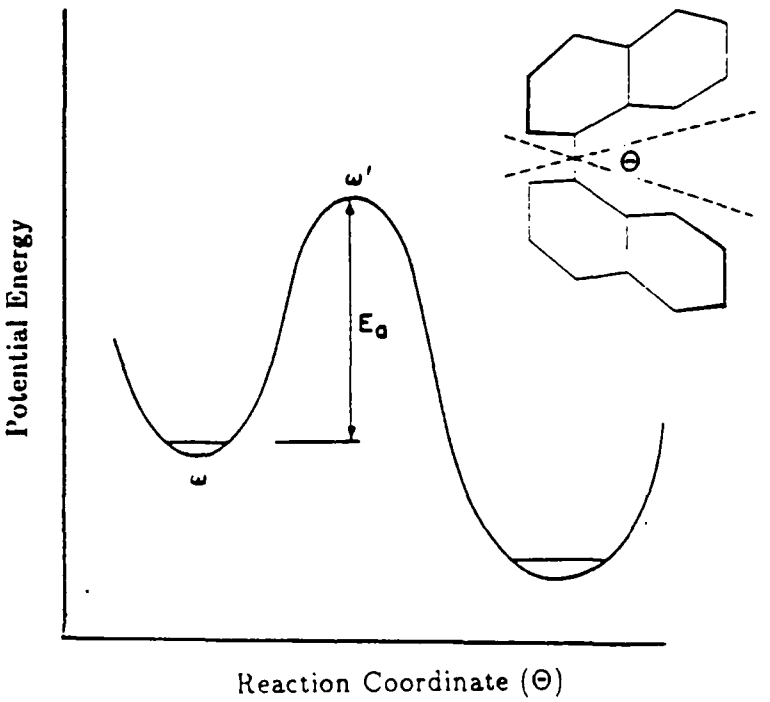

In our earlier work[9] we have shown that the twisting time of 1,1'-binaphthyl in several linear alcohols exhibits excellent agreement with Kramers' theory (Fig. 1). The agreement was obtained using the hydrodynamic model which relates the frictional drag coefficient to viscosity, where viscosity is a known macroscopic property of each solvent. The dynamics of 1,1'-binaphthyl in alcohols was the first

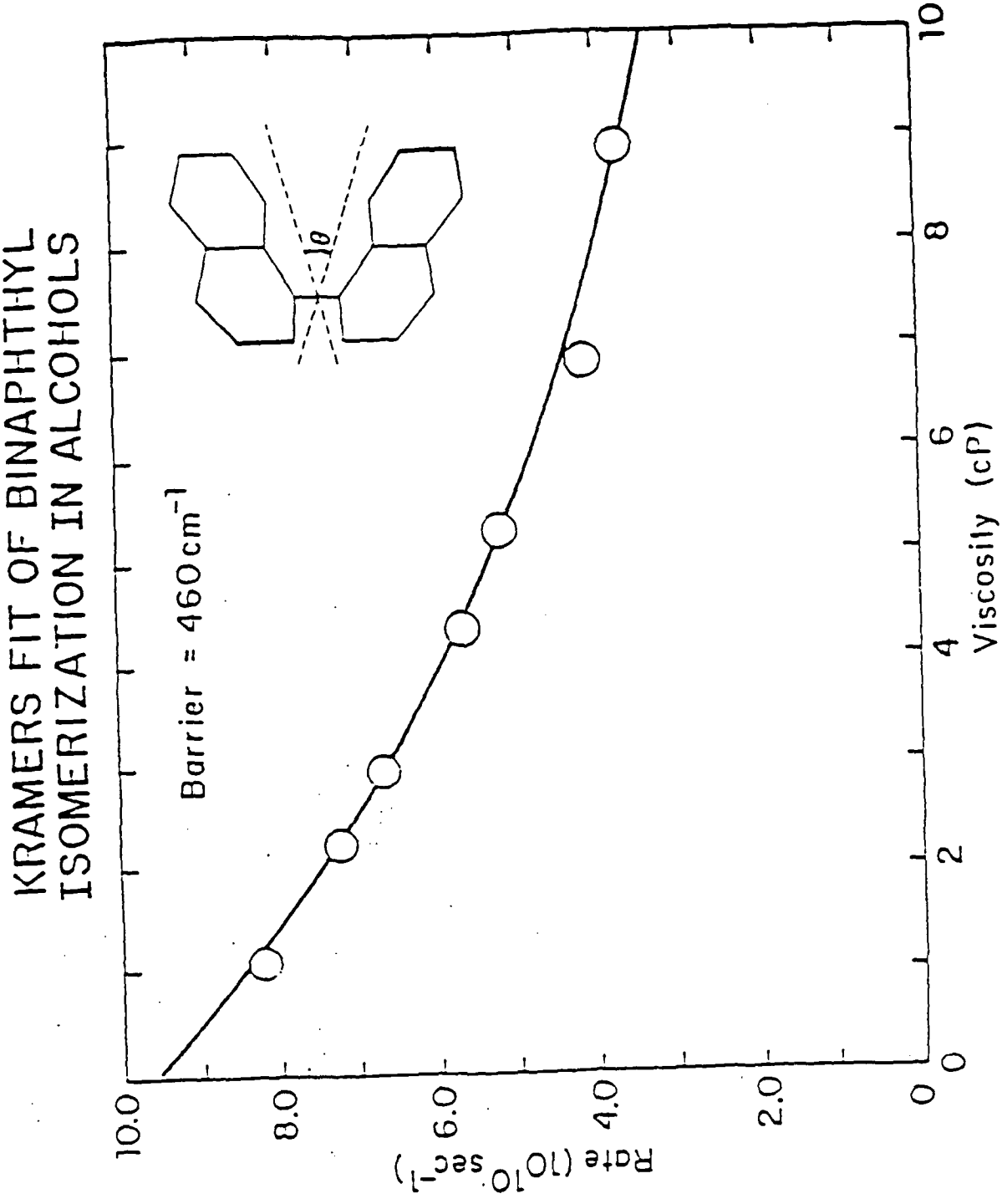

Figure 1: Barrier Crossing Rate of 1,1'-Binaphthyl versus Solvent Shear Viscosity in Alcohols.

observation of Kramers' behavior in the intermediate friction regime.

A crucial issue now is to see if Kramers' behavior is observed for 1,1'-binaphthyl in other solvent series. In our current work[10] we have measured the twisting times of 1,1'-binaphthyl in linear alkanes. The agreement of the alkane data with Kramers' theory is poor when using the hydrodynamic model. We are, however, able to get good agreement of Kramers' theory with experiment if we use the orientational relaxation times as a measure of solvent friction (Fig. 2). In this new approach we measured the orientational relaxation rate of 1,1'-binaphthyl in each alkane. By using time correlation functions we were able to relate the orientational relaxation times to the frictional drag coefficients, as originally suggested by Velsko et. al.[11] For completeness we measured the orientational relaxation rates for the linear alcohols. A good fit to Kramers' theory was also obtained for alcohols using the orientational relaxation times as a measure of the solvent friction.

It can be seen in the case of alcohols (Fig. 3) that viscosity scales linearly with orientational times. Because of this linearity both viscosity and orientational relaxation times turn out to be a good measure of solvent friction. On the other hand in alkane solvents there is a clear nonlinear dependence of the rotational reorientation time on the solvent viscosity (Fig. 4), which is especially seen at low viscositites, i.e. < 1 cP. In this case, only orientational relaxation is a good measure of friction. The problem now turns to understanding why orientational relaxation is a good measure of friction and where the discrepancy between solvent classes originates, i.e. why hydrodynamics appears to break down in alkanes. Since the energy barrier for excited state isomerization is similar in both alcohols (460 cm^{-1}) and in alkanes (480 cm^{-1}) we expect the solute-solvent interactions for the binaphthyl molecule to be similar in both solvent systems. We note, however, that the solvent-solvent interaction in alcohol will be larger than in alkane. This arises by virtue of the fact that alcohol possesses a hydroxyl group, which permits the solvent molecules to cluster via secondary hydrogen bonding. This is just one of several possible solvent-solvent interactions that may account for the underlying differences between the two solvent classes in terms of affecting the dynamics of conformational change in 1,1'-binaphthyl. In

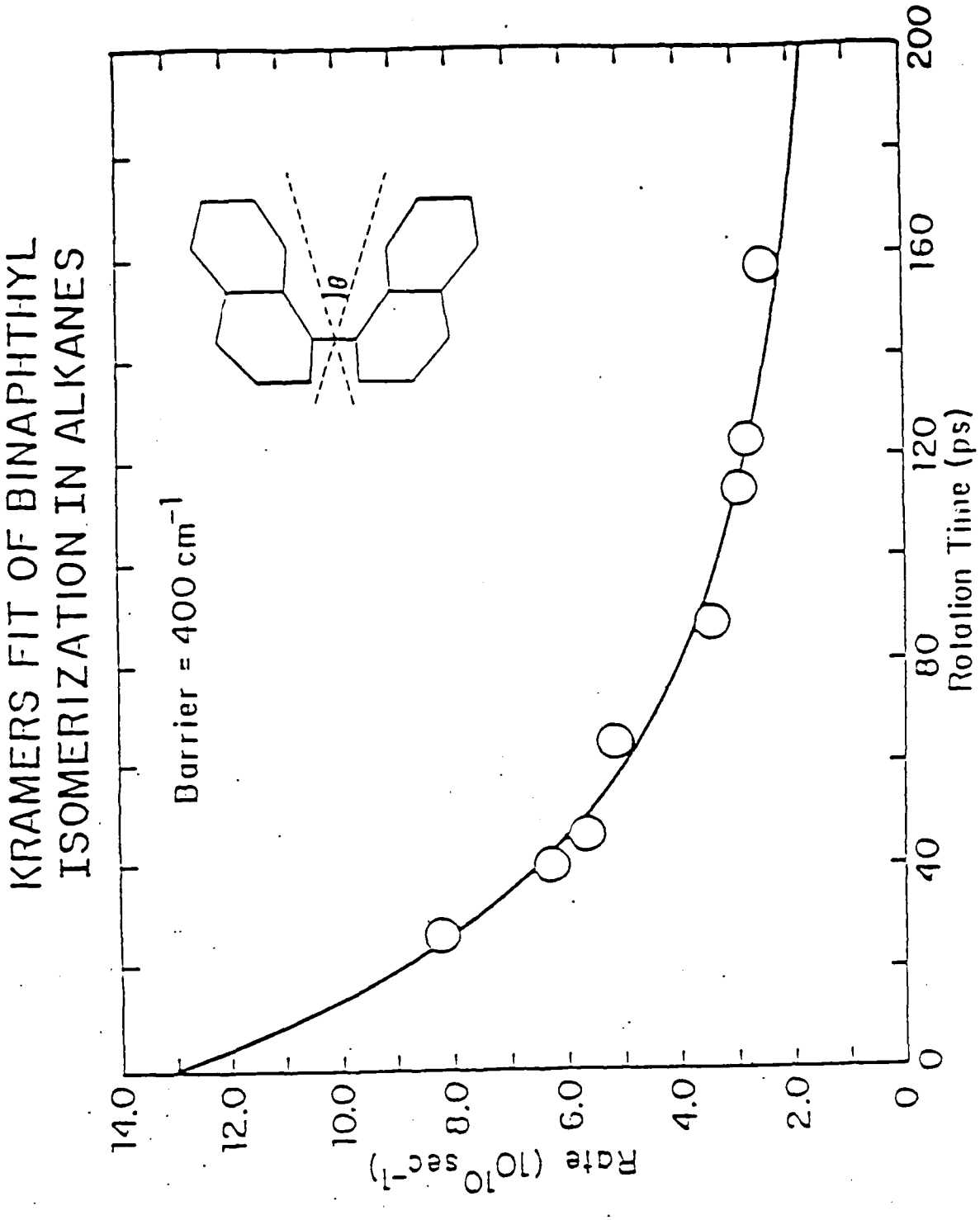

Figure 2: Barrier Crossing Rate of 1,1'-Binaphthyl versus Rotation Time in Alkanes.

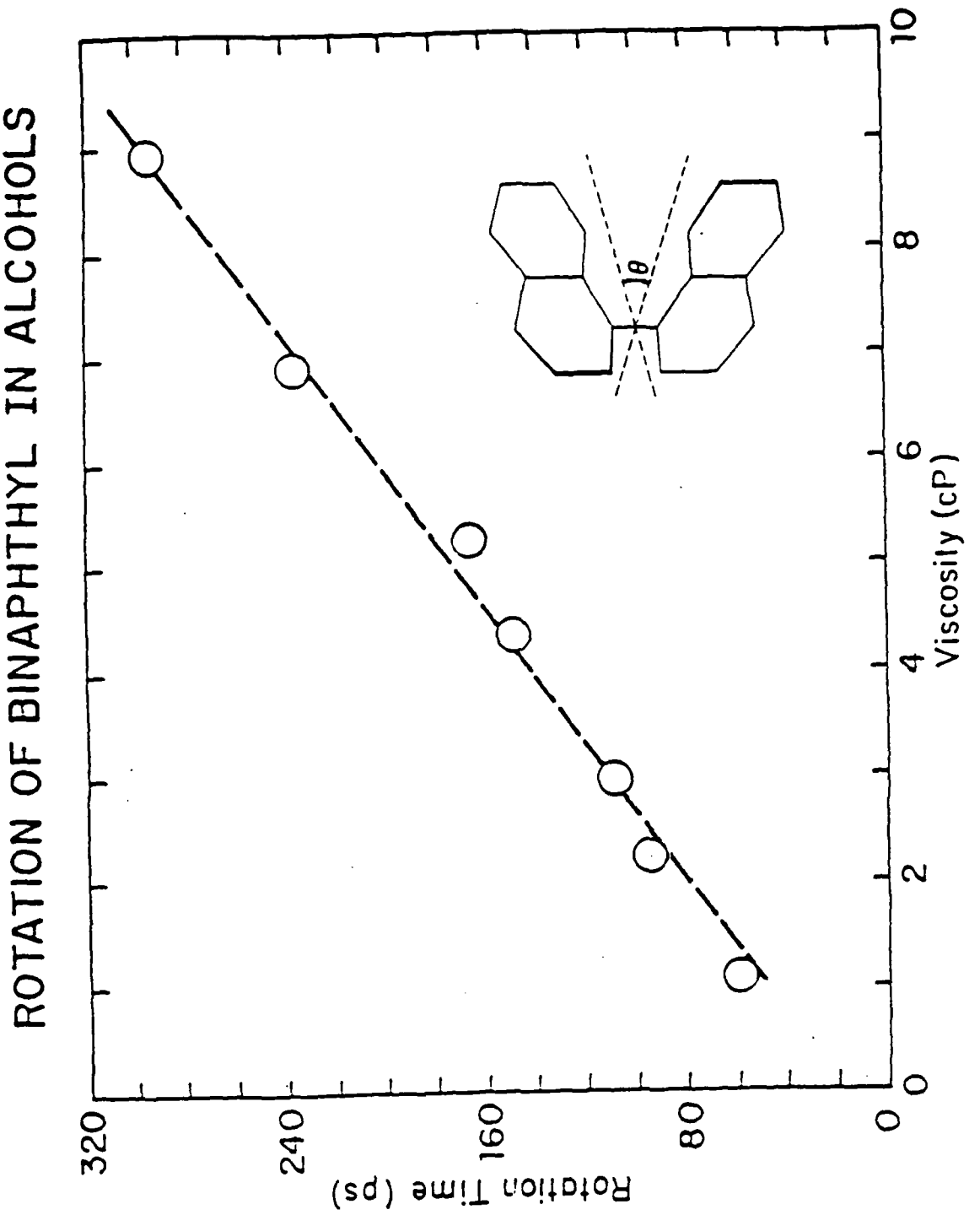

Figure 3: Plot of Rotation Re-orientation Time of 1,1'-Binaphthyl versus Solvent Shear Viscosity, in Alcohols.

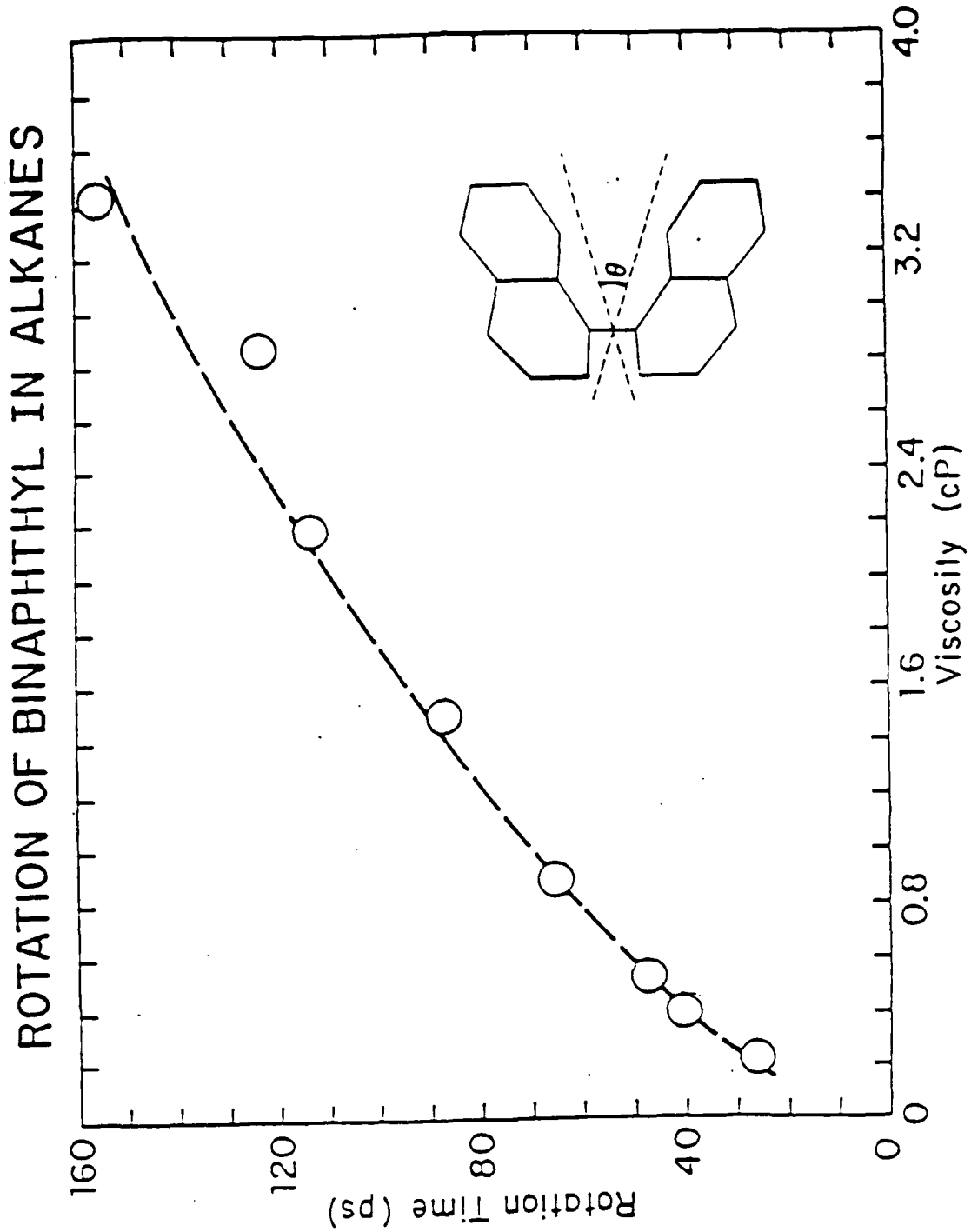

Figure 4: Plot of Rotation Re-orientation Time of 1,1'-Binaphthyl versus Solvent Shear Viscosity, in Alkanes.

summary, we have found that the photo-isomerization dynamics in 1,1'-binaphthyl follows Kramers' behavior in both alcohol and alkane solvent systems. It is also found that the use of orientational relaxation times as a measure of the solvent friction is crucial to the success of fitting Kramers' theory to the experimentally observed rates.

This research was also supported by the Air Force Office of Scientific Research under Contract 84-0013B and by the National Science Foundation under Grants NSF-CHE 85-13553 and NSF-CHE 82-11593.

(1) R.A. Friedel, M. Orchin, and L. Reggel, J. Am. Chem. Soc. 70, 199 (1948).

(2) R.M. Hochstrasser, Can. J. Chem. 39, 459 (1961).

(3) M.F. Post, J. Langelaar, and J.D.W. van Voorst, Chem. Phys. Lett. 32, 59 (1975).

(4) M.J. Riley, A.R. Lacey, M.G. Sceats, and R.G. Gilbert, Chem. Phys. 72, 83 (1982).

(5) B.J. Berne, J.L. Skinner, and P.G. Wolynes, J. Chem. Phys. 73, 4314 (1980).

(6) D.K. Garrity and J.L. Skinner, Chem. Phys. Lett. 95, 46 (1983).

(7) R.O. Rosenberg, B.J. Berne, and D. Chandler, Chem. Phys. Lett. 75, 162 (1980); J.A. Montgomery, Jr., D. Chandler, and B.J. Berne, J. Chem. Phys. 70, 4056 (1979).

(8) H.A. Kramers, Physica 7, 284 (1940).

(9) D.P. Millar and K.B. Eisenthal, J. Chem. Phys. 83, 5076 (1985).

(10) R.M. Bowman, D.P. Millar, and K.B. Eisenthal, manuscript in preparation.

(11) S.P. Velsko, D.H. Waldeck and G.R. Fleming, J. Chem. Phys. 78, 249 (1983).

C. POLARITY DEPENDENT BARRIERS AND THE PHOTOISOMERIZATION DYNAMICS OF POLAR MOLECULES IN SOLUTION

(J.M. Hicks, M.T. Vandersall, E.V. Sitzmann and K.B. Eisenthal)
(JSEP work unit 6, 1985 - 1988)
(Principal Investigator: K.B. Eisenthal (212) 280-3175)

There has been recent theoretical and experimental interest in potential energy barrier descriptions of molecular structural changes in solution.[1-9] For example, the dependence of photoisomerization kinetics on solvent viscosity has been studied to test barrier crossing models.[1-6] Changes in the photoisomerization rates through a solvent series or as a function of temperature have been attributed to viscosity and thermal effects; other possible effects, such as solvent dependent excited state potential surface variations, have generally not been considered.[9] In particular, strong interactions with polar solvents are expected for molecules that undergo a major charge redistribution on isomerization, whether they be polar molecules such as p-dimethylamino-benzonitrile (DMABN),[8] or nonpolar molecules that pass through very polar intermediate structures such as t-stilbene.[3-6] These polar interactions can be important factors in the dynamics of isomerization, as we will show in this paper.

1. DMABN - Case of a Polar Molecule -- DMABN is a classic example of a molecule that exhibits strong solute-solvent interactions, as demonstrated by the fact that its excited state isomerization occurs in polar solvents but not in nonpolar solvents.[10] A general scheme of the dynamics is given in Scheme I.[11]

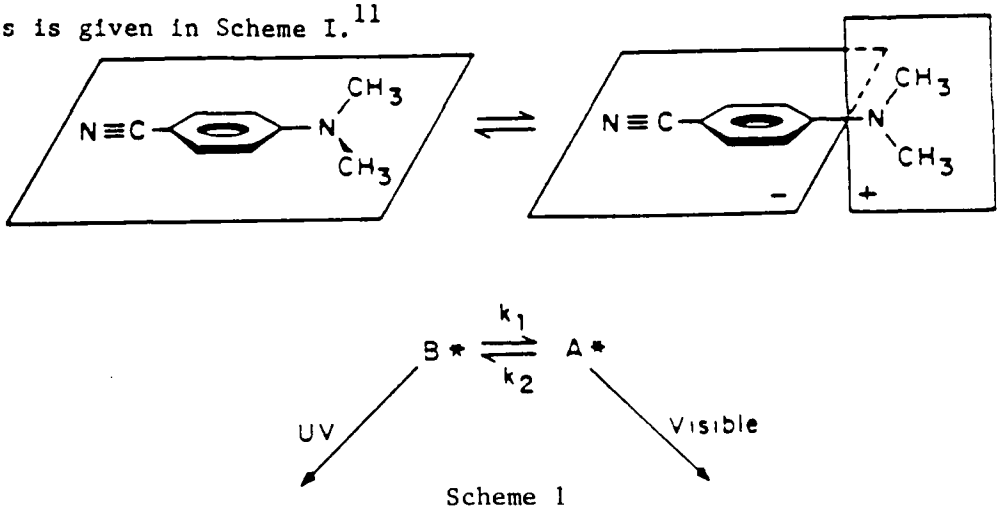

Scheme 1

The isomerization takes place on an excited singlet potential surface and involves a 90^{o} rotation of the dimethylamino group about the aminophenyl bond.[11] This twisting structural change produces an increase in the excited state dipole moment from 6 D to 16 D.[12] In polar solvents, a new visible emission appears due to the solvent stabilized twisted form. Due to a rapid equilibration between the planar (B^{*}) and twisted (A^{*}) structures two emissions are observed. The one in the ultraviolet is due to the planar form and the visible emission is due to the twisted polar form. In alkanes, only the uv emission from B^{*} is observed. Many time-resolved studies have been conducted on DMABN, yet the role of the solvent is still not clear.[8,13-17]

To investigate the effects of the solvent on the photoisomerization kinetics of DMABN, we have carried out studies in a series of linear alcohols, alcohol/alkane mixtures, linear nitriles and nitrile/alkane mixtures (part of the data has been reported[8,13]). A single pulse from the output of a Nd^{+3}/glass laser was frequency quadrupled to 265 nm and used to excite DMABN. The fluorescence from the B^{*} and A^{*} states was time-resolved with a streak camera detection system that had a resolution of 7 ps.[14]

An important aspect of the solute/solvent interactions is the effect of solvent viscosity on the kinetics of a reaction. From studies in neat liquids, we find a viscosity dependence in nitriles of $\eta^{-2/3}$ and in alcohols, η^{-1}. These can be interpreted as cases of intermediate and strong solute-solvent coupling, respectively. Of key importance in obtaining these viscosity dependences of k_1 is the assumption that only the viscosity differences among the various members of the solvent series affect the rate. The possibility that the potential surface may change in different solvents is not considered, nor are the possibilities that boundary conditions, entropy or dynamic polarity effects vary with solvent. For a polar structural transition such as in DMABN, the invariance of the potential cannot be assumed. Specifically, the changes in solvent polarity, even within a polar series, can be of sufficient magnitude to produce marked changes in the excited state barrier height. It has long been recognized that there are barrier height changes in going from a nonpolar to a polar solvent. The issue

here is that these barrier effects can come into play within a solvent family, e.g. the polar alcohol series, or in one solvent at different temperatures.

To separate the effects of solvent polarity and viscosity, we have used two techniques: (i) k_1 was measured at room temperature in isoviscous mixtures of a polar solvent and an alkane, where the polarity of the mixture was controlled by the concentration of the polar solvent, and (ii) the temperature was varied for the neat solvents so that the solutions had the same viscosity but different polarity values. We find that the isomerization rate increases exponentially with increasing solvent polarity as measured by the widely used[18] empirical solvent polarity parameter $E_T(30)$. It is important to emphasize that the rate dependence on $E_T(30)$ occurs when both viscosity as well as temperature remains constant.

Further support for the effects of solvent polarity on the isomerization dynamics is obtained from the second technique where the same viscosity is obtained by adjusting the temperatures of the neat liquids. The different rates measured have previously been assumed to be due to the different Boltzmann factors. This can be seen in the following Arrhenius-type expression

$$k = A\, f(\eta)\, \exp(-E_a/RT) \qquad (1)$$

where E_a is the barrier height, $f(\eta)$ is the viscosity function (which is a constant for the isoviscosity experiment) and A is the pre-exponential frequency factor. We carried out these measurements in both the neat alcohols and neat nitriles, and found that the rate increases as the temperature is lowered in both solvent families. This result of a "negative" activation energy is contrary to what would be the case if only the Boltzmann factor is changing. To explain these results, we propose that the barrier height is not independent of temperature, but decreases due to a higher solvent polarity at lower temperatures. The polar twisted form of DMABN (A^*) is stabilized relative to the initially excited planar form (B^*), which thereby leads to a smaller barrier. This decrease in the barrier overcomes the usual Boltzmann effect and is responsible for the increased rate at lower temperature. When we correct for the temperature induced polarity changes, we find that the corrected rate decreases as the temperature is lowered, i.e. a normal

positive activation energy is obtained.

We can explain the dynamics of TICT formation of DMABN in both alcohol and nitrile solvents by introducing a polarity dependent barrier E_a:

$$E_a = E_a - A(E_T(30)-30) \quad (2)$$

where E_a is the activation energy in an alkane solvent having an $E_T(30)$ of 30 and A is an experimentally determined factor that determines how strongly the barrier height changes with solvent polarity. The correct rate, κ, may be expressed as

$$\kappa = k_1 \exp(-A(E_T(30)-30)/RT) = C \exp(-E_a/RT) \quad (3)$$

where C is the Arrhenius pre-exponential factor. It is found that ln varies linearly with 1/T with negative slope, and thus permits the evaluation of the intrinsic value of E_a. The values of E_a are found to be 8.0 kcal/mole in the nitriles and 14.0 kcal/mole in the alcohols. Comparing the nitriles and alcohols at a given solvent polarity, we see that the barrier E_a is apparently higher in alcohols by about 6 kcal/mole.[20-23] One explanation for this is the presence of hydrogen bonding between the dimethylamino group of DMABN and the alcohol hydroxy group. The hydrogen bond withdraws electrons from the electron donating dimethylamino part of DMABN and thereby opposed the electron transfer to the benzonitrile part of DMABN. For the intramolecular charge transfer in DMABN to occur, the hydrogen bond must be broken. This increases the barrier for the isomerization in alcohols relative to nitriles by about 6 kcal/mole, roughly the energy of typical hydrogen bonds. Previously, by using linear free energy relations, Kupfer and Abraham also noted this fundamental difference in the solvation of the excited DMABN in protic versus aprotic solvents.[24]

Having obtained a quantitative expression for the polarity dependence of the rate k_a, we can now correct for the polarity differences in neat nitriles and alcohols in order to investigate the viscosity dependence of the isomerization. It is found that there is a negligible dependence of the polarity-corrected rate, κ(from (3)), on the viscosity for both nitriles and alcohols. From this result we conclude that the major role played by the solvent in the isomerization of DMABN is in stabilizing the more polar twisted form via dielectric interactions, and not in providing friction against which the

dimethylamino group must twist.

2. t-Stilbene - Case of a Polar Intermediate Structure -- The photoisomerization of t-stilbene has been studied by many groups to gain insight into how the solvent affects this simple chemical change.[3-6] The observed rate has been discussed in terms of (1), where $f(\eta)$ is either the Kramers function (which gives poor agreement with the observed rates)[3] or more often[6] $\eta^{-\alpha}$. This latter form can be obtained from a free volume[26] or frequency dependent friction model.[27-28] This general equation predicts that at constant viscosity, a plot of lnk versus T^{-1} should have the slope $-E_a/R$. We have tested this prediction by studying the rates of photoisomerization of stilbene in alcohols at various temperatures under constant viscosity conditions. A Nd^{3+}/YAG laser with pulses 30 ps in duration was used to excite the t-stilbene, and the fluorescence was detected using a streak camera, as for DMABN. A polarizer oriented at 54.7^{o} was placed in the collection optics to avoid the effects of time-dependent depolarization of fluorescence.

In Fig. 1 it is shown that the slopes of these lines depend on viscosity, contrary to what the equation predicts. The apparent E_a's vary from 2.6 to 1.2 kcal/mole. A similar deviation from (1) is shown by the dependence of the rate on viscosity at different fixed temperatures. We find that the value of α varies by a factor of two over a 50 K temperature range. This result conflicts with the constant α value predicted by the $\eta^{-\alpha}$ dependence of the rate equation.

Since the isomerization involves an intermediate structure that is highly polar, we ask whether polarity dependent barrier effects are important in the isomerization process. Accordingly, we carried out measurements in neat alcohols at various solvent polarities and temperatures, analogous to our DMABN study. We found that static polarity effects alone do not explain our stilbene results in alcohols. In stilbene, dynamic polarity effects could be important since extensive solvent rearrangements are required in the isomerization from the initial nonpolar form to the twisted charge separated form. This is not expected for DMABN because its transition involves an increase in dipole moment along the same axis from a polar (6 Debye) to a more polar (16

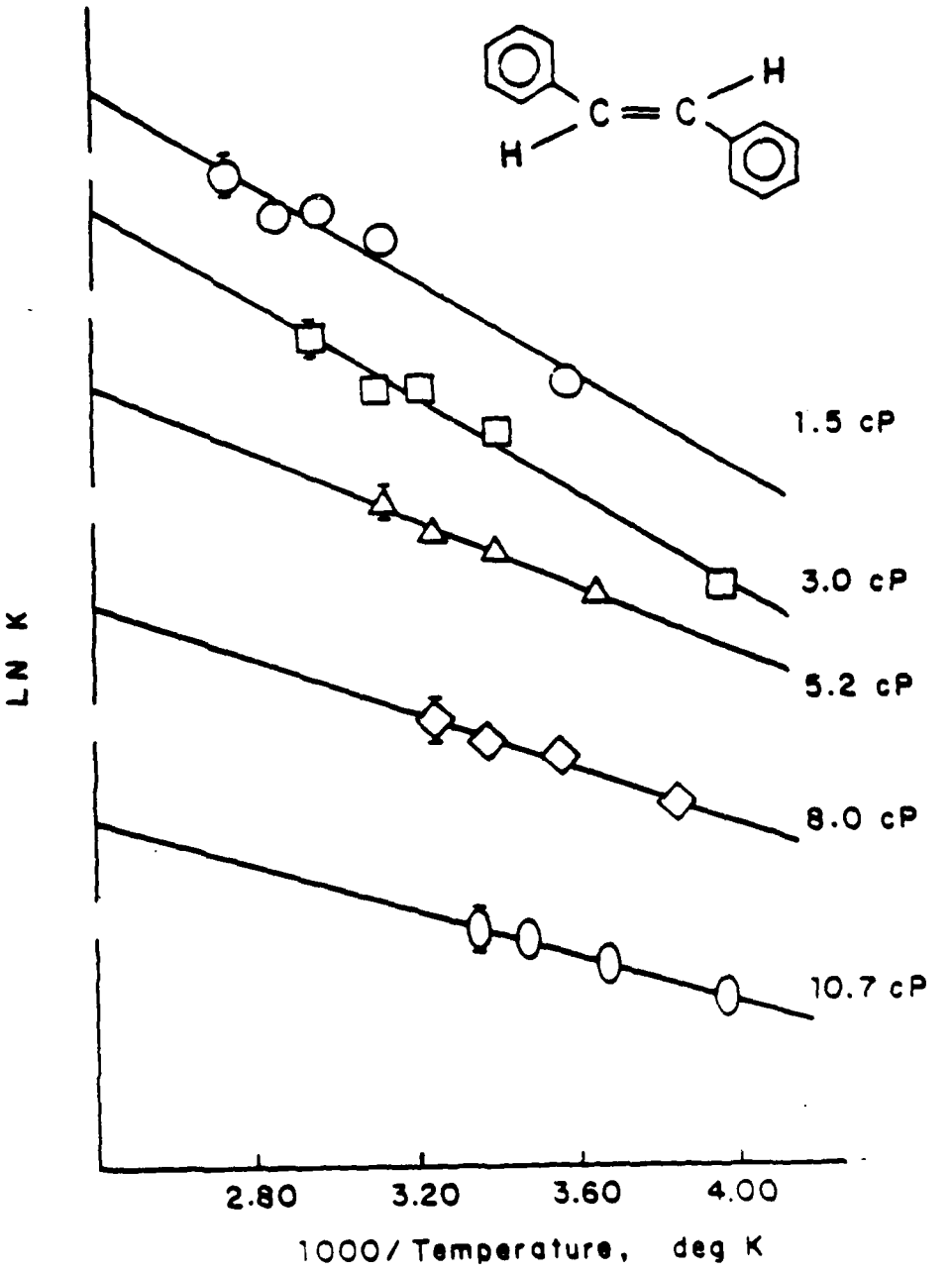

Figure 1: Arrhenius plot of the logarithm of k_1 for t-stilbene in isoviscous alcohols: the ordinate axis is offset for each viscosity line for viewing purposes

Debye) form. The solvent is already arranged about the large dipole in the initially excited DMABN, unlike the case for stilbene, where the initial solvent arrangement is that appropriate to a nonpolar solute molecule. If the solvent motions are not very rapid compared to the isomerization time, then the isomerization dynamics would depend on the dielectric relaxation properties of the solvent.[29-36] The energy separating the trans and intermediate form would therefore depend upon the positions of the surrounding solvent molecules, and thus be dependent on the rate of change of the solvent arrangement. Further work is underway to resolve the role of polarity and other solvent factors in the stilbene isomerization.

3. Conclusions -- We find that the isomerization dynamics of molecules that involve a large charge redistribution, such as in DMABN, are strongly dependent on the polarity of the solvent. The solute/solvent interaction can be described in terms of a polarity dependent barrier that separates the two structural forms of the molecule. In addition to the well-recognized effects in going from a nonpolar to a polar solvent, we find that the effects of polarity change within a series of related polar liquids, e.g. linear alcohols or nitriles, and the effects of the change in polarity with temperature are crucial to the observed kinetics. We have also found that hydrogen bonding of DMABN with alcohols impedes the isomerization relative to that of nonhydrogen bonding polar solvents such as nitriles. For t-stilbene in alcohols, we have found from measurements at various viscosities and temperatures that the isomerization cannot be described in terms of frequently applied equations that contain an $\eta^{-\alpha}$ power dependence. Although the t-stilbene isomerization passes through a very polar intermediate structure, we are not able to adequately fit the data using a static polarity correction as we did for DMABN. The possibility of a dynamic polarity effect due to a large solvent rearrangement in going from the nonpolar initially excited t-stilbene to the polar twisted intermediate stilbene structure is discussed.

This research was also supported by the Air Force Office of Scientific Research under Contract 84-0013B and by the National Science

Foundation under Grants NSF-CHE 85-13553 and NSF-CHE 82-11593.

(1) D.P. Millar and K.B. Eisenthal, J. Chem. Phys. 83, 5076 (1985).

(2) H. Courtney and G.R. Fleming, Chem. Phys. Lett. 103, 443 (1984); K.M. Keery and G.R. Fleming, Chem. Phys. Lett. 93, 322 (1982); S.P. Velsko and G.R. Fleming, J. Chem. Phys. 76, 3553 (1982); S.P. Velsko, D.H. Waldeck and G.R. Fleming, J. Chem. Phys. 78, 249 (1983).

(3) G. Rothenberger, D.K. Negus and R.M. Hochstrasser, J. Chem. Phys. 79, 5360 (1983); M. Lee, G.R. Holtom and R.M. Hochstrasser, Chem. Phys. Lett. 118, 359 (1985).

(4) V. Sundstrom and T. Gillbro, Ber. Bunsen. Phys. Chem. 89, 222 (1985); Chem. Phys. Lett. 109, 538 (1984); E. Akesson, H. Bergstrom, V. Sundstrom and T. Gillbro, Chem. Phys. Lett. 126, 385 (1986); Chem. Phys. 106 (1986) 269.

(5) G. Maneke, J. Schroeder, J. Troe and F. Voss, Ber. Bunsen. Phys. Chem. 89, 896 (1985).

(6) S.H. Courtney and G.R. Fleming, J. Chem. Phys. 83, 215 (1985).

(7) J.T. Hynes, Ann. Rev. Phys. Chem. 36, 573 (1985) and references therein.

(8) J.M. Hicks, M.T. Vandersall, Z. Babarogic and K.B. Eisenthal, Chem. Phys. Lett. 116, 18 (1985).

(9) Cases where it has been considered include: Ref. 8, J. Troe, Chem. Phys. Lett. 114, 241 (1985); 116, 453 (1985); J. Phys. Chem. 90, 357 (1986); W.L. Hase, J. Phys. Chem. 90, 365 (1986); E. Akesson et. al. of Ref. 4, V. Sundstrom and T. Gillbro, J. Chem. Phys. 81, 3463 (1984).

(10) E. Lippert, W. Luder and H. Boos, in Advanced in Molecular Spectroscopy, ed. by A. Mangini (Pergamon Press, Oxford, 1962) p. 443.

(11) K. Rotkiewicz, K.H. Grellman and Z.R. Grabowski, Chem. Phys. Lett. 19, 315 (1973); Z.R. Grabowski, K. Rotkiewicz, W. Rubaszewska and E. Kirkor-Kaminska, Acta Phys. Pol. A 54, 767 (1978).

(12) W. Baumann, personal communication; Z. Naturforsch. 36A, 868 (1981).

(13) Y. Wang and K.B Eisenthal, J. Chem. Phys. 77, 6076 (1982).

(14) Y. Wang, M. McAuliffe, F. Novak and K.B. Eisenthal, J. Phys. Chem. 85, 3736 (1981).

(15) D. Huppert, S.D. Rand, P.M. Rentzepis, P.F. Barbara, W.S. Struve

and Z.R. Grabowski, J. Chem. Phys. 75, 5714 (1981).

(16) F. Heisel and J.A. Miehe, Chem. Phys. Lett. 100, 183 (1983); Chem. Phys. 98, 233 (1985); with J.M.G. Martino, 98, 243 (1985).

(17) S.R. Meech and D. Phillips, Chem. Phys. Lett. 116, 262 (1985).

(18) C. Reichardt, in Molecular Interactions, vol. 3, ed. by H. Ratajcak and W.J. Orville-Thomas (John Wiley, New York, 1982) p. 241.

(19) E. Lippert, Z. Naturforsch. 10a, 541 (1955); N. Mataga, Y. Kaifu and M. Koizumi, Bull. Chem. Soc. Jap. 29, 465 (1956).

(20) The hydrogen bonding contributions to the $E_T(30)$ polarity parameter (as discussed in references 21-23) could also account for some of the differences observed in the data for nitriles and alcohols. However, the different lines in Figs. 1, 2 and 4 are not mere artifacts of the choice of polarity parameter. These differences appear when the data is plotted against different polarity parameters such as the emission energy of DMABN itself, the function $\Phi = (\varepsilon-1)/(\varepsilon+2)$, and Δf[19].

(21) B.S. Neporent and N.G. Bakshiev, Opt. and Spect. 8, 408 (1960).

(22) M.J. Kamlet, J.L. Abboud and R.W. Taft, J. Am. Chem. Soc. 99, 6027 (1977).

(23) R.W. Taft and M.J. Kamlet, J. Am. Chem. Soc. 98, 2886 (1976).

(24) M. Kupfer and W. Abraham, Chem. Phys. Lett. 122, 300 (1985).

(25) D. Rehm and A. Weller, Israel J. Chem. 8, 259 (1970).

(26) A.H. Alwattar, M.D. Lumb and J.B. Birks, in Organic Molecular Photophysics, ed. by J.B. Birks (John Wiley, New York, 1973) ch. 8.

(27) R.F. Grote, G. van der Zwan and J.T. Hynes, J. Phys. Chem. 88, 4676 (1984).

(28) B. Bagchi and D.W. Oxtoby, J. Chem. Phys. 78, 2735 (1983).

(29) The effects of solvent dielectric relaxation time on processes such as barrierless charge transfer reactions, electron solvation, and rotations of dipolar solute molecules, has been the subject of important experimental and theoretical activity (see refs. 30-36).

(30) P. Madden and D. Kivelson, J. Phys. Chem. 86, 4244 (1982).

(31) D. Kivelson and K.G. Spears, J. Phys. Chem. 89, 1999 (1985).

(32) H.E. Lessing and M. Reichert, Chem. Phys. Lett. 46, 111 (1977).

(33) B. Bagchi, D.W. Oxtoby and G.R. Fleming, Chem. Phys. 86, 257 (1984).

(34) G. van der Zwan and J.T. Hynes, Chem. Phys. 90, 21 (1984); J. Chem. Phys. 89, 4181 (1985); Chem. Phys. Lett. 101, 367 (1983).

(35) G.W. Kenney-Wallace and C.D. Jonah, Chem. Phys. Lett. 47, 362 (1977).

(36) L.A. Phillips, S.P. Webb, L.F. Buhse and J.H. Clark, in Ultrafast Phenomena IV, ed. by D.H. Auston and K.B. Eisenthal, (Springer Verlag, Berlin, 1984).

D. PICOSECOND LASER STUDIES ON THE PHOTODISSOCIATION OF TETRAPHENYLOXIRANE: EFFECT OF CARBENE PRECURSOR DISSOCIATION AND ENERGY DECAY ON PATHWAYS AND DYNAMICS

(E.V. Sitzmann, J. Langan and K.B. Eisenthal)
(JSEP work unit 6, 1985 - 1988)
(Principal Investigator: K.B. Eisenthal (212) 280-3175)

The sequence of energy relaxing steps following optical excitation of a carbene precursor are essential to unravelling the chemistry of the carbene. For example the primary steps leading to the carbene are important in that energy decay in the excited state precursor can alter the dynamics and channels of carbene formation. In some precursors the quantum yield is wavelength dependent,[1] indicating an extremely rapid fragmentation. A particularly important example of this effect is found for aromatic diazo compounds. In the case of diphenyldiazomethane, ultraviolet photoexcitation leads to C-N bond rupture on the order of less than 10 ps.[2]

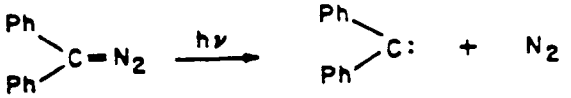

DIAZO CARBENE

Very little is known about other carbene precursors. In particular, kinetic details for other carbene precursors remain largely unknown.[3] With this in mind we have investigated the photophysics of tetraphenyloxirane (TPO), which like diphenyldiazomethane, undergoes photodecomposition to yield diphenylcarbene.[4,5]

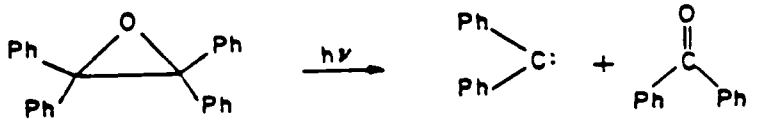

OXIRANE CARBENE KETONE

We find that irradiation of TPO at 266 nm produces two transients, which are observed by laser induced fluorescence at 500 nm and 580 nm, respectively. The transient that emits at 580 nm grows in as a single exponential with a time constant that is < 30 ps, and persists for several nanoseconds. The formation kinetics of this transient are not

found to exhibit a significant solvent dependence. We identify this species as a 1,3-biradical that is directly formed as a result of C-C cleavage of ^{1} TPO (see path A in Scheme 1). It is noteworthy that this biradical is similar to a ketyl radical, with the exception that the oxygen bearing hydrogen has been replaced by $-C(Ph)_2$. Since the chromophores are similar, it is expected that they will have similar spectral properties. For example, it is known that the ketyl radical has a higher extinction coefficient at 355 nm than at 266 nm. We therefore would expect the transient formed via path A to absorb light in a similar way. Confirmation of this is shown by the fact that the laser induced fluorescence (LIF) at 580 nm depends on the probe wavelength. Using a 355 nm picosecond laser pulse as the probe produces strong LIF at 580 nm. In contrast, when the probe wavelength is changed from 355 nm to 266 nm the LIF signal is negligible. We also note that the ketyl radical is known to fluoresce strongly at 580 nm,[6] and thus substantiates this assignment of the transient produced by the photodecomposition of TPO. Finally, the fast formation time (< 30 ps) of this biradical is consistent with the mechanism involving its direct formation from the photodissociation of TPO, as shown in path A of Scheme 1.

The second transient that emits at 500 nm is assigned to the triplet ground state of diphenylcarbene (^{3}DPC).[7,8] The formation time of ^{3}DPC was found to have an induction period of 70 ps before single exponential behavior was observed. The formation rate of ^{3}DPC was thus found to obey the kinetics of a sequential first order process involving two elementary steps. After accounting for the 70 ps induction period, it is found that the rate of formation of ^{3}DPC in several different solvents matches precisely the intersystem crossing rate (k_{ST}) as observed when

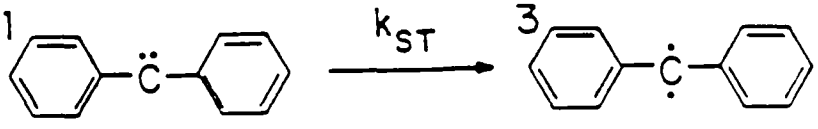

using diphenyldiazomethane as the carbene precursor,[9-11] see Table 1. Consistent with this kinetic evidence we postulate that carbene formation proceeds via C-O bond rupture in the ^{1*} TPO to produce an

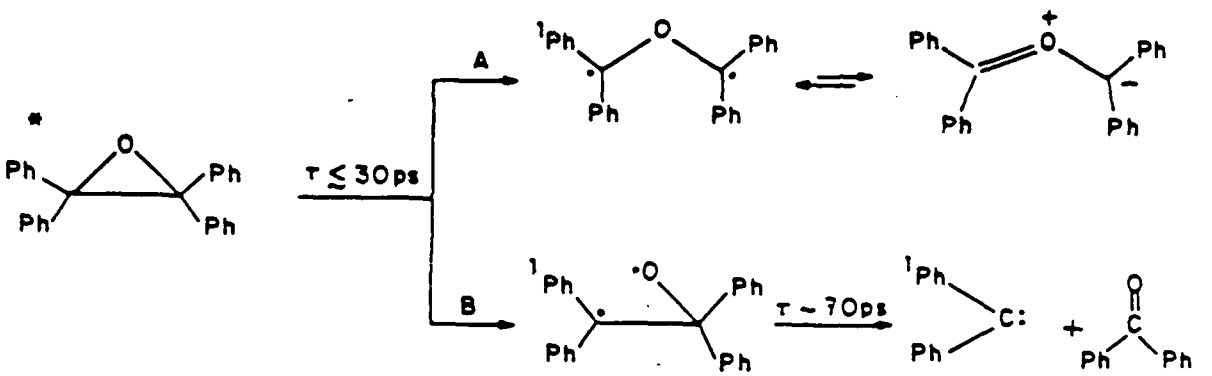

Scheme 1. Photodecomposition of Tetraphenyloxirane in fluid solution at room temperature

Table 1

Kinetics of ^{3}DPC Formation Following Photodecomposition of Tetraphenyloxirane (TPO) in Various Solvents at Room Temperature

Solvent	T_1 (ps)[a]	T_2 (ps)[a]	$1/k_{ST}$ (ps)[b]
3-methylpentane	70±14	95±11	95±12
isooctane	70±12	95±10	95±9
diethylether	80±15	135±14	130±11
1,4-dioxane	65±10	153±12	
tetrahydrofuran	75±10	183±15	180±14
1,3-dioxolane	50±10	190±15	190±15
acetonitrile	67±14	313±25	310±18

[a] T_1 and T_2 are optimized rate parameters obtained by fitting a two step sequential rate process to the LIF data, using TPO as the carbene precursor.

[b] obtained using diphenyldiazomethane as the carbene precursor.

intermediate 1,3-biradical. This 1,3-biradical persists on the order of 70 ps before it suffers annihilation via C-C cleavage to produce ^{1}DPC, see path B in Scheme 1. From our picosecond time resolved experiments we thus find that photodissociation of tetraphenyloxirane does not lead directly to the carbene. We find that photo-induced ring opening of tetraphenyloxirane proceeds sequentially and involves the competition between C-C cleavage (path A) and C-O cleavage (path B), to produce two distinct species. Furthermore, we find that only one route is responsible for carbene formation, i.e. path B, which involves a short lived (70 ps) singlet 1,3-biradical intermediate.

This research was also supported by the Air Force Office of Scientific Research under Contract 84-0013B and by the National Science Foundation under Grants NSF-CHE 85-13553 and NSF-CHE 82-11593.

(1) W. Kirmse, Carbene Chemistry, 2nd ed., chap. 1 (Academic Press, New York, 1971).

(2) C. Dupuy, G.M. Korenowski, M. McAuliffe, W.M. Hetherington and K.B. Eisenthal, Chem. Phys. Lett. 77, 275 (1981).

(3) L.E. Manring and K.S. Peters, J. Am. Chem. Soc. 106, (1984).

(4) K.B. Eisenthal, N.J. Turro, E.V. Sitzmann, I.R. Gould, G. Hefferon, J. Langan and Y. Cha, tetrahedron 41, 1543 (1985).

(5) R.S. Becker, R.O. Bost, J. Kolc, N.R. Bertoniere, R.L. Smith, and G.W. Griffin, J. Am. Chem. Soc. 92, 1302 (1970).

(6) B.W. Hodgson, J.P. Keene, E.J. Land, A.J. Swallow, J. Chem. Phys., 63, 3671, 1975.

(7) A.M. Trozzolo and W.A. Gibbons, J. Am. Chem. Soc. 89, 239 (1967).

(8) Y. Wang, E.V. Sitzmann, F. Novak, C. Dupuy, and K.B Eisenthal, J. Am. Chem. Soc. 104, 3238 (1982).

(9) E.V. Sitzmann, J.G. Langan and K.B. Eisenthal, J. Am. Chem. Soc. 106, 1868 (1984).

(10) E.V. Sitzmann, J.G. Langan, and K.B. Eisenthal, Chem. Phys. Lett. 112, 521 (1984).

(11) J.G. Langan, E.V. Sitzmann, and K.B. Eisenthal, Chem. Phys. Lett. 110, 521 (1984).

V. OPTICAL TRANSIENT SPECTROSCOPY

A. SPECTROSCOPIC AND MULTI-WAVE-MIXING STUDIES IN SOLIDS AND MOLECULAR DYES.

(F. Moshary and S. R. Hartmann)
(JSEP work unit 2, 1985-1988)
(Principal Investigator: S. R. Hartmann (212)280-3272)

1. Introduction--In the last year we have received and have been testing an Air Products and Chemicals Inc. closed cycle cryogenic refrigerator unit for optical study of solids at Liquid Helium temperatures. This unit, which will soon be fully operational, has made it possible to operate at LHe temperature continuously and at low cost. Also, the high temperature stability and controllability of this unit will increase the speed and accuracy of future temperature dependent experiments as well. In continuation of our previous research efforts, using the above unit, we have performed a variety of experiments in Pr^{3+} electronic transitions in the LaF_3 crystal field at 4.2 K. These include non-degenerate four wave mixing experiments for the study of three level coherence and inhomogeneous broadening and also further study of satellite echoes in this sample. In the near future we will also be studying dependence of relaxation rates in the above system on Pr^{3+} and Nd^{3+} ion concentration and investigate the possibility of Ion-Ion energy transfer in this crystal.

Another part of our effort has been aimed at the development and study of incoherent light sources to be used in the broad-band incoherent spectroscopy experiments. These experiments are currently in progress in Molecular dyes in solutions, and glass doped with semiconductor Microcrystallites . In the near future we plan to apply this technique to the study of excitons in GaAs multi-quantum well system as well.

2. Experiment.(a) Pr3+ Ion In LaF_3 (Figure 1) -- In the previous photon echo studies performed on the $^3P_0$-$^3H_6$ and $^3P_0$-$^3H_4$ transitions, we have observed anomalously fast photon echo relaxation rates which are not explainable by the known relaxation processes in this system. Further more, stimulated photon echo experiments seem to indicate that the above relaxation rates observed are in fact due to

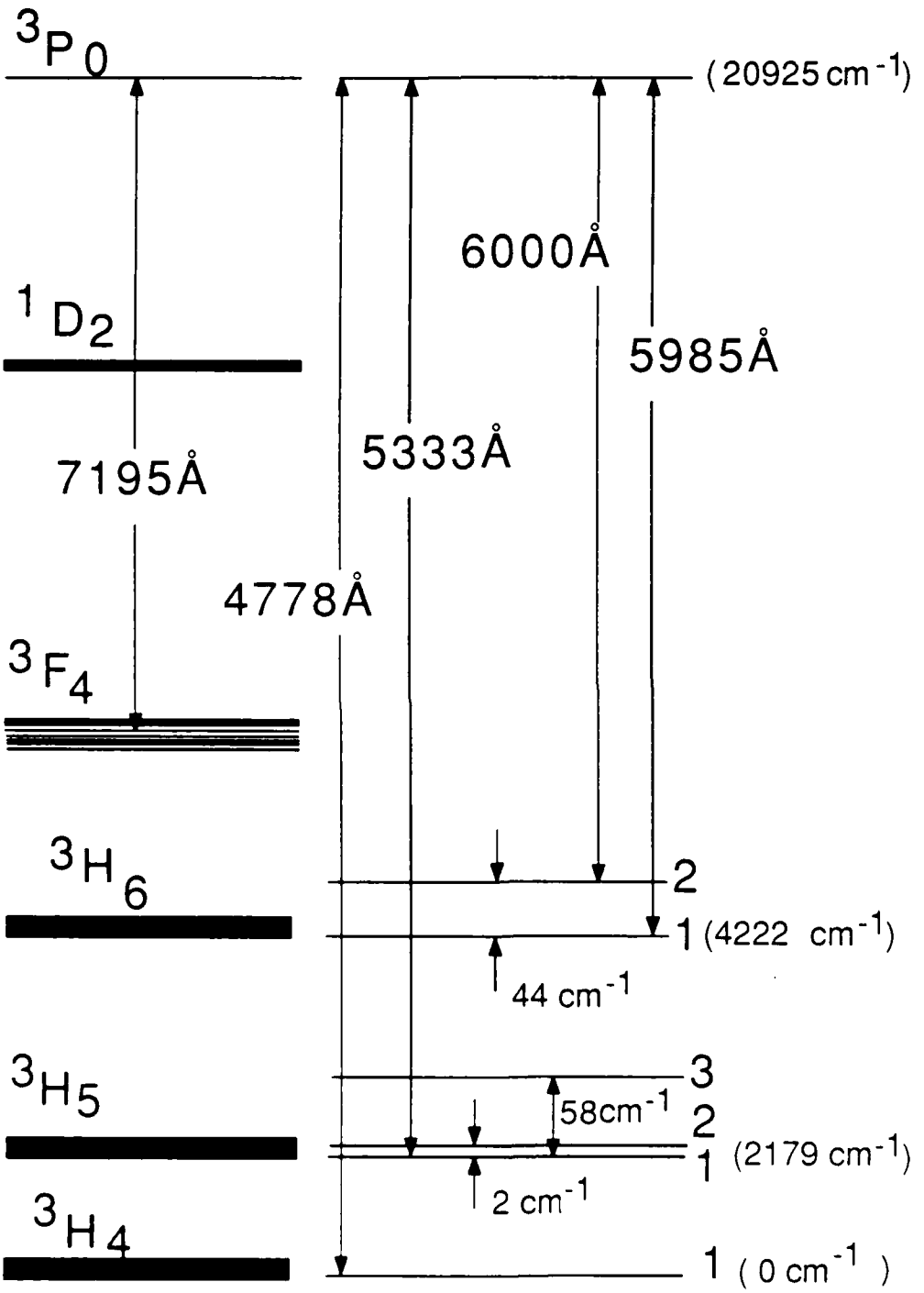

Figure 1. Energy level diagram of Pr^{3+}:LaF_3

population transfer from the terminal levels of these transitions. We are in the process of performing a grating echo experiment to isolate the $^3P_0$ contribution to the previously observed Stimulated echo data on the $^3P_0$-$^3H_6$ transition and therefore deducing the contribution of the $^3H_6$ level. This is achieved by first creating $^3P_0$ and $^3H_4$ population gratings by applying two simultaneous laser pulses at the $^3P_0$-$^3H_4$ transition frequency and at some later time interrogating only the $^3P_0$ grating by scattering a pulse at the $^3P_0$-$^3H_6$ transition frequency off this grating (see figure 2).

A photon echo experiment has given an even faster relaxation rate in a crystal of lower Pr^{3+} concentration (see figure 3) pointing to the possibility that the fast relaxation rate may actually be due to Pr^{3+}-Impurity Ion interaction. This would explain the above result if the lower concentration crystal had in fact a higher concentration of the impurity ion. Other investigators have suggested the possibility of the existence of such an energy transfer process between Pr^{3+}-Nd^{3+} ions.[1-3] We have obtained and prepared various sets of double doped samples to perform a comprehensive concentration dependent study to verify this effect and the possible nature of the interaction which is expected to be of dipolar or spin exchange type.

We have also performed nondegenerate four wave mixing experiments using the $^3H_4$- $^3P_0$-$^3H_6$ levels. The main purpose of these experiments were to observe a tri-level echo in this sample. However, the observation of a trilevel echo requires that the inhomogeneous widths of the two transitions involved be highly correlated. Our failure to observe a trilevel echo signal is in agreement with the experimental results of Flach et al[4] who have observed accidental coincidence broadenings even at low Pr^{3+} concentrations of as large as 1 GHz. Such an observation in conjunction with a two parameter model for the inhomogeneous broadening indicates that we do not have the time resolution (using 7 nsec pulses) to detect a tri-level echo signal. For the future, we plan to try the trilevel echo experiment in a LaF_3:Pr^{3+} sample which has a higher site symmetry and possibly more highly correlated inhomogeneous widths for the two transitions under

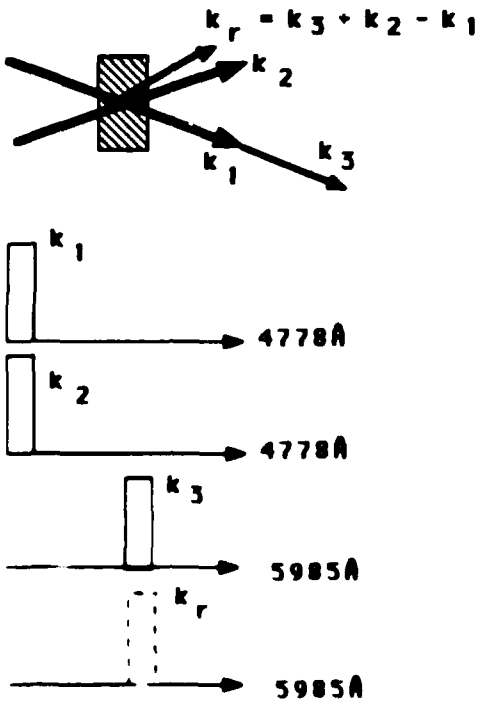

Figure 2- Grating echo.

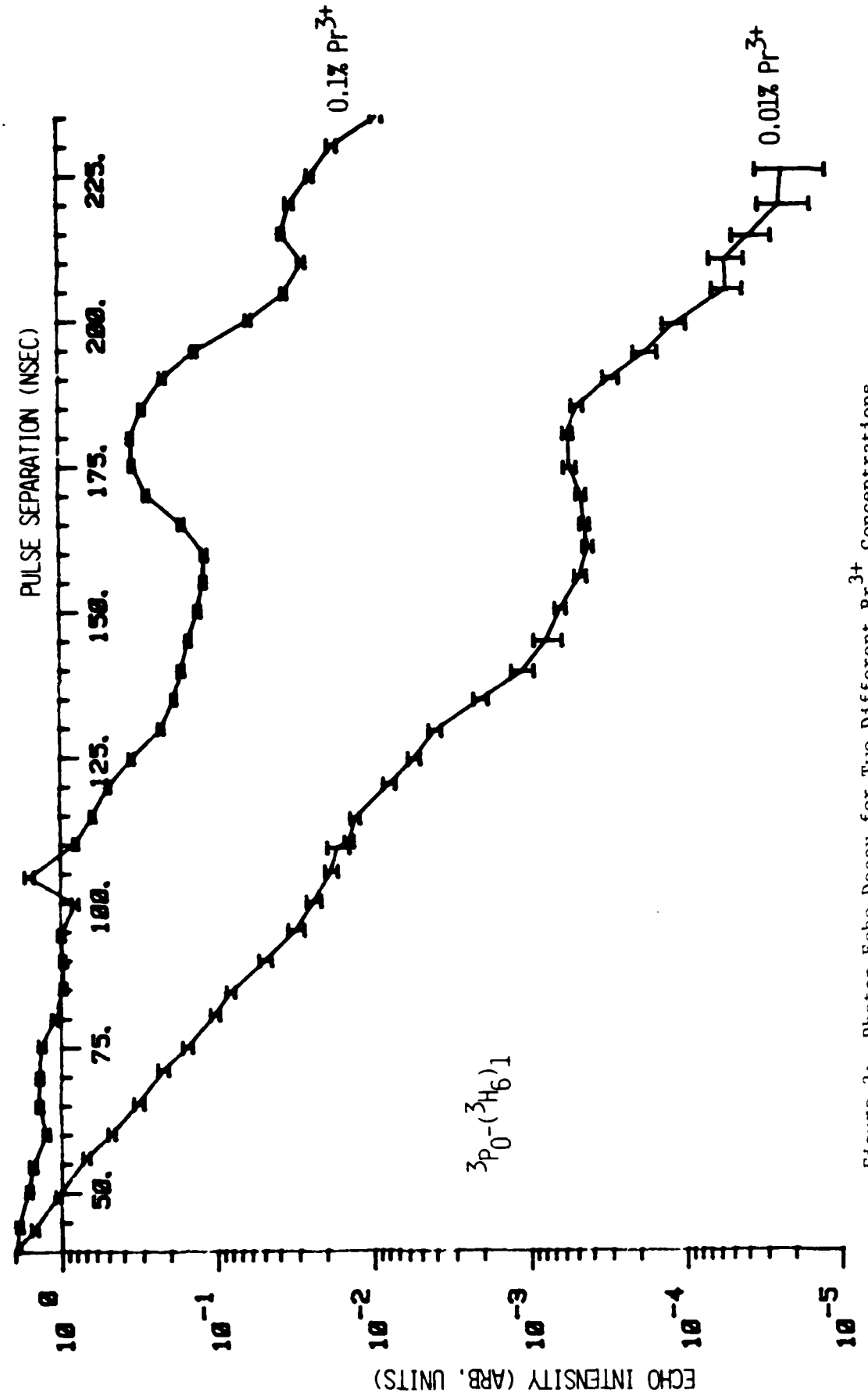

Figure 3: Photon Echo Decay for Two Different Pr^{3+} Concentrations

investigation. Also we plan to look for the trilevel echo using other transitions in the LaF_3 crystal, one possibility is the three levels $^3P_0$, $(^3H_5)_1$, and $(^3H_5)_2$. The two lowest levels of the $^3H_5$ multiplet are only separated by $2cm^{-1}$ and some hints of a trilevel echo signal has been observed on the two transitions from the $^3P_0$ level. However for a more precise study, we are awaiting construction of single mode dye lasers with mode bandwidths of about 100 MHz to make sure that a given pulse is not exciting both of the transitions.

These single mode dye lasers will also be useful in the study of $^3P_0$-$^3H_4$ satellite echoes already observed and documented by us. Echoes generated on the satellite lines of the $^3P_0$-$^3H_4$ transition will enable us to study these lines which are suggested to be due to Pr^{3+}-Pr^{3+} nearest neighbor interactions. These lines are thought to be very active in Ion-Ion energy transfer processes that lead to the observation of blue fluorescence from the $^3P_0$ level after the laser excitation of the $^1D_2$-$^3H_4$ transition.[5,6]

(b) Broad-Band Time-Delayed Four-Wave-Mixing--Construction and understanding of incoherent light sources in the visible region is essential to carrying out spectroscopic experiments utilizing the large spectral content and the resulting short correlation time of such sources for picosecond and femtosecond spectroscopy. It is relatively easy to obtain sources with spectral widths of 10 to 100 Å using amplified spontaneous emission from a single stirred dye cell with a mirror or grating placed at one side and pumped by a pulsed YAG laser (figure 4). We are interested in developing sources with spectral widths as narrow as 10 GHz to be able to study transitions in solid systems such as Pr^{3+}:LaF_3 where inhomogeneous widths of transitions at LHe temperatures is on the order of 10 GHz and due to small transition oscillator strengths Large power per bandwidth is required to carry out time delayed four wave mixing experiments. Additionally, were also interested in constructing ultra-broad band sources with correlation times of a few femtoseconds for carrying out relaxation studies in dye solutions, semiconductors, and glass color filters. Using a mixture of Rhodamine 640 and DCM dyes in a Methanol solution in a single Flow

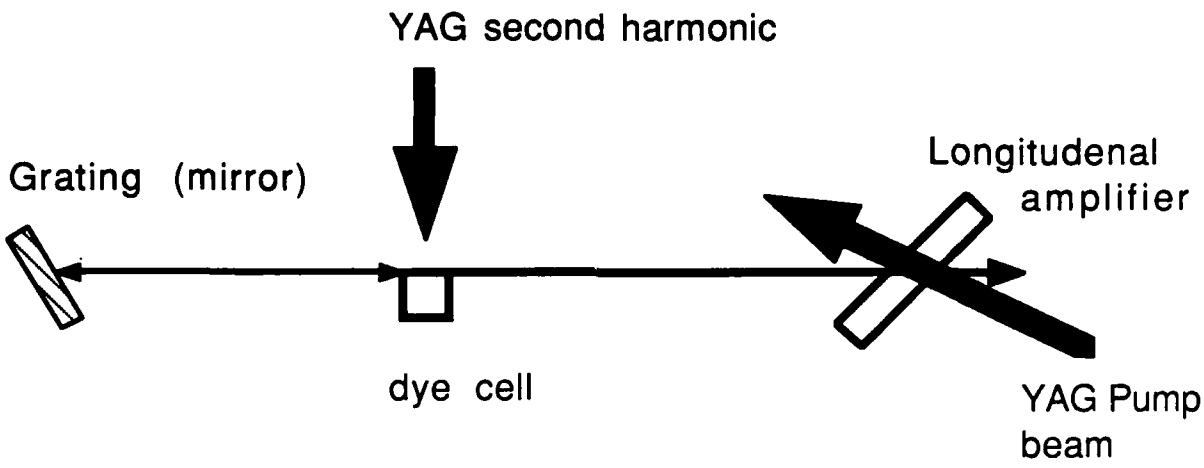

Figure 4- Typical arrangement for the spontaneous emission amplifier

Through dye cell, we have obtained a source at 6250 Å with as much as 400 Å bandwidth. We have also been successful in developing a broad-band source at 5150 Å using Cumarin 500 dye in conjuction with LD489 and Fluorescein 548 dyes; correlation times as short as 30 femtoseconds have been observed from a single dye cell containing a mixture of these dyes in methanol. Future efforts to obtain even broader sources will include: combining the output of several spontaneous emission amplifiers, use of a dye jet instead of a dye cell in the spontaneous emission design, and use of nonlinear effects in optical fibers for broadening our pulses.[7]

Recently we have been able to detect femtosecond coherent transients in glass doped with CdS_xSe_{1-x} microcrystallites using a 250 Å sources centered at 515 nm. The experimental set up is shown in figure 5 and the experimental traces is shown in figure 6. The sample is excited by two incoherent broad band pulses propagating in the $\mathbf{k}_1$ and $\mathbf{k}_2$ directions and the signals emitted in the phase matched $2\mathbf{k}_2-\mathbf{k}_1$ and $2\mathbf{k}_1-\mathbf{k}_2$ directions are monitored as a function of delay between the second and the first pulse. The above observation suggests that for the first time we have been able to observe processes on the femto second time scale using incoherent 7 nsec pulses. Figure 6 contains two plots: a and b. Figure 6(a) is the time delayed four-wave mixing in Nile Blue, which we believe to be the square of the autocorrelation function of the source. The relaxation times in this sample is suggested to be faster than 20 fsec[8], and above observations indicate the relaxation time to be under 10 fsec. For sources with correlation times considerably larger than the sample relaxation time, the experimental trace obtained will be the square modulus of the autocorrelation signal.[9] The autocorrelation trace is related to the power spectrum of the pulse by a fourier tranformation. The traces obtained in two directions seem to be identical and overlap for all delays, supporting the above hypothesis. Figure 6(b) is traces obtained from OG-530 Schott glass filter (transmission curve in figure 7). These traces have the same general characteristics of previous theoretical and experimental works[9-11] and indicated existence of phase relaxing processes of approximately 16 fsec. Recently,

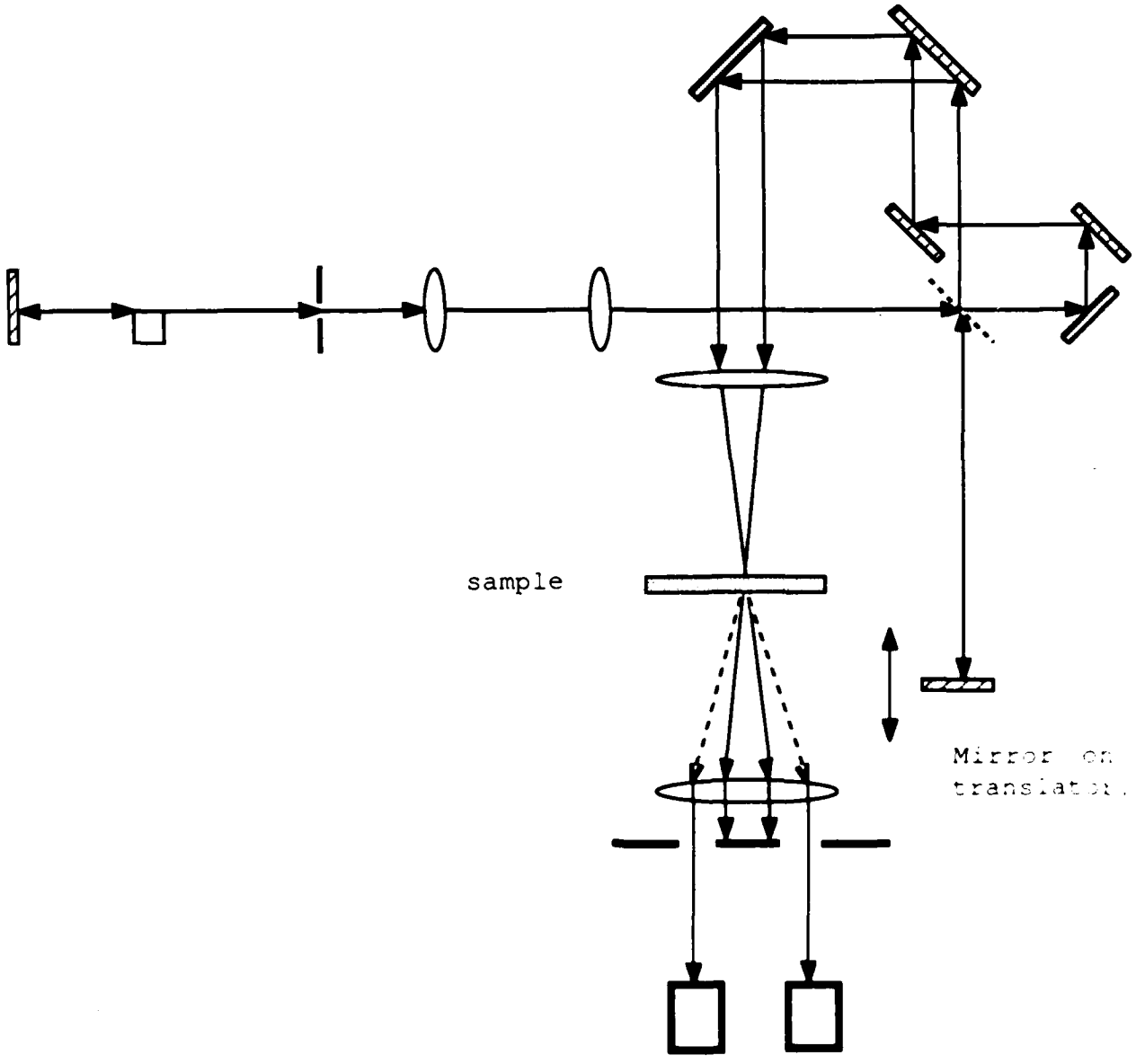

Figure 5- Experimental set up [illegible] mixing in [illegible].

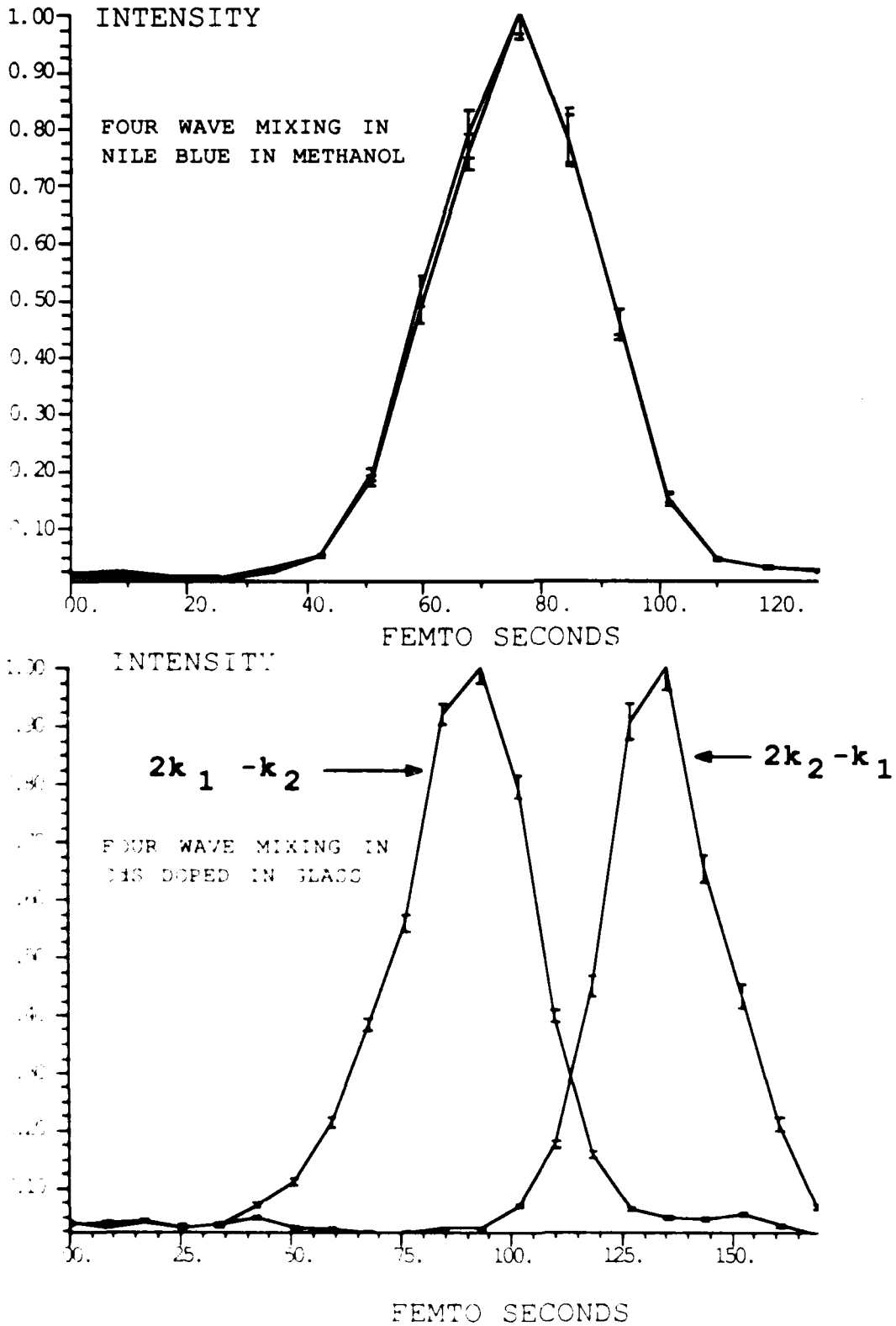
INTENSITY
1.00
0.90
0.80
0.70
0.60
0.50
0.40
0.30
0.20
0.10
FOUR WAVE MIXING IN
NILE BLUE IN METHANOL
00.
20.
40.
60.
80.
100.
120.
FEMTO SECONDS
INTENSITY
$2k_1 - k_2$
$2k_2 - k_1$
FOUR WAVE MIXING IN
DIS DOPED IN GLASS
00.
25.
50.
75.
100.
125.
150.
FEMTO SECONDS

FIGURE 6

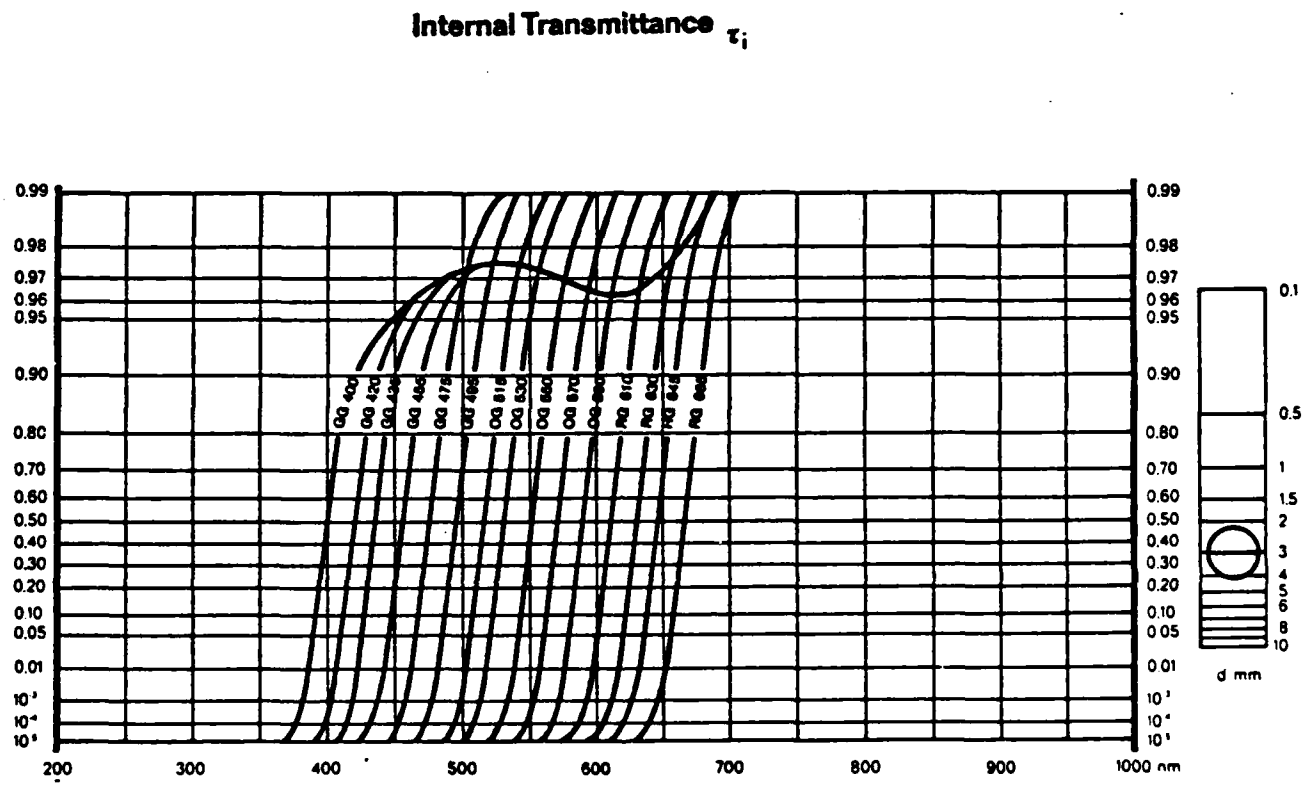

Figure 7: Internal Transmittance for OG530 Color Filter

semiconductor-doped glasses have gained importance due to their potential application in nonlinear optics. Of particular interest are their applications in four-wave mixing, phase conjugation, and optical bistability in these systems.[12-16] We are also currently studying longitudinal relaxation processes in these systems using the grating echo technique.

Hegarty an co-workers[17] have reported observation of photon echoes from two dimentional GaAs-AlGaAs quantum well structure at LHe temperatures using 13 psec excitation pulses. The phase relaxation time obtained in this manner is used to study exciton localization in such structures. Presently, we are in the process of obtaining and preparing such multiquantum well systems to repeat their experiment using our incoherent broad-band sources. Additionally Ippen and co-workers[8] have studied femtosecond dephasing of dye molecules in polymer hosts at various temperatures. Duplicating their experiments with our technique will lead to a greater understanding of the experimental results obtained using the broad band spectroscopy.

This research was also supported by the Office of Naval Research under Contract N00014-78-C-0517.

(1) M.R. Brown, J.S.S. Whiting and W.A. Shand, J. Chem. Phys. 43, 1 (1965).

(2) W.M. Yen, R.I. Greene and W.C. Scott, Phys. Rev. 140, A1188(1965).

(3) N. Krasutsky and H.W. Moos, Phys. Rev. B 8, 1010(1973).

(4) R. Flach, D.S. Hamilton, P.M. Selzer and W.M. Yen, Phys. Rev. B 15(1977).

(5) J.C. Vial, R. Buisson, F. Madeore and M. Poirier, J. De Phys 40, 913(1979).

(6) R. Buisson and J.C. Vial, *J. Physique* Lett. 42, L115(1981).

(7) S.L. Palfrey and D Grischkowsky, Optics Lett. 10, 562(1985).

(8) A.M. Weiner, S. DeSilvestri and E.P. Ippen, J. Opt. Soc. Am. B 2, 654(1985).

(9) N. Morita and T. Yajima, Phys. Rev A 30, 2525(1984).

(10) H. Nakatsuka, M. Tomita, M. Fujiwara and S. Asaka, Optics Comm.

52, 150(1984).

(11) M. Fujiwara, R. Kuroda and H. Nakatsuka, JOSA B 2, 1634(1985).

(12) G.R. Olbright and N. Peyghambarian, Appl. Phys. Lett. 48, 1184(1986).

(13) S.S. Yao, C. Karaguleff, A. Gabel, R. Fortenberry, C.T. Seaton and G. I. Stegeman, Appl. Phys. Lett. 46, 801(1985).

(14) R.K. Jain and R.C. Lind, JOSA 73, 647(1983).

(15) J. Warnock and D.D. Awschalom, Phys. Rev. B 32, 5529(1985).

(16) M. Dagenais and W.F. Sharfin, JOSA B 2, 1179(1985).

(17) L. Schultheis, M.D. Sturge and J. Hegarty, Appl. Phys Lett. 47, 995(1985).

B. TIME-DELAYED FOUR-WAVE MIXING USING INCOHERENT LIGHT

(L.G. Van Wagenen and S. R. Hartmann)
(JSEP work unit 2, 1985-88)
(Principal Investigator: S. R. Hartmann (212)280-3272)

Of continuing interest have been investigations in the use of chaotic (thermal) excitation pulses to generate Four Wave Mixing signals.[1] Previous experimental work on Time Delayed Four Wave Mixing (TDFWM) in sodium has shown that the TDFWM signal created by intense incoherent excitation pulses results in an unexpected decay of the signal intensity with increasing pulse separation as compared with the theoretical results of Morita and Yajima[2] (see figure 1). The cause of the signal decay with increasing pulse separation is due to the inability of the intense broad band excitation pulses to interrogate the grating.

Excitation pulses made from broadband light can be regarded as a train of incoherently phased noise spikes. In the original paper on tne subject[3] we considered the situation in which the output of a single chaotic source was divided into two pulses, $\mathbf{k}_1$ and $\mathbf{k}_2$, $\mathbf{k}_2$ was delayed with respect to $\mathbf{k}_1$ by up to several hundred picoseconds , this time is referred to as τ, and, $\mathbf{k}_2$ is in a slightly different direction than $\mathbf{k}_1$. These two pulses were then sent into a heatpipe containing sodium and the TDFWM signal was seen in the $2\mathbf{k}_2-\mathbf{k}_1$ direction. What we have is two trains of correlated noise spikes. Although the phase of each noise spike is random , each noise spike pair is correlated, having the same relative phase. This correlated relative phase contributes coherently to the $\mathbf{k}_1-\mathbf{k}_2$ momentum component of the ground state amplitude. The first noise spike pairs act to set up the accumulated gratings, then these gratings are interrogated by the selfsame fields to generated a TDFWM signal along the $2\mathbf{k}_2-\mathbf{k}_1$ direction. (This is explained in more detail in last years progress report.)

With high intensity pulses, such as we were using, it is necessary to consider how the excitation pulses themselves affect the generated superposition states and cause the grating and hence the

signal to be degraded. In our previous work we were concerned only with degradation effects that depend on τ, the pulse separation. Although both grating formation and interrogation are effected by the degradation mechanism, we were only interested in calculating the signal degradation due to intense self interrogation.

The noise spike degradation is explained by the fact that we had launched a radiating superposition state in the regime where the pulse area of the noise spikes were small, but not so small that the combined action of successive noise spikes could not have a sizable effect on the magnitude of the superposition state. Each successive noise spike reduces the amplitude of each of the superposition states by cos(spike area/2). Thus we can arrive at a noise spike degradation factor for the radiated intensity. The experimental data was in agreement with this theory. As can be seen from figure 1 our previous data for the signal intensity vs pulse separation agrees with the theoretical results for intensity when the noise spike degradation term is included.

The next situation of interest was to see if by probing a grating formed by intense broadband excitation pulses $\mathbf{k}_1$ and $\mathbf{k}_2$ as discussed above with a third broadband, but weak, excitation pulse, $\mathbf{k}_3$, we would still see the same signal degradation due to interrogation.

The experimental set up is shown in figure 2. 7 nsec long incoherent excitation pulses were generated by pumping a dye laser with the second harmonic of a Quanta Ray DCR-1a YAG laser. The dye laser consisted of a stirred dye cell of 50% by volume R610 (10^{-3}M) and 50% by volume kiton red (10^{-3}) placed in an open ended cavity with a diffraction grating in the Littrow configuration to provide bandwidth narrowing. The output was amplified by two longitudinally pumped flowing dye cells containg a solution of R610 and ethanol. A spectroscopic analysis of the output pulses showed them to have a full width at half maximum of 8 - 12 A centered around 5893 A. The angle between the beams was the order of a few milliradians. $\mathbf{k}_1$, $\mathbf{k}_2$ and $\mathbf{k}_3$ were sent through a 10 cm sodium sample cell and the TDFWM signal was detected in the $\mathbf{k}_3+\mathbf{k}_2-\mathbf{k}_1$ phase matching direction with and EG&G FND 100 photodiode using spatial filtering. The probe pulse $\mathbf{k}_3$ was 2 - 10

times less intense than the excitation pulses $\mathbf{k}_1$ and $\mathbf{k}_2$, and was split from the same source. The delay between $\mathbf{k}_1$ and $\mathbf{k}_2$ was from -30 psec to more than a hundred psec and $\mathbf{k}_3$ was delayed by 8 nsec from $\mathbf{k}_2$. Both the $2\mathbf{k}_2-\mathbf{k}_1$ signal and the $\mathbf{k}_3+\mathbf{k}_2-\mathbf{k}_1$ signals were monitered and as is shown by the data in figure 3 the signal degradation with increasing pulse separation is still evident although the parameter regime in which this data was taken ($\alpha l>1$) makes it difficult to assign a unique interpretation for the effects seen. But it is clear that the signal intensity is still degraded as the pulse separation increases.

This evidence that the noise spike induced degradation is still present even when the interrogation is done with weak excitation pulses indicates that the preceeding theory needs to be extended with respect to the degradation mechanisms at work in the grating formation and interrogation, and that more sophisticated experiments need to be undertaken to ascertain the nature of the signal decay with increasing pulse separation.

Collaboration with R. Friedberg has produced a more general theory. The new theory is an exact non perturbative and includes the case of intense incoherent pulses The time evolution of a two level atomic system interacting with a radiation field is best expressed in terms of the equation

$$\mathbf{P} = \gamma\mathbf{P} \times \mathbf{E} - \mathbf{z}(p_z - 1) \cdot T_1 - \mathbf{x} \cdot \cdot y$$

where $\gamma\mathbf{E} = \sqrt{2}\ (\mathbf{x}R_e R + \mathbf{y}\cdot\cdot) \cdot \cdot \mathbf{z}$

detuned by ω from exa

described by a time

$\langle R(t) \cdot$

$\cdot R(\cdot$

the

AD-A175 644 RESEARCH INVESTIGATION DIRECTED TOWARD EXTENDING THE USEFUL RANGE OF THE ELECTROMAGNETIC SPECTRUM(U) COLUMBIA RADIATION LAB NEW YORK G W FLYNN ET AL. 3/3

UNCLASSIFIED 31 DEC 86 DAAG29-85-K-0049 F/G 20/14 NL

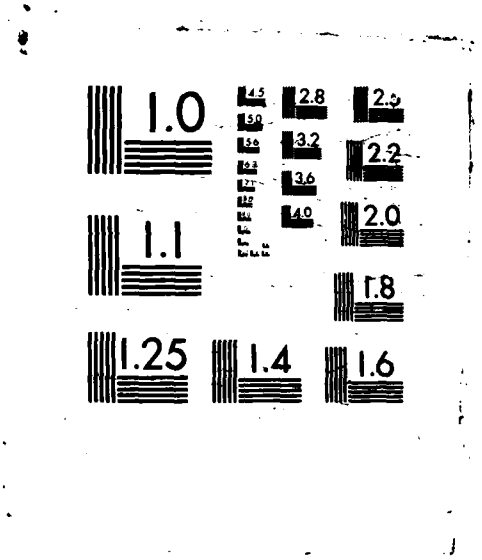
1.0
1.1
1.25
1.4
1.6
1.8
2.0
2.2
2.8
3.2
3.6
4.0

$$q_z = p_z(\omega)p_z(\omega')$$

$$q_- = p_-(\omega)p_+(\omega')$$

where $p_\pm = (1/\sqrt{2})[p_x \pm ip_y)$ and we have explicitly noted the dependence on ω and ω' to show that the q's are associated with atomic pairs. The advantage of this description is that the equations of motion, omitting an inhomogeneous term, are simply given

$$\begin{matrix} q_+ \\ q_z \\ q_- \end{matrix} = \begin{matrix} -i\Omega - 1/T_s - 2/T_2 & 1/T_s & 0 \\ 1/T_s & -2/T_1 - 2/T_s & 1/T_s \\ 0 & 1/T_s & i\Omega - 1/T_s - 2/T_2 \end{matrix} \begin{matrix} q_+ \\ q_z \\ q_- \end{matrix}$$

where $\Omega = \omega - \omega'$.

The Greens function for the coherent case is given by

$$G(T,\omega) = e^{-MT}$$

and for incoherent pulses it is given by

$$G(T,\Omega) = e^{-mT}$$

where M is given by

$$M = \begin{matrix} -i\omega - 1/T_2 & iR & 0 \\ iR & -1/T_1 & -iR \\ 0 & -iR^* & i\omega - 1/T_1 \end{matrix}$$

and m is obtained from M with the substitutions:

$$1/T_1 \rightarrow 2/T_s + 2/T_1 \,, \quad 1/T \rightarrow 1/T_s + 2/T_2$$

$$\omega \rightarrow \Omega \,, \quad \pm iR \rightarrow 1/T_s \,, \quad \pm iR^* \rightarrow 1/T_s$$

Experiments are now underway to verify the theory.

This research was also supported by the Office of Naval Research under Contract N00014-78-C-0517.

(1) R. Beach and S.R. Hartmann, Phys. Rev. Lett. **53**, 663 (1984)

(2) N. Morita and T. Yajima, Phys. Rev. A **30**, 2525 (1984)

(3) R. Beach, D. DeBeer, and S.R. Hartmann, Phys. Rev. A **32** 3467 (1985)

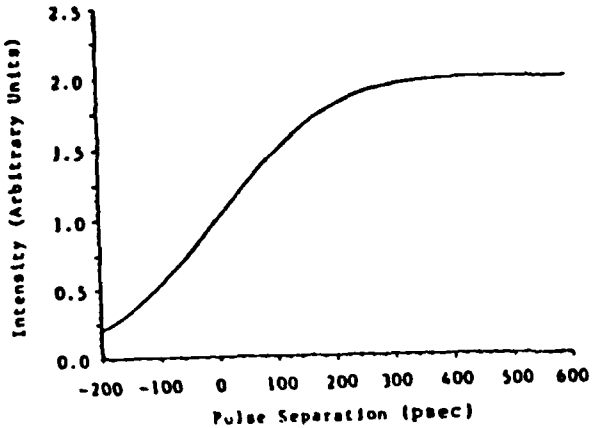

Fig. 1. Signal intensity vs excitation pulse separation after Morita and Yajima.

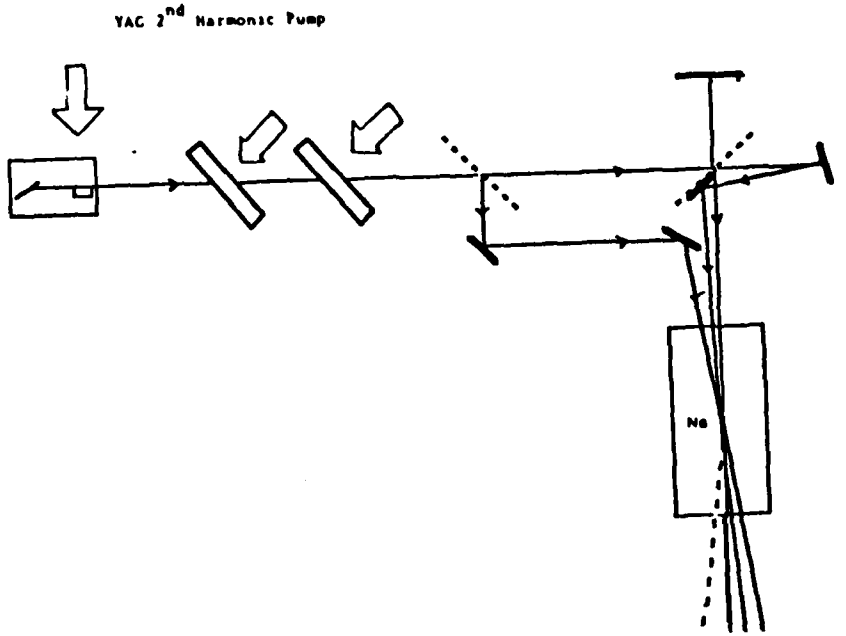

Fig. 2. Schematic of experimental setup.
The TDFWM signal is indicated by the dotted line.

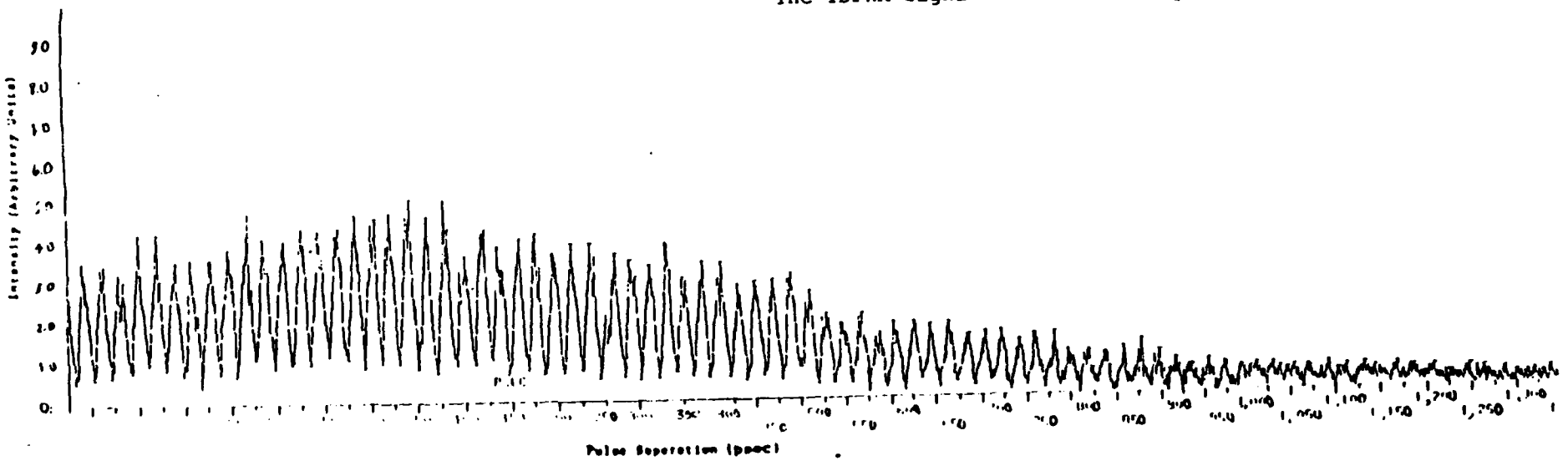

Fig. 3. Experimentally measured signal intensity vs exciation pulse separation using a weak probe beam.

C. PICOSECOND COHERENT TRANSIENTS.

(D. P. DeBeer and S. R. Hartmann)
(JSEP work unit 2, 1985-88)
(principal Investigator: S. R. Hartmann (212)280-3272)

A recent addition to our laboratory facilities is a picosecond laser. This system involves a mode-locked CW Nd:YAG synchronously pumping a dye laser which produces 1.7 psec pulses with 1 nJ of energy at a repetition rate of 82 MHz. To obtain higher peak powers a dye amplifier is used resulting in .5 GW pulses at a 10 Hz repetition rate. This laser system is now operational and allows us to continue previous work in a new time domain as well as providing us with the tools to progress in many new directions. Two experiments are planned for the immediate future. The first continues previous explorations in this lab of photon echo techniques applied to various problems. The second initiates a new study of superfluorescence.

Previous studies in this lab have used photon echo techniques to investigate relaxation processes[1], to do spectroscopy[2], and to characterize collisions between gaseous alkali atoms and various inert gasses[3]. These studies can all be advanced using picosecond pulses. The extension of the work of Ref. 1 will be particularly interesting. In Ref. 1 a photon echo signal on the 3S-3P transition in atomic Sodium was observed as a function of pulse separation over a range of 11 decades of intensity as shown in Fig. 1. This involved observing light emitted from an atom which was excited more than 23 lifetimes earlier. We can improve on the dynamic range of this experiment significantly at both short and long separations using psec. light pulses. For short pulse separations we can do better than before because the pulse durations are four orders of magnitude smaller and allow shorter pulse separations than before without temporal overlap. For large separations there is an improvement in that the signals are larger due to the fact that the psec pulses interact with the entire Doppler broadened line of Sodium atoms. We anticipate being able to observe the signal over many more decades of intensity allowing us to look for deviations from exponential decay as predicted by several theoretical investigations. This same experimental setup will allow us to continue the spectroscopic work begun in Ref. 2. In this work a technique was

developed to measure energy level splittings in systems such as that shown in Fig 2a. As discussed in Ref. 2 it promises to be a potentially very high resolution method. This is because the echo intensity, which can be expressed as:

$$\int dt\ I_{echo} \propto 1 + \exp\{-[\tau v_p(\Omega'-\Omega)/c]^2/8\}\ \cos[(\Omega-\Omega')\tau(1+v_{avg}/c)]$$

is modulated as a function of pulse separation, τ. Typical data for such an experiment performed on the Sodium $3S\text{-}3P_{1/2}\text{-}3P_{3/2}$ system is shown in Fig. 2b. As mentioned above this signal is observable over many lifetimes making it possible to observe on the order of 100,000 beats. Thus the energy-level splitting would be measurable to very high precision. In addition the technique is Doppler free if the entire velocity distribution of atoms can be evenly excited. Since a psec. pulse has a spectrum very wide compared to the Doppler width this requirement is met and we will be able for the first time to really push this technique to its limits.

We are also initiating a study of two-photon superfluorescence. Superfluorescence has been studied extensively in two level systems. In such a system one initially inverts the population and then observes the fluorescence. This fluorescence is at first incoherent but later becomes, under certain conditions, coherent. This buildup of coherent, or superradiant, emission occurs in some characteristic build up time and is called superfluorescence. We are undertaking similar studies on three level atomic systems. An initial psec. pulse will coherently excite a 1-3 superposition, where 1 and 3 indicate the ground and the upper excited states respectively. This results in the 2-3 transition being inverted and thus the system will superfluoresce on this transition (given the proper experimental parameters). The question then is whether the superfluorescence continues to the ground state on the 2-1 transition. This has never been observed experimentally. One would expect that when the sample superfluoresces from 3 to 2 it would transfer the 1-3 coherence into a 1-2 coherence and radiate since the 1-2 transition is dipole allowed. For this to occur requires that the 1-3 coherence dephasing time be long compared to the superfluorescence buildup time on the 2-3 transition. Unfortunately this condition is not easily obtainable. For alkali atoms typical dephasing time are .1

nsec whereas typical superfluorescence buildup times are about 1 nsec. We have devised a scheme, though, for preparing a sample of Cesium atoms with an artificially long coherence time on the order of tens of nanoseconds. The scheme involves optically pumping the atoms to obtain a "cool" sample and which therefore has a reduced Doppler broadening. The results of this experiment should prove to be very interesting. Preliminary calculations show that superfluorescence in the forward direction is suppressed while that in the backward direction is not. This has never been observed.

This research was also supported by the Office of Naval Research under Contract N00014-78-C-0517.

(1) R. Beach, B. Brody, and S.R. Hartmann, J. Opt. Soc. Amer. B **1**, 189 (1984).

(2) D. DeBeer, L.G. Van Wagenen, R. Beach, and S.R. Hartmann, Phys. Rev. Lett. **56**, 1128 (1986).

(3) T.J. Chen, D. DeBeer, and S.R. Hartmann, J. Opt. Soc. Amer. B **3**, 493 (1986).

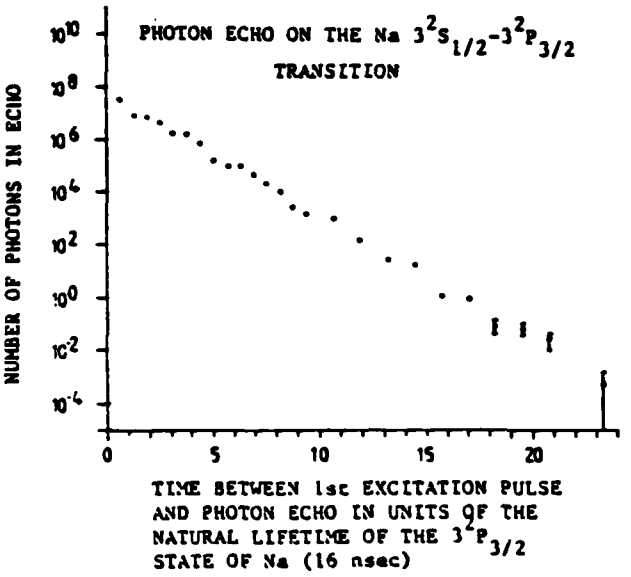

Figure 1: Photon echo intensity as a function of pulse separation.

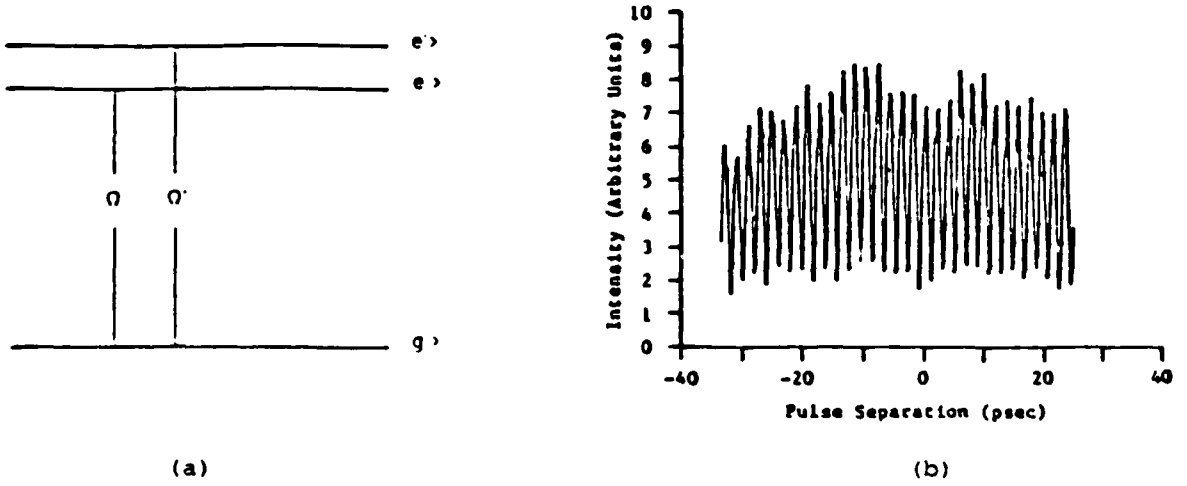

(a) (b)

Figure 2: (a) Energy level diagram for an ultrafast modulation spectroscopy (UMS) experiment. (b) Typical data obtained from an UMS experiment; in this case performed on the Sodium 3S-$3P_{1/2}$-$3P_{3/2}$ system.

SIGNIFICANT ACCOMPLISHMENTS AND TECHNOLOGY TRANSITION REPORTS

Significant Accomplishments

1. The usual semiclassical theory of light detection turns out to be incorrect when feedback is present from detector to source. A revised theory has been developed.

2. Laser light can be converted into amplitude-squeezed light by use of a lly designed quantum-well heterostructure.

3. The noise properties of superlattice avalanche photodetectors have been derived. The results show that the residual hole ionization must be kept extremely low to realize the potential advantages of such detectors.

4. A new formalism of the Kronig-Penney model which yields the minimum and maximum energies of superlattice energy subbands and their envelope wave functions by taking into consideration the effective mass differences of carriers in the well and barrier layers has been developed. This new formalism yields results equivalent to those obtained via the conventional formalism but in a much simpler fashion. The new formalism has been applied to the design of multiple quantum well electro-absorptive optical modulators. In this application, a single parameter defined as the critical barrier thickness becomes the paramount figure of merit for optimization of modulator design. The new formalism yields critical barrier thickness easily, simplifying the task of modulator design significantly.

5. The ultrahigh-vacuum surface analysis system, which was made operational last year, has been used in three important experiments in semiconductor electronics: UV-laser-assisted oxidation of GaAs, ion-beam assisted oxidation of Si, and laser-assisted etching of GaAs.

6. Laser-light has been used to desorb discharged-formed polymers from

a silicon surface. The experiment uses light to photogenerate carriers in a silicon sample; the carriers diffuse to the surface and assist in desorbing the polymer precursor molecules. The technique allows maskless patterning of a silicon wafer in a plasma reactor.

7. The evolution of metal semiconductor interface states upon formation of silicide in palladium silicon diodes was observed. The investigation implied a reduction in trap density as the interface moved into the silicon upon annealing.

8. Negative capacitance was reported for the first time in the forward bias capacitance measurement. A preliminary model attributes the negative capacitance to impact ionization of trap states by energetic mobile charges.

9. The oxidation of silicon by the use of a low energy ion beam has been studied. The electrical properties of the ultra-thin oxide layer has been investigated. The chemical properties of the oxide have been studied using Auger electron spectroscopy (AES) and angle resolved x-ray photoelectron spectroscopy (XPS). Experiments to study the effect of process parameters such as beam energy, composition, and substrate temperature have been performed.

10. Reverse bias leakage current in aluminum-gallium arsenide Schottky diodes has been reduced by over a factor of 25 by increasing the surface arsenic content.

11. Diode lasers have been used to probe for the first time the exact quantum states of molecules ejected from a surface following chemical reaction.

12. The CO_2 ν_3 mode ladder climbing rate has been measured accurately and can be used to improve modelling calculations for carbon dioxide lasers.

13. The interaction between an electronically excited metal atom and a

small polyatomic molecule has been investigated by probing for the first time the final quantum states of the polyatomic bath modes. These experiments are prototypical and can be expected to provide insight into the mechanisms responsible for energy transfer and chemical reactivity between metals and polyatomic molecules.

14. Collision processes have been investigated on a submicrosecond time scale in an energy range appropriate to plasmas (25,000 K). For the first time these high energy atom-molecule collision events have been studied in quantum state detail with a resolution of 0.0003 cm^{-1}.

15. The first measurement of the absolute phase of surface nonlinear susceptibility was achieved using a novel application of second harmonic generation techniques. This information, which cannot be obtained directly from ordinary linear optical methods, allowed us to determine the absolute molecular orientation of molecules at air-liquid interfaces.

16. Picosecond laser techniques were used to study the basic question of how the solvent can affect the probability of energy barrier crossing in molecules. The dynamics of barrier crossing in systems that do not involve large electric dipole moment changes were found to be dependent on the solvent friction. The optically induced conformational change in 1,1'-binaphthyl was shown to fit into this category. In this case we have found that the dynamics followed the one-dimensional barrier crossing theory of Kramers. On the other hand, for systems that do manifest a significant charge redistribution in the course of reaction we have found that the solvent polarity (as opposed to the solvent friction) can be the most important parameter. In this case there is a dramatic breakdown in the one-dimensional barrier crossing theory. The photoisomerization of dimethylaminobenzonitrile (DMABN) and of t-stilbene were found to be two such examples. In the case of DMABN we have found that solvent polarity strongly affects the height of the energy barrier, which in turn affects the rate of reaction.

17. It has been determined that a photochemical ring opening of a

substituted oxirane proceeds along two competitive routes, which lead to the formation of either an ylide or a carbene. Furthermore, the pathway that yields the carbene was found to involve a singlet 1,3-biradical as a short lived intermediate. These results are important in terms of showing the effect of the precursor to the formation and energy decay of carbenes, which are important chemical intermediates.

18. Broad-Band Time-Delayed Four-Wave-Mixing using incoherent broad band (200-300 Å) light has been observed in semiconductor-doped glasses. We have studied these extremely inhomogeneous systems at the band edge where they are highly non-linear. Evidence of phase relaxations of approximately 16 fsec have been observed in the Schott sharp cut-off colored glass OG-530 at room temperature. We have also observed grating echoes for long pulse delays (approximately 1 μsec) which may be evidence of a long longitudinal relaxation process.

Technology Transition Reports

1. The laser etching techniques under investigation are of interest for several DOD programs in diode laser technology. Both McDonald-Douglas and Livermore have discussed using the techniques in their diode laser programs. In general, the attractive features have been damage-free surfaces and smooth, high-aspect-ratio microfabricated features.

2. Prof. Fossum's work on CCD devices and circuits in GaAs and Si has attracted much industrial interest and support. In particular, his work in implementing pixel scale computation elements for image preprocessing has attracted supported from Hughes Aircraft.

PERSONNEL

Faculty

K. Eisenthal, Professor of Chemistry
G. Flynn, Professor of Chemistry, Co-Director
E. Fossum, Assistant Professor of Electrical Engineering
S. Hartmann, Professor of Physics
R. Osgood, Professor of Electrical Engineering and Applied Physics
P. Prucnal, Associate Professor of Electrical Engineering
M. Teich, Professor of Engineering Science
E. Yang, Professor of Electrical Engineering

Visiting Scientists

Dr. B. Brody
Dr. B. Saleh
Dr. Chen Xi Wang

Research Associates

Dr. R. Beach
Dr. L. Chia
Dr. H. Evans
Dr. H.H. Gilgen
Dr. T. Kreutz
Dr. K. Matsuo
Dr. D. Podlesnik
Dr. S. Shih
Dr. E. Sitzmann
Dr. C.F. Yu (IBM Fellow at Columbia Rad. Lab)

Post-Doctoral Research Scientist

J. Hershberger

Graduate Research Assistants

R. Ade
R. Bowman
B. Brady
B. Burke
T. Cacouris
R. Campos
L. Chen
R. Colbeth
D. DeBeer
N. Doudoumopoulos
E. Eid
S. Hewitt
B. Farahani
S. Kemeny
R. Krchnavek
J. Langan
T. Li
K. Luo
Q-Y Ma
P. Meyer
F. Mitlitzky
T. Licata
F. Moshary
J. O'Neill
G. Pinto
D. Rossi
E. Sanchez
M. Santoro
M. Schmidt
P. Shaw
K. Shoop
T. Tanabe
S. Todorov
F. Tong
V. Treyz
Y. Jiang
L. Van Wagenen
A. Willner
E. Xu

Administration

Ms. Cynthia Leslie
Ms. Marie Santoro
Ms. Maura Schreiner
Ms. Glady White
Ms. Karen Wingate

Technician

Dave Rivera

Undergraduate Technicians

A. Cubina
C. Delos-Reyes
D. Eiref
N. Joshi
P. Landsberg
M. Levy
A. Mehta
N. Ramlagan
S. Ross
S. Seshadri
S. Shillinger
N. Shoshilas
B. Wendemagegnehu
K. Wong
M. Yang
J. Yee
J. Yves

Dr. Jimmie R. Suttle
U. S. Army Research Office
P. O. Box 12211
Research Triangle Park, NC 27709

Mr. Charles Graff
U. S. Army Comm. - Electronics Command
ATTN: DRSEL-COM-RF-2
Fort Monmouth, NJ 07703

Mr. Edward Herr
U. S. Army Comm. - Electronics Command
ATTN: DRSEL-COM-RX-4
Fort Monmouth, NJ 07703

Mr. Roland Wright
Night Vision & Electro-Optics Labs
Fort Belvoir, VA 22060

Dr. Robert Rohde
Night Vision & Electro-Optics Labs
Fort Belvoir, VA 22060

Dr. Donn V. Campbell
U. S. Army Comm. - Electronics Command
ATTN: DRSEL-COM-RN-4
Fort Monmouth, NJ 07703

Dr. Nick Karayianis
Harry Diamond Laboratories
ATTN: DELHD-RT-CA
2800 Powder Mill Road
Adelphi, MD 20783

Dr. T. N. Chin
U. S. Army ARRADCOM
ATTN: DRDAR-SCF-10
Dover, NJ 07801

Dr. John Malamus
Night Vision & Electro-Optics Labs
Fort Belvoir, VA 22060

Dr. Rudolf G. Buser
Night Vision & Electro-Optics Labs
ATTN: DELNL-L
Fort Belvoir, NJ 22060

Dr. W. Ealy
Night Vision & Electro-Optics Labs
ATTN: DELNV-AC
Fort Monmouth, NJ 22060

Dr. J. Hall
Night Vision & Electro-Optics Labs
ATTN: DELNV-AC
Fort Belvoir, NJ 22060

Dr. J. Burgess
Night Vision & Electro-Optics Labs
ATTN: DELNV-RM-RA
Fort Belvoir, NJ 22060

DEPARMENT OF THE AIR FORCE

Dr. E. Champagne
AFWAL/AADD-I
Wright-Patterson AFB, OH 45433

Mr. W. Edwards, Chief
AFWAL/AAD
Wright-Patterson AFB, OH 45433

Professor R. E. Fontana
Head, Department of Electrical Engineering
AFIT/ENG
Wright-Patterson AFB, OH 45433

Dr. Alan Garscadden
AFWAL/POOC-3
Air Force Aeronautical Labs
Wright-Patterson AFB, OH 45433

Mr. Alan R. Barnum (CO)
Rome Air Development Center
Griffiss AFB, NY 13441

Chief, Electronic Research Branch
AFWAL/AADR
Wright-Patterson AFB, OH 45433

Mr. John Mott-Smith (ESD/ECE)
HQ ESD (AFSC), Stop 36
Hanscom AFB, MA 01731

Dr. J. Ryles
Chief Scientist
AFWAL/AS
Wright-Patterson AFB, OH 45433

Dr. Allan Schell
RADC/EE
Hanscom AFB, MA 01731

Dr. J. Bram
AFOSR/NM
Bolling AFB, DC 20332

Dr. David W. Fox
AFOSR/NM
Bolling AFB, DC 20332

Dr. J. Neff
AFOSR/NE
Bolling AFB, DC 20332

Dr. N. H. DeAngelis
RADC/ESR
Hanscom AFB, MA 01731

Dr. Gerald L. Witt
Program Manager
Electronic & Material Sciences Directorate
Department of the Air Force
AFOSR
Bolling AFB, DC 20332

Mr. Allan Barnum
RADC/IS
Griffiss AFB, N.Y. 13411

Dr. Tom Walsh
AFOSR/NE
Bolling AFB, DC 20332

Dr. Edward Altshuler
RADC/EEP
Hanscom AFB, MA 01731

DEPARTMENT OF THE NAVY

Naval Surface Weapons Center
ATTN: Technical Library
Code DX-21
Dahlgren, VA 22448

Dr. Gernot M. R. Winkler
Director, Time Service
U. S. Naval Observatory
Massachusetts Avenue at 34th Street, NW
Washington, DC 20390

G. C. Dilworth, Jr.
Technical Director
Naval Coastal Systems Center
Panama City, FL 32407

Naval Air Development Center
ATTN: Code - 301 A. Witt
Technical Library
Warminster, PA 18974

R. S. Allgaier, R-43
Naval Surface Weapons Center
Silver Spring, MD 20910

Office of Naval Research
800 North Quincy Street
ATTN: Code 250
Arlington, VA 22217

Office of Naval Research
800 North Quincy Street
ATTN: Code 414
Arlington, VA 22217

Office of Naval Research
800 North Quincy Street
ATTN: Code 411MA
(Dr. Stuart L. Brodsky)
Arlington, VA 22217

Commanding Officer
Naval Research Laboratory
ATTN: Dr. S. Teitler, Code 6601
Washington, DC 20375

Commanding Officer
Naval Research Laboratory
ATTN: Mrs. D. Folen, Code 5227
Washington, DC 20375

Commanding Officer
Naval Research Laboratory
ATTN: Mr. A. Brodzinsky, Code 5200
Washington, DC 20375

Commanding Officer
Naval Research Laboratory
ATTN: Mr. J. E. Davey, Code 5810
Washington, DC 20375

Commanding Officer
Naval Research Laboratory
ATTN: Mr. B. D. McCombe, Code [illegible]
Washington, DC 20375

Commanding Officer
Naval Research Laboratory
ATTN: Mr. W. L. Faust, Code 6504
Washington, DC 20375

Technical Director
Naval Underwater Systems Center
New London, CT 06320

Naval Research Laboratory
Underwater Sound Reference Detachment
Technical Library
P. O. Box 8337
Orlando, FL 32856

Naval Ocean Systems Center
ATTN: Dr. P. C. Fletcher, Code 92
San Diego, CA 92152

Naval Ocean Systems Center
ATTN: Mr. W. J. Dejka, Code 8302
San Diego, CA 92152

Naval Ocean Systems Center
ATTN: Dr. Alfred K. Nedoluha,
Code 922
San Diego, CA 92152

Naval Weapons Center
ATTN: Dr. G. H. Winkler, Code 381
China Lake, CA 93555

Dr. Donald E. Kirk (62)
Professor and Chairman, Electrical
Engineering
SP-304
Naval Postgraduate School
Monterey, CA 93940

Dr. D. F. Dence
Naval Underwater Systems Center
New London Laboratory
ATTN: Code 34
New London, CT 06320

Director, Technology Assessment
Division (OP-987)
Office of the Chief of Naval Oper.
Navy Department
Washington, DC 20350

Mr. J. W. Willis
Naval Air Systems Command
AIR-310
Washington, DC 20361

Naval Electronics Systems Command
NC #1
ATTN: Code 61R
2511 Jefferson Davis Highway
Arlington, VA 20360

Department of the Navy
Naval Sea Systems Command
ATTN: W. W. Blaine (SEA-92R)
Washington, DC 20362

David Taylor Naval Ship Research
and Development Center
ATTN: Mr. G. H. Gleissner, Code 18
Bethesda, MD 20084

Mr. Martin Mandelberg
Coast Guard R&D Center
Avery Point
Groton, CT 06340

Naval Underwater Systems Center
New London Laboratory
ATTN: 101E (Dr. Edward S. Eby)
New London, CT 06320

Mr. Thomas J. Manuccia, Head
Chemistry and Application Section
Code 6543
Naval Research Laboratory
Washington, DC 20375

Dr. Stephen G. Bishop, Head
Semiconductor Branch
Code 6870
Naval Research Laboratory
Washington, DC 20375

Dr. John W. Rockway
Comm. Technology Prog. Off.
Code 8105
Naval Ocean Systems Center
San Diego, CA 92152

Dr. Barry P. Shay
Joint Program Office,
ODUSD(P)
The Pentagon, Rm 40825
Washington, DC 20301

Dr. Sydney R. Parker
Professor, Electrical Engineering
Code 62PX
Naval Postgraduate School
Monterey, CA 93940

Dr. George B. Wright
Office of Naval Research
Code 427
Arlington, VA 22217

OTHER GOVERNMENT AGENCIES

Dr. Ronald E. Kagarise
Director
Division of Materials Research
National Science Foundation
1800 G Street
Washington, DC 20550

Director
Division of Electrical, Computer
and Systems Engineering
National Science Foundation
Washington, DC 20550

Dr. Dean L. Mitchell
Section Head
Condensed Matter Sciences Section
Division of Materials Research
National Science Foundation
1800 G Street, N. W.
Washington, DC 20550

Judson C. French, Director
Center for Electronics and Electrical
Engineering
B 358 Metrology Building
National Bureau of Standards
Washington, DC 20234

NON-GOVERNMENT AGENCIES

Director
Columbia Radiation Laboratory
Columbia University
538 West 120th Street
New York, NY 10027

Director
Coordinated Science Laboratory
University of Illinois
Urbana, IL 61801

Associate Director of Materials
and Electronics Research
Division of Applied Sciences
McKay Laboratory 107
Harvard University
Cambridge, MA 02138

Director
Electronics Research Center
University of Texas
P. O. Box 7728
Austin, TX 78712

Director
Electronics Research Laboratory
University of California
Berkeley, CA 94720

Director
Electronics Sciences Laboratory
University of Southern California
Los Angeles, CA 90007

Director
Microwave Research Institute
Polytechnic Institute of New York
333 Jay Street
Brooklyn, NY 11201

Director
Research Laboratory of Electronics
Massachusetts Institute of Technology
Cambridge, MA 02139

Director
Stanford Electronics Laboratory
Stanford University
Stanford, CA 94305

Director
Edward L. Ginzton Laboratory
Stanford University
Stanford, CA 94305

END

2-87

DTIC